Robust Approaches for Structural Load Mitigation and Prognosis-based Lifetime Control of Commercial Wind Turbines

Von der Fakultät für Ingenieurwissenschaften,
Abteilung Maschinenbau und Verfahrenstechnik
der
Universität Duisburg-Essen
zur Erlangung des akademischen Grades
eines
Doktors der Ingenieurwissenschaften
Dr.-Ing.
genehmigte Dissertation

von

Edwin Kipchirchir
aus
Nandi, Kenia

Gutachter: Univ.-Prof. Dr.-Ing. Dirk Söffker
Univ.-Prof. Dr.-Ing. Andreas Reuter

Tag der mündlichen Prüfung: 14. Juni 2024

DOI: 10.17185/duepublico/82108
URN: urn:nbn:de:hbz:465-20240620-082336-4

Acknowledgements

First and foremost, I would like to express my sincere gratitude to Univ.-Prof. Dr.-Ing. Dirk Söffker for giving me the opportunity to conduct my research at the Chair of Dynamics and Control (SRS) at the University of Duisburg-Essen. His guidance, motivation, and valuable advice throughout my research period contributed immensely to the successful completion of my studies. Secondly, I would like to thank Univ.-Prof. Dr.-Ing. Andreas Reuter from the Institute for Wind Energy Systems at the Leibniz University Hannover for agreeing to review my thesis and for his valuable comments as the second examiner.

I would like thank to my colleagues at the Chair of Dynamics and Control (SRS) for their kind support, encouragement, and for making my stay in Germany an unforgettable experience. Special thanks go to my predecessors and former SRS members Dr.-Ing. Jackson G. Njiri and Dr.-Ing. Manh Hung Do for their guidance and cooperation.

This work could not have been possible without the support of the research collaboration between the Kenya Ministry of Education through the administration and implementation of the National Research Fund (NRF), and the German Academic Exchange Service (DAAD). This disseration is printed with the support of the DAAD. I would also like to thank the administration of Jomo Kenyatta University of Agriculture and Technology (JKUAT) for granting me study leave for the entire duration of my research.

I would like to thank my dear wife from the bottom of my heart for making so much sacrifice by taking care for our children and home while I was away for study purposes. Her unwavering love, encouragement, and prayers went a long way in making my research journey worthwhile. My deepest gratitude goes to my son and daughter who gave up playtime and important experiences with their daddy. Their young understanding hearts were a constant source of encouragement. I would also like to thank my parents who laid a solid foundation by instilling good moral and spiritual values in me.

Finally and most importantly, I would like to thank God for His provision, protection, loving care, and wisdom that He has given me throughout my research.

Duisburg, June 2024 Edwin Kipchirchir

Kurzfassung

Um den ständig wachsenden weltweiten Bedarf an erneuerbaren Energien zu decken, hat der Windenergiesektor in den letzten Jahrzehnten ein exponentielles Wachstum der physischen Größe und Leistung von Windkraftanlagen (WEA) erlebt, um mehr Energie aus Wind zu gewinnen. Mit zunehmender Größe von WEA wird erwartet, dass die strukturelle Belastung der WEA-Komponenten aufgrund des zusätzlichen Gewichts und der Flexibilität zunimmt. Diese erhöhte Belastung hat Auswirkungen auf die Betriebssicherheit von WEA-Anlagen hinsichtlich Ermüdungsschäden, Lebensdauer, Ausfallzeiten und der damit verbundenen Zuverlässigkeit der Energieversorgung.

Dynamische Schwankungen im Windfeld einer WEA sind für die Ermüdungsbelastungen ihrer Komponenten bei der Stromerzeugung verantwortlich. Räumlich-zeitliche Veränderungen des Rotorwindfeldes wirken sich störend auf das WEA-System aus. Dies erfordert Steuerungsschemata, um diese Störung für einen optimalen Betrieb zu kompensieren. Um die Auswirkungen unterschiedlicher Belastungen auf WEA-Komponenten zu minimieren, wurden fortschrittliche Multi-Input-Multi-Output-Steuerungsschemata (MIMO) vorgeschlagen, die geeignete Windstörungsmodelle integrieren. Diese Methoden dienen in der Regel anderen Steuerungszielen, wie z. B. der Generatorgeschwindigkeits-/-leistungsregelung für den Betrieb von Windenergieanlagen bei überdurchschnittlichen Windgeschwindigkeiten. Die meisten dieser Regler basieren jedoch auf linearen Modellen, die aus nichtlinearen WT-Modellen reduzierter Ordnung gewonnen werden. Die bei der Extraktion dieser linearen Modelle getroffenen Annahmen führen zu Modellierungsfehlern im WEA-Betrieb. Darüber hinaus werden Nichtlinearitäten, die durch sich ändernde Betriebsbedingungen verursacht werden, nicht berücksichtigt. Obwohl robuste Regler die mit Systemnichtlinearitäten und Modellierungsfehlern verbundenen Unsicherheiten berücksichtigen, werden sie immer noch nur für Entwurfssituationen entwickelt. Daher kann sich ihre Leistung unter äußerst unsicheren Betriebsbedingungen erheblich verschlechtern. Darüber hinaus enthalten nominell robuste Regler keine Windstörungsmodelle, die die Auswirkungen von Windstörungen auf die WEA-Leistung unterdrücken können. Es wurden Versuche unternommen, einen robusten störungsadaptiven Controller (RDAC) zu entwickeln, um Modellierungsfehler und Nichtlinearitäten aufgrund von Windstörungen zu verringern. Dieser Regler wurde jedoch an einer kleineren 1,5-MW-Referenz-WEA getestet, die strukturell nicht so stark belastet ist wie größere kommerzielle WEA nach dem neuesten Stand der Technik (SOTA). Seine Leistung wurde auch nicht mit den neuesten Referenz-WT-Controllern (RWT) verglichen. Darüber hinaus basiert der Entwurf von RDAC auf nominalen Modellen, die keine Beschreibung des Unsicherheitsmodells enthalten, was zu einer konservativen Robustheit führt. Adaptive Regler hingegen sind darauf ausgelegt, mehrere Betriebspunkte im Design zu berücksichtigen. Allerdings berücksichtigen die meisten adaptiven Regler nicht die Optimierung von Kompromissen im Zusammenhang mit dem Betrieb der WEA bei Windgeschwindigkeiten über der Nennwindgeschwindigkeit,

einschließlich struktureller Lastreduzierung und Geschwindigkeitsregelung. Ähnlich wie RDAC basieren die meisten branchenbasierten Steuerungen für diesen Betriebsmodus auf der kollektiven Pitch-Steuerung (CPC) und berücksichtigen daher nicht die Rotorblattlasten von Windkraftanlagen, die nur durch unabhängige Pitch-Steuerung (IPC) gemindert werden können.

In den letzten Jahren haben Strategien zur Steuerung und Verlängerung der Lebensdauer von WEA immer mehr an Bedeutung gewonnen. Wenn sie nicht überwacht werden, können strukturelle Belastungen, insbesondere in großen Onshore- und Offshore-WEA-Anlagen, zu einer Verkürzung der Lebensdauer oder einem frühen Ermüdungsversagen aufgrund von Schadensanhäufungen führen. Daher ist eine kontinuierliche Überwachung des Gesundheitszustands (State of Health, SOH) von WEA von entscheidender Bedeutung, um solche Folgen zu vermeiden und die Energieversorgung und Betriebssicherheit sicherzustellen. Aus diesem Grund wurden Zustandsüberwachungssysteme (Condition Monitoring Systems, CMS) zur Fehlererkennung und Zustandsüberwachung von WEA-Strukturen entwickelt. In den letzten Jahren wurden Strategien für die Überwachung des strukturellen Zustands (Structural Health Monitoring, SHM) von Windkraftanlagen zur Schätzung des Ermüdungsschadens (SOH) und zur Vorhersage der verbleibenden Nutzungsdauer (RUL) entwickelt. Prognosebasierte Kontrollstrategien basieren in der Regel auf einem Bewertungskriterium für Ermüdungsschäden, um die verbrauchte Lebensdauer von WEA-Komponenten zu bestimmen. Basierend auf dem SOH werden Steuersollwerte angepasst, um eine gewünschte Lebensdauer der Komponenten zu erreichen. Allerdings erschwert die stochastische Winddynamik die Schätzung des SOH in einer WEA. Daher sind lebenslange Kontrollmethoden auf Basis von RDAC erforderlich. Die meisten der gemeldeten prognosebasierten Steuerungsmethoden konzentrieren sich auf die Steuerung der Lebensdauer einer einzelnen WEA-Struktur, typischerweise des Turms oder der Rotorblätter. Darüber hinaus sind diese zuverlässigkeitsorientierten Regler häufig für bestimmte Betriebspunkte ausgelegt und weisen daher bei wechselnden Windfeldern eine verminderte Leistung auf. Dadurch können sie bei dynamischen Windverhältnissen nicht die gewünschte Lebensdauer gewährleisten. In jüngster Zeit werden robuste Steuerungen in Kombination mit Echtzeitmodellen zur Beurteilung von Ermüdungsschäden eingesetzt, um Prognoseziele zu erreichen. Die meisten verlassen sich auf modellbasierte Online-Lastzykluszählalgorithmen, um die Schadensakkumulation zu bestimmen, wobei analytische Modelle die Verschlechterungsschätzung liefern. Sie stützen sich auch auf WEA-Lastmessungen, von denen einige in kommerziellen WEA nicht verfügbar sind, was ihre Praktikabilität einschränkt.

In dieser Arbeit werden verschiedene RDAC-Regelungsansätze zur strukturellen Lastreduzierung und Geschwindigkeitsregelung von kommerziellen WEA vorgestellt, die bei Betrieb mit hoher Windgeschwindigkeit betrieben werden. Die entwickelten Regelungsansätze werden dann in zuverlässigkeitsorientierten Prognoseverfahren zur Lebensdauerregelung von WEA eingesetzt. Zunächst wird ein CPC-basierter RDAC-Regler vorgestellt, der mit nicht glatter H_∞-Synthese entwickelt und um ein adaptives IPC-Schema (aIPC) zur Geschwindigkeitsregelung und Lastreduzierung im Turm und den Rotorblättern erweitert wird. Diese adaptive, robuste, beobachterbasierte Kontrollstrategie (RDAC+aIPC) wird an einem Onsore-RWA mit 1,5 MW getestet. Simulationsergebnisse zeigen, dass die vorgeschlagene Regelungsstrategie im Vergleich zu einem Gain-Scheduled-Proportional-Integral (GSPI) und einem RDAC-Regler strukturelle Belastungen in mehreren WTG-Komponenten reduziert, ohne nennenswerte Auswirkungen auf die Rotorgeschwindigkeit

oder die erzeugte Leistung unter unterschiedlichen Betriebsbedingungen. Zweitens wird ein H_∞ RDAC-Regler entwickelt und auf ein größeres 5-MW-Onshore-WEA angewendet, um seine Eignung für die kommerzielle WEA-Steuerung zu beweisen. Seine Leistung wird mit einem SOTA RWT-Controller, dem GSPI-basierten Referenz-Open-Source-Controller (ROSCO), verglichen. Simulationsergebnisse für verschiedene Windbedingungen zeigen eine verbesserte Leistung bei der Reduzierung der Turmlast und der Regelung der Generatordrehzahl. Drittens wurde der RDAC-Controller mithilfe des μ-Synthese-Ansatzes entwickelt, um eine verbesserte robuste Leistung zu erzielen. Eine aus der 5-MW-WEA extrahierte Anlagenfamilie ermöglicht die Erstellung einer Unsicherheitsbeschreibung, aus der ein unsicheres Modell der WEA entwickelt und für den Reglerentwurf verwendet wird. Simulationsergebnisse zeigen, dass der RDAC-Regler mit μ-Synthese im Vergleich zu ROSCO- und H_∞-RDAC-Reglern eine bessere Leistung bei der Reduzierung der Turmlast und der Generatorgeschwindigkeitsregelung erzielt. Dies wird erreicht, ohne dass die Pitchgeschwindigkeitsbeschränkung der Turbine verletzt wird oder zusätzliche Belastungen in den Rotorblättern entstehen. Abschließend wird ein IPC-basierter RDAC-Controller vorgestellt, der mithilfe des μ-Synthese-Ansatzes entwickelt wurde. Der Regler wird beim 5-MW-RWA eingesetzt, um die Generatorgeschwindigkeit zu regulieren und die Blatt- und Turmlasten zu reduzieren. Simulationsergebnisse zeigen eine verbesserte Leistung bei der strukturellen Lastreduzierung im Vergleich zu ROSCO-, H_∞ RDAC- und μ-Synthese-RDAC-Reglern. Es bietet auch einen optimalen Kompromiss bei der Generatordrehzahl-/Leistungsregelung.

Vor der Entwicklung von Prognoseschemata auf Basis der oben genannten Kontrollstrategien wird zunächst eine Literaturrecherche von SHM und Prognose sowie prognosebasierten Kontrollmethoden für WEA durchgeführt, um bestehende Lücken zu identifizieren. Widersprüchliche Anforderungen wie Produktionszuverlässigkeit, Reduzierung der Betriebs- und Wartungskosten (O&M) und lebenslange Garantien werden diskutiert. Aktuelle Entwicklungen bei modellbasierten, datengesteuerten und hybriden SHM-Prognosansätzen für die SOH-Schätzung, die RUL-Vorhersage und die Lebensdauersteuerung von WEA werden hervorgehoben. Zweitens wird eine modellbasierte adaptive robuste Lebensdauerkontrollstrategie basierend auf dem RDAC+aIPC-Regler für die kontrollierte Alterung von WEA-Rotorblättern vorgestellt. Das vorgeschlagene Prognoseschema wird am 1,5-MW-RWA evaluiert. Es wird ein Online-Schadensbewertungsmodell implementiert, um die Controller-Gewinne basierend auf dem SOH zu variieren. Das Prognoseschema reduziert strukturelle Belastungen in den Rotorblättern, um ein vordefiniertes Schadensniveau bei einer gewünschten Lebensdauer sicherzustellen, ohne die Geschwindigkeitsregulierungsleistung der WEA zu beeinträchtigen. Darüber hinaus ist auch eine deutliche Reduzierung der Turmermüdungsschäden zu beobachten. Abschließend wird ein hybrides Prognoseschema vorgestellt, das datengesteuerte Lastvorhersage und modellbasierte Schadensschätzungsmodelle für eine robuste Lebensdauersteuerung in kommerziellen WEA kombiniert. Ein Support Vector Machine (SVM)-Regressionsmodell wird mithilfe von Zeitreihen-Ladedaten trainiert, die aus dynamischen Simulationen mit dem μ-Synthese-RDAC-Controller erhalten wurden. Das Regressionsmodell nutzt verfügbare WT-Messungen, um die Turmlast vorherzusagen. Basierend auf dieser Vorhersage schätzt ein Online-Schadensbewertungsmodell das Schadensniveau und die Lebensdauer des Turms. Die Lebensdauergewinne des Controllers werden dynamisch angepasst, um eine vordefinierte Schadensgrenze und Lebensdauer zu erreichen. Ergebnisse dynamischer Simulationen mit dem 5-MW-RWA zeigen die Effizienz des vorgeschlagenen Ansatzes bei der Kontrolle der

Ermüdungsbelastung in WT-Komponenten.

Abstract

To meet the ever-growing global demand for renewables, the wind energy sector has seen exponential growth in the physical size and power of wind turbines (WTs) in recent decades to capture more energy from wind. As WTs increase in size, structural loads on WT components are expected to increase due to the additional weight and flexibility. This increased load has an impact on the operational safety of WT systems in terms of fatigue damage, service life, downtime, and the associated reliability of power supply.

Dynamic fluctuations in the wind field experienced by a WT is responsible for the fatigue loads in its components during power generation. Spatio-temporal changes in the rotor effective wind field act as a disturbance to the WT system. This requires control schemes to compensate for this disturbance for optimal operation. To minimize the effects of varying stresses on WT components, advanced multi-input multi-output (MIMO) control schemes which integrate suitable wind disturbance models have been proposed. These methods usually serve other control objectives such as generator speed/power regulation for WT operation in above-rated wind speed regime. However, most of these controllers are designed using linear models obtained from reduced-order nonlinear WT models. The assumptions made in extracting these linear models lead to modeling errors during WT operation. In addition, nonlinearities caused by changing operating conditions are not considered. Although robust controllers address uncertainties associated with system nonlinearities and modeling errors, they are still only developed for design situations. Therefore, their performance can degrade significantly under highly uncertain operating conditions. Furthermore, nominal robust controllers do not include wind disturbance models that can reject the effect of wind disturbances on WT performance. An attempt has been made to develop a robust disturbance accommodating controller (RDAC) to mitigate modeling errors and nonlinearities due to wind disturbances. However, this controller has been tested on a smaller 1.5 MW reference WT which is not structurally stressed as larger state-of-the-art (SOTA) commercial WTs. Its performance has also not been benchmarked against the latest reference WT (RWT) controllers. Furthermore, RDAC is designed based on nominal models that do not include an uncertainty model description, resulting in conservative robustness. Adaptive controllers on the other hand are designed to consider multiple operating points in the design. However, most adaptive controllers do not consider the optimization of trade-offs related to operation of the WT in above-rated wind speed, including structural load reduction and speed control. Similar to RDAC most industry-based controllers for this operating regime are based on collective pitch control (CPC), hence do not address WT rotor blade loads, which can only be mitigated through independent pitch control (IPC).

In recent years, strategies to control and extend the service life of WTs have become increasingly important. If not monitored, structural loads, especially in large onshore and offshore WT installations, can result in lifetime shortening or early fatigue failure

due to damage accumulation. Therefore, continuous state-of-health (SOH) monitoring of WTs is crucial to avoid such consequences and to ensure energy supply and operational safety. For this reason, condition monitoring systems (CMSs) have been developed for fault detection and health monitoring of WT structures. In recent years, strategies for structural health monitoring (SHM) of WT have been developed for fatigue damage SOH estimation and remaining useful life (RUL) prediction. Prognosis-based control strategies usually rely on a fatigue damage evaluation criterion to determine the consumed lifetime of WT components. Based on the SOH, control setpoints are adjusted to achieve a desired lifetime of the components. However, stochastic wind dynamics complicates estimation of the SOH in a WT. Therefore, lifetime control methods based on RDAC are required. Most of reported prognostics-based control methods focus on controlling the lifetime of a single WT structure, typically the tower or rotor blades. Moreover, these reliability-oriented controllers are often designed to be valid for specific operating points, hence show degraded performance in changing wind fields. As a result, they are not able to guarantee a desired service life under dynamic wind conditions. Recently, robust controllers have been used in combination with real-time fatigue damage assessment models to achieve prognosis goals. Most rely on model-based online load cycle counting algorithms to determine damage accumulation, with analytical models providing the degradation estimate. They also rely on WT load measurements, some of which are not available in commercials WTs, limiting their practicality.

In this thesis, different RDAC control approaches for structural load reduction and speed control of commercial WTs operating in above-rated wind speed operation are presented. The developed control approaches are then applied in reliability-oriented prognosis schemes for lifetime control of WTs. First, a CPC-based RDAC controller developed using nonsmooth H_∞ synthesis is presented and extended with an adaptive IPC (aIPC) scheme for speed regulation and load reduction in the tower and rotor blades. This adaptive robust observer-based control strategy (RDAC+aIPC) is tested on a 1.5 MW onsore RWT. Simulation results show that the proposed control strategy reduces structural loads in several WTG components without significant effects on rotor speed or generated power under different operating conditions compared with a gain-scheduled proportional integral (GSPI) and an RDAC controller. Secondly, a H_∞ RDAC controller is developed and applied to a larger 5 MW onshore RWT to prove its suitability for commercial WT control. Its performance is compared with a SOTA RWT controller, the GSPI-based reference open-source controller (ROSCO). Simulations results for different wind conditions show improved performance in tower load mitigation and generator speed regulation. Thirdly, the RDAC controller is designed using μ-synthesis approach to achieve improved robust performance. A family of plants extracted from the 5 MW RWT enables the generation of an uncertainty description, from which an uncertain model of the WT is developed and used for controller design. Simulation results show that the RDAC controller with μ-synthesis achieves better performance in tower load mitigation and generator speed regulation compared with ROSCO and H_∞ RDAC controllers. This is achieved without violating either the turbine's pitch rate constraint or inducing additional loads in the blades. Finally, an IPC-based RDAC controller developed using the μ-synthesis approach is presented. The controller is applied to the 5 MW RWT to regulate generator speed and reduce blade and tower loads. Simulation results show the best performance in structural load reduction compared with ROSCO, H_∞ RDAC, and μ-synthesis RDAC controllers. It also offers an optimal compromise in generator speed/power regulation.

Before developing prognosis schemes based on the above control strategies, a comprehensive review of SHM and prognosis as well as prognostics-based control methods applied to WTs is first carried out to identify existing gaps. Conflicting requirements such as production reliability, operation and maintenance (O&M) cost reduction, and lifetime guarantees are discussed. Recent developments in model-based, data-driven, and hybrid SHM prognosis approaches for SOH estimation, RUL prediction, and lifetime control of WTs are highlighted. Secondly, a model-based adaptive robust lifetime control strategy based on the RDAC+aIPC controller for controlled aging of WT rotor blades is presented. The proposed prognostics scheme is evaluated on the 1.5 MW RWT. An online damage evaluation model is implemented to vary the controller gains based on the SOH. The prognostics scheme reduces structural loads in the rotor blades to ensure a predefined damage level at a desired service life without compromising the speed regulation performance of the WT. Moreover, a significant reduction in the tower fatigue damage is also observed. Finally, a hybrid prognosis scheme which combines data-driven load prediction and model-based damage estimation models, for robust lifetime control in commercial WTs is presented. A support vector machine (SVM) regression model is trained using timeseries loading data obtained from dynamic simulations using the μ-synthesis RDAC controller. The regression model uses available WT measurements to predict the tower load. Based on this prediction, an online damage evaluation model estimates the damage level and lifetime of the tower. The lifetime controller gains are dynamically adjusted to achieve a predefined damage limit and lifetime. Results of dynamic simulations using the 5 MW RWT demonstrate the efficacy of the proposed approach in controlling fatigue loading in WT components.

Contents

List of Figures

List of Tables

List of Abbreviations

aIPC	adaptive Independent Pitch Control
AM	Attention Mechanism
ANFIS	Adaptive Neuro-Fuzzy Inference System
ANN	Artificial Neural Networks
ARE	Algebraic Riccati Equation
BECCS	Bioenergy with Carbon Capture and Storage
BM	Bayesian Method
CAGR	Compound Annual Growth Rate
CBM	Condition-Based Maintenance
CCS/U	Carbon Capture and Storage/Utilization
CM	Condition Monitoring
CMS	Condition Monitoring System
CNN	Convolutional Neural Network
CPC	Collective Pitch Control
DAC	Disturbance Accommodating Control
DBN	Deep Belief Network
DEL	Damage Equivalent Load
DFIG	Doubly-Fed Induction Generator
DLC	Design Load Case
DOF	Degree Of Freedom
DTU	Technical University of Denmark

E-W	Edge-Wise
F-W	Flap-Wise
F-A	Fore-Aft
FARE	Filter Algebraic Riccati Equation
FAST	Fatigue, Aerodynamics, Structures, and Turbulence
FDA	Fisher Discriminant Analysis
FDD	Fault Detection and Diagnosis
FFT	Fast Fourier Transform
FL	Fuzzy Logic
FLORIS	FLOw Redirection and Induction in Steady State
FOWT	Floating Offshore Wind Turbine
FTC	Tault Tolerant Control
GA	Genetic Algorithm
GPR	Gaussian Process Regression
GSPI	Gain-Scheduled Proportional Integral
HAWC2	Horizontal Axis Wind turbine simulation Code 2nd generation
HAWT	Horizontal Axis Wind Turbine
HPF	High-Pass Filter
HSS	High Speed Shaft
ICA	Independent Component Analysis
IEA	International Energy Agency
IEC	International Electrotechnical Commission
IPC	Independent Pitch Control
KF	Kalman Filter
LCOE	Levelized Cost Of Energy
LFT	Linear Fractional Transformation
LIDAR	Light Detection and Ranging

LMI	Linear Matrix Inequalities
LPF	Low-Pass Filter
LQG	Linear Quadratic Gaussian
LSTM	Long Short-Term Memory
LTI	Linear Time Invariant
LTP	Lifetime Prognosis
MBC	Multi-Blade Coordinate
MCMC	Markov Chain Monte Carlo
MIMO	Multi-Input Multi-Output
MISO	Multi-Input Single-Output
ML	Machine Learning
MLP	Multi-Layer Perceptron
MPPT	Maximum Power Point Tracking
MSE	Mean Square Error
N	Number of cycles
NLS	Nonlinear Least Squares
NN	Neural Networks
NREL	National Renewable Energy Laboratory
NS	Nominal Stability
O&M	Operation and Maintenance
OpenFAST	Open-source Fatigue, Aerodynamics, Structures, and Turbulence
PCA	Principal Component Analysis
PD-MFAC	Proportional-Derivative Model-Free Adaptive Control
PDF	Probability Density Function
PF	Particle Filter
PI	Proportional Integral
PID	Proportional Integral Differential

PR	Pitch Rate
PSD	Power Spectral Density
PSO	Particle Swarm Optimization
RDAC	Robust Disturbance Accommodating Controller
RFC	Rain-Flow Counting
RMS	Root Mean Square
RMSE	Root Mean Square Error
RNN	Recurrent Neural Networks
ROSCO	Reference Open-Source Controller
RP	Robust Performance
RS	Robust Stability
RUL	Remaining Useful Life
RWT	Reference Wind Turbine
S	Stress amplitude
SAP	Subspace Aided Approach
SCADA	Supervisory Control and Data Acquisition
SHM	Structural Health Monitoring
SISO	Single-Input Single-Output
SMC	Sliding Mode Control
SOH	State-Of-Health
SOTA	State-Of-The-Art
SS	Side-Side
SSV	Structured Singular Value
SV	Singular Value
SVM	Support Vector Machine
SVR	Support Vector Regression
TI	Turbulence Intensity

TOF	Time-Of-Failure
TSR	Tip-Speed Ratio
UPF	Unscented Particle filter
VAWT	Vertical Axis Wind Turbine
WECS	Wind Energy Conversion Systems
WindPACT	Wind Partnership for Advanced Component Technologies
WT	Wind Turbine

List of Symbols

$\tau_{g,ar}$	Above-rated generator torque
$\tau_{_\beta}$	Actuator time constant
P	Aerodynamic power
τ_a	Aerodynamic torque
ρ	Air density
ζ_{avg},ζ_{tilt},ζ_{yaw}	Average, tilt, and yaw blade-root F-W bending moments
ψ	Azimuth angle
β	Blade pitch angle
ζ_1,ζ_2,ζ_3	Blade-root F-W bending moments
β_{com}	Commanded pitch angle
D_k	Damage accumulation
ω_g	Generator speed
τ_g	Generator torque
$\|.\|_\infty$	H_∞ norm
$C_{p_{max}}$	Maximum power coefficient
β_{opt}	Optimal pitch angle
λ_{opt}	Optimal tip-speed ratio
K_i	Integral gain
K_p	Proportional gain
C_p	Power coefficient
$\omega_{g,rated}$	Rated generator speed
P_{rated}	Rated power

ω_r	Rated rotor speed
R	Rotor radius
ω	Rotor speed
ω_e	Rotor speed error
A	Rotor swept area
C_t	Thrust coefficient
λ	Tip-speed ratio
C_q	Torque coefficient
K_t	Torque control gain
J	Total rotational inertia
γ	Tower F-A acceleration
δ	Standard deviation
μ	Structured singular value
ζ	Tower F-A bending moment
ϕ	Tower-top pitch angle
d	Wind disturbance
v	Wind speed

1 Introduction

Increase in the global demand for electricity coupled with concerns related to climate challenges have led to commitment to renewable energy development. Traditional energy systems designed around high-carbon fossil fuels such as coal and crude oil need to be replaced with zero- or low-carbon alternatives. Alongside solar, wind is the leading renewable power source and is expected to remain so for the foreseable future. In tandem with increasing demand for wind energy, there has been an upscale in the size and power rating of wind turbines (WTs) making them succeptible to fatigue loads and performance degradation. Advanced control methods have been employed to curb this shortfall, albeit with persistent challenges related to variability of wind dynamics. This is especially the case for commercial WTs, typically located in harsh environments having stochastic variations of wind loads. Therefore, WT components are subjected to varying loads, which also complicates determination of the health state and lifetime prognosis. In this chapter, a brief background on wind energy generation, developments in WT installation, and future trends are discussed. The problem related to WT control for fatigue load reduction and structural health monitoring (SHM), and remaining uselful life (RUL) prognosis is defined. The objectives addressed in this thesis are also presented.

1.1 Motivation and problem statement

Nowadays, fossil-based energy sources are being faced out in favour of renewable energy sources due to increasing environmental concerns. The major contributor to global carbon emissions are the by-products of energy generation from fossil fuels such as coal and crude oil. Another factor for increased uptake of renewable energy is the scarcity of non-renewable fossil fuels. Global concerns related to climate challenges have led to prioritization of renewable energy development to achieve net-zero energy targets [IRE21; LZ22]. According to the 1.5 ^{o}C transition scenario developed by [IRE23], the use of renewables in power generation together with energy conservation and efficiency sectors will each contribute the largest share of up to 25 % in achieving net-zero global CO_2 emissions by 2050 as illustrated in Fig. 1.1. Other sectors such as direct eletrification, hydrogen and its derivatives, carbon capture and storage/utilization (CCS/U), and bioenergy with carbon capture and storage (BECCS) are expected to cut about half of the emissions. This projected high share of renewables in the energy mix requires a dramatic reduction in reliance on fossil fuels and a rapid development in the key renewable energy technologies such as solar and wind. This is particularly crucial considering that power generation needs to more than triple from 27 PWh in 2020 to 90 PWh by 2050 [IRE23].

After solar, wind is one of the fastest growing renewable energy sources and is expected to remain so in the medium-term [Mar23]. This is due to its higher capacity factor compared to other renewable sources [LZ21]. It is the most widely adopted renewable energy source

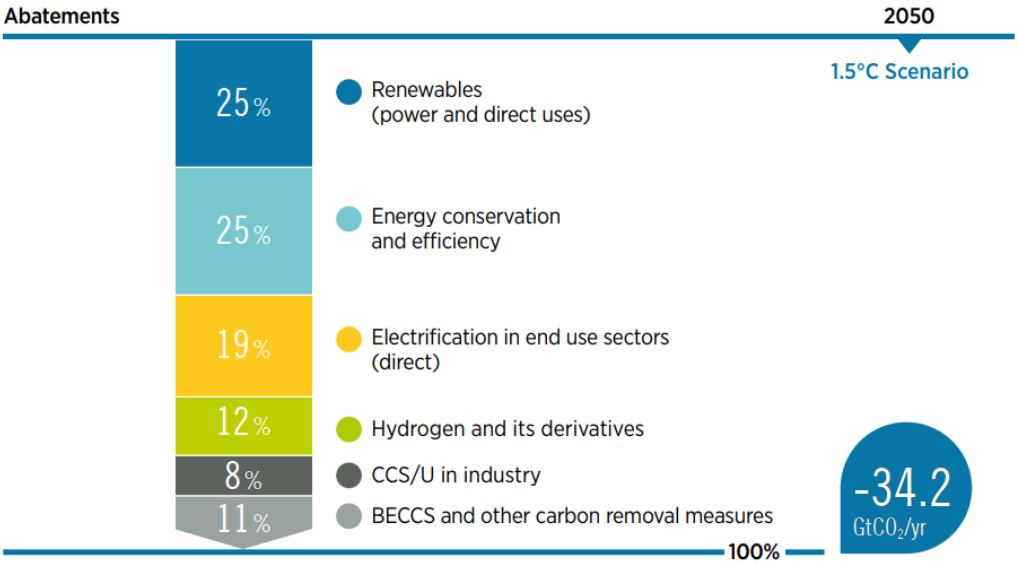

Figure 1.1: Carbon dioxide emissions abatement under the 1.5 ^{o}C scenario in 2050 [IRE23]

due its minimal negative environmental impact and global availability, making it suitable for meeting the ever increasing global energy needs. To meet this clean energy demand, the physical size of WTs and the number of wind energy projects are expected to increase in the coming years. In the short-term, global WT installations are expected to grow at a compound annual growth rate (CAGR) of 15 % [Mar23]. An additional 680 GW of wind capacity is expected to be added between 2023 and 2027, much of this coming from onshore wind. A 2 TW milestone of total wind power capacity is projected to be reached by 2030 [IEA21; Mar23] as shown in Fig. 1.2. However, this growth rate does not correspond to the 1.5 ^{o}C pathway [IRE21] as it results in a shortfall of 32 %. Furthermore, the data does not take into account decommissioned projects, which is significant given that the first generation of wind farms have been decommissioned or will soon reach their estimated 20-year end of life [ZGR^{+}18; BZJ^{+}22]. Although offshore WT installations are expected to increase in the coming years, onshore WTs will still account for a larger share of new WT installations due to their comparatively lower levelized cost of energy (LCOE) [LZ21]

The need to generate more energy from wind has led to a progressive increase in the size of WTs in recent decades [LZ20]. This has resulted in larger, heavier, and highly flexible rotors and towers. This, coupled with stochastic wind inflow conditions, has exacerbated the fatigue loading of these structural components due to increased inertial, gyroscopic, and gravitational loads during operation. This consequently, impacts reliability and increases operation and maintenance (O&M) costs, known to contribute between 25 % and 40 % to the LCOE in WTs [PFR17]. Wind turbines are typically located in harsh environments, with unsteady fluctuations of wind loads responsible for their relatively high failure-rate [LLJ19]. Therefore, almost all WT components are subjected to different combinations of loads during operation due to stochastic wind fields. Utility-scale WTs are particularly sensitive as they are less tolerant to faults and system performance degradation [GL21].

Modern WTs are instrumented with several sensors and actuators, which enables the implementation of multiple control objectives, including load mitigation, power optimiza-

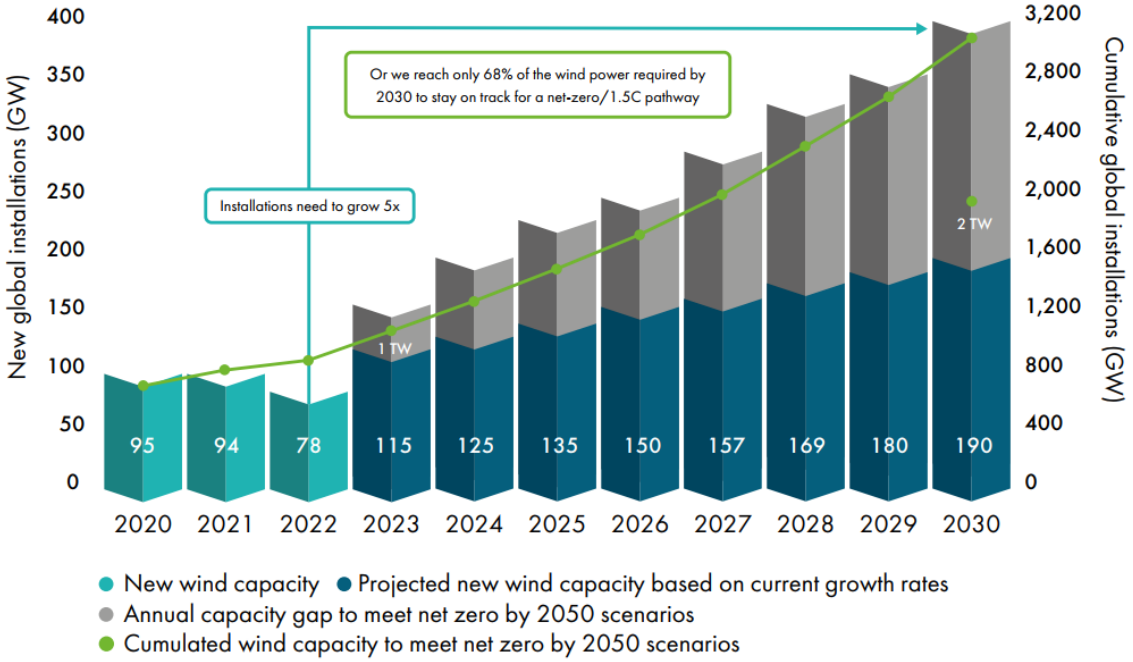

Figure 1.2: The 2 TW milestone is expected to be achieved in just seven years [Mar23]

tion, and lifetime control. Classical single-input single-output (SISO) controllers such as proportional integral differential (PID) control are becoming increasingly less effective in meeting the requirements of these multi-input multi-output (MIMO) systems. Due to coupling between the different dynamics of WTs, SISO controllers are not only difficult to design but also unsuitable for control of modern WT systems [Nji16]. Structural load mitigation of commercial WTs requires the use of advanced control strategies, albeit with collateral effects such as induced loads in other components, trade-off in speed regulation performance, and increased pitch activity [WF08]. Therefore, MIMO controllers are utilized to solve such multi-objective problems that require a balance between conflicting control objectives. However, achieving an optimal compromise is still a challenging and open problem.

To ensure that utility-scale WT perform within their design lifetime, advanced MIMO control approaches have been developed in recent years to reduce structural loads particularly in structures with high failure rates such as rotor blades, tower, and drive-train components. These control schemes include additional objectives such as power optimization and generator speed control. However, due to hardware limitations, most industry controllers still rely on classical approaches such as proportional integral (PI) control [AZPW22]. Structural loads in WTs are more pronounced in when operating in above-rated than in low wind speed regime due to higher wind speeds. For this reason, more emphasize has been placed on developing advanced MIMO controllers for load mitigation of WTs in above-rated operation. Stochastic wind fluctuation is considered a disturbance and leads to nonlinearities in a WT system. In conjuction with other uncertainties such as modeling errors, advanced WT control approaches should not only be robust but also reject effects of wind disturbances [RD18; DS22].

When operating in above-rated wind speed, collective pitch control (CPC), where the

rotor blades are pitched together, is used to regulate speed/power, reduce symmetrical loads in the tower, and stabilize platform pitch motion in floating offshore WTs. To reduce structural loads, individual control loops have been added to the classical CPC generator speed controller. However, coupling between different WT dynamic modes such as blade flap-wise (F-W) and tower fore-aft (F-A) with the drive-train can result in performance deterioration [GC08]. To attenuate periodic loads in rotor blades caused by asymmetric wind fields and gravity, independent pitch control (IPC) is required [YCT20]. Information related to design aspects of commercial WTs are not publicly available due to intellectual property rights. Nevertheless, in tandem with the advancement in WTs, state-of-the-art (SOTA) reference WTs (RWTs) closely reflecting the current and future trends in wind energy have been developed to study new technologies, advance the next generation of WTs, and test modern control techniques for improving the performance of WTs [RGZ$^+$20]. Among the first and most widely used RWTs is the 5 MW RWT developed by the National Renewable Energy Laboratoty (NREL) [JBMS09]. In the recent past, newer and larger RWT been developed to capture the current trends in commercial WT technology. A typical example is the International Energy Agency (IEA) Wind 15 MW RWT [GRS$^+$20] developed by NREL in collaboration with Technical University of Denmark (DTU). This RWT is implemented in NREL and DTU toolchains, which provide high blade fidelity including both bending and torsional deflections, representative of aeroelastic responses of modern long, slender, and highly flexible rotors. However, recent RWTs are yet to be widely adopted by control researchers and are biased towards offshore applications. Therefore, in this thesis, the 5 MW NREL RWT is used for evaluating the developed control approaches. To keep up with the advancement of RWTs, the wind industry has experienced a growing need for baseline controllers. In the recent past, reference controllers that are adaptable across different platforms of RWTs have been developed [AZPW22]. This has enabled a common framework for evaluating newly developed control approaches.

Wind turbines are designed for a service life of at least 20 years or 2.7 $\times 10^8$ fatigue load cycles [ZGR$^+$18]. Faults or failures experienced by WTs are due to component degradation through aging or extreme load events, resulting in system downtime and economic losses. Most WT component failures are attributed to fatigue loads caused by wind speed fluctuations and operational loads such as gyroscopic and inertial loads [NBDS19]. To ensure operational safety and reliability of WT systems, SHM and prognosis schemes that not only monitor degradation but also incorporate control of the life consumption of WT components are required. In recent years significant improvements in SHM have been achieved through online fault detection and condition monitoring [BNS18]. As part of SHM, appropriate measures are taken to address detected faults. This may include corrective or emergency maintenance. However, it is desirable to take action in anticipation of failure. Therefore, preventive maintenance is carried out at predefined intervals or service times, reducing system O&M costs and downtime by avoiding premature breakdowns [BS16]. Reliability-based maintenance combines knowledge of the system's current and previous SOH to determine the probability of failure. The system's reliability is then estimated and the SOH or remaining useful life (RUL) is predicted to determine whether a maintenance action should be performed or postponed.

Diagnosis and prognosis methods, integrated into SHM systems enable decision-making on maintenance or replacement actions. They are also used as modules in a prognosis-based control scheme that ensures reliable system operation and maintenance planning. Prognosis is the process of predicting the progression of a monitored component from undamaged

to failed states [GL21]. Using the damage evolution of a component, prognosis seeks to estimate the SOH and predict the RUL of a component before faults lead to failure. The progression of SOH from an undamaged state to the exhaustion of its structural reserves is predicted. From condition monitoring (CM), degradation patterns can be obtained. This enables the implementation of prognostic schemes for failure prediction.

Structural health monitoring and prognosis techniques are broadly classified into model-based, data-driven, and hybrid approaches. Model-based methods, using models obtained either through physical modeling or system identification are preferred for fault prognosis of WTs in real operating conditions due to their real-time capability. Although nonlinear models accurately represent WT behavior, most model-based approaches are based on linear models despite the inconsistency in behaviors that exists between the linearized model and the highly nonlinear WT [HHS19]. Furthermore, model-based approaches require complex predefined physics or analytical models. Instead of explicit input-ouput models, data-driven approaches use featured data containing system degradation process along with suitable machine learning (ML) techniques to establish a knowledge-base that represents an explicit dependency on system variables [LLJ19]. The ability to work with limited process data as well as its scalability makes data-driven approaches attractive for lifetime modeling of WTs [JKS19]. However, their ability to learn complex signals with nonlinear characteristics is limited. They also have slow convergence speed and low prediction accuracy when applied to big data [XWY+21]. In recent years, hybrid methods that combine the aforementioned approaches have been proposed for fault prognosis in WTs. These techniques capitalize on the advantages of each method and counteract their individual limitations. Hybrid prognosis methods are attractive for lifetime prediction in WTs due to huge amount of operational data generated by high frequency (1 kHz) supervisory control and data acquisition (SCADA) systems found in modern commercial WTs, as well as model-based high fidelity softwares developed for simulating the different dynamics of commercial WTs.

In recent years, lifetime control of WTs using the above-mentioned SHM and prognosis methods has become increasing important. In these approaches, advanced MIMO controllers are preferred for controlling the fatigue damage accumulation in components while considering other objectives [DS21]. A generalized representation of a prognostics-based lifetime control scheme applied to WTs is shown in Fig. 1.3. Online prognosis for determining the SOH or RUL of a WT component under consideration is usually achieved through ideal fatigue load measurements y. However, if WT measurements are unreliable or unavailability, such as tower F-A bending moments, it makes sense to estimate or predict the fatigue load using a suitable prognosis models. The predicted SOH or RUL is used for threshold evaluation, which determines suitable parameters for adapting the lifetime controller to achieve the desired control signal u. In this thesis model-based and hybrid lifetime control schemes are developed for controlling the life consumption of WT blades and tower, respectively. Advanced MIMO robust control methods are developed and used as lifetime controllers.

1.2 Thesis objectives and scope

From the foregoing discussion, it has been shown that the challenge of fatigue loads is more pronounced in utility-scale WTs, particularly in above-rated operation. Therefore, the scope of this thesis is limited to commercial WTs operating in above-rated wind speed

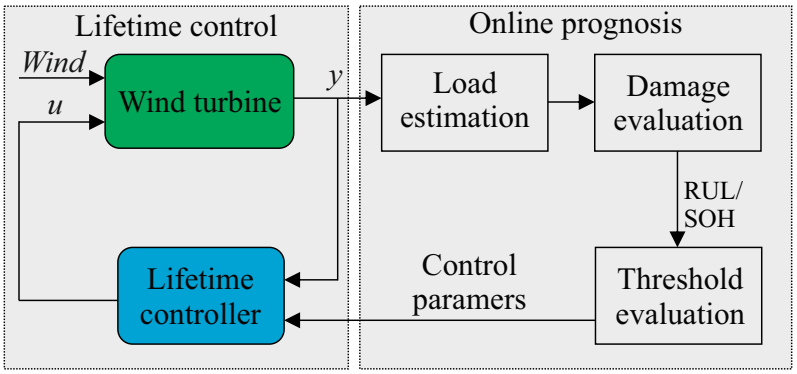

Figure 1.3: Generalized block diagram of a prognostics-based lifetime control strategy

regime. First, advanced MIMO robust control methods are developed for speed regulation and structural load mitigation in the tower and blades. These approaches compensate for uncertainties due to inaccurate nominal models and nonlinearities associated with dynamically fluctuating wind fields. Furthermore, the trade-off between speed regulation and fatigue load reduction control objectives is optimized. The developed approaches are then integrated as reliability controllers in model-based and hybrid SHM and prognosis schemes to achieve the desired service life of WTs.

The advanced MIMO robust control and lifetime approaches are evaluated on a high fidelity reference softwares [JB05; NRE21] using two onshore RWTs developed by NREL. The approaches are first illustrated on smaller Wind Partnership for Advanced Component Technologies (WindPACT) 1.5 MW RWT [RD18] and then applied to the larger 5 MW NREL RWT [JBMS09], which reflects the typical size of onshore commercial WTs. A Kaimal spectral model is used for generating stochastic wind fields for simulations. Although advanced models such as flow redirection and induction in steady state (FLORIS) [NRE24], have been developed for simulating complex wind wake interactions in wind farms, these are relevant for farm-level control which is outside the scope of this thesis.

This thesis is based on published/accepted/in preparation results that can be accessed in the following journal papers [KDNS23; KS24; KDNS24; KLS24] and conference proceedings [KDNS22; KBS23]

1.3 Thesis outline

This thesis is organized six chapters. In chapter 1, the motivation and problems related to the development of advanced control approaches for fatigue load mitigation and speed regulation, as well as SHM and prognosis approaches for improved reliability of commercial WTs are introduced.

In chapter 2, a background on wind energy generation and standard WT control is discussed. The influence of wind inflow coditions on structural loading in WTs is discussed. A review on advanced MIMO control approaches for fatigue load reduction is given. Additionally, a review of SHM and prognosis methods in WT systems and their application in lifetime control of WTs is discussed. Open research gaps from the review are presented.

In chapter 3, an overview of the WT models used in the thesis is given. The baseline

a gain-scheduled PI (GSPI) and ROSCO controllers used to evaluate the efficacy of the developed advanced robust controllers are discussed.

In chapter 4, development of the advanced MIMO robust control methods accommodating wind disturbances and model uncertainties for structural load mitigation and speed regulation of commercial WTs are presented. Using closed-loop dynamic simulation results for different wind conditions, performance of the control approaches are evaluated against the aforementioned baseline controllers. The control methods are compared against each other and practical recommendations for each are given.

In chapter 5, prognostics schemes utilizing the developed advanced MIMO robust control methods are presented. First, a model-based adaptive lifetime prognosis scheme, combining CPC and IPC control loops is applied to the WindPACT 1.5 MW RWT for controlled aging of the blades to avoid early fatigue without sacrificing speed regulation and tower load mitigation. Secondly, a hybrid (model-based data-driven) prognosis scheme for robust lifetime control of the 5 MW RWT is outlined. Simulation results for both of the prognostics-based robust lifetime control approaches are presented and discussed.

In chapter 6, a summary of the developed methods is given. The main design steps of the approaches are described. Scientific contributions that have been achieved are highlighted. Remaining limitations are discussed and the future direction of the work is given.

2 Background and Literature Review

As a preample to the advanced multi-input multi-output (MIMO) control methods and prognostics-based lifetime control schemes developed in this thesis, background information on wind energy generation and standard control methods for WTs are presented. To avoid knowledge duplication, an extensive literature review covering advanced control methods and SHM and prognosis approaches employed primarily for fatigue load reduction and lifetime control of WTs is discussed. From the review, existing research gaps are outlined.

The figures, tables, and content in this chapter are partly based on the published journal papers [KS24; KDNS24] and the journal paper in preparation [KLS24].

2.1 Fundamentals of wind turbine energy generation and control

2.1.1 Wind turbine energy extraction

The occurence of wind is attributed to processes driven by solar irradiation, whose energy produces temperature differences that lead to air circulation. As hot air rises, a reduction in local atmospheric pressure causes nearby cooler air to flow into this low pressure region, resulting in wind. Wind is a free energy resource that can be harnessed using wind energy conversion systems (WECS). This is achieved primarily using WTs, which convert the kinetic energy of the wind into electrical power. To maintain structural integrity and ensure high energy generation efficiency, it is crucial to install WTs in regions with stable wind flows and consistent speeds. Variability in wind characteristics results in wind shear and wake forces [And19].

The two main configurations of WTs are horizontal axis WTs (HAWT) in which the rotation axis of the rotor blades faces the wind flow, and vertical axis WTs (VAWT), whose blades rotate perpendicular to the wind stream [Ass12]. Horizontal axis wind turbines sare further divided into upwind and downwind WTs, in which the rotor blades are posistion into or away from the wind, respectively. A three-bladed HAWT configuration, is preferred for commercial power plants due to several advantages. These include high power density, the ability to mount the rotor on a tall tower to harness more energy from high wind speeds, easy installation and maintenance due to modular structure, and high power efficiency achieved using a yaw mechanism which positions the rotor to face the wind direction [Ass12; Hau13]. On the other hand, VAWTs are used for small-scale applications. They are suitable for urban areas with low wind speeds, high turbulence, and noise restrictions as they produce less noise due to their low tip speed. They are adaptable to unstable wind fields of urban terrains and are easily integrated into available infrastructure [KRF18].

Wind turbines can be manufactured with either fixed- or variable-pitch. Because structural loads are reduced by controlling of the blade pitch angle, fixed-pitch WTs are not suitable for commercial applications where high structural loads occur [NS16]. Therefore,

utility-scale WTs are equiped with pitch actuator drives that are used to vary the blade angle of attack. The rotor blades can be varied either together via collective pitch control (CPC) or independently via independent pitch control (IPC). While CPC is used primarily to regulate rotor speed, IPC is used to mitigate periodic loads in the blades caused by asymmetric wind fields and gravitational forces [GC08; YCT20].

Wind turbines can operate at either fixed or variable speed. Because its speed almost corresponds the grid fequency, the generator of a fixed speed WT is connected directly to the grid. Although they are simple and robust, wind turbulence leads to undesirable power fluctuations and induction of mechanical stress to the drivetrain [Thi05; NS16]. A variable speed WT can be operated close to its optimal efficiency because its speed is decoupled from the grid frequency [PJ11]. To achieve this, the generator is controlled by a power electronic converter, ensuring that high quality power is delivered to the grid. By varying the rotor speed via the electrical torque of the generator, power fluctuations caused by wind fluctuations can be compensated for. Therefore, modern commercial HAWTs are designed to have variable pitch and speed to reduce structural loads and maximize energy production by ensuring the rotor speed tracks the prevailing wind speed.

A variable speed HAWT has three operating regions defined by its power curve. In Figure 2.1, a generic power curve for a WT is shown. The power coefficient C_p of the available wind power is assumed to be 1, where C_p is the ratio of aerodynamic power to wind power [JPBL06]. The theoretical maximum extractable power from wind is 0.593, known as the Betz limit [Bet14]. In practice, C_p is between 0.4 and 0.45 [AYTS12]. Region 1 is the area below the cut-in wind speed in which power generated by the WT would not be sufficient to overcome frictional losses, which is why the turbine is stopped. Region 2 is the partial-load or below-rated region between the cut-in and rated wind speed. The main control objective for this region is to maximize power from the varying wind speeds. This is achieved by fixing the pitch angle at fine pitch, to ensure maximum aerodynamic efficiency, and varying the generator speed using a torque controller to follow the incoming wind speed. In this regime, maximum power point tracking (MPPT) control approaches based on torque control, pitch control or a combination of both are used [AYTS12; SKSR20]. Region 3, also known as above-rated or full-load region, is the region above the rated wind speed. Here, the main control goal is to ensure that the WT's rotor speed and power are controlled to their rated values to avoid exceeding its mechanical and electrical limits. This is achieved by pitch control using either CPC or IPC methods. In region 4, the rotor blades are pitched to feather resulting in zero thrust and thus triggers a shutdown maneuver of the WT for safety reasons. This region is not of interest for standard control. To ensure a smooth transition from one region to the next, a transition logic is usually implemented [AZPW22]. Most control strategies for load mitigation have been applied to region 3 due to the high structural loads experienced by WTs as a result of from high wind speeds.

Structural loads in wind turbines

Wind power is essential for generating energy in WTs. However, as a consequence of rotational sampling of spatio-temporally distributed wind field, asymmetric aerodynamic loads are induced on the rotor disc [CS16]. Subsequent rotor imbalance is the main cause of structural loads in WTs. Others include gravitational and gyroscopic forces resulting from a combined effect of nacelle yaw, blade pitch, and rotary motions. This results in cyclic loading of the blades, hub, and fixed components, which is a major cause of

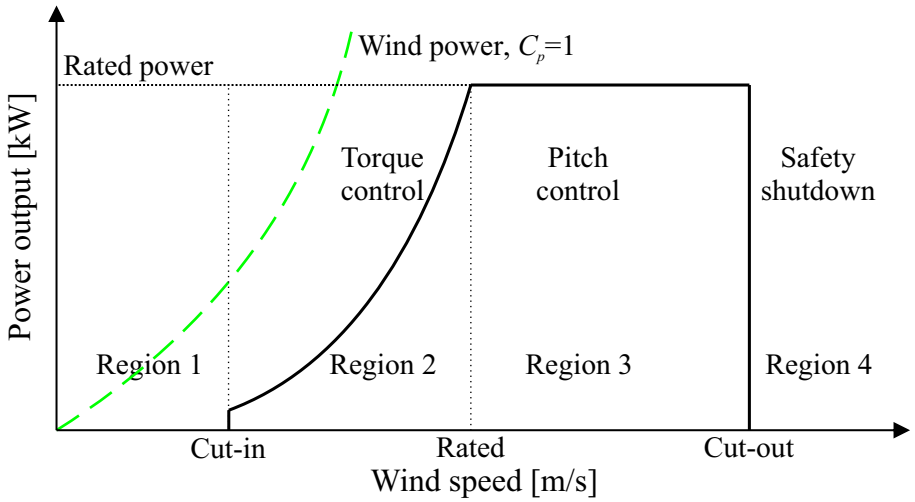

Figure 2.1: Generalized power curve of a variable speed wind turbine (modified from [NS16])

fatigue stress and can lead to premature failure if not controlled. Due to heavy rotational components, commercial WTs are exposed to high inertial forces. The simultaneous action of aeroydynamic, gravitational, gyroscopic, and inertial forces makes it difficult to quantify the contribution of each load to total structural loads experienced by a WT system [Nji16].

Wind experienced by a utility-scale WT generates significant vibrations and dominant design loads, which can lead to fatigue damage and failure [XA20]. Turbulent wind dynamics can cause imbalance of loads with stochastic properties. However, structural loads due to vertical wind shear and tower shadow are considered determistic due to their once per revolution (1P) periodicity. The tower shadow effect is more prominent in downwind WTs. This configuration is unusual in commercial WTs because their rotors face the wind and therefore the contribution of tower shadow to the structural load is neglible. On the other hand, vertical wind shear is the cause of asymmetric loads across the rotor disc. Wind shear is the horizontal change in wind speed with altitude, as illustrated in Fig. 2.2. As shown, intermittent changes in the rotor-effective wind field leads to deflections of the blades, tower and drivetrain in different modes, hence causing structural loads. The tower experiences fore-aft (F-A) and side-side (S-S) deflection modes, while the blades experience flap-wise (F-W) and edge-wise (E-W) deflection modes [Nji16]. Blade damping in the F-W mode is more critical than the E-W direction. However, with low aerodynamic damping in E-W mode, there is still a risk of fatigue damage [XA20]. Torsional stresses in the drive-train result from wind speed fluctuations during power production [CS16]. Due to coupling between different modes, load reduction in several load components should be considered.

Most commercial WTs have a three-bladed configuration with a blade separation of 120^o. Therefore, each blade samples unequal aerodynamic forces at every azimuth position due to vertical wind shear. This causes 1P cyclic loads acting on each blade and subsequent 3P loads on the tower and fixed structure. Gravitational forces due to centrifugal effect also contribute to cyclic loads due to 1P changes in blade stiffness. On the other hand, asymmetric wind inflow causes both variation in aerodynamic damping and blade stiffness [SMBN09; HMHN14]. However, aerodynamic loads due to 1P, 3P,

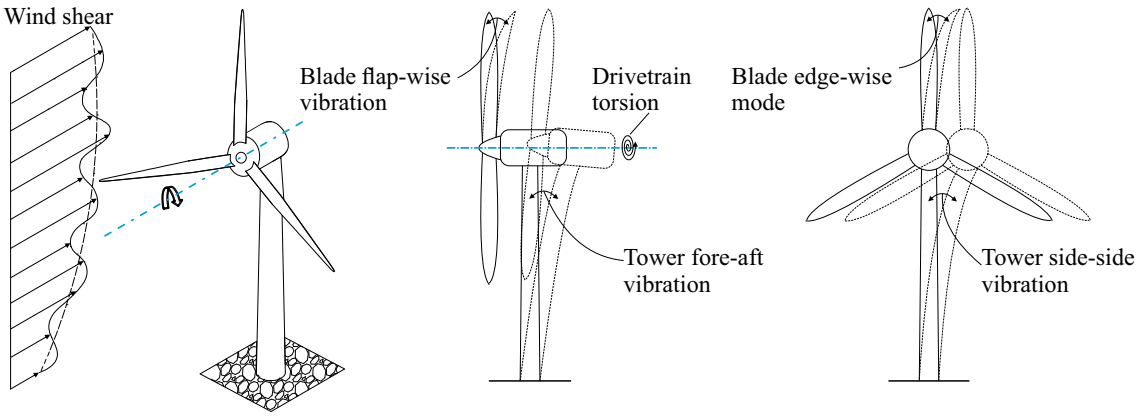

Figure 2.2: Deflection modes in commercial wind turbines (modified from [NS16])

and higher order harmonics contribute the most to the structural loads in WTs. When transmitted to the drivetrain, these loads can potentially excite poorly damped vibration modes, which can damage the gearbox, rotor blades, and other components. In addition, the quality of power delivered to the grid can be effected due to flickers in the system [CS16].

Due to their dominance and proximity to the resonance frequencies of the blades and tower, most advanced controllers are aimed at reducing either 1P loads via IPC [GC08; Par14; WWB17] or 3P loads via CPC [DPAE$^+$12; DS22]. However, in the realm of commercial WTs having highly flexible structures and lowly damped modes that are subjected to high aerodynamic loads [XA20], it is beneficial to develop controllers to reduce loads in the blades and tower components. Drivetrain torsional dampers are typically designed to reduce the large torque that occurs due to heavy loads during operation [DPAE$^+$12; FVS$^+$13]. Harmonics beyond 4P are usually neglected due to bandwith limitation of the blade pitch actuator [GC08; YCT20]. A large bandwidth can potentially excite different modes of the WT with low natural frequencies and damping such as the tower F-A mode [Wri04]. From the foregoing discussion, the importance of structural load mitigation in commercial WTs has been shown. Due to coupling between different modes and other conflicting objectives such as speed regulation and power maximization, development of advanced single-loop MIMO controllers is required to achieve these goals.

Fundamental WT equations are required for mathematical modeling of a nonlinear WT. The amount of power generated by a WT is given by

$$P = \frac{1}{2} A C_p(\lambda, \beta) v^3, \tag{2.1}$$

where ρ denotes the air density, $A = \pi R^2$ the rotor swept area, R the rotor radius, and v the wind speed. The power coefficient C_p is a nonlinear function of blade pitch angle β and tip-speed ratio λ expressed as

$$\lambda = \frac{\omega R}{v}, \tag{2.2}$$

where ω is the rotor speed. For any given v there are optimal values of tip-speed ratio λ_{opt} and pitch angle β_{opt} that yield the maximum power coefficient $C_{p_{max}}$. These parameters can be obtained from experiments or theoretical methods, from which a 3D C_p surface

of a WT is generated [Nji16]. The ideal control objective is to operate the WT at the peak of the C_p curve during operation, with β as the control variable, while λ is controlled indirectly using generator torque control [JPBL06]. Similar parameter surfaces for thrust and torque coefficients, C_t and C_q, respectively can be generated [JPBL06; AZPW22].

From (2.1) and (2.2), aerodynamic rotor power is given by $P = \tau_a \omega$, where τ_a is the aerodynamic torque expressed as

$$\tau_a = \frac{1}{2}\rho R^3 \frac{C_p(\lambda, \beta)}{\lambda} v^2. \tag{2.3}$$

2.1.2 Standard wind turbine control

Wind turbines are complex nonlinear systems that are affected by gravitational, gyroscopic, and stochastic aerodynamic loads. Therefore, the dynamics of WTs are nonlinear, unsteady, and complex, with the fatigue loading caused by turbulent wind inflow [WF08]. To accurately model WTs, several degrees of freedom (DOFs) that capture the most important dynamics should be considered. However, this increases model complexity, which is undesirable for control design. Therefore, a balance between accuracy and complexity is required. Classical control techniques are used in commercial WTs primarily for power maximization in below-rated wind speed regime using standard generator torque control and for speed/power regulation in the above-rated operation using PI-based CPC. Active yaw control is also used to orient the WT to face the wind stream.

A first order model of a WT with rigid rotor assumption is typically used for standard control design [PJ11]. This simple one-mass model is given by

$$\dot{\omega} = \frac{1}{J}(\tau_a - \tau_g), \tag{2.4}$$

where τ_g denotes the generator torque and J the total rotational inertia of the rotor, gearbox, generator, and shafts. In transient condition, the rotor either accelerates or decelerates to maintain λ_{opt} to deliver maximum power. By holding the blades at a fine pitch for maximum aerodynamic efficiency, power can be maximized if the generator torque controller tracks λ_{opt}.

The steady-state condition for (2.4), such that $\dot{\omega} = 0$, provides the basic law for optimal torque control of variable speed WTs operating in region 2 [JPBL06], which is given by

$$\tau_g = K_t \omega^2, \tag{2.5}$$

where the torque control gain K_t is given by

$$K_t = \frac{1}{2}\rho R^5 \frac{C_{p_{max}}}{\lambda_{opt}^3}. \tag{2.6}$$

Therefore, wind speed tracking is achieved by accelerating or decelerating the rotor to follow the λ_{opt} that corresponds to $C_{p_{max}}$. Despite its simplicity, there are no accurate approaches for designing K_t as they are subject to modeling and assumption errors [JFPB05]. This is particularly exacerbated in commercial WTs having highly flexible rotors, because the assumption that R is constant across all wind speeds does not apply. Therefore, a PI-based TSR tracking generator torque controller is becoming an industry

standard [AZPW22]. Furthermore, strict tracking of the incoming wind speed induces high torsional loads to the drivetrain, which can excite lowly damped modes [WF08].

Conventional control for above-rated region is to regulate the turbine's rotor speed and power to their rated values while holding the generator torque or power constant [AZPW22]. Most commercial WTs use a reference-tracking PI-based CPC scheme expressed as

$$\beta(t) = K_p\omega_e(t) + K_i \int_0^t \omega_e(t)d_t, \tag{2.7}$$

where K_p and K_i denote the proportional and integral gains, respectively, $\omega_e = \omega_r - \omega$ the rotor speed error, and ω_r the rated rotor speed. Appropriate values of K_p and K_i are designed for a specific operating point defined by wind speed, rotor speed, and pitch angle to maintain closed-loop stability and achieve good response [WF08]. To compensate for deviations in operating points due to varying wind speeds, a gain-scheduled PI (GSPI) controller should be used [WF08; RD18; AZPW22]. In this case, the K_p and K_i are scheduled as a function of β prescribed using linearization tools [JBMS09; MV18] or the C_p surface [MV18]. In addition, saturation limits and anti-windup are usually added to address issues related to integration of negative speed error, which can result from gusty winds. In this thesis, GSPI controllers described in [RD18; AZPW22] are used as baseline controllers.

The major drawback of PI- and GSPI-based CPC schemes is that all blades are assumed to be subjected to equal aerodynamic loads during operation. This is not the case particularly with commercial WTs that have large rotor dimensions. Therefore, the rotor is subjected to large asymmetric loads, hence inducing stresses that can lead to fatigue failure. For this reason, WT controllers should provide an additional structural load mitigation goal. To reduce loads, individual control loops have been added to the classic CPC generator speed controller. However, coupling between different WT dynamics such as blade F-W and tower F-A modes with the drive-train can result in performance deterioration [GC08]. Therefore, the use of multiple SISO control loops to damp flexible modes or mitigate asymmetric wind loads could interfere with each other and lead to WT instability. The risk of destabilizing a commercial WT is high due to a high degree of coupling between different modes [WF08]. Therefore, advanced MIMO controllers are required to handle this multi-objective control problem.

2.2 Advanced control approaches for wind turbine structural load mitigation

2.2.1 Influence of environmental conditions on structural loading

Information about environmental conditions such as wind, and ocean waves and currents is essential for estimating and monitoring of fatigue loads in WTs [BS16]. However, environmental and operational loads are usually unknown and/or difficult to define, making it difficult to predict the load profile. In contrast to many other control problems, dynamics in WTs are driven by wind speed disturbance. Therefore, in addition to excitation of vibrations in different structural components, wind is one of the main variables for selecting the operating condition of a WT [ØBS07]. Fluctuating wind loads can lead to fatigue failure of WT components, particularly blades and tower. Furthermore, wind loads from extreme events such as hurricanes or tropical cyclones can cause damage because WTs are not operated under extreme loads [XA20]. Wind turbine operation is governed by the

interaction between the incoming wind profile and the rotor blades. Aerodynamic thrust and torque is applied to the rotor shaft due to the aerodynamic design of the blades. The rotor-effective wind speed can be considered as the sum of the average value and stochastic perturbations caused by turbulence and gusts [HHS19]. While turbulence models such as Von Karman and Kaimal have been used to model stochastic terms of wind speed, a low-pass filter can be used to estimate the average term [JBB+21]. The deterministic terms of the wind profile such as the wind shear and tower shadow have analytical expressions that can be integrated into a wind model.

Wind turbines are typically located in harsh environments. Unsteady fluctuations in wind loads are responsible for the relatively high failure-rate of these machines, with typical faults occuring in gearboxes, rotor blades, generators, and power electronics [LLJ19]. In offshore WTs, both aerodynamic and hydrodynamic loads contribute to fatigue loading [XA20]. This can cause fatigue damage if the corresponding structural loads become significant. Therefore, the relationship between the inflow conditions and accumulated damage or fatigue in a structure is important in reducing structural load. Fatigue loads are related to operating parameters of the system. Fatigue testing of components is generally performed under specific laboratory conditions that are not representative of real-world system dynamics. To analyze fatigue in WTs, it is necessary to install additional sensors for mechanical stress analysis. However, this causes uncertainties and increases operation costs.

To reduce the risk of failure, the resultant force on a WT should be estimated. The wind force acting on a WT is generally estimated either through quasi-steady analysis or simulation [XA20]. Fluid dynamics modeling and subsequent load prediction can be used to reduce structural loads and adapt WT operation to predicted environmental conditions. A mix of mathematical, probabilistic, empirical, and statistical models can provide approximate wind and wave dynamics. However,in most cases wind dynamics modeling is based on empirical and long-term measurement data collected from in-service WTs [BGEJ14]. To improve the prediction accuracy, uncertainties related to the model, measurements, environment, human factors, and fluid properties should be taken into account when modeling wind inflow characteristics [QSL+14].

Wind inflow related parameters are considered in [RDT20; NCK21; HYS+22] for fatigue load prediction. In [RDT20], a physics-based load evaluation model is proposed for WT lifetime prediction. The work considers wind inflow effects such as turbulence, surface roughness, side winds, yaw misalignment, rotor tilt, blade cone angle, and blade pitching. It is shown that actual wind speed distribution has a strong correlation to lifetime prediction. Dynamic field data including acceleration and strain measurements influenced by environmental loads from wind and wave action as well as nonlinear soil dynamics are used in [NCK21] for estimation of natural frequencies and damping in offshore WTs with monopile foundations. Based on simulation results, a reduction of first natural frequency and increased damping ratio with increasing load level is observed. However, this effect is found to be smaller than that of field measurements, suggesting that other factors could influence the estimation. In [HYS+22], a machine learning (ML) support vector regression (SVR)-based method is proposed for predicting fatigue loads and power in WTs with yaw misallignment. Input features considered for prediction include different wind speeds, yaw angles, turbulent intensities, and shear exponents. The effect of wind inflow and wake conditions are considered by integrating active yaw control, ensuring the accuracy of the proposed scheme. A statistical method for online estimation of extreme loads in WT

towers is proposed in [YLL+22]. The empirical method based on statistical extrapolation considers both mean and fluctuating moments, resulting thrust force on the rotor, drag forces on the tower and nacelle, and gravitational forces on the nacelle and rotor. The efficacy of the method is assessed through validation using a simulated one-year load. Good accuracy is reported in various wind conditions for both short- and long-term extreme loads.

From the foregoing discussion, it is shown that environmental conditions have a strong influence on fatigue loading of WTs. Therefore, there is need for SHM approaches for fault prognosis of WT systems.

2.2.2 Advanced control approaches

In this section, a review of advanced MIMO control approaches for WTs is presented. A summary of these methods is given in Table 2.1.

Table 2.1: Advanced MIMO control methods applied to wind turbines

Control approach	Reference	Advantages	Limitations
DAC	[WWJ16; WWB17; NARG18; JSY14]	Disturbance rejection	Not robust to uncertainties
Adaptive control	[Fro09; MBF13; YT16; CGP17; NBDS19; LWZQ21; WWYC23]	Adaptable to changing operations	Not robust to uncertainties
H_∞ robust control	[GC08; CPaN+11; DPAE+12; PN20; DABB21]	Robust to uncertainties	Uncertainties are assumed No disturbance rejection
μ-synthesis robust control	[MNP11; Par14; MV15; YCT20]	Uncertainties are modeled	Chattering phenonenon
Nonlinear robust control	[ZTG+19; ANSM19; NMV20]	Robust to uncertainties	No disturbance rejection No load mitigation
Robust adaptive control	[BGMO20; DMR20; FMC21; MT22; RJ22]	Uncertainties are modeled Adaptable to changing operations	No disturbance rejection
H_∞ robust DAC	[DS19; DS22]	Robust to uncertainties Disturbance rejection	Uncertainties are assumed No blade load mitigation

The stochastic nature of wind is considered a disturbance to a WT system. Consequently, its influence on the performance of a WT should be reduced. In [WWJ16; WWB17], IPC-based disturbance accommodating control (DAC) is proposed for regulating rotor speed and reducing asymmetric 1P blade F-W load in above-rated operation. In [NARG18], a CPC-based DAC controller is used to actively damp tower F-A vibrations and regulate rotor speed in the 5 MW National Renewable Energy Laboratory (NREL) RWT. Unlike conventional DAC based on assumed waveform structured disturbances, in [JSY14] a DAC controller is designed considering random process theories that simulate stochastic wind conditions to regulate rotor speed and alleviate fatigue load in WTs in above-rated operation. The proposed controller exhibits improved performance compared with CPC and IPC controllers. Although DAC controllers have been shown to improve performance in wind energy conversion systems by rejecting wind disturbance effects, they are not robust to model uncertainties and nonlinearities. To achieve this, robust control methods should be employed.

Adaptive controllers are designed to be valid across multiple operating points. In [Fro09; MBF13], adaptive CPC controllers are proposed to regulate rotor speed and accommodate wind disturbances. In [CGP17], adaptive control is implemented for power regulation and tracking without prior knowledge of system parameters, wind field, or rotor speed. Asymptotic stability of the power error is demonstrated using Lyapunov method. An adaptive PI controller is proposed in [DDMB19] to address uncertainties in wake center measurements of a light detection and ranging (LIDAR) sensor for improved wake steering in wind farms. Despite improved speed regulation performance in these contributions

[Fro09; MBF13; CGP17; DDMB19], structural load mitigation is not implemented. In [YT16], a model reference adaptive controller is implemented to regulate generator speed and mitigate blade F-W loads in the 5 MW NREL RWT, where a slight increase in power fluctuation is observed. Blade F-W load are reduced in [NBDS19] using a variable gain IPC scheme for WT speed regulation and lifetime extension. In [LWZQ21], a proportional-derivative model-free adaptive control (PD-MFAC) is proposed for independently actuating trailing edge flaps mounted on each rotor blade. Compared with H_∞ and GSPI controllers, the PD-MFAC controller shows improved blade load alleviation. In[WWYC23], a stochastic model predictive controller, which uses an adaptive scenario generation is proposed for active yaw control for an offshore wind farm. The adaptive controller shows improved energy harvesting compared with a baseline predictive controller. The adaptive control schemes in [Fro09; MBF13; YT16; CGP17; NBDS19; LWZQ21; WWYC23] are not robust to modeling errors resulting from model-system mismatch and inherent WT nonlinearities due to operating point changes caused by wind fluctuations.

In recent years robust control methods have attracted increasing interest in WT applications due to their inherent robustness to model uncertainties and system nonlinearities. Independent controllers synthesized using H_∞ optimization are used to realize multi-objective control problems in [GC08; CPaN$^+$11; DPAE$^+$12]. In [GC08], two H_∞ controllers are designed and applied to an analytical model of a WT in above-rated regime. One CPC-based controller regulates generator speed and uses tower F-A acceleration measurement to reduce the first tower axial bending moments, while the other IPC-based controller reduces 1P blade vibrations. In [CPaN$^+$11; DPAE$^+$12], a set of two H_∞ multi-input single-output (MISO) controllers are proposed for controlling of a 5 MW WT in above-rated operation. A H_∞ controller is designed for generator speed control and tower load reduction, while a H_∞ generator torque controller reduces drive-train torsional load. Significant improvements are achieved compared with a baseline PI controller with tower F-A and drive-train torque dampers. In [DABB21], a nonlinear robust controller based on an improved MPPT algorithm is proposed for maximum power extraction in a small scale WT operating in various wind speed regimes. A two-DOF H_∞ controller is proposed in [PN20] for drive-train torsional damping on a 2 MW WT in above-rated operation. Significant robust performance is achieved compared with a GSPI and DAC controllers. Nevertheless, the H_∞ control synthesis procedure yields conservative because plant uncertainties are not modeled.

To obtain a robust controller for a plant with parametric and/or dynamic uncertainties, μ-synthesis approach which extends H_∞ optimization can be employed [MSMD21]. Robust controllers based on μ-synthesis using DK-iteration procedure are proposed in [MNP11; Par14; MV15; YCT20]. In [MNP11], parametric uncertainties in the drive-train are considered in designing a robust controller for better regulation of generated power and rotor speed. However, its influence on the turbine's component loads is not studied. This is also the case in [MV15], whereby the approach is designed only for speed and power regulation of WTs in the presence of model/parametric uncertainties. Robust μ-synthesis approaches based on IPC is proposed in [Par14; YCT20], to reduce periodic blade F-W loads. In both cases, a CPC controller is designed as a separate loop for generator speed regulation. However, overall closed-loop optimality and stability ared not investigated. Although this approach is promising, the effect of wind disturbances is not considered and its impact on load channels that are highly coupled to the blades, such as tower F-A moment, is not investigated.

Nonlinear robust control methods such as sliding mode control (SMC) applied to WTs are investigated in [ZTG+19; ANSM19; NMV20]. Considering that SMC controllers suffer from chattering effect in the control input due to high frequency switching, adaptive methods have been employed to mitigate this phenomena. In [ZTG+19], a CPC-based adaptive robust controller based on high order sliding mode is proposed for regulating rotor speed and reducing platform pitch motion of floating offshore WTs (FOWTs). Although chattering effects are reduced, its effectiveness in structural load mitigation is not studied. In [ANSM19], adaptive output feedback SMC is employed with satisfactory results, to regulate the rotor speed and power on a 5 MW RWT in the presence of uncertainties and actuator faults. A comparative study in [NMV20] focusing on SMC and H_∞ control designed via μ-synthesis concludes that SMC approach provides better tracking and transient performance albeit with slight chattering effect. In general SMC is mainly employed in WT for regulation and tracking problems. However, its effectiveness in handling multi-objective control problems involving load mitigation has not been extensively studied.

In [BGMO20], a robust adaptive controller for torque and pitch control is proposed for optimal rotor speed regulation of WTs operating in below- and above-rated wind speed regions. Switching in the transition region is implemented using wind speed approximated using Gaussian probability distribution functions. In [DMR20], an adaptive robust control design based on an adaptive second-order integral terminal sliding mode speed control is proposed to maximize power extraction in WTs in the presence of model uncertainties and input saturation. An auxiliary dynamic variable is added to the tracking error to compensate for the effect of input saturation. In [FMC21], an adaptive fault tolerant control (FTC) based on SMC and an adaptation law that estimates the upper bounds of uncertainties, is proposed for pitch actuator fault mitigation and power regulation. The proposed approach outperforms a standard SMC. An uncertainty estimator-based dual layer adaptive FTC for the blade pitch system of a WT in the presence of actuator and sensor faults, uncertainties, and disturbances is implemented in [MT22]. Improved performance compared with nonlinear PI and feedback linearized control schemes is reported. In [RJ22], a robust adaptive controller that estimates parametric uncertainties in WTs is proposed for improved robustness and MPPT efficiency. However, in [BGMO20; DMR20; FMC21; MT22; RJ22], structural load migation is not considered.

In [DS19; DS22], a CPC-based robust DAC (RDAC) controller is implemented for generator speed regulation and tower load mitigation. Contrary to the DAC controllers proposed in [WWJ16; WWB17; NARG18], the disturbance observer, state feedback, disturbance rejection gain matrices are synthesized simultaneously, hence ensuring overall system optimality and robustness. Furthermore, compared with the aforementioned robust controllers, integration of a step disturbance model in control synthesis improves the rejection of persistent wind disturbance effects on the controlled outputs. The CPC-based RDAC controller is designed using nonsmooth H_∞ synthesis approach. However, because CPC control is implemented, mitigation of periodic blade loads is not considered. The proposed control method is evaluated on a 1.5 MW RWT, which is not representative of state-of-the-art (SOTA) commercial WTs. Although simulation results show improved disturbance rejection, uncertainties are assumed rather than modeled, hence the resulting controller may not be adequately robust. Therefore, there is a need for an IPC-based robust controller that can reject wind disturbances with improved robustness to model uncertainties having an approximate description, to solve the multi-objective problem of speed regulation and load mitigation in commercial WTs. Collective pitch control can

only reduce structural loading of components in the fixed reference frame, like the tower and drive-train. On the other hand, IPC control relies on multi-blade coordinate (MBC) transformation [Bir10] to transform blade dynamics in the rotating frame to the fixed frame, hence, both symmetric and asymmetric blade loads can be reduced. In this thesis, the RDAC controller is extended for structural load mitigation and speed control in the larger 5 MW NREL RWT. To improve robustness, μ-synthesis approach is used for design. Blade load mitigation is included by designing a IPC-based RDAC controller.

Reference WTs and their respective controllers such as [JBMS09; BZB$^+$13; Mor13] have provided a standardized platform on which researchers can evaluate their control schemes. However, to assess the efficacy of advanced control algorithms, there is a need to benchmark them against SOTA reference WT controllers such as [MV18; AZPW22], that reflect industry-standard control functionalities and are designed to work across different WT platforms to aid the wind energy research community. In this thesis, the SOTA RWT controller [AZPW22] is used to evaluate the performance of developed control methods.

2.3 Structural health monitoring and prognosis of wind turbine systems

Wind turbines usually experience faults or failures due to component degradation through aging or ephemeral events [GL21]. This leads to system downtime and economic losses for wind farm operators. Reduced reliability of components occurs due to change in their material properties with use. Abnormal behaviours of WTs are classified into faults or failures. While a fault is an unacceptable deviation measured parameters from the normal values, which could signal a damage to a system, a failure is a complete loss of functionality of the system [BS16]. When a fault occurs, fault diagnosis is carried out to identify the type, location, criticality, and patterns of faults at an early stage. As part of SHM systems, appropriate maintenance actions are taken to correct detected faults. When an incipient fault in a WT is identified through condition monitoring (CM) or its RUL predicted by a SHM and prognosis system, the decisions to be made include shutdown, reducing loads by derating, or implementing maintenance [LS18]. The maintenance actions taken may include corrective maintenance, which involves restoring the system to its undamaged state, emergency maintenance, which aims to avoid complete failure of components, or predictive maintenance, which relies on predicted future failure based on the current state-of-health (SOH), or reliability of the system to plan maintenance ahead of time [BS16; LS18]. To achieve this, CM of system's health is required.

Integration of CM systems (CMS) in WTs enables advanced techniques such as fault detection and diagnosis (FDD) and lifetime prognosis (LTP) [BZJ$^+$22]. They also enable cost-effective preventive maintenance, called condition-based maintenance (CBM). In CM, a system's operational parameters are continuously monitored to identify significant variations that indicate incipient faults. Therefore, CM of critical components seeks to detect significantly large deviations in SOH from a healthy state and take measures to avoid catastrophic failure. While CMS monitor key parameters including drive-train vibration, oil quality, component or system temperatures, etc., they are usually deployed as add-ons to the WT. However, a supervisory control and data acquisition (SCADA) system is included in every utility-scale WT for performance monitoring [PAD23]. It is employed to collect parameters relevant to the operating characteristics of a WT including wind speed, power, current, voltage, temperature, etc. Due to its low-cost as no additional sensor installation is required, a wide variety of methods employing SCADA data for fault prognosis have

been developed.

Fully- or semi-automatic diagnostic schemes detect and localize potential faults in a WT. This allows optimization of the maintenance procedure, reduces downtime and economic loss, and avoids complete failure [XWY+21]. To improve the reliability of a system, fault diagnosis is usually employed using either hardware or software/analytical redundancy [GCD15]. Hardware redundancies such as sensors and actuators can be implemented in WTs to automatically detect faults based on the residual signatures of collected data. However, this comes at a high price of increased data acquistion complexity, weight, and space requirements. On the other hand, software redundancies that use mathematical models to generate residuals overcome these limitations [HHS19]. Because an analytical model of the system is used, software redundancy is also called model-based fault diagnosis [LLJ19]. By extracting hidden features within SCADA data, the operating state of the WT can be identified and early failures can be detected and predicted [XWY+21].

Prognosis is the process of predicting the progression of a monitored component from undamaged to failed state [GL21]. Using the damage evolution or aging of a component, prognosis attempts to estimate the SOH and predict the RUL of the component before faults ultimately lead to failure. It predicts the progression of SOH from undamaged state of a WT component to when its structural reserves are consumed. Prognostic algorithms use long-term predictions to describe the evolution of a fault indicator, so as to estimate the time-of-failure (TOF), or RUL of a faulty component or system [RJP+20]. To achieve this, a thorough knowledge of the degradation processes, anticipated future loading profiles, and characteristics of all sources of uncertainty is required [JGO+22]. The RUL prediction made at any given time uses a mathematical model of the failure criterion adapted to online measurement data. Therefore, a robust technique should be used to predict an optimal RUL for the component under consideration based on a predefined failure criterion [RKO+21]. Furthermore, uncertainties including unknown future operation conditions and damage process, should be considered in the RUL prediction with associated confidence interval. Based on various fault diagnosis and CM strategies, WT health status can be assessed. Therefore, degradation patterns can be established, allowing for implementation a prognostic scheme for failure prediction [GL21]. By measuring system performance degradation from normal operation, the RUL can be estimated through fault prognosis. Diagnosis and prognosis schemes are usually incorporated in SHM systems. Structural health monitoring and prognosis systems are employed as modules in reliability-oriented control to aid in decision-making about maintenance and replacement of components for lifetime control and extension [BS16]. Fault prognosis techniques are broadly classified into physics/model-based, data-driven, and hybrid approaches [GL21; RKO+21].

2.3.1 Model-based prognosis approaches

Model-based methods are suitable for fault prognosis of WTs in real-world operating conditions. They employ physical or mathematical models of the degradation trend, and leverage knowledge of the system's dynamical behavior, CM data, and damage evaluation models to predict RUL of critical components in real-time [RKO+21]. Model-based approaches are developed assuming that the failure process conforms to a physical law such as fatigue cracking, which obeys the Paris-Erdogan model [THH+20]. The required mathematical models, obtained using theoretical or experimental modeling approaches such as finite element methods and fatigue propagation models, respectively [DTZX18],

are usually developed as degradation models to describe the degraded process for LTP [BZJ+22]. Therefore, WT models obtained either through physical modeling of the degradation process based on mathematically formulated natural laws, or by experimental modeling, where the model is identified from the process measurements using system identification techniques that express the input-output relationship in a mathematical model. Measured monitoring data is used to identify model parameters, which are then used to predict future damage/degradation evolution, hence determining the RUL. The choice of which model to use is problem-specific. The degradation model is a function of loading conditions, elapsed time/cycle, and model parameters. Loading conditions and time are often assumed to be given [KAC17].

Although model-based prognosis approaches require a relatively small amount of observed data to predict the future damage behavior, the measured data must be directly related to the physical model. Furthermore, failure prediction of complex systems without well-defined physics describing the degradation process is challenging [KAC17]. An accurate physical model that describes the damage degradation as a function of time does not exist in practice. In addition, the future usage condition is the most significant source of uncertainty. Imperfections in the degradation model are caused by uncertain future loading/operating conditions, measurement errors and noise from onboard sensors and actuators used to quantify damage growth, and variations associated with the data used in system identification. These cause uncertainty in the estimated model parameters and thus, the predicted RUL [KAC17]. Therefore, to improve the degradation model by taking future uncertainties into account, parameters of the model should be estimated in real-time using Bayesian algorithms such as the overall Bayesian method (BM) and recursive Bayesian (filtering-based) methods such as Kalman filter (KF), extended/uncented KF, and particle filter (PF) [BZJ+22]. It relies on measurement data to reduce the uncertainty of model parameters. It is preferred over other parameter estimation techniques such as nonlinear least squares (NLS) and maximum likelihood estimation methods due to its ability to estimate the uncertainty of identified model parameters. Therefore, most model-based approaches are based on Bayesian inference [KAC17; BZJ+22]. Parameter estimation algorithms form the basis for classification of model-based approaches. For a degradation model that is a nonlinear function of model parameters, the regression process to find unknown parameters is known as NLS. The KF-family and PF are based on the filtering techniques that recursively update the parameters using one measurement data at a time. In contrast to PFs, which have no restrictions on systems and noise types, factors such as initial conditions and variance of the parameter as well as approximation in linearization affect the performance of KF-family [KAC17]. The choice on which filtering method to use is dictated by the dynamics of the system (linear/nonlinear) and the type of noise distribution (Gaussian or non-Gaussian) [SBBB17]. A summary of the model-based prognosis approaches reviewed in this thesis is given in Table 2.2.

Model parameters of the overall Bayesian approach are estimated as a posterior probability density function (PDF), which is proportional to the product of the likelihood of the observed data and the prior probability distribution [CAG+10]. The main challenge of this method is choosing the right options for the sampling process. Markov chain Monte Carlo (MCMC) method is the most effective sampling method [KAC17]. Bayesian inference-based methods are proposed in [DTZX18; HRBA+18; RKO+21] for fatigue life prediction of WT drive-train components. In [DTZX18], an approach which integrates gear physics models and health condition data for RUL prediction of a WT gearbox under

Table 2.2: Examples of existing literature on model-based prognosis of wind turbines [KLS24]

Approach	**BM**	**PF**	**BM+KF**
References	[DTZX18; HRBA$^+$18; RKC$^+$20b; RKO$^+$21]	[FYLW15; SBBB17; VP19]	[THH$^+$20; WLZ$^+$20; JGO$^+$22]
Component	Gearbox	Drivetrain	Bearing
	Bearing	Rotor blades	Rotor blades
Advantages	Have excellent real-time capability due to their online implementation		
	Require a relatively small amount of observed data to predict future damage		
Limitations	Failure prediction of complex systems without well-defined physics of degradation process is challenging		
	Measured data must be directly related to the physical model		

instantaneously varying wind load conditions is developed. The focus of the work is on prognosis of fatigue crack at the root of a spur gear. The uncertain distribution of material parameter in the modified Paris crack propagation model is estimated using a Bayesian inference based on CM data at each inspection interval and the predicted failure time is updated. Improved prediction accuracy is claimed compared to a constant-load method. Prognosis methods for WT bearings are proposed in [HRBA$^+$18; RKC$^+$20b; RKO$^+$21]. Wind turbine bearing failure prediction is proposed in [HRBA$^+$18] by abstracting bearing residual states using a Bayesian inference and Gaussian processes. The model is trained using run-to-failure bearing timeseries, assuming that the feature space is described by a multi-variate Gaussian process. A high failure prediction horizon of approximately a month is achieved for bearing over-temperature. In [RKC$^+$20b], an adaptive Bayesian algorithm for RUL prediction of faulty WT bearings based on extracted features is developed. To improve RUL prediction accuracy, a fusion strategy based on an ordered weighted average operator is used. In [RKO$^+$21], estimation of RUL of WT drivetrain bearings via an adaptive Bayesian algorithm based on failure dynamics and prevailing operating conditions is proposed. The influence of environmental conditions such as ambient temperature and wind speed on bearing failure dynamics is defined by SCADA data and vibration signals. The method provides a higher RUL prediction than a naive Bayesian algorithm.

The Bayesian framework is a probabilistic algorithm for sequential state estimation using Bayes rule, which is suitable for solving the problem of characterizing the posterior PDF of the state vector in dynamical systems [JGO$^+$22]. For a dynamical system which is linear with Gaussian disturbances or smooth nonlinearity, the Bayesian framework problem can be solved using the KF, extended KF or unscented KF. However, in practice state dynamics are usually nonlinear, time-varying, and affected by non-Gausssian disturbances. This requires PFs to compute the sub-optimal solution of the Bayesian framework. Also known as sequential Monte Carlo method, a PF is the most popular model-based technique for prognosis [KAC17]. It has a similar framework to recursive Bayesian update. A PF aims to represent the posterior PDF of the state vector at each time step using a set of random samples and weights called particles/samples [JGO$^+$22]. In fault diagnosis and prognosis, PFs are used for online estimation of states which are unmeasurable or would require costly sensors. State estimation can also be performed for nonlinear processes with non-Gaussian uncertainties [PNJ$^+$12]. If one of the states in the state vector is a SOH indicator, the magnitude of incipient faults can be estimated. Fault isolation can also be realized if different fault modes present in the state vector are estimated [JGO$^+$22]. Uncertainties associated with PF-based fault prognosis may arise from the model, future usage/load profile, and the prognostic algorithm. Approaches for WT drivetrain prognosis using PF are proposed in [FYLW15; SBBB17]. In [FYLW15], RUL prediction of a WT

gearbox is implemented. To validate the approach, measurement data from a SCADA system for a WT gearbox is used. Moreover, the model is verified using real-time data, with results showing the practical value of the approach. A PF-based approach for prognosis of track degradation on a WT high speed shaft (HSS) bearing is proposed in [SBBB17]. Validation results on real drivetrain data show that the method outperforms both SVR and Kalman smoother approaches. In [VP19], PFs are used to estimate the RUL of a fatigue damaged WT blade subjected to turbulence. The PDFs for RUL of WT blades are estimated for different initial crack sizes, while PF is used for predicting fatigue damage evolution by considering nonlinearity and uncertainty in crack propagation.

Approaches based on integrated Bayesian framework and PF are proposed in [THH$^+$20; WLZ$^+$20; JGO$^+$22]. To solve the nonlinear tracking problem, uncented PF (UPF), which combines unscented Kalman transform and PF is used in [VDDW00]. An approach based on improved UPF is developed in [THH$^+$20] for RUL prognosis of WT bearings. Its practicality for field use is attributed to its high dependence on measurement data rather than on parameters of the initital degradation model. The efficacy of the approach is verified using three life-cycle bearings from an on-site WT. A combined diagnosis and prognosis approach for predictive maintenance of WT bearings with limited degradation data is developed in [WLZ$^+$20]. Bearing incipient fault signatures are diagnosed using wavelet transform, and an algorithm is used to represent the bearing defects. This feature and the physics behind this degradation process is modeled in a Bayesian framework. A PF is used for online estimation of model parameter and prediction of RUL with recursive quantification of the uncertainty. Validated results using real WT bearing aging data as in [HRBA$^+$18] demonstrated the significance of the approach compared with a data-driven technique. In [JGO$^+$22], a robust monitoring for online damage diagnosis and prognosis of WT blades is proposed. Identified modal frequencies of the rotor blades are selected as a SOH indicator to quantify the damage level, while features extracted from vibration signals are used to obtain inputs for a Bayesian framework based on PF. The algorithm generates long-term predictions of the SOH to estimate the TOF probability mass function for the monitored blade. However, in contrast to [HRBA$^+$18; WLZ$^+$20], experimental data from fatigue tests is used for validation.

Spatio-temporal variation in wind speed, subjects WTs to varying loads, which lead to fatigue loading of structural components during operation. A number of models have been proposed for lifetime prediction, including fatigue life and progressive damage models, probabilistic damage growth models, and those based on virtual fatigue estimators. To estimate the lifetime from given fatigue stress data, rain-flow counting (RFC) algorithm is used in combination with Palmgren-Miner rule of linear damage accumulation and material-specific fatigue stress amplitude (S) vs. cycles number (N) curve, well known as S-N curve [CCC$^+$19]. The S-N curve defines the allowable fatigue cycles to failure. Fatigue life models calculate the RUL of a WT through extrapolation of fatigue data. Variables describing component deterioration are used in progressive damage models to estimate damage. In [MNG22; MN22], RUL prognosis of offshore WT drivetrains based on digital twin concept is realized. A virtual sensor using a digital twin framework is proposed in [MNG22] for RUL assessment of WT gearbox bearings. The virtual sensor combines data from CMS and SCADA systems, with a physics-based gearbox model. Load estimation is realized using KF, least squares, and quasi-static methods. Accumulated damage obtained from a Palmgren-Miner model is employed as a SOH indicator for RUL assessment. In [MN22], a digital twin consisting of a torsional dynamic model, online measurements, and

fatigue damage model, is used for RUL estimation. The approach is successfully evaluated on a 10 MW WT.

Although nonlinear models accurately represent the WT behavior, most model-based fault diagnosis and prognosis methods have been developed for linear models despite the inconsistency in behavior that exists between the linearized model and the highly nonlinear WT [HHS19]. To increase model accuracy, nonlinear WT modeling frameworks such as linear parameter varying and fuzzy Takagi-Sugeno prototypes, both of which use a set of linear models, have been developed [HHS19]. Several high-fidelity reference WT toolchains such as OpenFAST developed by NREL [NRE21], horizontal axis wind turbine simulation code 2nd generation (HAWC2) developed by the Aeroelastic Design Research Program at Technical University of Denmark (DTU) [LTA07], among others, are used by researchers and WT manufacturers. These have facilitated the development of SHM and prognosis schemes for WTs.

2.3.2 Data-driven prognosis approaches

Also known as knowledge-based fault diagnosis and prognosis, this approach relies on featured data containing system degradation process instead of explicit input-ouput models, and integrates it to a suitable ML technique or statistical model to establish a knowledge-base which represents an explicit dependency of system variables, hence enables prediction of future conditions [DTZX18; LLJ19; JKS19; GL21]. Therefore, the degradation model is based on black-box modeling methods such as NN [BZJ$^+$22]. With the aid of a classifier, a diagnostic decision can be arrived at by comparing the operational behavior of the real WT system with the knowledge-base. The advantage of using data-driven approach for lifetime modeling of WTs lies in its ability to work with insufficient information from process data as well as its scalability and rapid deployment for various industries [JKS19]. Data-driven approaches are widely used in practice because physical degradation models are rare [KAC17]. Wind turbines are instrumented with SCADA systems, whose timeseries signals such as vibration and acoustic measurements are used in fault diagnosis and prognosis.

In the absence of a physical model describing the degradation process, model-based prognosis may not be suitable. However, data-driven prognosis relies on observed data, not necessarily related to the degradation process, to identify patterns and predict future state [KAC17]. Although a physical model is not used, data-driven methods use mathematical models that are unique to the monitored system. While degradation data is required by model-based approaches for parameter estimation, aging data as well as observed data is used to train mathematical models in data-driven methods [KAC17]. Data-driven fault diagnosis and prognosis approaches have a limited ability to learn complex signals with nonlinear characteristics. When used in processing big data, traditional data-driven methods exhibit slow convergence speed and low prediction accuracy [XWY$^+$21]. Athough modern deep-learning methods have accelerated convergence speed and improved prediction accuracy, most do not consider long-term dependencies hidden in sequential/timeseries data [LLJ19].

Historical WT performance data is used in ML to learn the performance dynamics of the WT, estimate the SOH from real-time data, and predict its RUL. Timeseries measurement data is used for fault diagnosis and prognosis of WTs as long-term dependencies hidden in this data is essential for generating classifiable features [LLJ19]. Based on the data extraction process, data-driven fault diagnosis and prognosis can be classified into qualitative

and quantitative approaches. Examples of qualitative approaches include, root-cause and fault tree analysis. Quantitative data-driven methods widely used in prognosis can be classified into statistical or nonstatistical (probabilistic or artificial intelligence) approaches [KAC17; LLJ19]. A summary of the data-driven prognosis methods reviewed in this thesis is given in Table 2.3.

Table 2.3: Examples of existing literature on data-driven prognosis of wind turbines [KLS24]

Approach	**SVM**	**ANN**	**LSTM**	**PSO-ANFIS**
References	[XLZZ19; LZTT20]	[ES19; OGGP21]	[DGS+20; XWY+21; VPCT23]	[AAMO21; GCB+21]
Application	HSS bearing Blade pitch system Power forecasting	Power forecasting Fault prediction	Main bearing Gearbox bearing Generator bearing	Power forecasting Bearing
Advantages	Rely on measured data not necessarily related to the degradation process Ability to work with insufficient information from process data			
Limitations	Require abundant data with many degradation sequences for training Traditional approaches require long training and validation time Most do not consider longterm dependencies hidden in sequential/timeseries data			

Common nonstatistical analysis approaches used for CM and fault diagnosis and prognosis in WTs include neural network (NN) and fuzzy logic (FL). In FL, which is inspired by human reasoning, a feature space is partitioned into fuzzy sets and fuzzy rules are then applied for reasoning. Some of the statistical data-driven methods include principal component analysis (PCA), independent component analysis (ICA), Fisher discriminant analysis (FDA), subspace aided approach (SAP), and support vector machine (SVM). Using dimensionality reduction to preserve crucial trends in the original dataset for successful fault extraction, PCA, ICA, SAP, and FDA are used. On the other hand, SVM, a nonparametric method is used to detect faults in WTs due to its supreme classification capability.

To improve reliability and accuracy of identification, statistical analysis-based methods can be coupled with suitable nonlinear kernels. In [SBBB17], vibration-based prognostic scheme using SVM regression (SVR) combined with spectral kurtosis-derived time domain indices is proposed for prognosis of WT HSS bearings. A novel area under spectral kurtosis is used as a health indicator to determine rolling bearing fault and an SVR model is trained for lifetime prognosis. The proposed method is promising for early failure detection and estimation of degradation trend. Approaches based on SVM are proposed in [XLZZ19; LZTT20]. In [XLZZ19], diagnosis and prediction of faults in a WT pitch system is realized using radar chart and SVM. Indicator data obtained from a SCADA system is used in constructing radar charts which correspond to normal and faulty operations of WT. Features from the radar charts are used for SVM prediction. The proposed method returns a higher accuracy than an SVR model. An SVM is developed in [LZTT20] for short-term forecast of WT power production. To select the optimal parameters for SVM, an improved dragonfly algorithm with an adaptive learning factor and a differential evolution strategy is used. The method shows superior prediction performance compared to a back-propagation NN and a Gaussian process regression (GPR).

Intelligent diagnosis involves feature extraction and fault classification. To classify faults, traditional methods such as SVM rely on suitable preselected features. On the other hand, modern deep learning algorithms such as multi-layer perceptron (MLP), convolutional NN (CNN), and recurrent NN (RNN) rely on hierarchical architectures with multiple nonlinear layers to obtain generalizable features from large scale training data [LLJ19].

Neural networks are the most common algorithms used for prognosis [KAC17]. Artificial neural networks (ANNs) are proposed in [ES19; OGGP21]. In [ES19], an ANN is trained for fault prediction in WTs using a novel training algorithm called Antrain ANN. In [OGGP21], wind power prediction with a 24-hour horizon is proposed using ANN and physics models, and a hybrid of both. The dataset used for training included two-year hourly measurements from a wind farm. A comparison of the prediction accuracy of the models used showed the superiority of ANN over the physics model, while the hybrid model had the best overall performance.

To capture long-term dependencies hidden in timeseries data, long short-term memory (LSTM) model based on RNN uses recurrent behavior and gates systems to learn features directly from multivariate timeseries signals. This can be combined with other ML methods to discover longer patterns leading to improved fault diagnosis and prognosis. In addition to a hidden state vector used in RNNs, LSTM includes a memory cell consisting of three gates, including the input, output and forget gates. It encodes the memory of observed information. In [DGS$^+$20; XWY$^+$21; VPCT23], approaches using LSTM and SCADA data for WT prognosis are proposed. In [DGS$^+$20], an LSTM network is used to predict WT gearbox bearing failures caused by axial cracking based on one month of timeseries data. However, the optimal time window for onset of failures could not be determined. In [XWY$^+$21], a method combining CNN and LSTM is proposed for fault detection and prediction of WT gearbox and generator bearings using SCADA data analysis. The CNN cascades to LSTM based on an attention mechanism (AM). The AM is used to enhance important information by assigning different weights to LSTM to improve its learning accuracy through mapping weight and parameter learning. Predictive maintenance of WT main bearings using LSTM and SCADA variables of rotor speed, generated power, and temperature is proposed in [VPCT23]. Target failure can be detected up to four months in advance, giving operators sufficient time to make informed maintenance decisions.

When measured data is stochastic in nature, it is challenging to establish the link between RUL and the degradation indicator due to uncertainties from operating conditions and existence of multiple fault mechanisms. In this case, probabilistic methods are used to make predictions about future failures. Probabilistic approaches that have been used for multi-state degradation include Markov Model, Weiner process, Bayesian network, and proportional hazard model [CSL$^+$18]. A Bayesian network consists of nodes that correspond to random variables. The nodes are interconnected using conditional dependencies and can take distinct states. On the other hand, Markov models are used to estimate probabilities of future failures. This is achieved by finding the probabilities of each state as well as those associated with state transitions. Future states only depend on prior states [RKC$^+$20a]. Given that WT components exhibit multi-state degradation due to varied operating conditions, aging, and other factors, probabilistic prognosis methods can be used for accurate prediction of RUL.

To overcome the limitations of each ML method and leverage individual advantages, data-driven prognosis methods can be merged to complement each other. An example of this is the adaptive neuro-fuzzy inference system (ANFIS), which takes advantage of the NN's extensive expert knowledge of system behavior available in datasets and required by FL systems. Due to the black-box data processing structure in NN, back-tracking of output is difficult, resulting in slow convergence. Due to their accuracy, reduced computational time, and robustness in searching for global optimal values of model parameters, hybrid ANFIS approaches optimized using particle swarm optimization (PSO) are proposed in

[AAMO21; GCB+21]. In [AAMO21], very short-term power output forecasting is realized using two hybrid models of ANFIS, including PSO and generatic algorithm (GA), with PSO-ANFIS returning a higher forecast accuracy. In [GCB+21], a PSO-ANFIS approach is proposed for modeling nonlinear degradation of extracted features to predict the RUL of a WT bearing using a vibration signal.

2.3.3 Hybrid prognosis approaches

By combining the aforementioned approaches for fault diagnosis and prognosis, hybrid techniques capitalize on the advantages of different methods while counteracting their individual limitations. Although model-based approaches require complex predefined physics or analytical models, they have excellent real-time capability due to their online implementation. In addition, model-based methods make use of fault information from measured data and empirical knowledge for reliable fault prognosis [PHCW20]. From an economics perspective relative to wind farms aiming at cost reduction, it is not practical to install sensors in every component that needs to be monitored. Therefore relying on available SCADA measurements instead of CMS for fault prognosis is a cost-effective solution [PAD23]. Data-driven methods rely on past operational data, usually acquired using SCADA and ML algorithms to build a knowledge-base used for CM and prediction of future degradation patterns. However, they require abundant historical lifecycle data of many degradation sequencies from similar sensors/actuators to train the model [WLZ+20; RKC+20b]. In practice, most WTs have only limited degradation data available, which is not only costly and but also time-consuming to acquire. The degradation patterns are also nonstationary due to different failure modes and operating conditions [HRBA+18]. Data quality also affects the prediction accuracy of data-driven models [PHCW20]. Furthermore, the training and validation process required for data-driven algorithms is time-consuming [GL21].

In recent years, hybrid approaches for fault diagnosis and prognosis in WTs have been proposed. These techniques have good prediction performance because they accurately model of uncertainty. However, hybrid prognosis algorithms can be extremely sophisticated and are constrained by the requirement for physical modeling of degradation events [BMS23]. Therefore, for successful implementation of a hybrid model, the physical degradation model should be reliable and sufficient historical degradation data should be available. A summary of the hybrid prognosis approaches reviewed in this thesis is given in Table 2.4.

Table 2.4: Examples of existing literature on hybrid prognosis of wind turbines [KLS24]

Approach	**Physics-informed RNN**	**DBN+PF**	**ANFIS-PF**
References	[YV20]	[PHCW20]	[CQQ18; CQQH19]
Component	Main bearing	Gearbox	Gearbox Generator
Advantages	Capitalize on the advantages of different methods while counteracting their individual limitations Good prediction performance because they enable accurate modeling of uncertainty		
Limitation	Algorithms are extremely sophisticated and constrained by the requirement for physical modeling of degradation		

Hybrid physics-informed NN models are proposed in [YV20; PHCW20] for prognosis in WTs. In [YV20], the fatigue life of WT main bearing, which is typically influenced by lubricant condition, is modeled by incorporating RNN into a lubricant degradation model. The approach gives accurate fatigue life prediction of WT main bearings. In [PHCW20], RUL prediction of WT gearbox is realized using a hybrid approach based on deep belief

network (DBN) and improved PF. The DBN is used to denoise and merge vibrations to obtain the SOH indicator, while the PF is used for RUL prediction. A Wiener model is used to characterize the randomness of WT gearbox degradation operation, hence improving RUL prediction efficiency. To validate the effectiveness of the approach, simulated and experimental vibration signals from a WT gearbox are used.

Bearing failure is the main cause of WT gearbox failures. Therefore, accurate prediction of RUL for gearboxes is critical for preventive maintenance. A WT drivetrain gearbox is a complex multi-component system, usually operating under varying load conditions. This makes it hard to obtain an accurate physical degradation model, especially for gearbox bearings. To solve this problem, approaches based on ANFIS-PF are developed in [CQQ18; CQQH19]. In [CQQ18], analysis of one phase stator current of a generator connected to a gearbox is used for prognosis and RUL prediction of WT gearboxes. The approach is realized using ANFIS for learning the fault feature state transition, and a PF algorithm is used to continuously predict the RUL based on the learned state transition and the new fault feature. To enhance the prediction performance of PFs by eliminating particle impoverishment in the resampling procedure due to low particle density, a particle modification method and improved multinomial resampling is proposed in [CQQH19]. On the other hand, an ANFIS is used to learn the state transition function in the fault degradation model using the SOH indicator obtained from monitoring data. The approach was evaluated on a doubly-fed induction generator (DFIG) of a 2.5 MW WT.

Wind turbines are designed to operate for decades. However, there is insufficient data at the beginning of their operational life. Therefore, databases do not cover the useful features needed for successful fault prognosis using data-driven methods because collected data charaterizes only normal system operation. To solve this, physical models can be used to generate useful features covering both normal and faulty operation [DBS18]. Therefore, hybrid models are suitable for fault prognosis of a WT over its entire life.

2.4 Application of structural health monitoring and prognosis in lifetime control of wind turbines

Commercial WTs are less tolerant to performance degradation and unplanned downtime. The SOTA in lifetime control and extension strategies for these systems is the use of resilient or FTC [ARTV16; ANSM19; EE20; JY20] to minimize the impact of unanticipated faults or unexpected dynamics by maintaining the operation of a WT under a tolerated performance degradation. However, FTC control is reactive as it relies only on detected faults and does not address the problem of controlling life consumption in WT components to avoid fatigue failures while ensuring other control objectives such as power maximization are achieved. Therefore, to compensate for faulty components, the WT is operated with restricted power output until repairs are made and normal operation is restored. This is undesirable considering a 20-year lifespan of a WT.

From the foregoing discussion in section 2.3, it has been shown that SHM and prognosis approaches are useful in establishing the SOH and predicting RUL of WTs. In recent years, integration of SHM and prognosis in control of WTs has attracted attention in the research community. Performance and reliability of any given system is affected by its SOH. Therefore, prognosis of SOH or RUL of WTs is useful in developing health-oriented control strategies for optimal performance. This concept of continuously optimizing the control strategy based on the SOH was first introduced by [SR97]. In the realm of WTs,

the main trade-off is related to lifetime extension and power maximization.

Within a wind farm, WTs impact each on power generation and structural loads through their wakes. Therefore, control strategies for mitigating wake effects are required. In [KSE18; VPPK19] approaches for lifetime control of wind farms are proposed. The benefits of active wake control for lifetime power production and fatigue loading in real commercial wind farms is extensively studied in [KSE18]. Active power control is employed in [VPPK19], to extend the service life of highly loaded WTs in a waked wind farm. The power reference signal of the entire wind farm is taken into account and fatigue loads in WTs are alleviated. Optimization of the control problem is based on a data-driven fatigue load model such that the lifetime tower F-A loads of the WTs operating within the wind farm are balanced. In [CCC+19], an approach based on a SMC controller for online fatigue life alleviation in WTs is developed. An online fatigue estimator is employed as a virtual sensor of fatigue damage, which is fed to the controller to reduce fatigue of WT components. The approach is validated on the 5 MW NREL RWT.

In [PSSC18; NBDS19], approaches for lifetime extension of WTs using IPC-based MIMO controllers are proposed. In [PSSC18], the trade-off between blade F-W load mitigation and pitch actuation for extending the lifetime of a 10 MW RWT is investigated. In [NBDS19], a WT lifetime extension scheme incorporating an online RFC damage evaluation model and a IPC-based MIMO controller is developed. Based on the accumulated damage the controller is continuously adapted to trade-off between power production and tower F-A load mitigation to extend the service life. In [DS20], an adaptive lifetime controller is proposed to achieve the desired lifetime of the tower. Depending on the damage accumulation and the predicted lifetime provided by an online damage evaluation model, the weights of the lifetime controller are varied. A health-oriented strategy for power control of a WT drive-drive to maximize its economic return over its entire lifecycle is proposed in [CWLW22]. A model-based approach is employed for RUL prediction of the WT's power converter. A receding horizon model predictive control is employed for extending the converter fatigue life.

Although hybrid SHM and prognosis approaches are widely used in SOH and RUL prediction of WTs, little has been reported on their application for lifetime control of WTs. Modern utility-scale WTs are instrumented with high frequency (1 Hz) SCADA systems [LL20]. Additionally, model-based high fidelity toolchains have been developed to simulate the different dynamics of commercial WTs. Therefore, by taking advantage of abundant data generated by modern SCADA systems and combining this with the model-based methods based on the digital twin concept, hybrid prognosis approaches can be developed for improved lifetime control and extension of WTs.

2.5 Open research gaps

From the foregoing review of advanced control methods for WT structural load reduction as well as application of SHM and prognosis approaches for lifetime control and extension of WTs, the following research gaps which are addressed in this thesis have been identified:

1. Wind inflow is known to have a strong influence on WT fatigue loads due to its stochastic dynamics. Therefore, it is treated as a disturbance to the WT system. Commercial WTs are especially succeptible to aerodynamic load due to their large, slender, and heavy structural components. In addition to addressing other control

objectives such as power maximization and speed regulation, advanced MIMO controllers incorporating disturbance models have been used for structural load mitigation of WTs. However, these controllers are not adaptable to fluctuating operating points due to changing wind dynamics.

2. To evaluate the performance of advanced control schemes for WTs, researchers typically test them on RWTs, which are available in high fidelity open-source softwares. However, most promising control approaches have been evaluated on small RWTs, which do not reflect the industry SOTA in terms of both physical size and power rating of commercial WTs. Therefore, practicality of these controllers cannot not guaranteed.

3. To enable researchers evaluate there control schemes across different RWT platforms, SOTA RWT controllers that mirror capabilities of industry controllers have been developed. Therefore, representative dynamic simulations performed using these controllers provide trustworthy results for benchmarking developed controllers. However, because these RWT controllers are relatively new, they have not been widely used to evaluate the efficacy of new control schemes.

4. Uncertainties in WTs arise from modeling errors and nonlinearities. While nonlinearities are associated with changing wind dynamics, modeling uncertainties result from the use of linear or reduced-order models for control design. Although most robust controllers are known to handle these uncertainties, they are only developed for design situations, hence provide conservative robust performance. By using robust control methods that incorporate model uncertainty descriptions to the nominal models used for design, robust performance can be improved.

5. With the ever increasing size of WTs, coupling between different dynamics is exacerbated. Therefore, structural load mitigation in multiple load components, particularly the main ones such as rotor blades and tower, should be considered. To realize this goal, advanced MIMO controllers based on IPC need to be developed. However, most advanced WT control schemes realize structural load mitigation on a single component, mostly the tower or blades based on CPC or IPC, respectively. The few control schemes developed for load mitigation in multiple WT components have achieved this using separate control loops, which do not consider overall system optimality.

6. Most prognosis approaches for lifetime control and extension of WTs are based on fault-tolerant control, where the WT is operated at reduced power output in case of faults. Therefore, these controllers are reactive and do not use the full benefits of SOTA SHM prognosis methods to continuously adapt the control setpoint and actively miminize fatigue loads in WT components over their lifetime.

7. Prognosis-based lifetime control and extension of WTs has been achieved using model-based or data-driven prognosis approaches. With modern commercial WTs instrumented with high frequency (1 Hz) SCADA systems, sufficient data is generated for developing data-driven prognosis models. On the other hand, the current high fidelity softwares for simulating several dynamics of commercial WTs can be used for developing model-based prognosis models for SOH and RUL prediction. However,

while hybrid methods take advantage of the benefits of individual approaches while compensating for its limitations, little has been reported on the use of hybrid prognosis methods for lifetime control of WTs.

3 Wind Turbine Model and Baseline Controllers

A brief overview of the Wind Partnership for Advanced Component Technologies (WindPACT) 1.5 MW and 5 MW National Renewable Energy Laboratory (NREL) reference wind turbines (RWTs) used for controller design and closed-loop response evaluation of the proposed control schemes are given. In addition, a brief description of the baseline gain-scheduled proportional integral (GSPI)-based standard controller and reference open-source controller (ROSCO) used to evaluate the performance of the control schemes developed in this thesis is given.

The figures, tables, and content in this chapter are based on the accepted/published journal papers [KS24; KDNS24] and conference proceedings [KDNS22; KBS23].

3.1 Wind turbine models

In the recent past, several RWTs reflecting current and future trends in the wind industry have been developed to investigate technologies for enhancing the performance of the next generation of turbines [RGZ+20]. In this section, a brief description of the two RWTs used for the design and simulation of the proposed control schemes is given.

3.1.1 WindPACT 1.5 MW reference wind turbine

The WindPACT 1.5 MW RWT developed by NREL [RD18], which is included in fatigue, aerodynamics, structures, and turbulence (FAST) design code [JB05] is selected as a test-bed for the design and simulation of some of the proposed control strategies. The WindPACT 1.5 MW RWT was designed to closely represent actual commercial WT technology. It was used extensively in the WindPACT program for studies of novel configurations and innovations of WT technology. It serves as a research tool for testing control schemes [RD18]. Here, a brief introduction and description of this RWT is given. A detailed description can be found in [JB05; RD18]. This onshore WT model, whose specifications are summarized in Table 3.1, was developed based on a real commercial WT used in the WindPACT program. It is a 3-bladed, upwind horizontal axis WT, having 16 degrees of freedom (DOFs) describing its flexibility. However, a few DOFs are enabled to obtain reduced-order linear time invariant (LTI) models used for controller design.

3.1.2 5 MW NREL reference wind turbine

The land-based 5 MW NREL RWT [JBMS09], which is domicile in the high fidelity open-source FAST (OpenFAST) software [NRE21], is used for the design and evaluation of the closed-loop coupled dynamic response of some of the proposed control schemes. In Table 3.2, a summary of the specifications of the 3-bladed, upwind RWT is provided. The 5 MW

Table 3.1: WindPACT 1.5 MW reference wind turbine specifications [RD18]

Parameter	Value	Unit
Rated power	1.5	MW
Hub height	84.288	m
Cut-in, Rated, Cut-out wind speed	4, 12, 25	m/s
Rated rotor speed	20.463	rpm
Gearbox ratio	87.965	-
Blade radius	35	m
Blade pitch range	0-90	$^\circ$
Pitch rate	10	$^\circ$/s
Optimal pitch angle (β_{opt})	2.6	$^\circ$
Optimal tip-speed ratio (λ_{opt})	7.0	-
Maximum power coefficient ($C_{p_{max}}$)	0.5	-

RWT model has 16 DOFs describing the blades, tower, drive-train, generator, and nacelle motions. However, a few DOFs are enabled to capture the most important dynamics corresponding to the desired closed-loop performance in terms of structural load mitigation and generator speed regulation. The enabled DOFs include first tower fore-aft and blade flap-wise bending modes, drive-train rotational flexibility, and generator motion.

Table 3.2: 5 MW NREL reference wind turbine specifications [JBMS09]

Parameter	Value	Unit
Rated power	5	MW
Hub height	90	m
Cut-in, Rated, Cut-out wind speed	3, 11.4, 25	m/s
Cut-in, Rated rotor speed	6.9, 12.1	rpm
Gearbox ratio	90	-
Rotor, Hub radius	63,1.5	m
Blade pitch range	0-90	$^\circ$
Pitch rate	8	$^\circ$/s
Optimal pitch angle (β_{opt})	0	$^\circ$
Optimal tip-speed ratio (λ_{opt})	7.55	-
Maximum power coefficient ($C_{p_{max}}$)	0.482	-

The nonlinear dynamics of the RWTs modeled in both the FAST [JB05] and OpenFAST [NRE21] softwares can be described using the generalized equation of motion expressed as

$$M(q,u,t)\ddot{q} + f(q,\dot{q},u,u_d,t) = 0, \tag{3.1}$$

where M denotes the mass matrix containing inertia and mass components, f the nonlinear function of the enabled DOFs q and their first derivative $\dot{q}$ as well as the control input u, wind disturbance u_d, and time t. The nonlinear model (3.1) is linearized about an operating point in above-rated WT operation. By enabling the DOFs that capture the key WT dynamics of interest and specifying the operating point defined by a constant wind speed, blade pitch angle, and rotor speed, linearization is performed numerically in FAST and OpenFAST softwares. Linearization takes place in two steps. First, a periodic steady-state

operating point for the enabled DOFs is computed. Secondly, the nonlinear model is numerically linearized around this operating point to form periodic state space matrices that depend on the defined azimuth positions around the rotor disc. These periodic models are then azimuth-averaged to obtain a nonperiodic or LTI model that is used for controller design. The above algorithm is known as *simsetup.m* and is implemented numerically in the softwares developed by NREL [JB05].

3.2 Baseline controllers

In this thesis, two baseline controllers developed by NREL are used to evaluate the performance improvement of the proposed control shemes. These include a standard GSPI controller [RD18] and the newly developed modularized ROSCO controller [AZPW22]. These controllers are briefly described for principal understanding.

3.2.1 Standard GSPI controller

A standard GSPI controller designed by NREL based on the guidelines in [WF08; RD18] is used as a reference baseline controller for the control schemes designed and simulated on the WindPACT 1.5 MW RWT. The GSPI controller is designed to regulate rotor speed to its rated value ω_r in above-rated operation. Therefore, it relies solely on rotor speed measurement to realize CPC control. In Figure 3.1, the implementation of this controller is illustrated. In region 3, generator torque is held constant at its rated value τ_{rated}. The PI gains K_p and K_i are scheduled with respect to β by multiplying each of the gains by a function GS. The operational point is defined by the actual blade pitch angle β. The scheduling coefficients of GS for the WindPACT 1.5 MW RWT are defined as follows

$$GS(\beta) = \begin{cases} 1 & \beta < 0.0454 \\ 0.213\beta^{-0.5} & 0.0454 \leq \beta \leq 0.5236, \\ 0.2944 & \beta > 0.5236 \end{cases} \tag{3.2}$$

here β is in radians [RD18]. By implementing GSPI control, the dynamic response of the WT is significantly improved across the entire above-rated wind speed operation range. However, uncertainties associated with nonlinearities and modeling errors are not considered, hence less robust performance is expected. Reduction of structural loads is critical for commercial WTs operating in above-rated wind speed regime. However, load reduction is not considered in the standard GSPI controller.

3.2.2 Reference open-source controller

In tandem with the evolution of WT models over the last decades, there has been a growing need in the wind industry for baseline RWT controllers that can be used on various RWT platforms. The modularized ROSCO controller [AZPW22] was developed by NREL to be adaptable across different RWTs platforms, including the 5 MW NREL RWT [JBMS09]. Its performance is comparable to existing baseline control platforms such as the 5 MW NREL [RD18] and Technical University of Denmark (DTU) 10 MW [MV18] controllers. A block diagram of the modularized controller framework in ROSCO is shown in Fig. 3.2. Generator torque τ_g and collective blade pitch β controllers are implemented for below

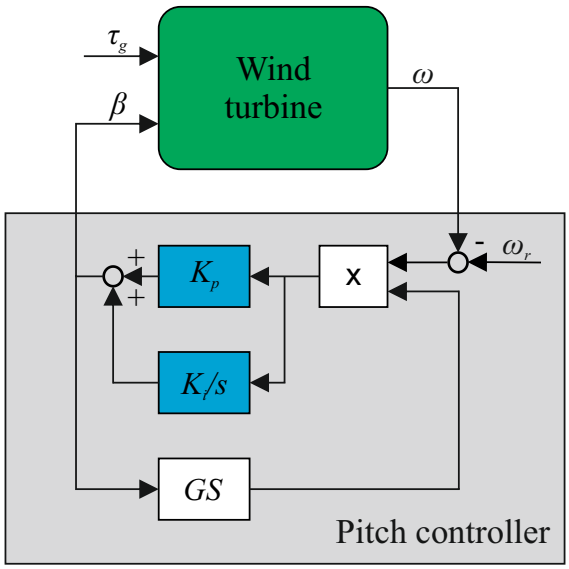

Figure 3.1: Standard GSPI controller for region 3

and above-rated operations, respectively. This controller has additional control features that reflect current trends in industry controllers. These include, tip-speed ratio (TSR) tracking generator torque control, which is suitable for modern WTs having larger and highly flexible blades, a pitch saturation module that sets the minimum blade pitch angle $\beta_{\min}$ to limit rotor thrusts near rated wind speed and to maximize power in the presence of rotor speed constraints at low wind speeds, and a setpoint smoother that uses a shifting term $\Delta\omega$ to avoid unwanted pitch and torque control interactions near rated operation. A wind speed estimator is used to realize TSR tracking generator torque control and pitch saturation by using a wind speed estimate v. Tower-top pitch angle measurement ϕ is fed to the floating feedback module for platform stabilization in floating offshore WTs (FOWTs) via an additional pitch angle β_{float}. Low-pass filters (LPFs) are used to filter out unwanted frequencies in the outputs. For brevity, only relevant control features implemented for above-rated WT operation are described. Further details can be found in [AZPW22].

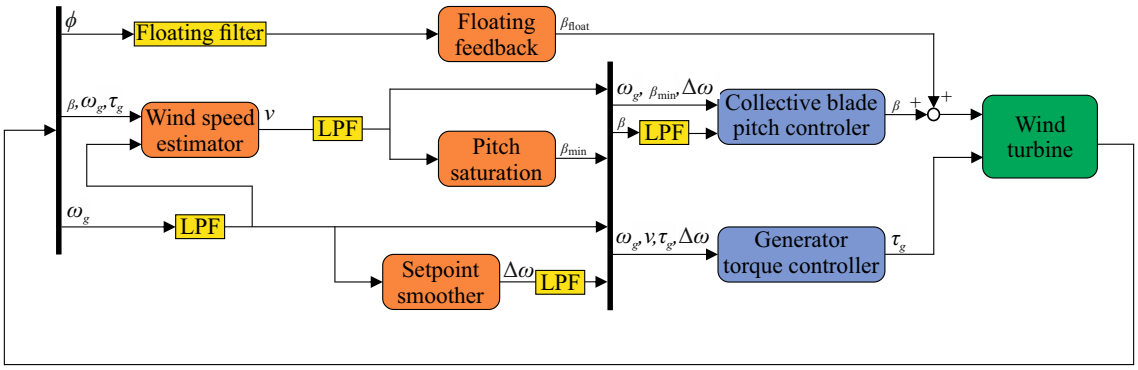

Figure 3.2: Block diagram of the general controller logic in ROSCO (modified from [AZPW22])

To improve speed regulation performance in above-rated operation, a GSPI controller

is implemented in ROSCO with the assumption of constant τ_g. For steady-state condition in above-rated operation TSR is only a function v (2.2), hence an optimal pitch angle which depends on prevailing wind speed $\beta_{opt}(v)$ can be defined. Therefore, scheduling of PI gains is realized using $\beta_{opt}(v)$ values obtained from a C_p curve of the 5 MW NREL RWT. This is slightly different from the 5 MW NREL reference controller which uses the linear relationship between pitch sensitivity and rotor collective pitch angle to implement gain-scheduling [JBMS09]. While generator torque in the 5 MW NREL RWT is kept constant in above-rated wind speed region, in ROSCO, a set-point smoothing algorithm is used to shift the reference generator speed to achieve either constant torque (3.3), where output varies proportionally to changes in generator speed or constant power (3.4), where slight and consistent changes in output power occur.

$$\tau_{g,ar} = \frac{P_{rated}}{\omega_{g,rated}}, \tag{3.3}$$

$$\tau_{g,ar} = \frac{P_{rated}}{\omega_g(t)}. \tag{3.4}$$

Here, $\tau_{g,ar}$ denotes the above-rated generator torque, P_{rated} the rated power, and $\omega_{g,rated}$ the rated generator speed.

Although GSPI control improves generator speed regulation over the entire range of above-rated operation, modeling errors and system nonlinearities associated with wind disturbance are not considered in ROSCO. Therefore, performance is expected to be less robust as operating conditions change. In addition, load mitigation is not considered in ROSCO. To address these limitations, robust multi-objective control schemes are developed.

4 Robust Disturbance Accommodating Control Methods For Wind Turbine Load Mitigation and Speed Regulation

The figures, tables, and content in this chapter are based on the accepted/published journal papers [KDNS24; KS24] and conference proceedings [KDNS22; KBS23].

With increasing demand for energy from renewables, wind energy has grown rapidly due to its high capacity factor compared to other renewables [GL21]. To generate more energy from wind, the physical size and nominal power of wind turbines (WTs) have gradually increased over the past decades [Mar23]. Therefore, modern commercial WTs have larger, slender, and highly flexible rotor blades and towers. Coupled with stochastic wind inflow conditions, this has exacerbated fatigue loading of these structural components, which in turn impacts reliability and increases operation and maintenance (O&M) cost of WTs. Control strategies for WTs have been developed to reduce structural loads and also address other objectives. Commercial WTs are multi-input multi-output (MIMO) systems with several sensors and actuators. This enables implementation of multiple control objectives including, load mitigation, power optimization, and lifetime control. However, due to hardware limitations, most industry controllers still rely on classical single-input singel-outpout (SISO) control approaches such as proportional integral (PI) control [AZPW22], which are less effective in solving the multi-objective control problem in modern WTs [Nji16]. For this reason, MIMO controllers are used to solve this problem, which requires a balance between conflicting control goals. However, achieving an optimal compromise is still a challenging and open problem.

Wind variability is considered a disturbance to a WT system. Therefore, disturbance accommodating control (DAC) approaches are used to suppress these disturbances using suitable disturbance models [WWJ16; WWB17; NARG18]. However, these controllers are designed based on linear models and are not robust against uncertainties due to modeling errors and WT nonlinearities caused by wind variability.. Adaptive controllers are designed to be valid across multiple operating points. In [YT16; NBDS19; LL20; WWYC23], adaptive controllers are developed for load mitigation in commercial WTs. However, similar to DAC, adaptive controllers are not robust to uncertainties. Due to their robustness against uncertainties, robust control methods have been widely applied to WTs. Robust control approaches designed based on H_∞ optimization are applied for structural load mitigation in [GC08; DPAE$^+$12; PN20]. However H_∞ synthesis yields conservative robustness because plant uncertainties are not modeled. Parametric and/or dynamic uncertainties are included in the μ-synthesis approach. Robust μ-synthesis approaches are proposed in [MNP11; Par14; YCT20] to reduce WT structural loads. However, rejection of wind disturbances is not considered. Nonlinear robust approaches have also found application in WTs. An example is sliding mode control (SMC) which is generally only used for speed control or platform stabilization in WTs [ZTG$^+$19; ANSM19; NMV20].

Chattering phenomenon in the control input due to high frequency switching is still an open problem in SMC. Robust adaptive control has also been applied to WT control mainly for speed/power regulation [BGMO20; FMC21] or to maximize power extraction [DMR20; RJ22]. Limited work is reported on its application for load reduction.

An approach based on robust H_∞ control and DAC concepts is proposed in [DS19; DS22]. A CPC-based robust DAC (RDAC) controller is used to regulate rotor speed and reduce tower load. In this approach, the disturbance observer, state feedback, disturbance rejection gain matrices are synthesized simultaneously to ensure optimality and robustness of the overall system. However, because the approach is based on CPC control, mitigation of periodic blade loads is not considered. Because H_∞ synthesis is used for optimization, model uncertainties are assumed rather than modeled, hence the proposed approach has conservative robustness. Furthermore, the control method is evaluated on a small 1.5 MW reference WT (RWT), which does not reflect the current trend in modern commercial WTs. In this thesis, the RDAC control approach [DS19; DS22] is extended to a larger 5 MW RWT for structural load mitigation and generator speed regulation. Independent pitch control (IPC) based on multi-blade coordinate (MBC) transformation [Bir10] is integrated into the design procedure for load reduction in the rotor blades. The μ-synthesis approach is used to design the RDAC controller by incorporating a description of model uncertainties. Performance of the proposed RDAC approaches is assessed against the latest baseline RWT controller [AZPW22], which mirrors industry-standard control functionalities and is designed for use on various WT platforms. Finally, the proposed control approaches are applied for WT lifetime control.

In this chapter, RDAC controllers developed for structural load reduction and speed regulation of WTs in above-rated WT operation are presented. These controllers are evaluated on the WindPACT 1.5 MW and 5 MW National Renewable Energy Laboratory (NREL) RWTs described in section 3.1. The baseline gain-scheduled PI (GSPI) controllers outlined in section 3.2, are used to evaluate the efficacy of proposed control methods. Furthermore, the approaches are evaluated against each other to determine performance improvements, limitations, and practical recommendations.

4.1 Extended H_∞ RDAC using adaptive IPC

In this section, an adaptive robust observer-based control strategy for structural load reduction and rotor speed regulation in commercial WTs operating in high wind speed regime is described. First, a previously proposed H_∞ robust disturbance accommodating controller (RDAC) [DS22] is discussed. This controller is extended with an adaptive independent pitch controller (aIPC), which adapts to fluctuations in wind speed to regulate rotor speed and reduce structural loading in both the tower and rotor blades of WTs in above-rated operation. The novelty of aIPC is that switching between a set of IPC controllers occurs based on prevailing operating conditions, ensuring a suitable trade-off between performance and robustness. Unlike previous attempts that have been applied for rotor speed regulation and/or load mitigation in a single WT structure like the tower or blades, the robust control scheme, henceforth denoted as RDAC+aIPC is designed to reduce loads in both these structures. To design the controller, the WT dynamics are modeled with respect to speed regulation and load mitigation using fatigue aeroelastic structures and turbulence (FAST) simulation tool [JB05]. The high fidelity WindPACT 1.5 MW RWT developed by the National Renewable Energy Laboratory (NREL) is selected for control

design and for conducting dynamic simulations. Although, real-time hardware-in-the-loop experiments are not carried out due to the unavailability of an actual WT or physical model, the high fidelity WindPACT 1.5 MW RWT closely represents actual commercial WT technology. It has been widely used by researchers in WT field as a testbed for evaluating new control algorithms [RD18]. The performance of RDAC+aIPC controller is evaluated against the standard GSPI [RD18] and RDAC [DS22] controllers.

4.1.1 H_∞ robust disturbance accommodating control

The RDAC controller for rotor speed regulation and tower load mitigation is hereby introduced. This controller, proposed in previous work [DS22], is extended with the view of achieving additional objectives. It is briefly repeated here for principal understanding.

To obtain a linear model for controller design, the nonlinear model (3.1) is linearized around an operating point in the high wind speed regime, which is defined by a constant hub-height wind speed of v_{op}=18 m s^{-1}, a pitch angle of $\beta_{op} = 20$ °, and a rotor speed of $\omega_{op} = 20.463$ rpm. Six DOFs are enabled to capture the most relevant dynamical parts in the linear model while avoiding unnecessary complexity. The DOFs considered include tower fore-aft (F-A) displacement in the first mode, variable speed generator, drive-train rotational flexibility, and first mode of blade flap-wise (F-W) displacement for all blades. These correspond to the desired closed-loop performance with respect to load mitigation and speed regulation. To capture the periodic behavior around the rotor disc due to vertical wind shear, 24 azimuth positions are selected for linearization. After linearization, the obtained mechanical states $x \in \mathbb{R}^{11x1}$, which are related to the aforementioned DOFs selected in the WindPACT 1.5 MW RWT are given as

$$x = \begin{bmatrix} \text{tower-top F-A displacement} \\ \text{drivetrain torsional displacement} \\ \text{blade 1 F-W displacement} \\ \text{blade 2 F-W displacement} \\ \text{blade 3 F-W displacement} \\ \text{generator speed} \\ \text{tower F-A velocity} \\ \text{drivetrain torsional velocity} \\ \text{blade 1 F-W velocity} \\ \text{blade 2 F-W velocity} \\ \text{blade 3 F-W velocity} \end{bmatrix}. \tag{4.1}$$

The 24 periodic models obtained by linearization are azimuth-averaged to obtain a reduced-order linear time invariant (LTI) model for controller design, expressed in state-space form as

$$\begin{aligned} \dot{x} &= Ax + Bu + B_d d \\ y &= Cx, \end{aligned} \tag{4.2}$$

where $A \in \mathbb{R}^{11x11}$ denotes the linearized system matrix, $B \in \mathbb{R}^{11x1}$ the control input matrix, $B_d \in \mathbb{R}^{11x1}$ the disturbance matrix, $C \in \mathbb{R}^{2x11}$ the output matrix, $u \in \mathbb{R}^{1x1}$ the perturbed collective pitch angle $\Delta\beta$, and $d \in \mathbb{R}^{1x1}$ the perturbed hub-height wind speed Δv. The measurements $y \in \mathbb{R}^{2x1}$ include rotor speed ω and tower-base F-A bending moment. Although nacelle accelerometer measurements are used to determine structural loading in

actual WT towers, F-A bending moment measurement is used in the proposed approach because it fits the state-space scheme and is required for the given task of providing insight into the influence of the wind field on tower loading.

Disturbance accommodating control design

Highly turbulent wind conditions influence the aerodynamic power and torque of a WT, and is responsible for cyclic loading of its components. Therefore, there is need to counteract these wind disturbances without affecting full-state feedback and observability. Assuming the disturbance structure as known, a wind disturbance state can be added to the model (4.2) to design a DAC controller. By augmenting the observer-based controller with an assumed waveform model, the disturbance observer estimates the wind disturbance state [Wri04], which in combination with a suitable disturbance gain can be used to accommodate persistent wind disturbances.

In the realm of WTs, spatial variation of rotor effective wind speed is considered an additive disturbance having a waveform model of the form [Wri04]

$$\begin{aligned} d &= \theta x_d \\ \dot{x}_d &= F x_d, \end{aligned} \tag{4.3}$$

where x_d denotes the wind disturbance state while θ and F denote the known disturbance state-space model.

Assuming a step disturbance model, which approximates sudden uniform rotor-effective wind velocity fluctuations, the state-space matrices are chosen as $\theta = 1$ and $F = 0$ [SYM95; Wri04; WF08]. In principle, combining the disturbance model with a suitable high gain yields a practical solution [SYM95]. Model (4.2) is extended to include the wind disturbance model as

$$\begin{aligned} \underbrace{\begin{bmatrix} \dot{x} \\ \dot{x}_d \end{bmatrix}}_{\dot{x}_e} &= \underbrace{\begin{bmatrix} A & B_d\theta \\ 0 & F \end{bmatrix}}_{A_e} \underbrace{\begin{bmatrix} x \\ x_d \end{bmatrix}}_{x_e} + \underbrace{\begin{bmatrix} B \\ 0 \end{bmatrix}}_{B_e} u \\ y &= \underbrace{\begin{bmatrix} C & 0 \end{bmatrix}}_{C_e} \begin{bmatrix} x \\ x_d \end{bmatrix}. \end{aligned} \tag{4.4}$$

The observability of the system (4.4), which is an extension of the LTI model (4.2), is tested and stated as observable. After establishing full observability, the system and disturbance states are estimated by designing an extended observer expressed as

$$\begin{aligned} \begin{bmatrix} \dot{\hat{x}} \\ \dot{\hat{x}}_d \end{bmatrix} &= \begin{bmatrix} A & B_d\theta \\ 0 & F \end{bmatrix} \begin{bmatrix} \hat{x} \\ \hat{x}_d \end{bmatrix} + \begin{bmatrix} B \\ 0 \end{bmatrix} u + L(y - \hat{y}) \\ \hat{y} &= \begin{bmatrix} C & 0 \end{bmatrix} \begin{bmatrix} \hat{x} \\ \hat{x}_d \end{bmatrix}, \end{aligned} \tag{4.5}$$

where the observer gain L is typically calculated using pole placement or LQR method. Using the estimated states, full-state feedback control is implemented as

$$u = u_x + u_d = K_x\hat{x} + K_d\hat{x}_d, \tag{4.6}$$

where K_x denotes the full-state feedback controller used to realize rotor speed regulation and tower load mitigation control objectives and K_d denotes the disturbance rejection controller, which is designed separately to cancel wind disturbances effects. Using the control variable in (4.6), (4.5) can be rewritten as

$$\begin{bmatrix}\dot{\hat{x}}\\ \dot{\hat{x}}_d\end{bmatrix} = \begin{bmatrix}A & B_d\theta\\ 0 & F\end{bmatrix}\begin{bmatrix}\hat{x}\\ \hat{x}_d\end{bmatrix} + \begin{bmatrix}B\\ 0\end{bmatrix}\begin{bmatrix}K_x & K_d\end{bmatrix}\begin{bmatrix}\hat{x}\\ \hat{x}_d\end{bmatrix} - \underbrace{\begin{bmatrix}L_1\\ L_2\end{bmatrix}}_{L}\begin{bmatrix}C & 0\end{bmatrix}\begin{bmatrix}\hat{x}\\ \hat{x}_d\end{bmatrix} + Ly, \tag{4.7}$$

where L_1 and L_2 denote the system observer and disturbance observer gain matrices, respectively. The observer gains are typically calculated using pole placement [SYM95] or LQR method. Similarly, K_x is usually designed using pole placement or LQR technique. In standard DAC approaches, K_d is chosen to minimize the norm $\|B_d\theta + BK_d\|$ by using Moore-Penrose Pseudoinverse (†) or Kronecker Product method [WWJ16; WWB17].

To meet the objective of rotor speed regulation with zero static tracking error, the DAC model (4.7) is extended with a partial integral action $\dot{x}_i = C_i y$, where C_i denotes the location of the rotor speed in the output measurements. Therefore, the dynamic DAC controller with partial integral action becomes

$$\begin{aligned}\underbrace{\begin{bmatrix}\dot{\hat{x}}\\ \dot{\hat{x}}_d\\ \dot{x}_i\end{bmatrix}}_{\dot{x}_r} &= \underbrace{\begin{bmatrix}A + BK_x - L_1C & B_d\theta + BK_d & BK_i\\ -L_2C & F & 0\\ 0 & 0 & 0\end{bmatrix}}_{A_r}\underbrace{\begin{bmatrix}\hat{x}\\ \hat{x}_d\\ x_i\end{bmatrix}}_{x_r} + \underbrace{\begin{bmatrix}L_1\\ L_2\\ C_i\end{bmatrix}}_{B_r} y,\\ u &= \underbrace{\begin{bmatrix}K_x & K_d & K_i\end{bmatrix}}_{C_r}\begin{bmatrix}\hat{x}\\ \hat{x}_d\\ x_i\end{bmatrix}.\end{aligned} \tag{4.8}$$

In existing approaches, DAC parameters including the state feedback controller K_x, disturbance rejection controller K_d, integral gain K_i, and observer gains L_1 and L_2, are calculated separately without considering the closed-loop system stability, robustness, and optimality. Therefore, a robust control method for obtaining optimal DAC parameters in a single step is required.

Robust disturbance accommodating control design

The standard H_∞ control problem is usually formulated as a task to minimize the H_∞ norm $\|.\|_\infty$ of the transfer function G_{zd} from the exogenous inputs d to the controlled outputs z expressed as

$$R^* = \underset{R\in\mathcal{R}}{argmin} \parallel G_{zd}(P,R) \parallel_\infty, \tag{4.9}$$

where R^* denotes the optimized controller, $\mathcal{R}$ a set of controllers R that stabilize the plant P. The effects of exogenous disturbances on the outputs is minimized by using R^*, hence increasing system robustness. This convex optimization problem can be solved using algebraic Riccati equations (ARE) or linear matrix inequalities (LMI). Standard H_∞ control cannot be applied in control systems with structural constraints such as the structured DAC control system (4.8), which depends smoothly on the design parameters K_x, K_d, K_i, L_1, and L_2.

To achieve a trade-off between robust stability and performance, weighting functions are usually introduced. Therefore, the optimization problem (4.9) is extended to become a mixed-sensitivity H_∞ problem expressed as

$$R^* = \underset{R\in\mathcal{R}}{argmin} \left\| \begin{matrix} W_1 S \\ W_2 RS \\ W_3 T \end{matrix} \right\|_\infty , \tag{4.10}$$

where, W_1, W_2, and W_3 denote the weighting functions, while S, RS, and T denote the sensitivity function, control effort, and complementary sensitivity function, respectively. This serves as a cost function for optimizing parameters of a structured DAC controller. The problem of finding the optimal RDAC controller $RDAC^*$ defining the optimal parameters $K^* = [K_x\, K_d\, K_i]$ and $L^* = [L_1\, L_2]^T$ is formulated as

$$RDAC^* = \underset{RDAC\in\mathcal{RDAC}}{argmin} \parallel G_{zd}(P, RDAC) \parallel_\infty, \tag{4.11}$$

where $\mathcal{RDAC}$ denotes a set of controllers $RDAC$ that stabilize the generalized plant P made up of weighting functions, pitch actuator (PA) dynamics, and a nominal model of the WT.

To ensure that $RDAC^*$ guarantees asymptotic stability of the closed-loop system, the optimization problem (4.11) is subjected to the Lyapunov stability constraint $\parallel C_r(sI - \mathcal{A}_{RDAC})^{-1}B_r \parallel_\infty < +\infty$, where $\mathcal{A}_{RDAC}$ denotes the closed-loop system matrix depending on RDAC controller. Therefore, the optimization problem becomes

$$\begin{aligned} RDAC = \underset{RDAC\in\mathcal{RDAC}}{argmin} & \parallel G_{zd}(P, RDAC) \parallel_\infty \\ s.t. \ & \parallel C_r(sI - \mathcal{A}_{RDAC})^{-1}B_r \parallel_\infty < +\infty, \end{aligned} \tag{4.12}$$

whose H_∞ norms are calculated from the closed-loop system using a bisection algorithm. The robust stability domain of (4.12) is defined by the structure of the observer-based DAC system (4.8). This is therefore independent of the external wind load fluctuations, provided that this disturbance is limited to operation by a maximum wind speed (Table 3.1). Given that (4.12) is non-convex, hence cannot be solved using AREs or LMIs, nonsmooth H_∞ synthesis [AN06], which is used for problems with structural and stability constraints is applied to find an optimal controller $RDAC^*$ for tower load mitigation and rotor speed regulation of WTs. The structurally constrained controllers K^* and L^*, are defined as tunable parameters that are optimized using nonsmooth H_∞ synthesis. This method is implemented in MATLAB using *hinfStruct* command [AN17]. It uses Clarke sub-differential and a multi-start steepest gradient descent method to minimize the H_∞ norms. Default values of the relevant hyperparameters of the optimizer including the maximum number of iterations for each optimization run and the allowable tolerance gain are maintained at 300 and 0.001, respectively. This is because varying the hyperparameters does not translate to any significant performance improvement.

The proposed RDAC approach is applied to the WindPACT 1.5 MW RWT as shown in Fig. 4.1. To account for PA dynamics, which is not integrated in FAST, an actuator transfer function is included in the generalized plant P. Because PA dynamics is faster than other WT dynamics, the actuator model is defined as a first-order lag (PT1) linear model

$$\frac{\beta}{\beta_{com}} = \frac{1}{s\tau_\beta + 1}, \tag{4.13}$$

where β_{com} denotes the commanded pitch angle, β the actual pitch angle, and τ_β the actuator time constant, which is chosen as 0.2 seconds according to the actuator characteristics. To avoid exceeding the turbine's maximum pitch rate (PR) of 10 °/s, a rate-limiter is implemented as a hard constraint.

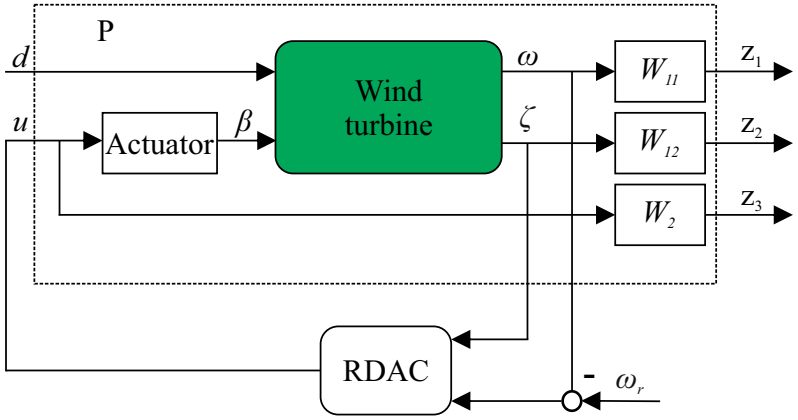

Figure 4.1: RDAC applied to the WindPACT 1.5 MW wind turbine (modified from [DS22])

The hub-height wind disturbance d excites WT dynamics in the above-rated wind speed region. The RDAC controller relies on measured outputs including rotor speed ω and tower F-A bending moment ζ, to generate a collective pitch angle β as a control signal for regulating rotor speed to the rated value and reducing tower F-A bending moment oscillations.

The weighting functions W_{11}, W_{12}, and W_2 are designed to achieve the desired robust performance. To effect rotor speed response and ensure robustness against wind disturbances, W_{11} is designed as an inverted high-pass filter (HPF). To reduce the first mode of tower F-A oscillation, which occurs at 2.56 rad/s, W_{12} is designed as an inverted notch filter centered at this frequency. Finally, to reduce controller activity at high frequencies and thus increase robustness, W_2 is chosen as an inverted low-pass filter (LPF).

Lower linear fractional transformation (LFT) is used to interconnect the generalized plant P and the observer-based DAC system (4.8), hence forming a generalized state-space system. While tunable elements of the control architecture K_x, K_d, K_i, L_1, and L_2 are contained in the observer-based system, P carries the fixed elements including the WT model, weighting functions, and PA. Nonsmooth H_∞ optimization [AN17], is used to synthesize the optimal RDAC controller that minimizes the maximum singular value of the closed-loop transfer function from d to $[z_1 \ z_2 \ z_3]^T$. Therefore, the obtained RDAC controller is considered to be robust against modeling errors and wind disturbances. This controller ensures both objectives of rotor speed regulation and tower load reduction for WTs in above-rated operation are achieved. However, the controller is only valid within its design operating point and suffers performance deterioration outside this envelop. Furthermore, its control input signal is a collective pitch angle, hence it cannot be used to reduce blade oscillations due to vertical wind shear as this can only be achieved via IPC.

To improve the performance of the RDAC controller, a novel aIPC controller, which is designed using the LQG method and implemented as a separate control loop is proposed. Whereas the RDAC controller provides the main CPC control signal to achieve the objectives

of tower load mitigation and rotor speed regulation, aIPC is designed to reduce 1P (0.333 Hz) blade F-W oscillations due to vertical wind shear by using additional IPC control signals. It is adaptive to change in operating point due to horizontal wind speed fluctuations. Control signals from both controllers are used to manipulate each blade independently to achieve the desired objectives.

4.1.2 Adaptive IPC

As WT rotor blades rotate, they experience varying aerodynamic loads at different azimuth positions due to wind shear. To counteract this periodicity, which is more pronounced in large WTs, rotor blades are pitched independently. In the proposed approach, vertical wind shear is only considered for turbine level control. However, in wind farms, partial wind wakes can cause horizontal shear, which contributes to periodic loading. The idea behind aIPC is to use 5 IPC controllers, each designed to be effective in a specified wind speed range/bin in above-rated operation. The linear models used to design respective IPC controllers are extracted from the nonlinear WT model (3.1) at different operating points shown in Table 4.1. Constant wind speeds and associated blade pitch angles define the operating points used to obtain linear models for designing each IPC controller. The wind speed bins serve as threshold values within which the associated controller is active during operation. Closed-loop dynamic simulations are performed using stochastic wind profiles.

Table 4.1: Design operating points for the IPC controllers [KDNS24]

IPC	**WS bin [m/s]**	**WS [m/s]**	**Angle [°]**	**Speed [rpm]**
1	12 - 15	14	13.10	20
2	15 - 17	16	16.75	20
3	17 - 19	18	19.83	20
4	19 - 21	20	22.47	20
5	21 - 25	22	24.84	20

To capture the most important dynamics with respect to blade load mitigation and rotor speed regulation, 7 states x including blade F-W displacement for each blade, their respective velocities, and generator speed are selected. To capture periodicity in aerodynamic loading due to vertical wind shear, 24 equispaced azimuth positions are selected for linearization. To incorporate this inherent periodicity into the controller design, MBC transformation [Bir10] is used to transform the individual blade dynamics from the rotating frame to the non-rotating frame. The transformed reduced-order models are then averaged to obtain an LTI model described in state-space form as

$$\begin{aligned} \dot{x_i} &= A_i x_i + B_i u_i + B_{di} d \\ y_i &= C_i x_i, \end{aligned} \tag{4.14}$$

where the index $_i$ denotes the systems used for aIPC design, $u_i \in \mathbb{R}^{3\times 1} = [\Delta\beta_1\, \Delta\beta_2\, \Delta\beta_3]^T$ the perturbed independent pitch angles, $d \in \mathbb{R}^{1\times 1}$ the wind disturbance. The matrices $A_i \in \mathbb{R}^{7\times 7}$, $B_i \in \mathbb{R}^{7\times 3}$, $B_{di} \in \mathbb{R}^{7\times 1}$, and $C_i \in \mathbb{R}^{3\times 7}$ denote the system, input, disturbance, and output matrices, respectively. The measurements $y_i \in \mathbb{R}^{3\times 1}$, which include the blade-root F-W bending moment for each blade are assumed to be distorted by noise v.

To implement full-state feedback control, the control gain matrix $K = R^{-1}B_i^T P$ is designed using LQR technique by minimizing the quadratic performance index

$$J_{QR} = \int_0^\infty (x_i^T Q x_i + u_i^T R u_i) dt, \tag{4.15}$$

while solving the ARE $A_i^T P + P A_i - P B_i R^{-1} B_i^T P + Q = 0$ assuming (A_i, B_i) is fully controllable. Here, Q and R denote symmetric positive definite state and control input weighting matrices, respectively. The elements of Q and R are chosen to achieve desired dynamic response with respect to blade load mitigation and rotor speed regulation. The symmetric positive definite matrix P is the solution to the ARE.

Some states might not be available for measurement, moreover, it is cost-effective to use a few measurements to reconstruct systems states using an observer. Because WT dynamics are excited by stochastic wind fields and that measurement signals are typically noisy, a Kalman state estimator is used to obtain estimated states $\hat{x}_i$ for implementing full-state feedback control. The process noise d and measurement noise v are assumed to be uncorrelated zero mean Gaussian white noise with process disturbance covariance matrix $Q_f = E(ww^T)$ and measurement noise covariance matrix $R_f = E(vv^T)$.

After determining that all (A_i, C_i) are fully observable, the observer gain $L = P_f C_i^T R^{-1}$ is designed by minimizing the state estimation error covariance $E((x_i - \hat{x}_i)(x_i - \hat{x}_i)^T)$, while solving the filter ARE (FARE) $A_i P_f + P_f A_i^T - P_f C_i^T R_f^{-1} C_i P_f + Q_f = 0$, where the index $_f$ denotes the observer-based system and $P_f = P_f^T \geq 0$ is the solution to the FARE. An optimal full-state feedback control is implemented using the estimated states as $u_i = -K_i \hat{x}_i$.

An implementation of one of the five IPC controllers is shown in Fig. 4.2. The wind profile d excites the dynamics of the WT in above-rated wind speed regime. The periodic blade-root F-W bending moment measurements y_o are transformed from the rotating to the fixed coordinate frame of controller design using the inverse MBC transformation matrix $T(\psi)^{-1}$, which relies on real-time rotor azimuth angle measurements ψ. The perturbed independent pitch angles $\Delta\beta_i$ are obtained by transforming the IPC control input u_i back to the rotating coordinate frame using the MBC transformation matrix $T(\psi)$. By summing $\Delta\beta_i$ and the collective pitch angle β_c from RDAC controller, the IPC signal β_i obtained.

To maintain robustness to changing wind conditions, the entire range of above-rated WT operation from 12 m/s to 25 m/s is divided into 5 regions defined by wind speed (WS) bins shown in Table 4.1. Using linear models obtained for each of these regions, corresponding controllers are designed. Optimal design of the gains ensures suitable performance in compromise between blade load reduction and rotor speed regulation. A technique for switching between the IPC controllers based on the incoming hub-height wind speed is implemented in MATLAB/Simulink using if-else logic. Depending on the hub-height wind speed measurement d, the if-else logic built using the wind speed bins determines the operation range of the WT. The switching logic activates a suitable controller from the IPC bank, ensuring that an appropriate controller is active over a specific wind speed bin for the prevailing wind conditions. This forms the adaptation mechanism. Therefore, the observer model shown in Fig. 4.2 is updated to match the wind conditions. The observer matrices A_i, B_i, and C_i including the corresponding full-state feedback gain K_i and observer gain L_i, are updated based on the identified operation range. The implementation is illustrated in Fig. 4.3. The observer models rely on the measurements y_i.

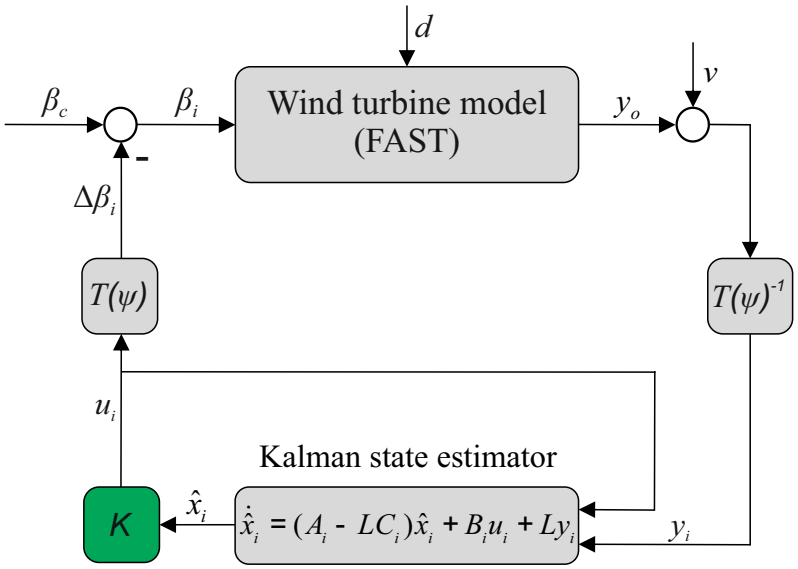

Figure 4.2: Independent pitch controller [KDNS24]

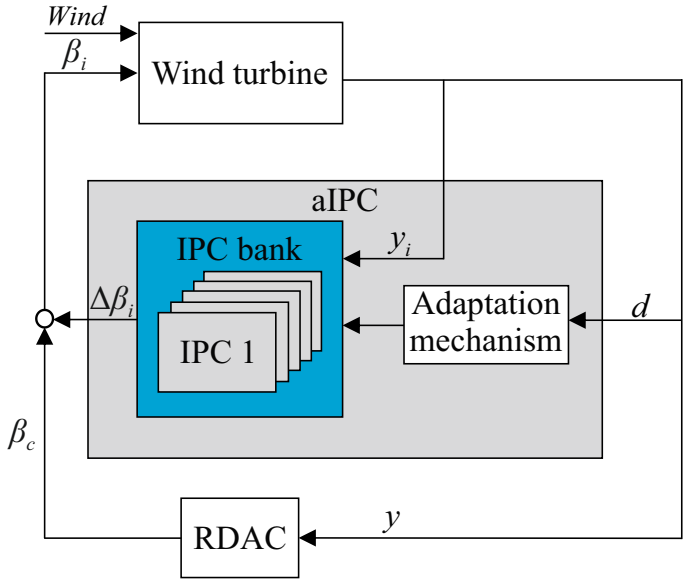

Figure 4.3: aIPC switching implementation [KDNS24]

The bank of five IPC controllers are individually designed using linear quadratic Gaussian (LQG) method based on linear models extracted from predefined operating points shown in Table 4.1, which cover most of the above-rated WT operation. It should be noted that wind speed bins only define the switching thresholds. Therefore, the highly uncertain WT anemometer measurement should suffice as strict accuracy is not required. Switching between IPC controllers during continuous operation constitutes aIPC control. The estimation quality of each observer is improved by using local models related to the range of WT operation determined by prevailing wind speeds. To compensate for uncertainties, the adaptation mechanism ensures that a valid model is active at any given

time. Because wind speed fluctuation is considered an input disturbance in a WT system, the use of local models reduces the impact of these disturbances on the blade loads. In addition, the RDAC controller reduces the effect of disturbances on the tower F-A mode and rotor speed regulation, as shown in section 4.1.4.

4.1.3 Extended H_∞ RDAC using adaptive IPC

The adaptive robust observer-based controller (RDAC+aIPC) is implemented using two control loops, as illustrated in Fig. 4.4. For above-rated operation, generator torque is kept constant at the rated value. The RDAC controller relies on tower-base F-A bending moment and rotor speed measurements to generate a collective pitch angle signal for tower load mitigation and rotor speed regulation. The aIPC controller relies on blade-root F-W bending moments and azimuth measurements to generate IPC signals used to mitigate blade load. The independent pitch angles are perturbed about the CPC signal and thus form the control input for the WT model in FAST. Because both RDAC and aIPC controller gains are designed using control methods that guarantee closed-loop stability and each addresses specific objectives, robustness and stability of the combined control strategy RDAC+aIPC is assured. Although reduced-order LTI models (4.2) and (4.14) are used for designing the proposed control scheme, the nonlinear model of the WindPACT 1.5 MW RWT (3.1) is used as the controlled plant in the closed-loop simulations performed with the proposed control method.

4.1.4 Simulation results and discussion

In this section, the simulation results obtained from the evaluation of adaptive robust observer-based control strategy using the Test 14 version of the WindPACT 1.5 MW NREL RWT in FAST v7 design code [JB05] are discussed. Both step and stochastic wind profiles are used to excite the WT dynamics in the above-rated wind speed region. The standard GSPI controller, which is designed based on the guidelines in [WF08; RD18], is used as a reference baseline controller. It is designed for speed regulation, hence rotor speed measurement is used to realize CPC control. The performance of the proposed control scheme (RDAC+aIPC) is compared with the standard GSPI and RDAC [DS22] controllers. Selected performance measures are used for comparison.

Performance measures for analyzing results

Timeseries simulation results are analyzed in time and frequency domains using a set of criteria to illustrate improvements in structural load mitigation and speed/power regulation of the proposed control scheme.

Time domain Timeseries results analyzed include blade F-W and tower F-A bending moments, rotor speed, generator power, and blade pitch angles. The timeseries data is plotted for a graphical illustration of the results. In addition, the mean and standard deviation δ of the data are computed.

Frequency domain While time domain analysis provides incite into the temporal behavior of signals, spectral analysis is necessary for estimating the frequency components in a timeseries signal. Power spectral density (PSD) analysis using Welch's method [Wel67]

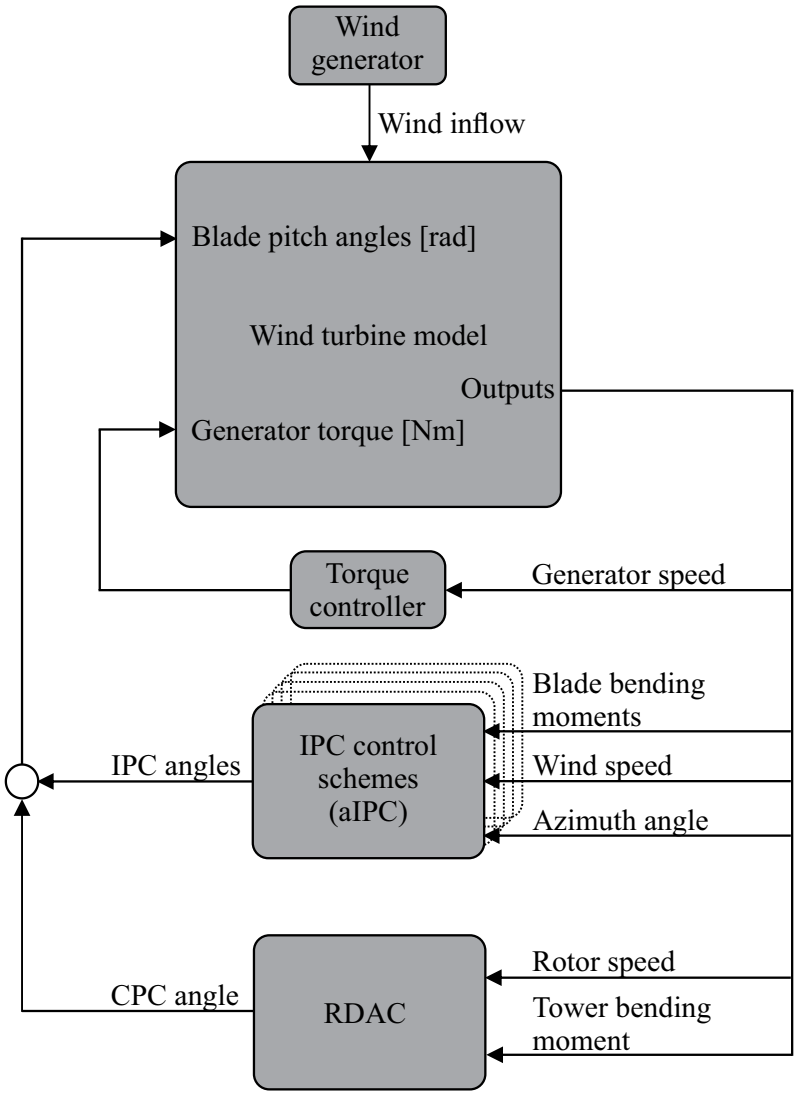

Figure 4.4: Adaptive robust observer-based controller [KDNS24]

is used to determine the frequency-dependence of the timeseries structural loading data from simulation. To improve the spectral estimation process, the method uses a windowing mechanism to shape the timeseries signal before the related PSD is computed. To achieve this, the timeseries signal is divided into small time-slices called windows and the percentage of overlap between windows is specified. The fast Fourier transform (FFT) of all windows are averaged to obtain a smooth signal, whose PSD is then computed. In this thesis, spectral analysis is used to analyze the contribution of 1P and 3P frequencies to blade and tower loading.

Power-load covariance Although previously outlined performance measures can yield meaningful information on structural load reduction or rotor speed regulation performance, they do not consider the correlation between structural loads and power regulation. To obtain a clear performance illustration of the proposed control scheme with respect to

both load mitigation and power regulation, power-load covariance criteria proposed in [DS20] is used. This graphical method uses a power-load distribution diagram and ellipse isocontours based on the power and load covariance matrices to obtain five performance metrics. These include the average and variance in power and structural load, as well as the power-load covariance level.

Damage equivalent loads Damage equivalent load (DEL) analysis is performed using MLife software [Hay12]. This is done according to the specifications of the International Electrotechnical Commission (IEC) 61400-1 standard for performing fatigue analysis.

Step wind profile results

To evaluate the closed-loop control performance in changing operating points, a step wind profile shown in Fig. 4.5a is used. It has vertical wind shear with a conservative power-law exponent of 0.2. The hub-height wind speed varies from 14 m/s to 22 m/s in 2 m/s increments. To compare the pitch activity of different blades, IPC control signals from RDAC+aIPC and control inputs from the CPC-based GSPI and RDAC controllers are plotted as shown in Fig. 4.5b. Additional pitching of each blade around the CPC signal is provided by the IPC controllers, each activated at different operating points to mitigate cyclic loading of blades due to vertical wind shear. In addition, smooth switching between the different controllers is observed.

Structural load mitigation performance in rotor blades and tower is also evaluated. As illustrated in Fig. 4.6a, the RDAC+aIPC controller shows a significant reduction in the blade-root F-W bending moment vibration amplitude. The standard deviation decreases by 28.9 % and 13.7 % compared with GSPI and RDAC controllers, respectively. Mitigation of tower-base F-A bending moment follows a similar trend as shown in Fig. 4.6b, with 59.2 % and 8 % reduction in δ against the GSPI and RDAC controllers, respectively.

Despite the improved performance in structural load mitigation achieved by the proposed controller, it is important to ascertain that this does not result in a trade-off in speed/power regulation performance. The rotor speed measurement is used to evaluate speed regulation as shown in Fig. 4.7a. The proposed controller shows improved transient performance attributed to aIPC. Despite higher overshoots, the GSPI controller shows consistent speed regulation in changing operating points. However, the proposed controller shows higher static variation in power regulation performance at higher wind speeds as shown in Fig. 4.7b. This is attributed to high pitch activity to alleviate blade and tower loads.

To give a clear illustration of the control performance in both load mitigation and speed/power regulation, generator power versus structural load covariance is evaluated (Fig. 4.8). First proposed in [DS20], the power-load covariance diagram is used to evaluate the overall performance and relationship in power regulation and load mitigation. This graphical method uses power-load distribution diagram and ellipse isocontours generated using the power and load covariance matrices to obtain relevant performance metrics, including the average and variance in both power and structural load as well as power-load covariance level. The GSPI controller has the highest variance in both power and structural loads because it has the largest ellipse. The proposed control strategy shows lower variance in both blade and tower loads σ_{x2}, and generated power σ_{y2} compared

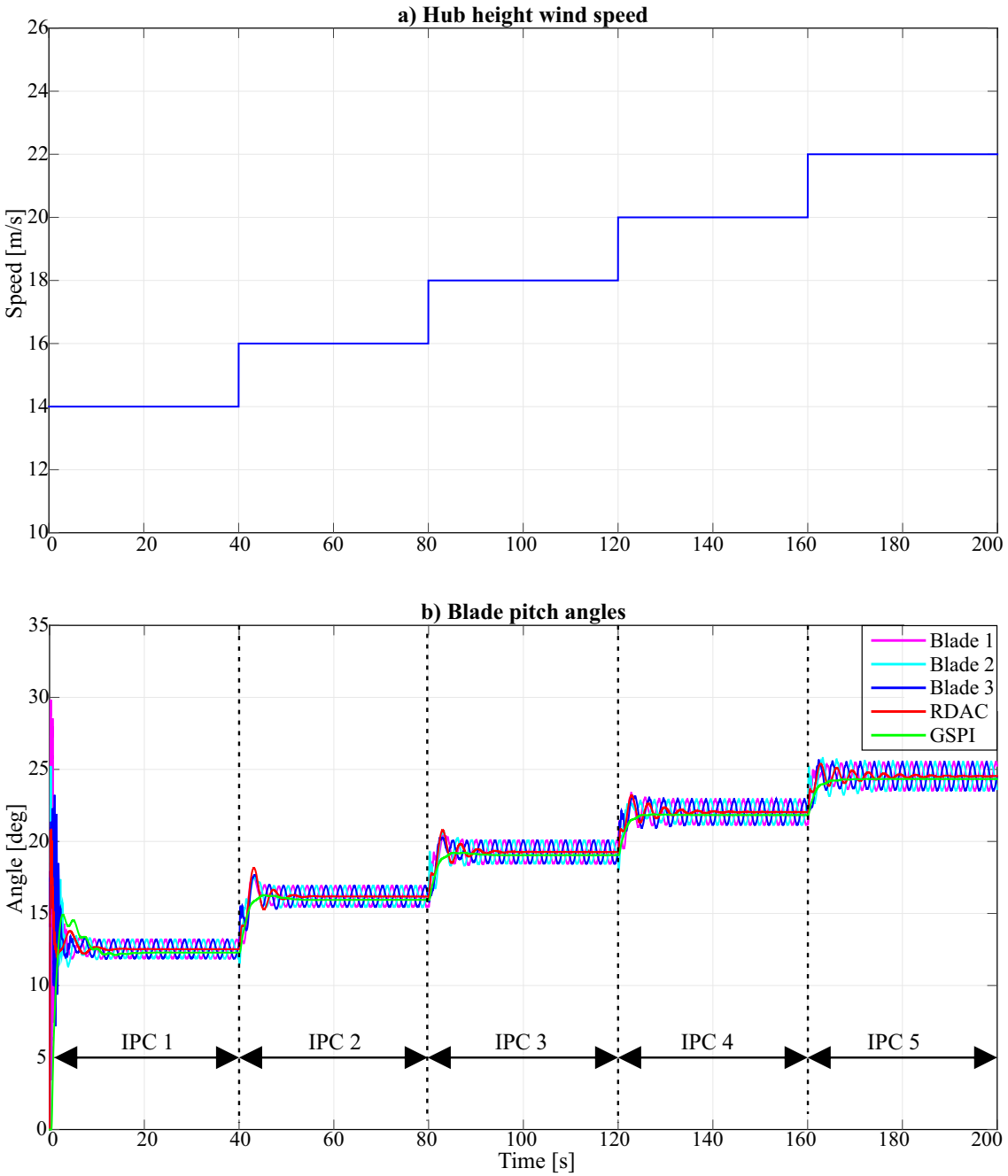

Figure 4.5: Step wind response [KDNS24]

with GSPI and RDAC controllers. Therefore, there is improved structural load mitigation without compromising speed and power regulation performance.

Stochastic Wind Profile Results

To evaluate the closed-loop performance of the proposed control strategy under more realistic wind conditions, stochastic wind profiles shown in Fig. 4.9a are used. These

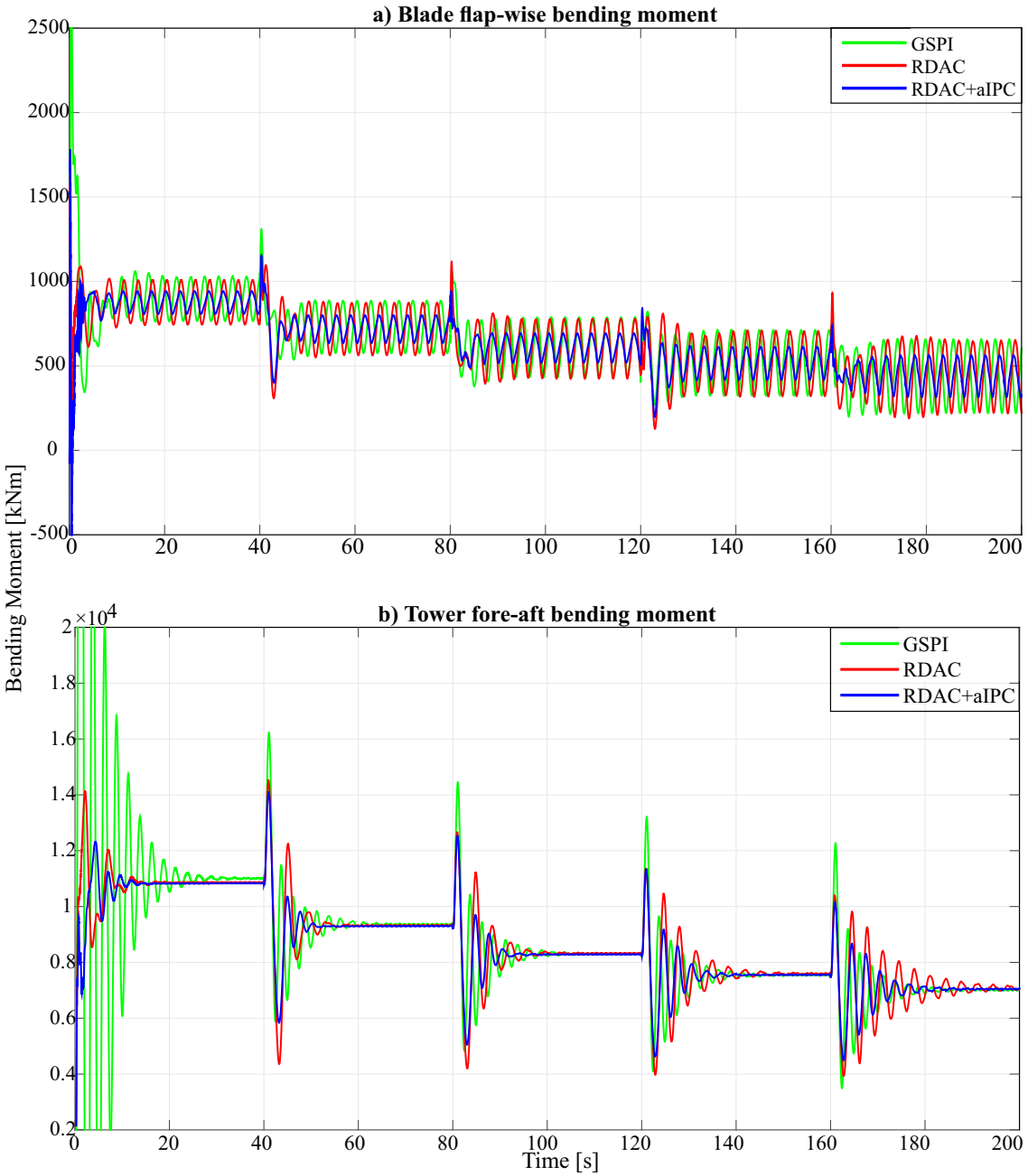

Figure 4.6: Structural loading in blades and tower [KDNS24]

are generated using TurbSim software [JK12] based on IEC von Karman spectral model, with a 13 by 13 grip-point matrix dimension. Following the IEC 61400-1 recommendation for fatigue load evaluation of WT structures, the wind fields are generated with various combinations of mean hub-height wind speeds, random seeds, and turbulence intensities (TIs). The TIs include type A (16 %), type B (14 %), and type C (12 %), all referenced to a wind speed of 15 m/s. All wind profiles exhibit vertical wind shear with a power law exponent of 0.2.

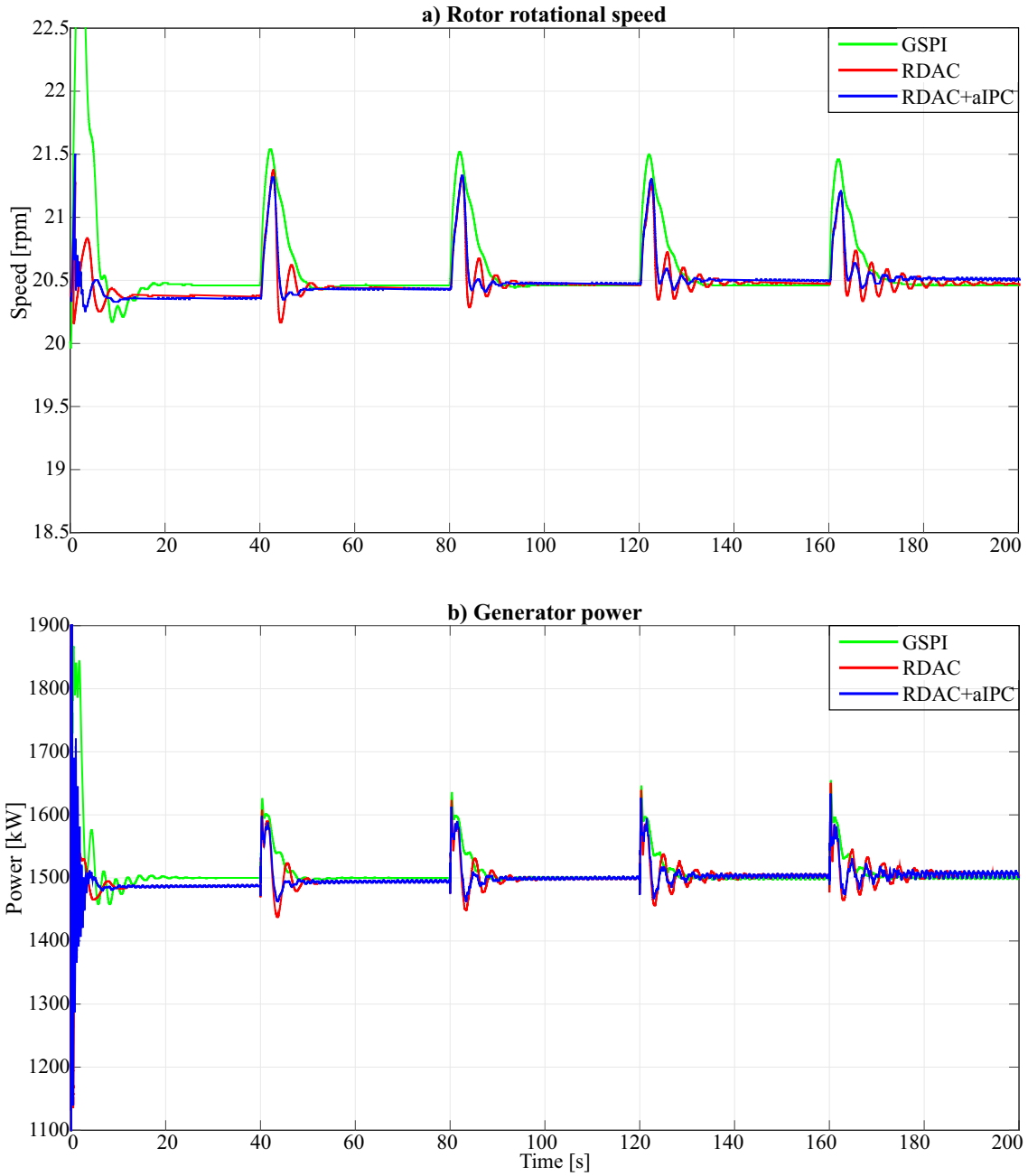

Figure 4.7: Speed/power regulation response [KDNS24]

Structural load mitigation analysis Structural load mitigation performance in the blades and tower is illustrated in Fig. 4.9. The proposed control scheme achieves significant reduction in both blade F-W and tower F-A bending moment variations. In Table 4.2, the load mitigation performance in these load channels for all wind fields is given. Compared with the GSPI and RDAC controllers, the average (for all wind fields) δ in blade F-W bending moment is reduced by 10.7 % and 9.2 %, respectively. Similarly, the δ in tower F-A moment reduces by 36.2 % and 8.4 %, respectively. Therefore, the proposed control

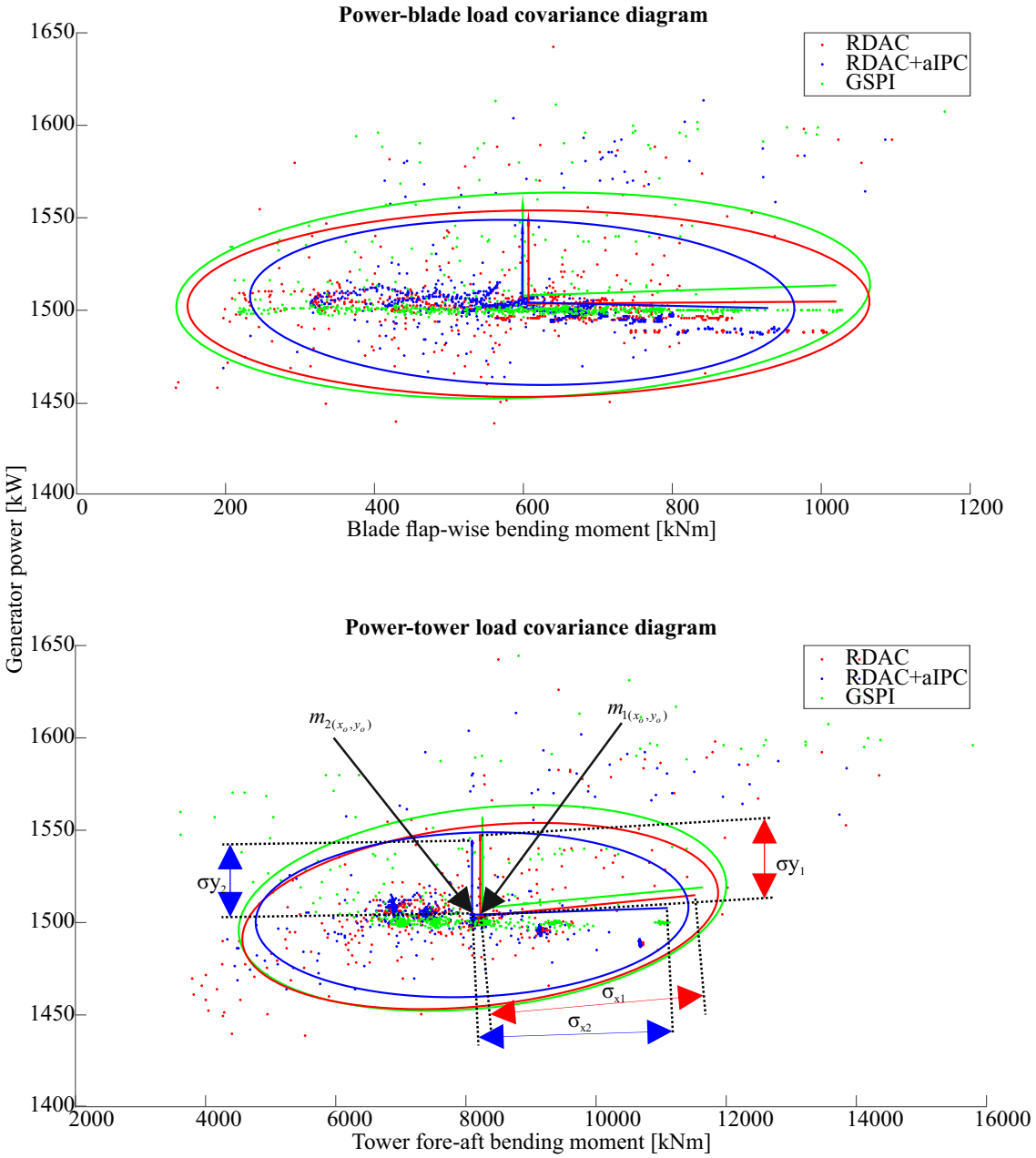

Figure 4.8: Power-load covariance analysis (according to [DS20])

scheme meets the challenge of load mitigation in multiple WT components under changing operating conditions.

Speed and power regulation analysis The speed and power regulation performance of the proposed control scheme compared with the GSPI and RDAC controllers is illustrated in Fig. 4.10. The RDAC+aIPC controller shows better speed and power regulation compared with the baseline GSPI controller. However, there is a slight deterioration in performance compared with RDAC. In Table 4.3, the performance analysis in PR and rotor speed/power

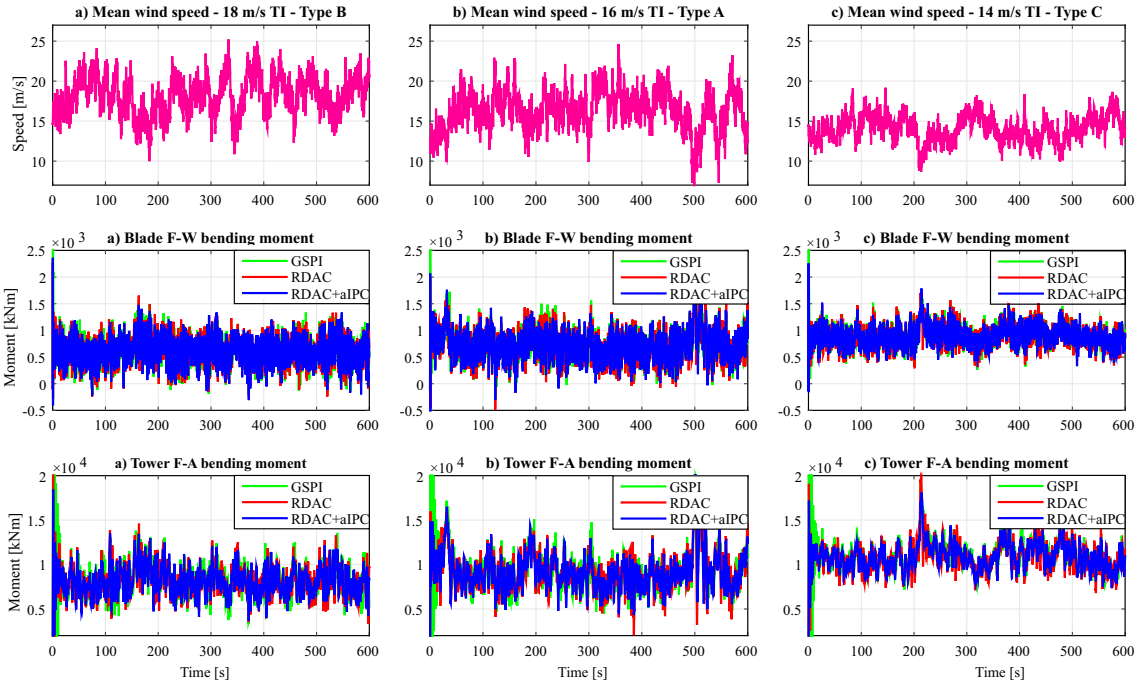

Figure 4.9: Structural loading in blades and tower [KDNS24]

Table 4.2: Load mitigation performance analysis (Key: best, worst) [KDNS24]

Load channel [kNm]	Controller	18 m/s	16 m/s	14 m/s	Avg.	%
Blade F-W (δ)	GSPI	264.97	277.99	213.56	252.17	-
	RDAC	259.6	277.87	206	247.82	-1.7
	RDAC+aIPC	235.57	255.05	184.77	224.21	-9.2
Tower F-A (δ)	GSPI	2769.6	2837.2	2580.5	2729.1	-
	RDAC	1737.5	2243.5	1720.3	1900.43	-30.4
	RDAC+aIPC	1585.5	2107.1	1529	1740.53	-36.2

regulation for all wind fields is given. Compared with the GSPI controller, the average δ in rotor speed is reduced by 41.1 % and% 37.2 % by the RDAC and proposed controllers, respectively. This performance is also reflected in the MSE values as the average MSE of rotor speed is reduced by 36.6 % and 31.4 % by the RDAC and RDAC+aIPC controllers, respectively, compared with the GSPI controller. In addition, the RDAC and RDAC+aIPC controllers reduce the δ in generator power by 15.6 % and 9.2 %, respectively, compared with the GSPI controller. Therefore, although the proposed controller shows improved speed regulation performance compared with GSPI controller, it realizes a slightly lower performance compared with RDAC. This is attributed to a greater need for trade-off between load mitigation and speed regulation. In Figure 4.11, the average normalized values of pitch activity and rotor speed regulation error is shown. The RDAC+aIPC controller has the highest total pitch travel due to the use of additional IPC control signals to mitigate blade loads. Nevertheless, the proposed controller does not violate the turbine's maximum PR of 10 °/s because the average root mean square (RMS) values for the GSPI, RDAC, and RDAC+aIPC are 0.87, 3.58, and 7.05, respectively, as shown in Table 4.3.

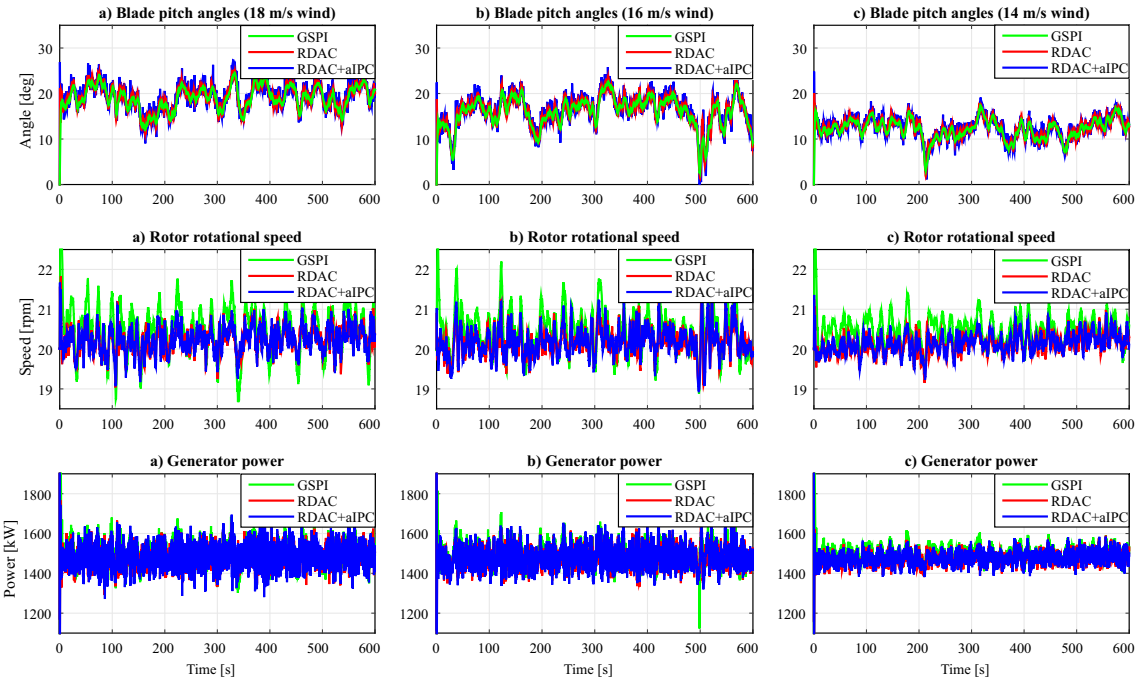

Figure 4.10: Speed and power regulation response [KDNS24]

Table 4.3: Pitch usage and speed/power regulation performance analysis (Key: best, worst) [KDNS24]

Parameter	Units	Controller	18 m/s	16 m/s	14 m/s	Avg.	%
Speed (δ)	rpm	GSPI	0.6182	0.5564	0.3835	0.5194	-
		RDAC	0.3225	0.348	0.2473	0.3059	-41.1
		RDAC+aIPC	0.3431	0.3831	0.2549	0.327	-37.0
Speed (MSE)	rpm	GSPI	0.3831	0.3096	0.1473	0.2800	-
		RDAC	0.1610	0.2005	0.1710	0.1775	-36.6
		RDAC+aIPC	0.1751	0.2260	0.1755	0.1922	-31.4
Power (δ)	kW	GSPI	60.62	54.88	38.36	51.29	-
		RDAC	50	47.4	32.48	43.29	-15.6
		RDAC+aIPC	55.42	51.24	33.08	46.58	-9.2
PR (RMS)	°/s	GSPI	0.9104	0.8946	0.8065	0.8705	-
		RDAC	3.7189	3.5209	3.4877	3.5758	310
		RDAC+aIPC	7.9071	7.2454	5.9896	7.0474	710

Analysis of the adaptation effectiveness To evaluate the effectiveness of the adaptation mechanism of the proposed control scheme, two experiments are conducted. First, the performance of the RDAC+aIPC controller is evaluated against the non-adaptive RDAC+IPC controller, which uses only a single IPC controller designed using a linear model obtained at a constant wind speed of 18 m/s. Using the results obtained for all wind fields shown in Fig. 4.9a, the performance in structural load reduction and speed/power regulation is shown in Table 4.4. In terms of structural load mitigation, RDAC+aIPC shows better performance in mitigating both blade F-W and tower F-A bending moments

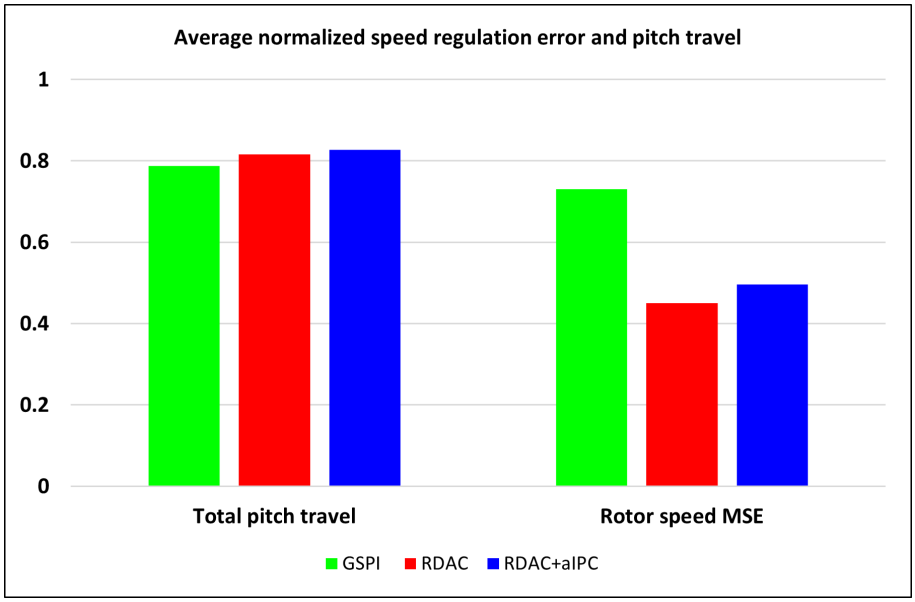

Figure 4.11: Pitch activity and speed regulation performance [KDNS24]

for wind speed outside the operating point, i.e., 14 m/s and 16 m/s. The RDAC+IPC controller performs better at this operating point (18 m/s). In addition, it achieves slightly better performance in regulating rotor speed and generator power. This is attributed to the lower trade-off required in adapting to changing wind speeds to mitigate loads. This is clearly seen in the lower RMS values of PR, indicating a lower PA demand. Therefore, the proposed adaptive controller shows better performance in load mitigation by adapting to changing wind speeds without significant trade-off in rotor speed and power regulation.

Table 4.4: Load mitigation and speed/power regulation performance analysis (Key: best) [KDNS24]

Parameter	**Units**	**Controller**	**18 m/s**	**16 m/s**	**14 m/s**
Blade F-W (δ)	kNm	RDAC+IPC	233.02	256.45	189.25
		RDAC+aIPC	235.57	255.05	184.77
Tower F-A (δ)	kNm	RDAC+IPC	1519.1	2111.9	1551.2
		RDAC+aIPC	1585.5	2107.1	1529
Speed (δ)	rpm	RDAC+IPC	0.3301	0.3766	0.2544
		RDAC+aIPC	0.3431	0.3831	0.2549
Speed (MSE)	rpm	RDAC+IPC	0.1673	0.2212	0.1731
		RDAC+aIPC	0.1751	0.2260	0.1755
Power (δ)	kW	RDAC+IPC	54.2	50.94	33.23
		RDAC+aIPC	55.42	51.24	33.08
PR (RMS)	°/s	RDAC+IPC	6.719	6.176	4.761
		RDAC+aIPC	7.907	7.245	5.990

Secondly, the sensitivity of the proposed adaptive controller to varying adaptation rates is evaluated. In the foregoing results, an adaptation rate of 100 Hz, which matches the simulation time-step is used. Wind measurement systems that comply with the IEC

61400 standard should have a minimum sampling rate of 0.5 Hz, but the recommendation is 1 Hz. Modern wind WTs are equiped with high frequency supervisory control and data acquisition (SCADA) systems that operate at a sampling frequency of 1 Hz [LL20]. Therefore, for practical implementation, 1 Hz frequency of the adaptation mechanism should be considered. The wind speed measurement is downsampled to 20 Hz to match the sample timeseries frequency of the wind profiles used in the simulation. In addition, an adaptation frequency of 1 Hz is used to comply with the minimum requirements of IEC 61400 standard. Therefore, lower adaptation rates of 1 Hz and 20 Hz are simulated. Analysis of the obtained simulation results are shown in Table 4.5. It is noted that the performance of the proposed RDAC+aIPC controller in structural load mitigation and regulation of rotor speed and power is similar across all adaptation rates. However, at lower rates of 1 Hz and 20 Hz, this performance is achieved with lower PRs compared to 100 Hz. This is attributed to the fact that less frequent adaptation leads to lower PA demand. Therefore, using the recommended 1 Hz adaptation frequency results in optimal performance.

Table 4.5: Load mitigation and speed/power regulation performance analysis for different adaptation frequencies (best, worst) [KDNS24]

Parameter	**Units**	**Freq. (Hz)**	**18 m/s**	**16 m/s**	**14 m/s**	**Avg**
Blade F-W (δ)	kNm	1	235.34	255.13	185.05	225.17
		20	236.12	254.78	184.97	225.29
		100	235.57	255.05	184.77	225.13
Tower F-A (δ)	kNm	1	1580	2111.7	1533.9	1741.9
		20	1584.4	2109.0	1531.3	1741.6
		100	1585.5	2107.1	1529	1740.5
Speed (δ)	rpm	1	0.343	0.3822	0.255	0.3267
		20	0.3435	0.3829	0.2549	0.3271
		100	0.3431	0.3831	0.2549	0.3270
Speed (MSE)	rpm	1	0.1751	0.2256	0.1748	0.1918
		20	0.1760	0.2251	0.1757	0.1923
		100	0.1751	0.2260	0.1755	0.1922
Power (δ)	kW	1	55.22	51.31	33.13	46.55
		20	55.37	51.24	33.07	46.56
		100	55.42	51.24	33.08	46.58
PR (RMS)	°/s	1	6.807	6.082	4.356	5.748
		20	6.822	6.075	4.353	5.750
		100	7.907	7.245	5.990	7.047

Spectral analysis Spectral analysis of the blade F-W bending moment illustrated in Fig. 4.12a shows a reduction around 1P frequency component. Similarly, the proposed controller achieves a slightly lower contribution of tower F-A bending moment load around 3P frequency as shown Fig. 4.12b. Therefore, decreased asymmetric loading on the blades contributes to lower tower vibration at 3P frequency. Therefore, the proposed control scheme meets the challenge of load mitigation in multiple WT components.

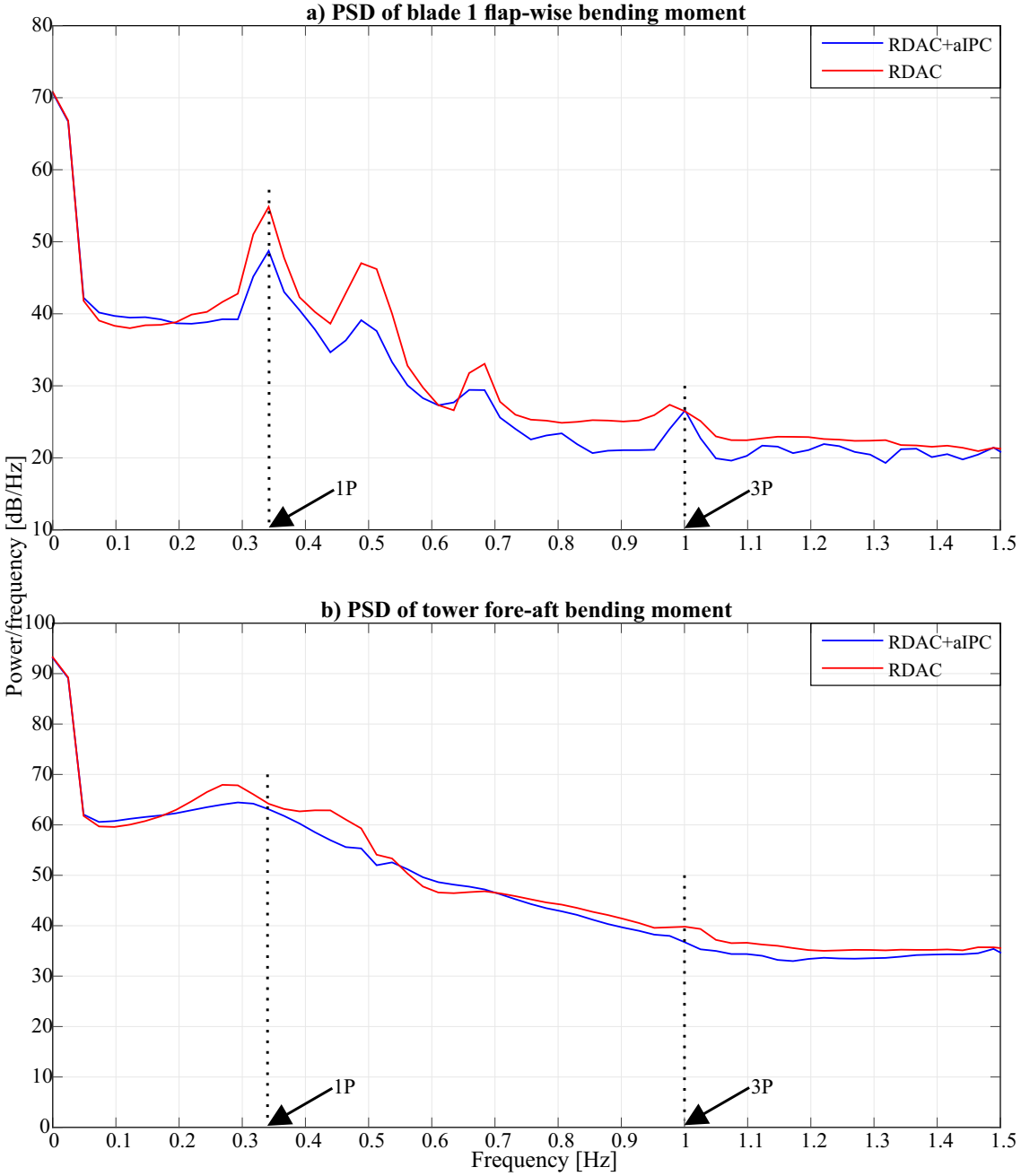

Figure 4.12: Spectral analysis of blade and tower loading [KDNS24]

Fatigue load analysis To evaluate fatigue loading, DEL evaluation with additional load channels is performed. Based on fatigue analysis carried out in MLife software [Hay12] using 10 minute simulation results, the proposed controller reduces blade F-W and tower F-A DELs in all wind fields as shown in Fig. 4.13. There is no significant improvement in blade edge-wise (E-W) DEL. However, a slight increase in tower side-side (S-S) DEL is observed. This is attributed to increased PA duty cycle when using of aIPC controller, which typically excites tower S-S vibration.

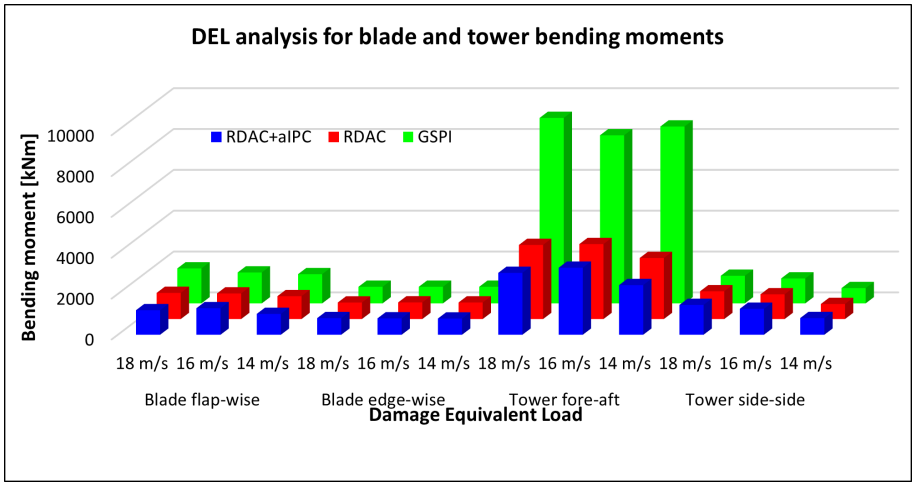

Figure 4.13: Damage equivalent load analysis [KDNS24]

4.1.5 Summary

A robust disturbance accommodating controller (RDAC), which is extended with a novel adaptive independent pitch controller (aIPC) is presented. This adaptive robust observer-based control concept (RDAC+aIPC) is used to reduce structural loads in both the tower and rotor blades without negatively affecting rotor speed control in WTs. The RDAC controller is designed to mitigate the tower load and to regulate rotor speed by minimizing the H_∞ norm of the mixed-sensitivity generalized WT system using the nonsmooth H_∞ synthesis approach. The aIPC controller is designed using the LQG method to attenuate asymmetric blade loads. Simulation results with different wind fields show that the proposed control approach performs significantly better in reducing structural loads in the rotor blades by 10.7 % and 9.2 % and in the tower by 36.2 % and 8.4 % compared with the GSPI and RDAC controllers, respectively. Fatigue analysis clearly shows a reduction of the DELs in most load channels. The control approach also exhibits improved speed control performance compared with the baseline GSPI controller, with the average MSE of the rotor speed reduced by 32.2 %. Although it shows a slight reduction in speed control under stochastic wind conditions in comparison with the RDAC controller, the improvement in load reduction far outweighs this trade-off.

The RDAC+aIPC controller shows overall superior performance in structural load reduction and speed control. It is robust to WT modeling errors and nonlinearities and adapts to operating point changes due to wind disturbances. The limitation of this control scheme is that the multi-objective optimization problem of regulating rotor speed and minimizing loads (in the blades and tower) is solved using a combination of the IPC and CPC control signals from aIPC and RDAC controllers, respectively. This could potentially lead to increased use of blade PAs. In addition, the control approach is evaluated on a smaller 1.5 MW RWT which is not representative of commercial WTs with higher power rating and larger physical size. These limitations are addressed by designing single-loop CPC- and IPC-based RDAC controllers, which are evaluated on a larger 5 MW RWT.

4.2 H_∞ RDAC applied to the 5 MW NREL reference WT

The H_∞ RDAC controller, first proposed in [DS22] and described in section 4.1, is evaluated on a small WindPACT 1.5 MW NREL RWT. In this section, the RDAC controller is redesigned and evaluated on the larger 5 MW NREL RWT [JBMS09], which reflects the current trend of commercial onshore WTs. The performance of the new RDAC controller, henceforth denoted as RDAC1, is benchmarked against the state-of-the-art (SOTA) baseline ROSCO controller described in section 3.2.2. This reference controller has features similar to those found in industry controllers. While ROSCO controller implements GSPI control for generator speed regulation, RDAC1 controller realizes both tower load mitigation and generator speed control in above-rated wind speed operation.

4.2.1 H_∞ RDAC design for the 5 MW NREL reference WT

The onshore NREL 5 MW RWT [JBMS09], which is domicile in OpenFAST software [NRE21], is selected for design and performance evaluation of the proposed control scheme. Specifications of this 3-bladed, upwind RWT are summarized in Table 3.2. A reduced-order model used to design the proposed RDAC1 controller is obtained by linearizing the nonlinear WT model (3.1) in OpenFAST around an operating point in the above-rated wind speed regime defined by 18 m/s hub-height wind speed, 12.1 rpm rated rotor speed, and related blade pitch angle of 14.6 °. Linearization is performed numerically in OpenFAST after steady-state is achieved, by linearizing the input-output coupling relations between modules in the OpenFAST glue-code around the specified operating point. All the linearized matrices are combined to form a full-system linear state-space model [JWHR19].

To capture relevant dynamics in the linear model for control design used to achieve desired closed-loop performance in terms of speed regulation and load reduction, six DOFs are enabled including first tower F-A and blade F-W bending modes, drive-train rotational flexibility, and generator motion. The linear state-space model used for control design is as expressed in (4.2). However, the measurements $y \in \mathbb{R}^{2x1}$ include generator speed ω_g and tower-base F-A bending moment ζ. The dynamic states $x \in \mathbb{R}^{11x1}$ related to the aforementioned DOFs selected in the 5 MW NREL RWT are given in (4.1). The design procedure for RDAC1 controller is similar to that of RDAC described in section 4.1.1. The unique information is highlighted below.

The proposed RDAC1 controller is applied to the 5 MW NREL RWT as shown in Fig. 4.14. The wind disturbance d excites the WT dynamics in above-rated operation. The controller relies on measured outputs including generator speed ω_g and tower F-A bending moment ζ, to generate a collective pitch angle u used to regulate ω_g to rated value $\omega_{g,rated}$ and to damp the first tower F-A vibration mode.

The weighting functions W_{11}, W_{12}, and W_2 are designed as transfer functions to achieve the desired performance in terms of closed-loop frequency response. To shape the desired profile of generator speed response and ensure robustness against wind disturbances, W_{11} is designed as an inverted HPF. To reduce tower F-A oscillation in the first mode TFA_1=2.06 rad/s, W_{12} is designed as an inverted notch filter centred at this frequency. Finally, W_2 is designed as an inverted LPF to reduce controller activity in high frequencies thereby increase robustness. In Figure 4.15, a Bode diagram of the open-loop transfer functions from wind speed to measurement outputs and the associated weighting functions is shown. As illustrated, $1/W_{11}$ and $1/W_{12}$ shape the respective open-loop responses to achieve the

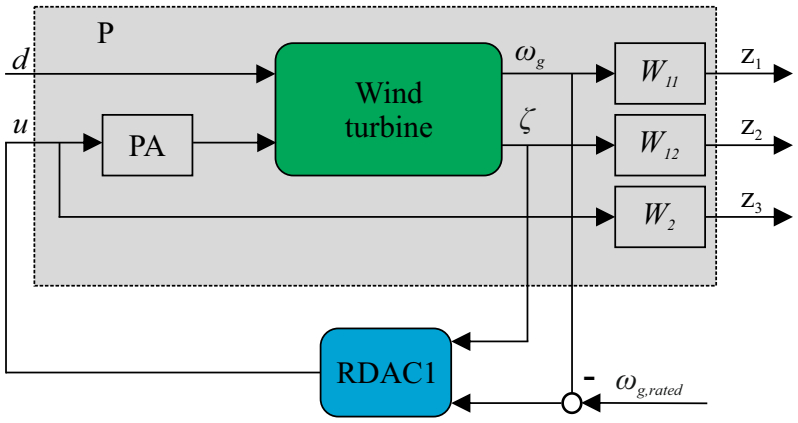

Figure 4.14: RDAC1 applied to the 5 MW NREL reference wind turbine [KDNS22]

desired closed-loop frequency response.

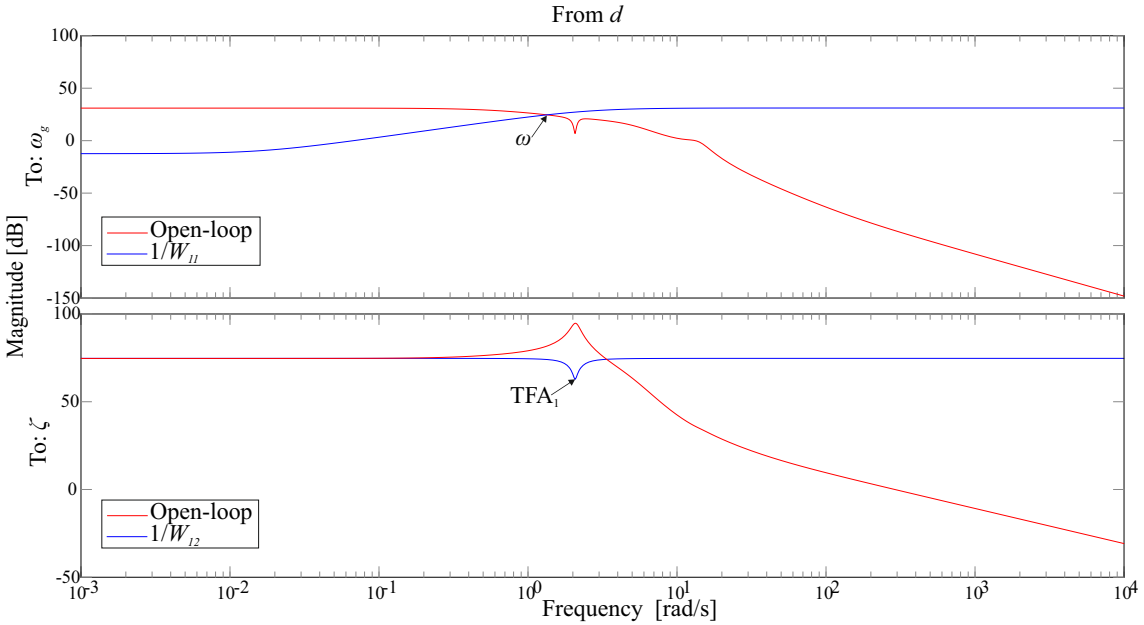

Figure 4.15: Bode plot of open-loop response and weighting functions for RDAC1 control design [KDNS22]

To account for the slow PA dynamics relative to other turbine dynamics, the WT model is supplemented with a PA modeled as a second order transfer function from the commanded pitch signal β_{com} to the actual pitch angle β expressed as

$$\beta = \frac{\omega_{PA}^2}{s^2 + 2\zeta\omega_{PA}s + \omega_{PA}^2}\beta_{com}, \tag{4.16}$$

where the natural frequency ω_{PA} is chosen to be four times the turbine's rated rotor speed $\omega_r = 1.267$ rad/s, and damping ratio ζ is 80% critical as recommended by NREL [RD18]. In [DS22; NS16; GC08], the actuator dynamics is modeled as a first-order lag filter that

simulates the time delay between β_{com} and β. In the proposed controller, a second order system is considered to improve transient response to stochastically varying wind field.

The generalized state-space system, which consists of the generalized plant P shown in Fig. 4.14 interconnected with the observer-based system (3.1) is implemented using lower LFT. Plant P contains fixed elements of the control architecture including the WT model, weighting functions, and PA. The observer-based system carries the tunable elements K_a, K_i, and L_a. Using nonsmooth H_∞ optimization, which minimizes the maximum singular value of the closed-loop transfer function from d to controlled outputs $[z_1\ z_2\ z_3]^T$, the RDAC1 controller is obtained. This controller is robust against modeling errors and disturbances and is used to regulate generator speed and reduce the amplitude of the first tower F-A vibration mode of the NREL 5 MW RWT using a CPC signal u.

4.2.2 Simulation results and discussion

The results from closed-loop dynamic simulations of 5 MW NREL RWT using ROSCO and RDAC1 controllers are discussed. Stochastic and step wind profiles are used to excite the WT dynamics in above-rated operation.

Step wind profile results

The step wind profile shown in Fig. 4.16 is used to evaluate control performance outside its design operating point. Hub-height wind speed varies in 2 m/s increments from 14 m/s to 22 m/s, which covers the WT's above-rated operation. To evaluate performance of the proposed RDAC1 controller in tower load mitigation, tower F-A bending moment is measured. As shown in Figure 4.17, RDAC1 controller achieves significant reduction in tower F-A bending moment compared with the baseline ROSCO controller. This is attributed to reduction of wind effect on the first tower F-A mode. To ascertain that this improvement does not compromise speed regulation performance, generator speed is evaluated. The proposed RDAC1 controller offers better performance expressed by improved transient response in changing wind speeds, as shown in Fig. 4.18.

4.2.3 Stochastic wind profile results

To evaluate the disturbance rejection performance of RDAC1 controller under more realistic wind conditions, a stochastic wind profile shown in Fig. 4.19 is used. The full-field IEC von Karman type B wind profile has a TI of 14.9 % and a mean hub-height speed of 18 m/s. In this scenario, the proposed controller shows better tower load mitigation response expressed by reduction in tower F-A bending moment variation in Fig. 4.20. The standard deviation is reduced by 34.6 %. In addition, RDAC1 controller shows improved generator speed regulation performance compared with ROSCO controller as shown in Fig. 4.21. A 41.7 % reduction in standard deviation is realized. This is attributed to the robustness of RDAC1 controller to wind disturbances. However, this improvement is accompanied by increased blade pitch activity leading to steady-state speed variations, especially in high wind speeds.

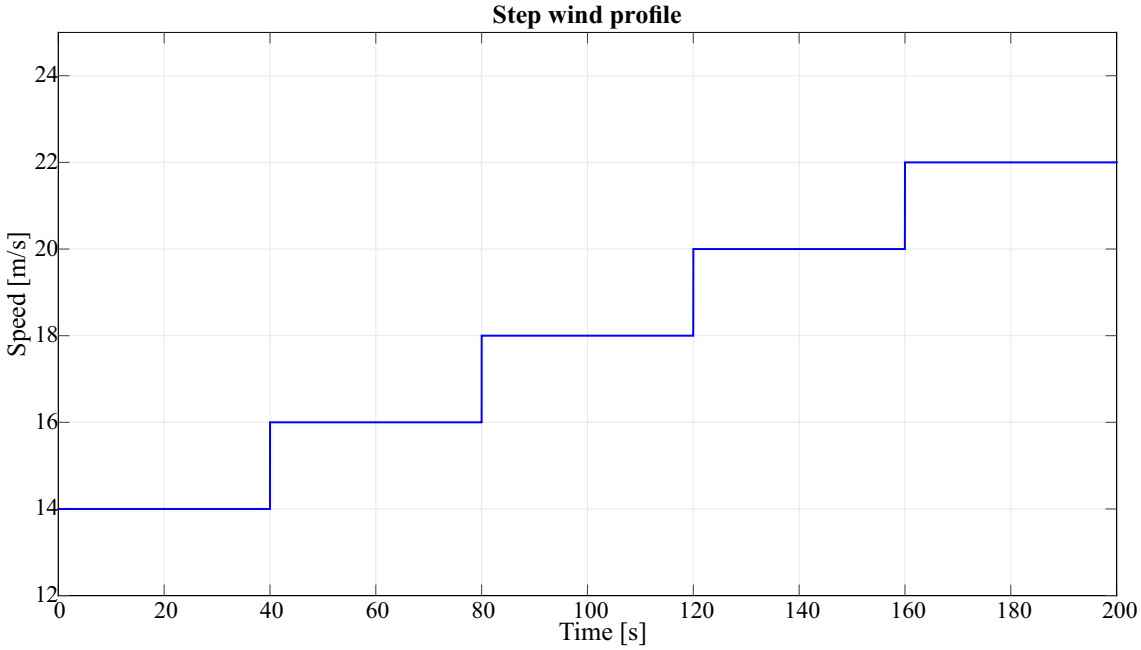

Figure 4.16: Step wind profile [KDNS22]

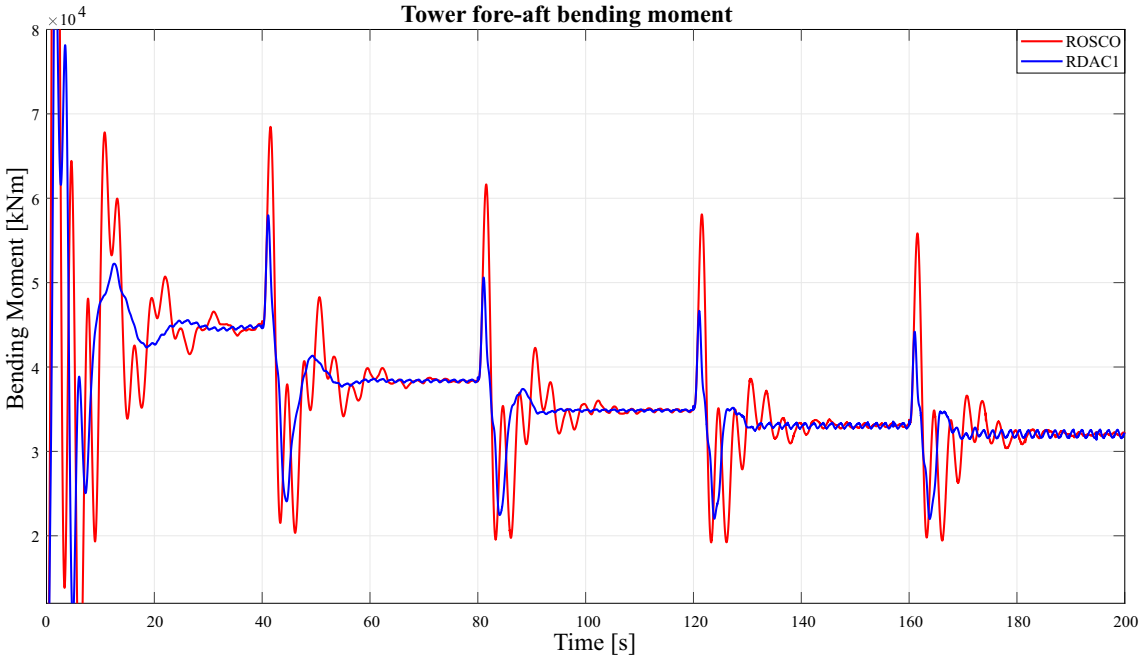

Figure 4.17: Tower load mitigation response to step wind profile [KDNS22]

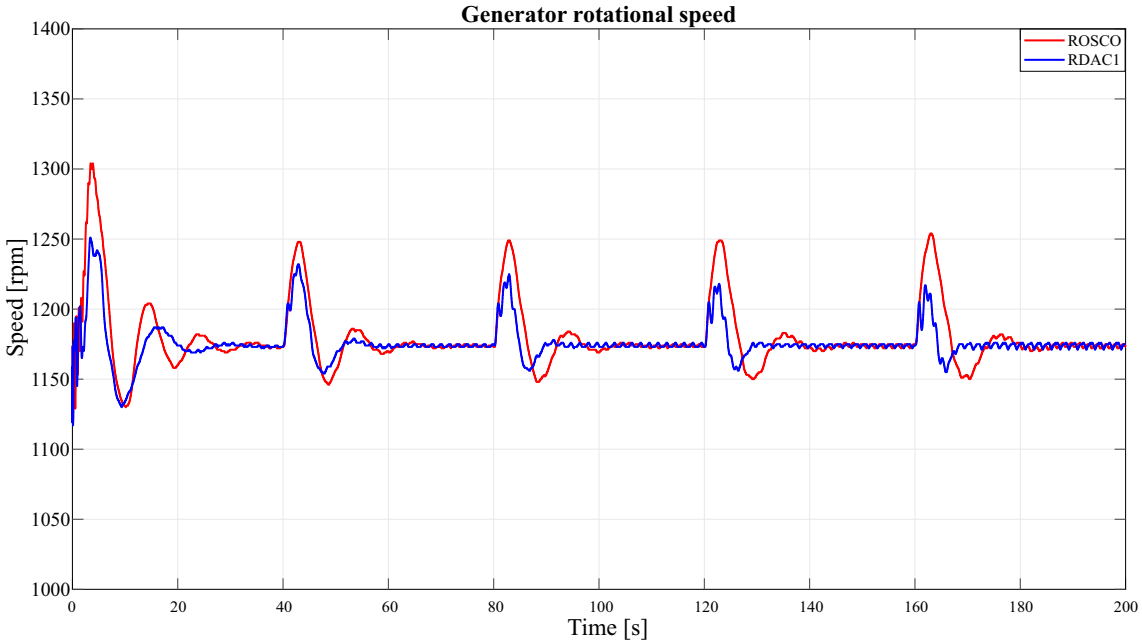

Figure 4.18: Generator speed regulation response to step wind profile [KDNS22]

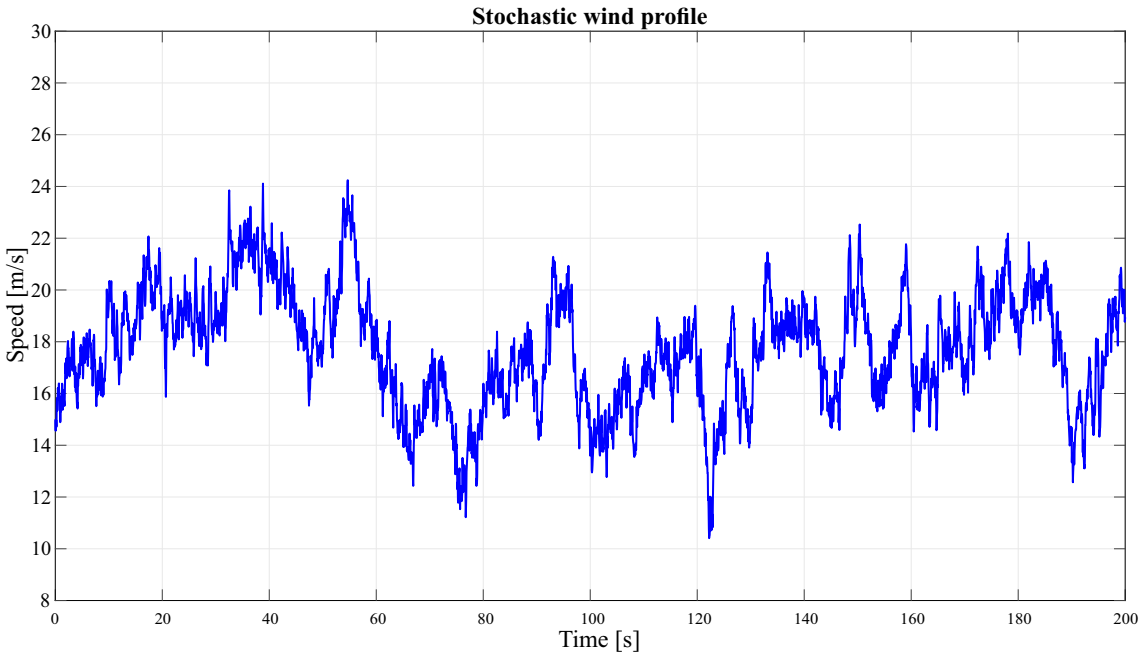

Figure 4.19: Stochastic wind profile [KDNS22]

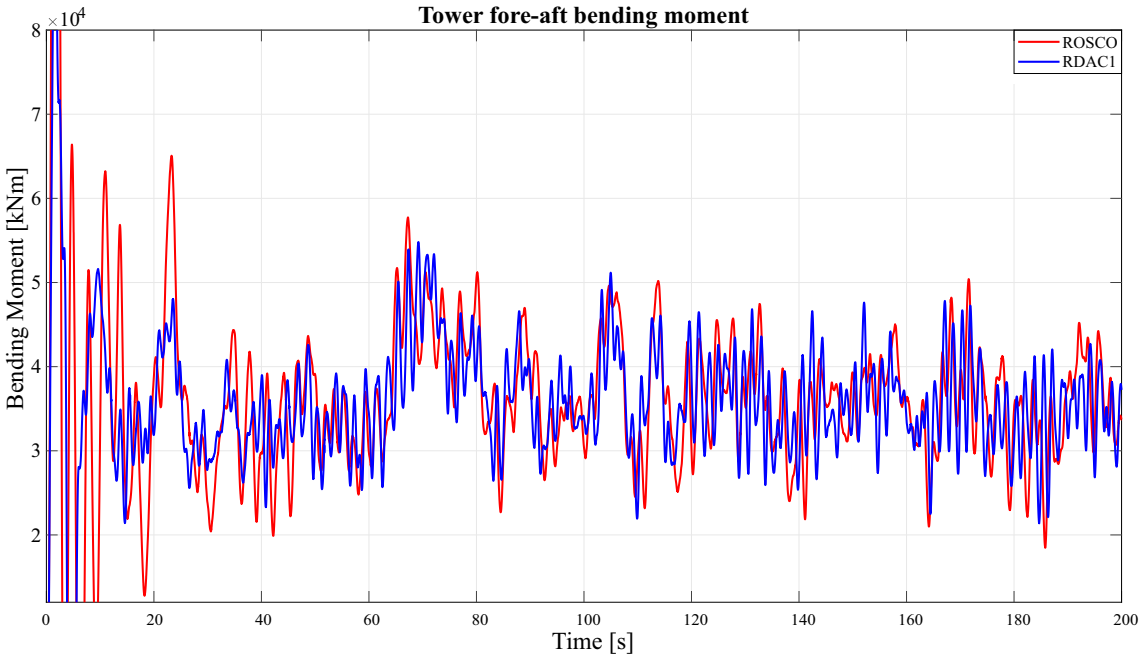

Figure 4.20: Tower load mitigation response to stochastic wind profile [KDNS22]

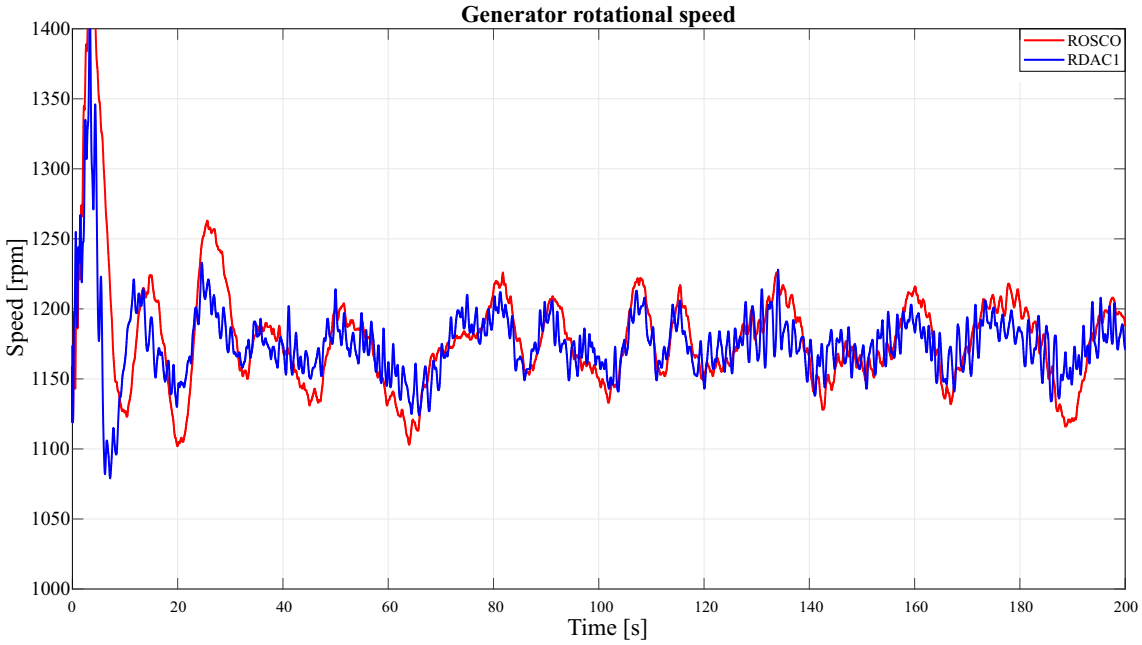

Figure 4.21: Generator speed regulation response to stochastic wind profile [KDNS22]

4.2.4 Summary

A robust disturbance accomodating controller designed for speed regulation and structural load mitigation of the onshore 5 MW NREL RWT is presented. The CPC-based RDAC1 controller is designed by minimizing the mixed-sensitivity H_∞ norm of the generalized WT system and is robust to modeling errors and nonlinearities caused by wind disturbances.

This controller is applied for the first time to the 5 MW NREL RWT. Compared with the CPC-based ROSCO baseline controller, simulation results show that the proposed control strategy reduces first-mode tower F-A vibration amplitude without significant compromise in generator speed regulation performance. The limitation of this H_∞-based RDAC1 controller is that uncertainties are assumed rather than modeled in the design process, resulting in conservative robustness. In addition, the use of CPC control limits its application to load mitigation in fixed frame WT components such as the tower. To address these limitations, an RDAC control approach that integrates uncertainty modeling in the design process is required for improved robust performance. Furthermore, IPC should be implemented for additional load mitigation in the rotor blades.

4.3 μ-synthesis RDAC approach

Robust controllers address system nonlinearities and modeling errors. However, most rely on nominal models without uncertainty description, resulting in conservative robustness. For instance, the RDAC1 controller described in section 4.2 is designed based on nonsmooth H_∞ synthesis [AN17], where a nominal model of the WT (4.2) is used in the design process. In this section, a μ-synthesis approach [Apk11] for designing the RDAC1 controller to improve robust performance is presented. A family of plants extracted from a nonlinear RWT at different operating points defined by wind speed enables the generation of an uncertainty description used for controller design. The efficacy of the new RDAC controller, henceforth denoted as RDAC2, is evaluated against RDAC1 and ROSCO controller [AZPW22] described in section 3.2.2. The μ-synthesis RDAC2 controller is applied to the 5 MW NREL RWT [JBMS09] to evaluate its closed-loop dynamic response in tower load mitigation and generator speed regulation in above-rated operation.

4.3.1 μ-synthesis RDAC design and implementation

Design of the μ-synthesis RDAC2 controller used to regulate the generator speed/power and reduce tower loads in the 5 MW NREL RWT is described. The process involves designing a generalized state-space system made up of a nominal WT model, actuator dynamics, weighting functions, and an observer-based control structure with tunable gains. In addition, an uncertainty description of the WT system is designed. By minimizing the structured singular value (SSV) μ, the tunable gains of the generalized state-space system with uncertainty description are synthesized using μ-synthesis approach.

The nonlinear model of the 5 MW NREL RWT described by (3.1) is linearized in OpenFAST software [NRE21] to obtain a reduced-order model used for designing the proposed controller. Linearization is performed by defining a steady-state operating point in the above-rated WT operation and selecting six DOFs to capture relevant dynamics in the LTI model corresponding to the desired closed-loop performance. The selected operating point and DOFs for linearization are same as those described in section 4.2.1.

The nominal model used for control design is as expressed in (4.2). However, the measurements $y \in \mathbb{R}^{2x1}$ include generator speed ω_g and tower F-A acceleration γ. The dynamic states $x \in \mathbb{R}^{11x1}$ related to selected DOFs are given in (4.1). Furthermore, an uncertain plant model is obtained by augmenting the nominal model (4.2) with plant uncertainty description to improve robust performance. The design procedure for RDAC2

controller is similar to that of RDAC described in 4.1.1. The difference is highlighted below.

The nominal model (4.2) defines the WT dynamics at a specific operating point defined by a hub-height wind speed of 18 m/s. In changing operating conditions, model uncertainties are expected to manifest as WT dynamics deviate from the model dynamics. To illustrate this, the open-loop frequency response of a sample of linear models obtained at different operating points (wind speeds of 14 m/s, 16 m/s, 20 m/s, and 22 m/s) is obtained as shown in Fig. 4.22. It can be seen that there is a noticeable variation in the responses between the nominal and uncertain models, particularly for the tower F-A acceleration at high frequencies above the rated rotor speed of 1.267 rad/s. Therefore, a description of these uncertainties should be included in controller design. Due to the modest variability in the frequency response of the uncertain models, the wind disturbance is assumed to produce an additive uncertainty.

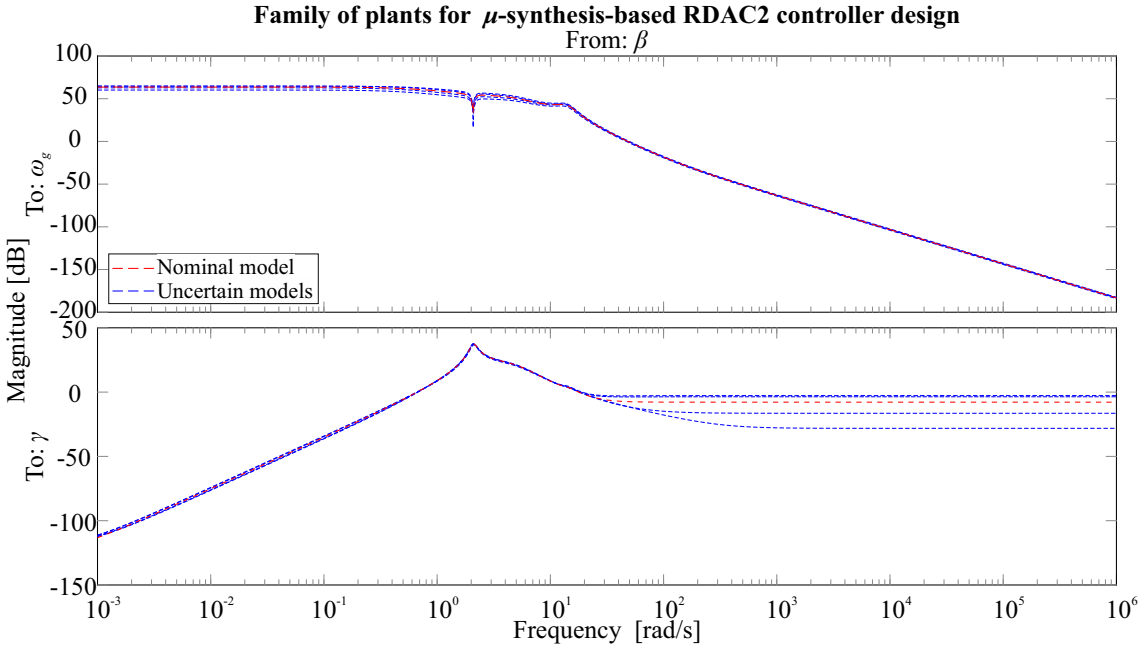

Figure 4.22: Comparison of open-loop frequency responses from collective pitch angle to measured outputs [KBS23]

The family of uncertain linear models (Fig. 4.22) is used to model an unstructured additive uncertainty description. Therefore, the frequency-dependent unstructured uncertainties resulting from unmodeled dynamics in the linearization process are included in the nominal plant model (4.2). In this way, an uncertain plant model $\tilde{G}$ of the form $\tilde{G} = G + W\Delta_a$ is obtained and used for controller design. Here, Δ_a denotes the uncertain dynamics with unit peak gain and W denotes a 2×2 diagonal shaping filter. The orders of individual diagonal elements are designed to adjust the degree of uncertainty at each frequency. This ensures that the gaps between the nominal and uncertain models are closely tracked, improving uncertainty estimation. In this thesis, the orders of each diagonal entry of W are designed to shape the uncertainty in the respective outputs y of the family of uncertain plants. The obtained uncertainty $\Delta = W\Delta_a$, which has a 2×2 block diagonal structure is used for designing the proposed RDAC2 controller. Structured or parametric

uncertainties, usually present at low frequencies as a result of plant perturbations [GC08] are not considered in this thesis. This is because in above-rated WT operation, variations in parameters of interest are small because the generator speed and power are regulated to their rated values.

μ-synthesis-based RDAC2 applied to the 5 MW NREL RWT

The proposed RDAC2 controller is applied to the 5 MW NREL RWT as shown in Fig. 4.23. The additive uncertainty Δ describes the variations between the nominal and uncertain family of plants in Fig. 4.22. Wind disturbance d excites the WT dynamics in above-rated operation. The generalized plant P, consisting of the nominal WT plant, PA, and weighting functions W_{11}, W_{12}, and W_2, is interconnected with the observer-based RDAC2 system (4.8) using lower LFT. On the other hand, upper LFT is used to interconnect P and Δ. The controlled outputs $\mathrm{z} = [\mathrm{z}_1 \ \mathrm{z}_2 \ \mathrm{z}_3]^T$ include the weighted measurements w_g and γ and control input u, respectively. The second order transfer function used to model the slow blade PA dynamics is described in section 4.2.1.

Using the DK-iteration process, the optimal RDAC2 is designed using μ-synthesis approach by minimizing SSV μ. The RDAC2 controller relies on generator speed ω_g and tower F-A translational acceleration γ to generate a CPC control input u for regulating generator speed to its rated value $\omega_{g,rated}$ and for damping the first-mode tower F-A vibration.

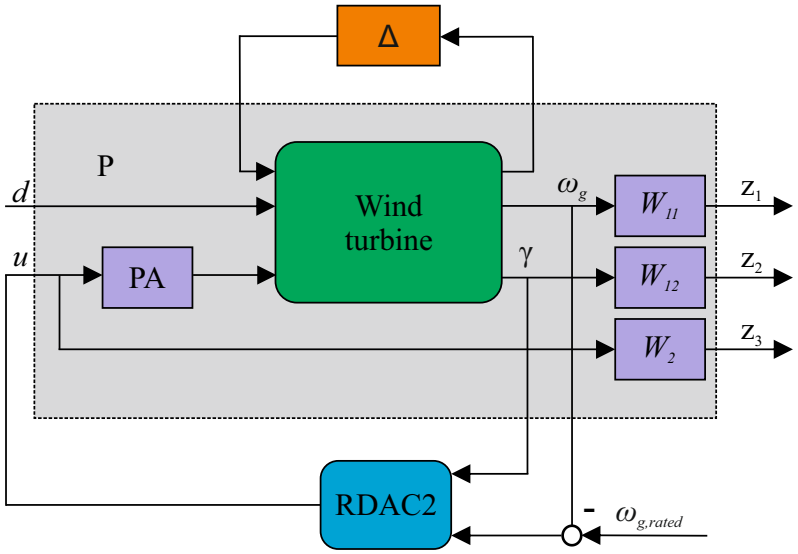

Figure 4.23: RDAC2 controller applied to the 5 MW NREL wind turbine model [KBS23]

Robust performance is dictated by appropriate selection of weighting functions. Closed-loop characteristics are shaped using the desired weighting functions that are rational, stable, and minimum phase [Sko05]. Therefore, the frequency-dependent weighting functions W_{11}, W_{12}, and W_2 are designed to shape system measurement signals and control input to achieve the desired closed-loop frequency response. In Figure 4.24, Bode diagrams of the open-loop transfer functions from wind disturbance d to measurement outputs compared with associated inverted weighting functions $1/W_{11}$ and $1/W_{12}$ are shown. A singular

value (SV) plot from control input β to the tower F-A acceleration γ compared with W_2 is also shown. As illustrated, $1/W_{11}$ and $1/W_{12}$ shape the respective open-loop responses to achieve the desired closed-loop frequency responses. To effect the generator speed response while ensuring robustness to wind disturbances, W_{11} is designed as an inverted HPF. To damp the first tower F-A vibration mode, W_{12} is designed as an inverted notch filter centred at this frequency TFA_1=2.08 rad/s. To reduce controller activity in high frequencies and thus increase robustness, W_2 is designed as an inverted LPF, with control bandwidth being limited to effect the desired frequency TFA_1.

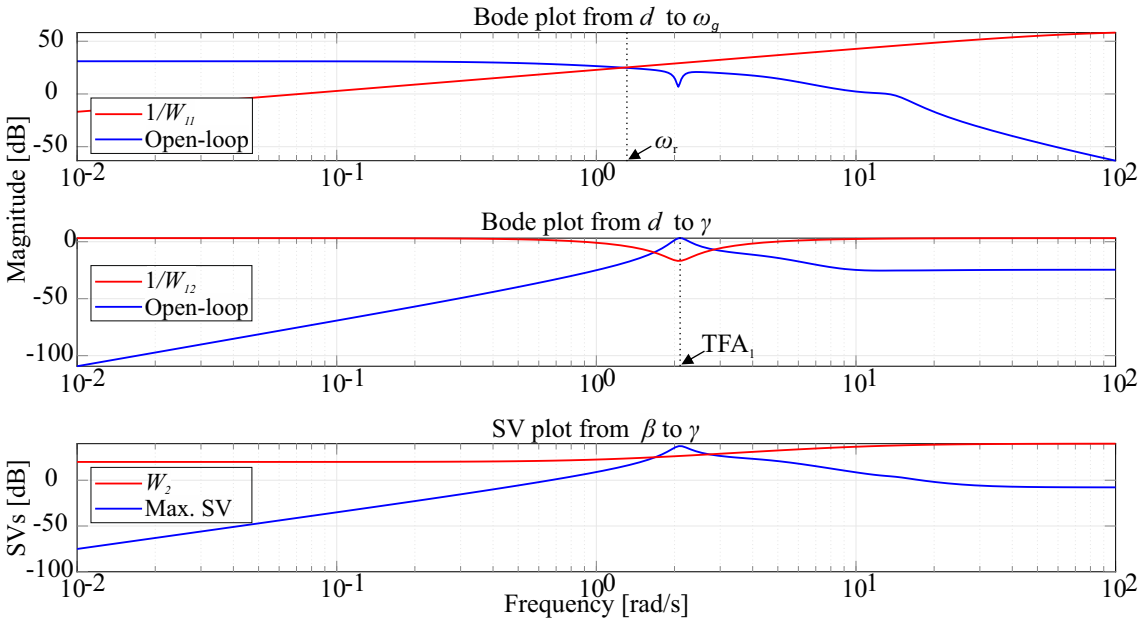

Figure 4.24: Comparison of open-loop frequency responses and weighting functions used in RDAC2 control design [KBS23]

The upper LFT $F_u(M, \Delta)$ in Fig. 4.23 consists of the transfer function M from the output to the input of the perturbation Δ, both of which are stable. The lower LFT $N = F_l(P, RDAC2)$ interconnects the plant P with the observer-based $RDAC2$ controller. For robust stability (RS), an RDAC2 controller can be obtained if the system remains stable for all uncertain plants shown in Fig. 4.22. Robust performance (RP) is guaranteed if RS condition is met and in addition, the performance objective can be achieved for all possible plants in the uncertainty set, including the worst-case plant. These criteria are expressed as

$$RS \Leftrightarrow F_u(M, \Delta) \text{ is stable for } \forall \Delta, \| \Delta \|_\infty \leq 1; \text{and NS}, \tag{4.17}$$

$$RP \Leftrightarrow \| F_l(N, \Delta) \|_\infty < 1 \text{ for } \forall \Delta, \| \Delta \|_\infty \leq 1; \text{and NS}, \tag{4.18}$$

where NS denotes nominal stability.

From small gain theorem, RS is expressed as

$$RS \Leftarrow \bar{\sigma}(M) < 1 \, \forall \omega, \tag{4.19}$$

which is a tight condition for any case of complex Δ satisfying $\bar{\sigma} \leq 1$. A more general tight condition is given as

$$RS \Leftrightarrow \mu(M) < 1 \, \forall \omega, \tag{4.20}$$

where the real non-negative $\mu(M)$ is the SSV which is expressed as

$$\mu(M) = \frac{1}{\min\{k_m | \det(I - k_m M\Delta) = 0}, \tag{4.21}$$

for structured Δ, $\bar{\sigma} \leq 1$. If no structured uncertainty Δ exists then $\mu(M) = 0$. The factor k_m is used to scale the uncertainty Δ to make the matrix $I - k_m M\Delta$ singular, hence the SSV is expressed as $\mu(M) = 1/k_m$ [Sko05].

Therefore, μ-synthesis is a important tool for RP analysis. To synthesize a controller to minimize a given μ condition, a scaled version of μ is needed [MNP11]. To synthesize an optimal RDAC2 controller that minimizes μ by guaranteeing RP and RS, the DK-iteration process is used in this thesis. The process solves a sequence of scaled H_∞ problems by using frequency-dependent scaling matrices, D and G, which take advantage of the uncertainty structure. First, nonsmooth H_∞ synthesis [AN17] is used to obtain an RDAC controller that minimizes the closed-loop gain of the nominal plant P. The process is summarized as

$$\min_{RDAC} (\min_{D \in \mathcal{D}} \parallel DN(RDAC2)D^{-1} \parallel_\infty). \tag{4.22}$$

In the D-step, the robust H_∞ performance of the closed-loop system using the current RDAC2 controller is estimated. The upper bound $\bar{\mu}$ of the robust H_∞ performance of RDAC2 is then computed using a suitable $D(j\omega)$ scaling which commutes with Δ. Rational functions $D(s)$ of a specified order are used to fit the $D(j\omega)$ scaling, yielding the scaled H_∞ norm μ_F. In the K step, a controller $RDAC2^*$ that minimizes μ_F to improve the robust performance obtained in the D-step is synthesized. The iterative process is repeated until no further improvement in μ is achieved by the optimal controller $RDAC2^*$. In this thesis, only D scaling is used because wind disturbance is assumed to produce a complex additive uncertainty.

4.3.2 Simulation results and discussion

The results from closed-loop dynamic simulations of the 5 MW NREL RWT with the baseline ROSCO, RDAC1, and the proposed RDAC2 controllers are discussed. Various stochastic wind fields excite the WT dynamics in the high wind speed region of interest.

Structural Load Mitigation

In Figure 4.25(a), the three stochastic wind profiles used in the simulations are shown. The 10-minute long full-field wind fields are based on the Kaimal spectral model. To obtain more representative results, various combinations of random seeds, mean wind speeds, and TIs are considered. In Figure 4.25(b), tower load mitigation response is shown. Compared with ROSCO, the proposed RDAC2 controller shows improved performance. In Table 4.6, the performance analysis of tower F-A and blade F-W moments is given. As shown, the average (for all wind fields) δ in the tower F-A moment reduces by 11.6 %. However, RDAC1 shows the best performance with a 14.8 % reduction in δ. It is important to evaluate the load mitigation performance in other load structures. The blade F-W load response is evaluated because it is the main blade structural load channel in above-rated operation. As illustrated in Fig. 4.25(c), the proposed controller shows insignificant performance deterioration compared with ROSCO, with the average δ slightly increasing by 0.95 %. In addition, RDAC2 exhibits better performance compared with RDAC1 as δ reduces by 4.8 %.

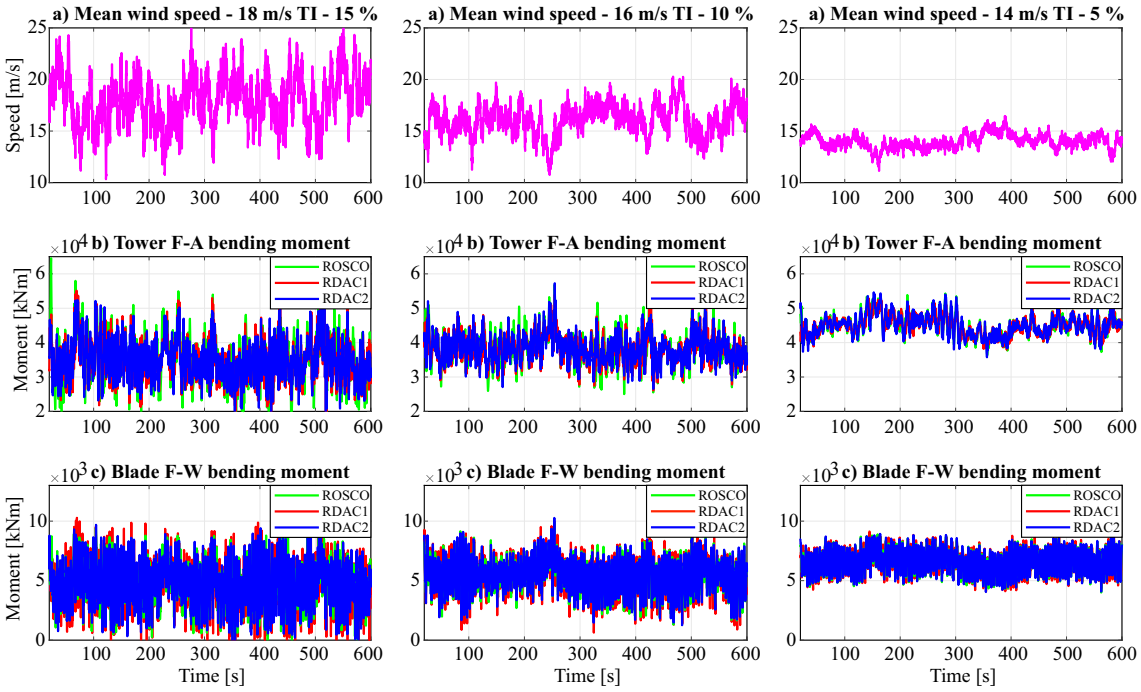

Figure 4.25: Tower and blade load mitigation response [KBS23]

Table 4.6: Load mitigation performance analysis (Key: best, worst) [KBS23]

Load channel [kNm]	Controller	18 m/s	16 m/s	14 m/s	Avg.	%
Tower F-A (δ)	ROSCO	6632.5	4758.7	3013	4801.4	-
	RDAC1	5610.4	3948.9	2706.9	4088.7	-14.8
	RDAC2	5658.4	4042.4	3039.2	4246.7	-11.6
Blade F-W (δ)	ROSCO	1805.8	1375.2	988.8	1389.9	-
	RDAC1	1972.8	1450.7	998.8	1474.1	6.1
	RDAC2	1836.2	1374.1	999.3	1403.2	0.95

Speed/Power Regulation

Using a CPC control input, the proposed RDAC2 controller is also designed to regulate the WT's generator speed to its rated speed of 1173.7 rpm. To achieve both speed regulation and load mitigation using the same control input, a trade-off between these two conflicting objectives is required. As illustrated in Fig. 4.26(a), the RDAC1 and RDAC2 controllers exhibit higher blade pitch usage to achieve both objectives. However, the proposed controller has a smaller increment in pitch usage compared with ROSCO. Pitch control effort is limited to avoid violation of the WT's PR constraint. In Table 4.7, the performance analysis in PR and generator speed/power is given. The average RMS value of PR is 0.37 $^\circ/s$, 4.78 $^\circ/s$, and 2.23 $^\circ/s$ for the ROSCO, RDAC1, and RDAC2 controllers, respectively. Therefore, the proposed controller does not violate the turbine's maximum PR constraint of 8 $^\circ/s$. Speed regulation performance is also evaluated as shown in Fig. 4.26(b). The proposed RDAC2 controller realizes the best generator speed regulation, with the average δ reducing by 42.6 % and 11.9 % compared with ROSCO and

RDAC1, respectively. Furthermore, the MSE reduces by 72.1 % and 25.8 %, respectively. In Figure 4.26(c), power regulation performance is illustrated. The proposed controller exhibits improved performance compared with RDAC1, with δ and MSE decreasing by 32.6 % and 55.7 %, respectively. However, a slight reduction in performance is realized against ROSCO, with δ and MSE values increasing by 7.1 % and 13.6 %, respectively. Although a slight reduction in power regulation is realized, this is an expected consequence of the trade-off between speed regulation and load mitigation, which results in the proposed RDAC2 controller achieving better generator speed regulation compared to ROSCO and RDAC1 controllers.

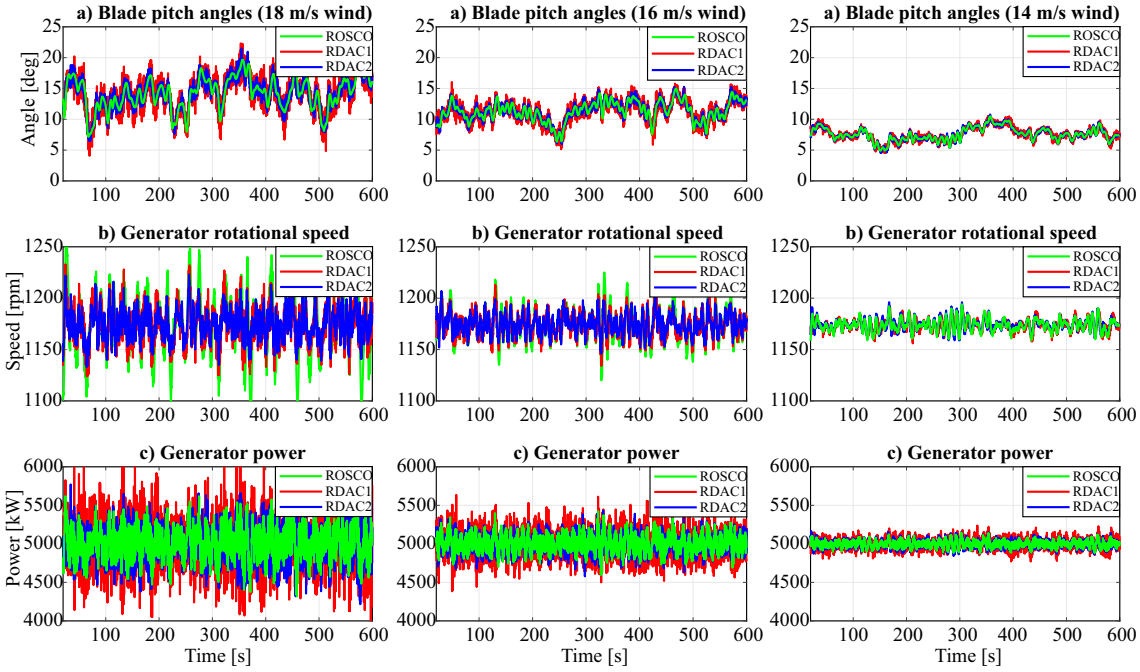

Figure 4.26: Pitch usage and generator speed/power regulation response [KBS23]

4.3.3 Summary

A robust disturbance accommodating controller for structural load reduction and speed regulation of the 5 MW NREL onshore RWT is presented. The CPC-based controller is designed using the μ-synthesis approach following the DK-iteration process. The synthesis is performed by minimizing the structured singular value μ of the generalized WT system, which consists of an uncertain WT plant, a PA system, and weighting functions. Compared with the baseline GSPI-based ROSCO and H_∞ RDAC controllers, simulation results show that the proposed controller achieves optimal performance in reducing tower loads and regulating generator speed without violating the turbine's maximum PR constraint. In addition, the controller does not induce significant loading in the blades. Despite improved performance, the proposed controller is based on CPC, hence blade load mitigation is not considered as this can only be realized via IPC. Therefore, an IPC-based RDAC controller should be designed to realize load mitigation in the blades. To apply the μ-synthesis RDAC2 controller for control of WTs operating in below-rated wind speeds, plant

Table 4.7: Pitch usage and generator speed/power regulation performance analysis (Key: best, worst) [KBS23]

Parameter	Units	Controller	18 m/s	16 m/s	14 m/s	Avg.	%
Speed (δ)	rpm	ROSCO	30.67	15.8	6.04	17.5	-
		RDAC1	17.54	11.07	5.56	11.39	-34.9
		RDAC2	14.61	9.62	5.88	10.04	-42.6
Speed (MSE)	rpm	ROSCO	943.8	250.4	36.49	410.2	-
		RDAC1	307.9	122.6	30.94	153.8	-62.5
		RDAC2	214.5	93.33	34.71	114.2	-72.1
Power (δ)	kW	ROSCO	190.2	104.2	40.12	111.5	-
		RDAC1	304.1	165.7	61.91	177.3	58.9
		RDAC2	204.0	107.3	47.21	119.9	7.1
Power (MSE)	kW	ROSCO	36236	10879	1610	16242	-
		RDAC1	92497	27473	3833	41268	154.1
		RDAC2	41613	11528	2230	18457	13.6
PR (RMS)	°/s	ROSCO	0.5136	0.3738	0.2178	0.3684	-
		RDAC1	7.947	4.486	1.895	4.776	1200
		RDAC2	4.09	1.912	0.693	2.231	510

parametric uncertainties that occur especially in below-rated WT operation, should be combined with unstructured uncertainties usually occuring at high frequencies to obtain a lumped uncertainty description for improved robust performance.

4.4 IPC-based μ-synthesis RDAC approach

A majority of robust controllers for structural load mitigation in WTs are based on collective pitch control (CPC). Therefore, structural load in WT rotor blades is not addressed. Despite performance improvements, the robust controllers described in sections 4.2 and 4.3 provide load mitigation in a single structural component, namely the tower. Although the controller described in section 4.1 is used for load mitigation in both the tower and blades, this is achieved through separate CPC and IPC control loops. This could result in high PA usage and overall system optimality is not guaranteed. To address these challenges, an IPC-based RDAC controller, henceforth denoted as IPC-RDAC for regulating generator speed and reducing structural loads in both the blades and tower using a single control loop is described in this section. It uses IPC to actively damp fatigue loading in rotor blades and tower by compensating for asymmetric wind inflow conditions. The IPC-RDAC controller is designed using μ-synthesis approach [Apk11] described in section 4.3.1. The description of model uncertainties is derived from a family of plants. The closed-dynamic dynamic response of IPC-RDAC is evaluated on the 5 MW NREL RWT [JBMS09]. The performance of this RDAC approach is evaluated against baseline ROSCO [AZPW22] and RDAC1 controllers described in sections 3.2.2 and 4.2.1, respectively.

4.4.1 IPC-based RDAC design and implementation

To obtain a reduced-order model used for designing the IPC-RDAC controller, the nonlinear model (3.1) is linearized in OpenFAST software [NRE21] around a steady-state operating

point in the above-rated wind speed region defined by a 18 m/s steady wind speed, 12.1 rpm rated rotor speed, and associated blade pitch angle of 14.6 °. Six DOFs described in section 4.2.1 are selected to capture relevant dynamics in the LTI model corresponding to the desired closed-loop performance. To design an independent pitch controller to mitigate periodic aerodynamic loading due to vertical wind shear, 36 equispaced rotor azimuth positions are selected in the linearization process. The obtained 36 linear models, which capture this periodicity are expressed in state-space form as

$$\begin{aligned} \dot{x}_m &= A_m(\psi)x_m + B_m(\psi)u_m + B_{d_m}(\psi)d \\ y_m &= C_m(\psi)x_m, \end{aligned} \tag{4.23}$$

where $A_m \in \mathbb{R}^{11x11}$, $B_m \in \mathbb{R}^{11x3}$, $B_{d_m} \in \mathbb{R}^{11x1}$, and $C_m \in \mathbb{R}^{4x11}$ denote the azimuth (ψ) -dependent system, control input, disturbance, and output matrices, respectively, all of which lie in the mixed coordinate frame. The perturbed independent pitch angles $[\Delta\beta_1\, \Delta\beta_2\, \Delta\beta_3]^T$ are denoted by $u_m \in \mathbb{R}^{3x1}$, and $d \in \mathbb{R}^{1x1}$ denotes the perturbed hub-height wind speed Δv. The measurements $y_m \in \mathbb{R}^{4x1}$ include generator speed ω_g and blade-root F-W bending moments ζ_1, ζ_2, and ζ_3. The dynamic states $x_m \in \mathbb{R}^{11x1}$ include the enabled DOFs displacements and their respective velocities.

In OpenFAST, the dynamics of the rotor blades are expressed in the rotating coordinate frame. To model the coupled dynamics of the tower-nacelle subsystem expressed in the fixed frame and the spinning rotor, MBC transformation [Bir10] is used to transform individual blade dynamics to the non-rotating frame. This transformation yields a model that describes WT coupled dynamics in the fixed frame, effectively facilitating IPC controller design. After performing MBC transformation, the obtained azimuth-dependent reduced-order models are averaged to obtain a weakly periodic linear model expressed as

$$\begin{aligned} \dot{x} &= Ax + Bu + B_d d \\ y &= Cx, \end{aligned} \tag{4.24}$$

where A, B, B_d, and C denote the system, input, disturbance, and output matrices, respectively. The measurements y include generator speed ω_g and the MBC transformed average, tilt, and yaw blade-root F-W bending moments ζ_{avg}, ζ_{tilt}, and ζ_{yaw}, respectively. The LTI model (4.24) is used to design the proposed IPC-RDAC controller.

The MBC transformation of the blade F-W moments from the rotating to the fixed frame is expressed as

$$\begin{bmatrix} \zeta_{avg} \\ \zeta_{tilt} \\ \zeta_{yaw} \end{bmatrix} = T(\psi) \begin{bmatrix} \zeta_1 \\ \zeta_2 \\ \zeta_3 \end{bmatrix}, \tag{4.25}$$

where

$$T(\psi) = \frac{2}{3} \begin{bmatrix} \frac{1}{2} & \frac{1}{2} & \frac{1}{2} \\ \cos(\psi) & \cos(\psi + \frac{2}{3}\pi) & \cos(\psi + \frac{4}{3}\pi) \\ \sin(\psi) & \sin(\psi + \frac{2}{3}\pi) & \sin(\psi + \frac{4}{3}\pi) \end{bmatrix} \tag{4.26}$$

is the transformation matrix. Here, ζ_{avg} denotes the symmetric moment, which represents the average bending moments at the blade-roots caused by the out-of rotor plane flapping of the rotor blades in unison, while ζ_{tilt} and ζ_{yaw} are asymmetric moments induced by tilt and yaw motions, respectively.

The design procedure for the IPC-RDAC controller is similar to that of RDAC described in section 4.1.1. The robust H_∞ control approach based on μ-synthesis [Apk11] described in section 4.3.1 is used to design the IPC-RDAC controller for load mitigation and speed regulation of the 5 MW NREL RWT. The uniqueness of this proposed control approach is highlighted below.

Open-loop response of the wind turbine model

The linear model (4.24) from MBC transformation is obtained from a specific operating point. However, model uncertainties are to be expected during operation due to variations in WT dynamics outside the design operating point of 18 m/s hub-height wind speed. Therefore, this uncertain behavior should be modeled. This is illustrated in Figure 4.27, where the range of open-loop frequency response behavior is captured using a sample of linear models obtained from a selection of operating points defined by 14 m/s, 16 m/s, 20 m/s, and 22 m/s wind speeds. In this thesis, only these frequency-dependent unstructured uncertainties resulting from unmodeled dynamics related to changes in turbine operating points are considered.

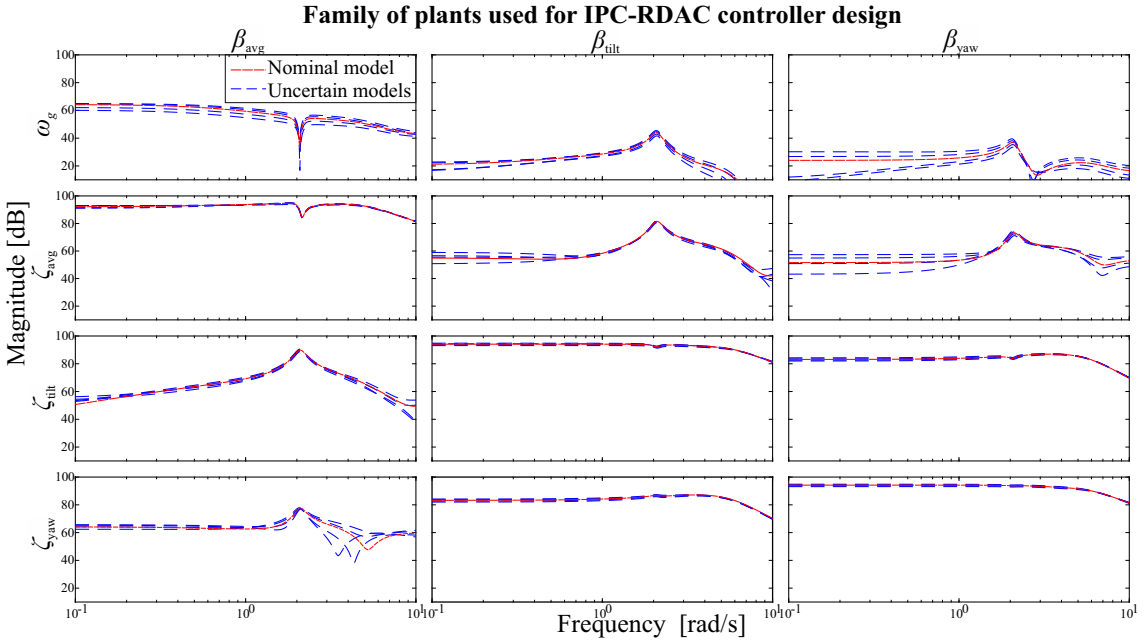

Figure 4.27: Comparison of open-loop frequency responses from pitch commands to measured outputs between nominal model and uncertain models [KS24]

The average (CPC) pitch command β_{avg} strongly influences generator speed ω_g and the average blade F-W moment ζ_{avg} as seen in larger magnitudes of the associated frequencies. It also has a strong influence on the first tower F-A frequency, which is reflected in the response peaks of ζ_{tilt} and ζ_{yaw} blade moments at 2.07 rad/s. The pitch commands β_{tilt} and β_{yaw}, which are responsible for mitigating asymmetric load on the blades, have a greater influence on ζ_{tilt} and ζ_{yaw} moments, respectively. Given the differences between the frequency responses of the nominal model and the uncertain models especially at high frequencies above the rated rotor speed $\omega_r = 1.267$ rad/s, relying only on the nominal

model obtained at 18 m/s would lead to high model-system mismatch.

Wind disturbances are assumed to generate additive uncertainty because the frequency responses of the family of uncertain plants produce modest variability compared with the nominal model. Therefore, these frequency responses are modeled using unstructured additive uncertainty and combined with the nominal WT plant G (4.24), yielding an uncertain plant $\tilde{G}$ of the form $\tilde{G} = G + W\Delta_a$, where Δ_a denotes the uncertain dynamics with unit peak gain and W denotes a 4×4 diagonal shaping filter. The orders of each diagonal entry of W are designed to shape the uncertainty in the respective outputs y of the family of uncertain plants. The obtained uncertainty $\Delta = W\Delta_a$, which has a 4×4 block diagonal structure is used to design the proposed IPC-RDAC controller.

IPC-based RDAC approach applied to the 5 MW NREL RWT

The proposed IPC-RDAC controller is applied and therefore used to control the 5 MW NREL RWT as shown in Fig. 4.28. The model-system mismatch due to variations in operating point is modeled as unstructured additive uncertainty Δ. Wind disturbance d excites the WT dynamics in above-rated operation. The generalized plant P, which consists of a combination of nominal WT plant, PA, and weighting functions W_{xy}, is interconnected with the observer-based IPC-RDAC system (4.8) using lower LFT, and Δ using upper LFT. The controlled outputs $\mathrm{z}=[\mathrm{z}_1\ \mathrm{z}_2\ \mathrm{z}_3\ \mathrm{z}_4\ \mathrm{z}_5\ \mathrm{z}_6\ \mathrm{z}_7]^T$ consist of the weighted generator speed, average, tilt, and yaw blade F-W bending moments, and weighted control signals. The IPC-RDAC controller relies on the generator speed ω_g and the MBC transformed blade F-W bending moments ζ_{avg}, ζ_{tilt}, and ζ_{yaw} to generate independent pitch angles $[\beta_{avg}\, \beta_{tilt}\, \beta_{yaw}]^T$. Inverse MBC transformation matrix $T(\psi)^{-1}$ transforms these control signals back to the rotating coordinate system to obtain IPC signals u. The optimal H_∞ structured controller IPC-RDAC is designed using DK-iteration process based on μ-synthesis by minimizing the SSV μ as described in section 4.3.1.

To account for slow PA dynamics relative to other turbine dynamics, the WT model is supplemented with a PA for each blade, modeled as a second order transfer function from the commanded individual pitch angle β_{com} to the actual pitch angle β. The PA model is described in section 4.2.1. Its parameters are designed as recommended by NREL [RD18]. The individual pitch angles are used to regulate generator speed to its rated value $\omega_{g,rated}$ and to damp the first-mode tower F-A vibration, average blade F-W mode, and asymmetric blade F-W vibrations, which include tilt and yaw F-W motions. This reduces the tower F-A load and damps the symmetric and asymmetric blade F-W load at 2P, 3P, and 4P frequencies. This is achieved by designing suitable weighting functions.

Weighting function selection

Periodic loading of WT structures are manifested as harmonics of the rotor frequency. The MBC transformation converts the 1P, 2P, 3P,... frequencies in the rotating frame to 0P, 3P, 6P,... frequencies in the fixed frame [SMBN09], as shown in Table 4.8. In this thesis, 2P, 3P, and 4P frequencies in the rotating frame are counteracted by designing appropriate weighting functions for shaping the respective closed-loop transfer function from the wind disturbance d to blade F-W bending moments ζ_{avg}, ζ_{tilt}, and ζ_{yaw}. Reduction at the stated frequencies is considered as these are close to the natural frequencies of the blades and tower shown in Table 4.9. Due to the blade PA bandwidth limitation, frequencies beyond

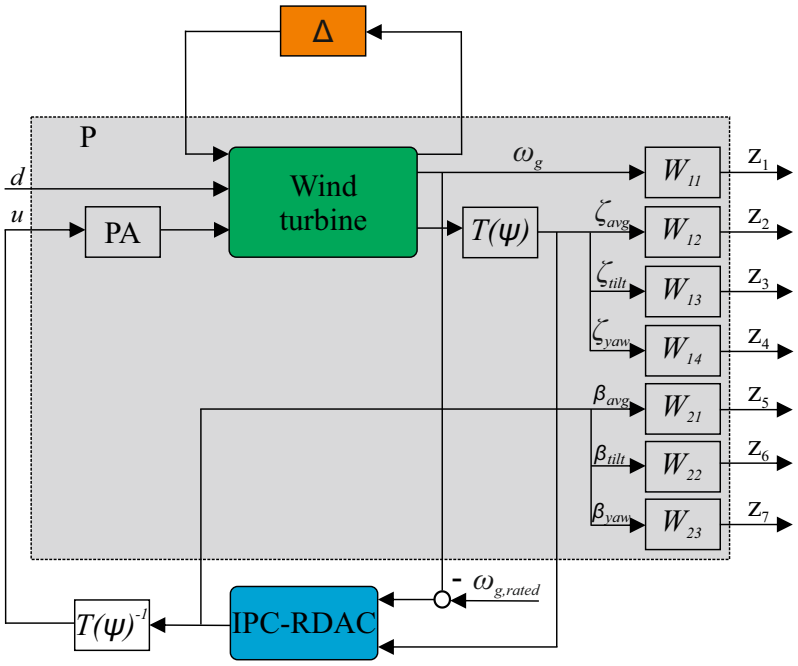

Figure 4.28: Block configuration of IPC-RDAC controller applied to the 5 MW NREL reference wind turbine [KS24]

4P are usually not considered in turbine control design.

Table 4.8: Correspondence of harmonics in rotating and fixed frames [KS24]

Rotating frame	Fixed frame
1P	0P @ ζ_{tilt} and ζ_{yaw}
2P	3P @ ζ_{tilt} and ζ_{yaw}
3P	3P @ ζ_{avg}
4P	3P @ ζ_{tilt} and ζ_{yaw}
5P	6P @ ζ_{tilt} and ζ_{yaw}
6P	6P @ ζ_{avg}
7P	6P @ ζ_{tilt} and ζ_{yaw}

To design the weighting functions, knowledge of the natural frequencies of the blades and tower components at different modes of vibration is crucial. The natural frequecies of the 5 MW NREL RWT are given in Table 4.9. The frequency-dependent weighting functions W_{11}, W_{12}, W_{13}, W_{14}, W_{21}, W_{22}, and W_{23} are designed and imposed on respective measurement signals or system inputs to achieve the desired closed-loop frequency response. To effect the generator speed response and to ensure robustness against wind disturbances, W_{11} is designed as an inverted HPF with the frequency at which W_{11}^{-1} crosses the open-loop response being adjusted to 0.1396 rad/s, which corresponds to the turbine's maximum PR, hence avoids violation of the turbines PR constraint [GC08]. To reduce vibrations in the tower and rotor blades, W_{12}, W_{13}, and W_{14} are designed as inverted notch filters centred at the respective frequencies. To reduce vibration at 3P frequency (3.8 rad/s) in both the fixed and rotating frames, the notch in filter W_{12} is centred at the 3P frequency.

Filters W_{13} and W_{14} have two notches centred at the first tower F-A frequency (2.07 rad/s) and at 3P frequency, which corresponds to 2P and 4P frequencies in the rotating frame. To reduce the controller activity in high frequencies and thereby increase robustness by limiting the control bandwidth, filters W_{21}, W_{22}, and W_{23} are designed as inverted LPF

Table 4.9: Natural frequecies for the 5 MW NREL RWT [JBMS09]

Vibration mode	**Frequency [rad/s]**
1st blade asymmetric flap-wise yaw	4.187
1st blade asymmetric flap-wise tilt	4.194
1st blade symmetric flap-wise average	4.394
1st blade asymmetric edge-wise yaw	6.781
1st blade asymmetric edge-wise tilt	6.847
1st tower fore-aft	2.036
1st tower side-side	1.960
1st drive-train torsion	3.899

The weighting functions are integrated to the linear WT model as illustrated in Fig. 4.28. This ultimately results in the three control inputs $u = [\beta_{avg}\, \beta_{tilt}\, \beta_{yaw}]^T$ and the four performance outputs ω_g, ζ_{avg}, ζ_{tilt}, and ζ_{yaw}. The weighting functions $1/W_{11}$, W_{12}, W_{13}, W_{14}, $1/W_{21}$, $1/W_{22}$, and $1/W_{23}$ are selected as

$$W_{11} = \frac{\frac{s}{M_s} + \omega_s}{s + \omega_s \epsilon_s}, W_{12} = (\frac{s^2 + 2\alpha_1 \omega_{3P} s + \omega_{3P}^2}{s^2 + 2\beta_1 \omega_{3P} s + \omega_{3P}^2}) \times \frac{1}{522.6}, \tag{4.27}$$

$$W_{13} = (\frac{s^2 + 2\alpha_{21} \omega_{3P} s + \omega_{3P}^2}{s^2 + 2\beta_{21} \omega_{3P} s + \omega_{3P}^2}) \times (\frac{s^2 + 2\alpha_{22} \omega_{tfa} s + \omega_{tfa}^2}{s^2 + 2\beta_{22} \omega_{tfa} s + \omega_{tfa}^2}) \times \frac{1}{115.8}, \tag{4.28}$$

$$W_{14} = (\frac{s^2 + 2\alpha_{31} \omega_{3P} s + \omega_{3P}^2}{s^2 + 2\beta_{31} \omega_{3P} s + \omega_{3P}^2}) \times (\frac{s^2 + 2\alpha_{32} \omega_{tfa} s + \omega_{tfa}^2}{s^2 + 2\beta_{32} \omega_{tfa} s + \omega_{tfa}^2}) \times \frac{1}{31.6}, \tag{4.29}$$

and

$$W_{21} = W_{22} = W_{23} = \frac{s + \frac{\omega_u}{\epsilon_u}}{s + \frac{\omega_u}{M_u}}, \tag{4.30}$$

where $M_s, \omega_s, \epsilon_s, \alpha_1$, β_1, α_{21}, β_{21}, α_{22}, β_{22}, α_{31}, β_{31}, α_{32}, $\beta_{32}, M_u, \omega_u$, and ϵ_u are tuning parameters of the respective inverted weighting filters, and $0 < \beta < \alpha < 1$.

In Figure 4.29, a Bode diagram of the open-loop transfer functions from wind speed to respective outputs and the associated inverse weighting functions is shown. As illustrated, $1/W_{11}$, $1/W_{12}$, $1/W_{13}$, and $1/W_{14}$ shape the respective open-loop responses to achieve the desired closed-loop frequency responses.

By using the DK-iteration process described in section 4.3.1, an optimal IPC-RDAC controller is designed based on μ-synthesis approach [Apk11] by minimizing μ. The obtained IPC-RDAC controller is applied to the 5 MW NREL RWT to damp blade F-W and tower F-A vibrations as well as control generator speed/power.

4.4.2 Simulation results and discussion

To validate the IPC-RDAC control method, closed-loop dynamic simulations are performed in OpenFAST design code [NRE21] using the 5 MW NREL RWT. While the controller is

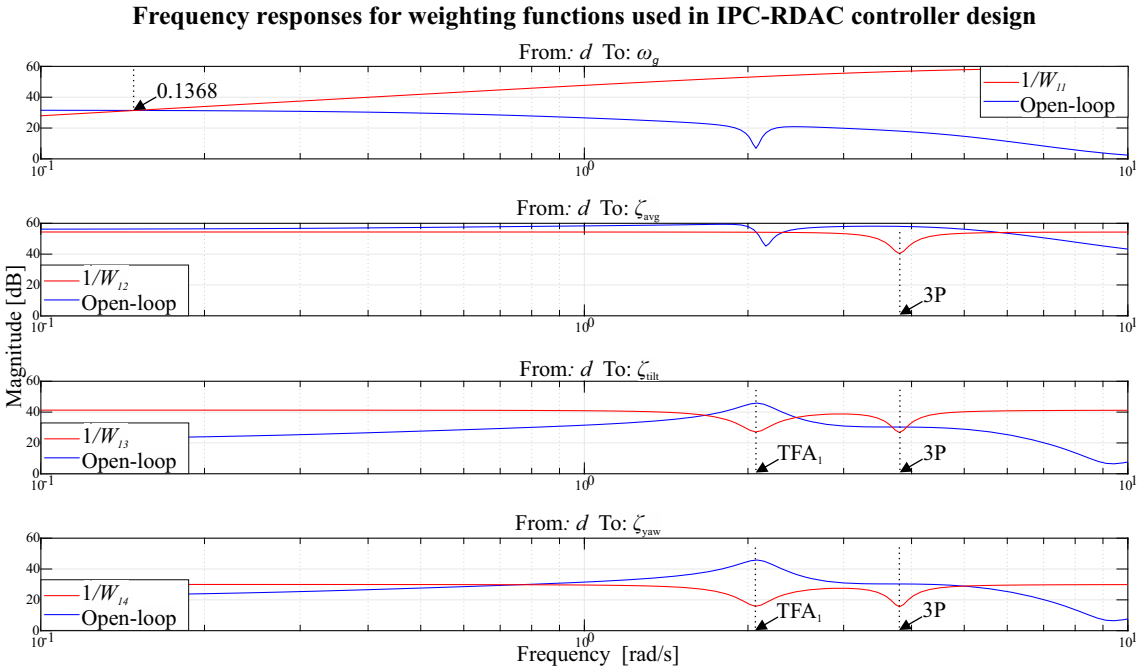

Figure 4.29: Comparison of open-loop frequency response and weighting functions used in IPC-RDAC control design [KS24]

designed using a reduced-order (linearized) model of the WT (4.24), a nonlinear model (3.1) is used in the simulations. This makes it possible to evaluate of control performance in the presence of modeling errors. The objectives of the proposed IPC-RDAC control scheme include regulation of generator speed to its rated value of 1173.7 rpm and reduction of structural loads in the blades (F-W mode) and the tower (F-A mode). Stochastic wind fields are used to excite the dynamics of the WT in above-rated operation. Using closed-loop simulation results, performance of the proposed IPC-RDAC controller is compared with the baseline ROSCO [AZPW22] and RDAC1 controllers described in sections 3.2.2 and 4.2.1, respectively. The obtained results are analyzed and discussed using selected performance metrics.

Structural load mitigation performance

A WT experiences spatio-temporal variations in the wind field acting on its rotor. To simulate the non-stationary wind conditions, stochastic wind profiles generated with TurbSim software [JK12] are used in closed-loop dynamic simulations. In Figure 4.30(a), the full-field wind profiles generated using the IEC Kaimal spectral model are shown. Following the recommendation of the IEC 61400-1 standard for design load case (DLC) 1.2, which is related to fatigue load evaluation in WT structures, 10-minute wind profiles are generated with different combinations of mean wind speeds, TIs, and random seeds. This covers most of the turbine's above-rated operation.

In Figure 4.30(b), the closed-loop blade F-W load mitigation response of the WT is shown. As illustrated the proposed IPC-RDAC controller shows improved performance in reducing the blade F-W bending moments in all wind field scenarios compared with

the baseline ROSCO and RDAC1 controllers. This performance is attributed to reduction in 2P, 3P, and 4P blades loads using IPC control signals. In Table 4.10, load mitigation performance in the blade F-W and tower F-A load channels for all wind fields is given. The proposed IPC-RDAC controller reduces the average δ in blade F-W bending moment by 9.8 % compared with ROSCO. However, RDAC1 shows the worst performance as δ increases by 6.1 % compared with ROSCO. The performance in tower F-A load reduction is shown in Fig. 4.30(c). The proposed controller exhibits improved tower F-A load mitigation performance compared with ROSCO as δ reduces by 9.8 % as shown in Table 4.10. The RDAC1 controller exhibits superior performance as δ is reduced by 14.8 % compared with ROSCO. This is attributed to less control objectives compared with IPC-RDAC, as it only trades off between tower F-A load mitigation and generator speed regulation. However, at lower mean wind speed of 14 m/s (treated as worst-case scenario), which is outside the 18 m/s control design working point and has a higher occurence probability in real turbine operation, IPC-RDAC achieves the best performance in both load channels, hence proves its robustness to model uncertainties. Therefore, the proposed controller realizes optimal performance in mitigating both the blade F-W and tower F-A loads.

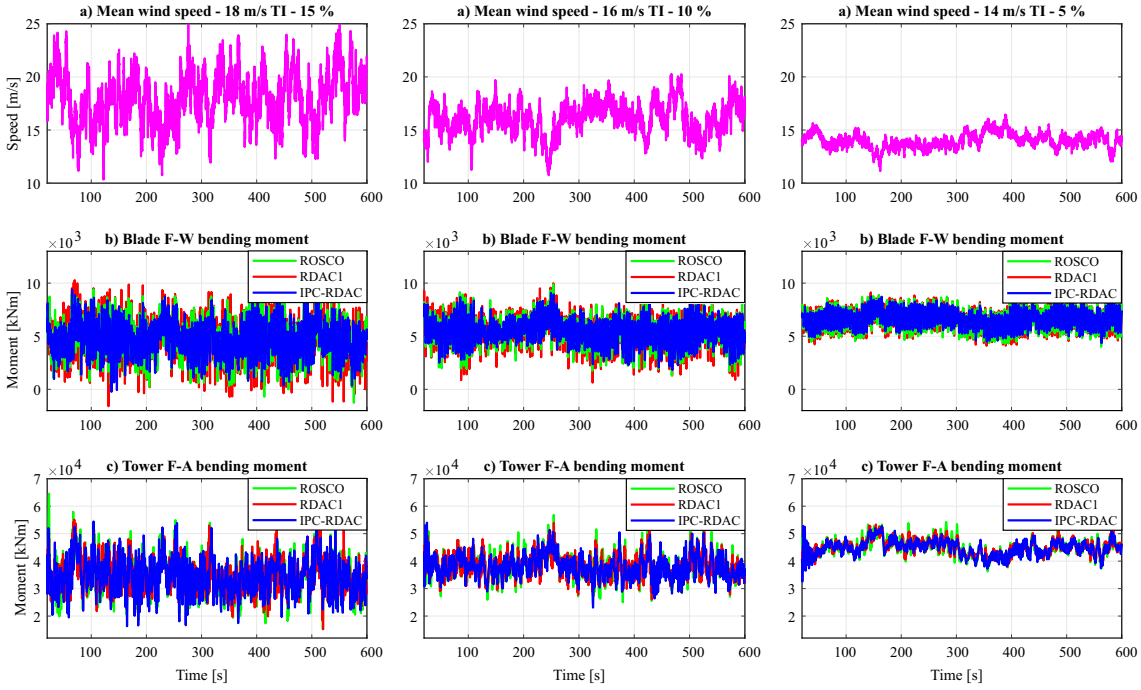

Figure 4.30: Blade F-W and tower F-A load mitigation response [KS24]

Generator speed and power regulation performance

Given that the proposed controller is designed for structural load reduction and generator speed regulation, it is necessary to ascertain that the foregoing improvement in load mitigation does not lead to deterioration of generator speed and power regulation performance. Therefore, the proposed IPC-RDAC controller is compared with the ROSCO and RDAC1 controllers as shown in Fig. 4.31. Due to additional blade load mitigation control objective, the IPC-RDAC controller has slightly higher pitch usage as shown in Fig. 4.31(a). Com-

Table 4.10: Blade F-W and tower F-A load mitigation performance analysis (Key: best, worst) [KS24]

Load channel [kNm]	Controller	18 m/s	16 m/s	14 m/s	Avg.	%
Blade F-W (δ)	ROSCO	1805.8	1375.2	988.8	1389.9	-
	RDAC1	1972.8	1450.7	998.8	1474.1	6.1
	IPC-RDAC	1494.3	1118.8	792.95	1135.35	-18.3
Tower F-A (δ)	ROSCO	6632.5	4758.7	3013	4801.4	-
	RDAC1	5610.4	3948.9	2706.9	4088.7	-14.8
	IPC-RDAC	6277.9	4019.7	2697.7	4331.8	-9.8

pared with both ROSCO and RDAC1, the proposed controller achieves improved generator speed regulation as illustrated in Fig. 4.31 (b). In Table 4.11, the performance analysis in blade pitch usage and generator speed and power regulation for all wind fields is given. As shown, both RDAC1, and IPC-RDAC realize a 34.9 % and 26.6% reduction in the average δ in generator speed, respectively, compared with ROSCO. This performance is also reflected in the MSE values. Compared with ROSCO, the average generator speed MSE reduces by 62.5 % and 51.5 % for RDAC1 and proposed controller, respectively. However, it is clear from Fig. 4.31 (c) that ROSCO achieves superior power regulation performance, with the generator power δ increasing by 59 % and 31.8 % for RDAC1 and IPC-RDAC, respectively, compared with ROSCO as shown in Table 4.11. A similar performance is also reflected in generator power MSE. Therefore, although RDAC1 has superior speed regulation performance, it comes at a penalty as it achieves the worst power regulation. However, the proposed controller achieves an optimal compromise between generator speed and power regulation. The mean blade pitch travel is used to evaluate the controllers' blade PA usage for all wind fields, as shown in Table 4.11. The proposed controller shows a marginal increase in PA usage compared with both ROSCO and RDAC1.

Table 4.11: Blade pitch usage and generator speed and power regulation performance analysis (Key: best, worst) [KS24]

Parameter	Units	Controller	18 m/s	16 m/s	14 m/s	Avg.	%
Speed (δ)	rpm	ROSCO	30.67	15.79	6.04	17.5	-
		RDAC1	17.54	11.07	5.56	11.39	-34.9
		IPC-RDAC	20.24	12.27	6.05	12.85	-26.6
Speed (MSE)	rpm	ROSCO	943.84	250.37	36.49	410.24	-
		RDAC1	307.94	122.62	30.94	153.83	-62.5
		IPC-RDAC	409.92	150.69	36.6	199.07	-51.5
Power (δ)	kW	ROSCO	190.24	104.22	40.12	111.52	-
		RDAC1	304.13	165.74	61.91	177.26	59
		IPC-RDAC	234.45	146.15	60.35	146.98	31.8
Power (MSE)	kW	ROSCO	36236	10879	1609.8	16241.6	-
		RDAC1	92497	27473	3833.5	41267.83	154.1
		IPC-RDAC	54966	21360	3642	26656.2	64.1
Pitch travel (mean)	°	ROSCO	14.251	11.331	7.574	11.052	-
		RDAC1	14.291	11.347	7.578	11.072	0.18
		IPC-RDAC	14.290	11.357	7.577	11.075	0.21

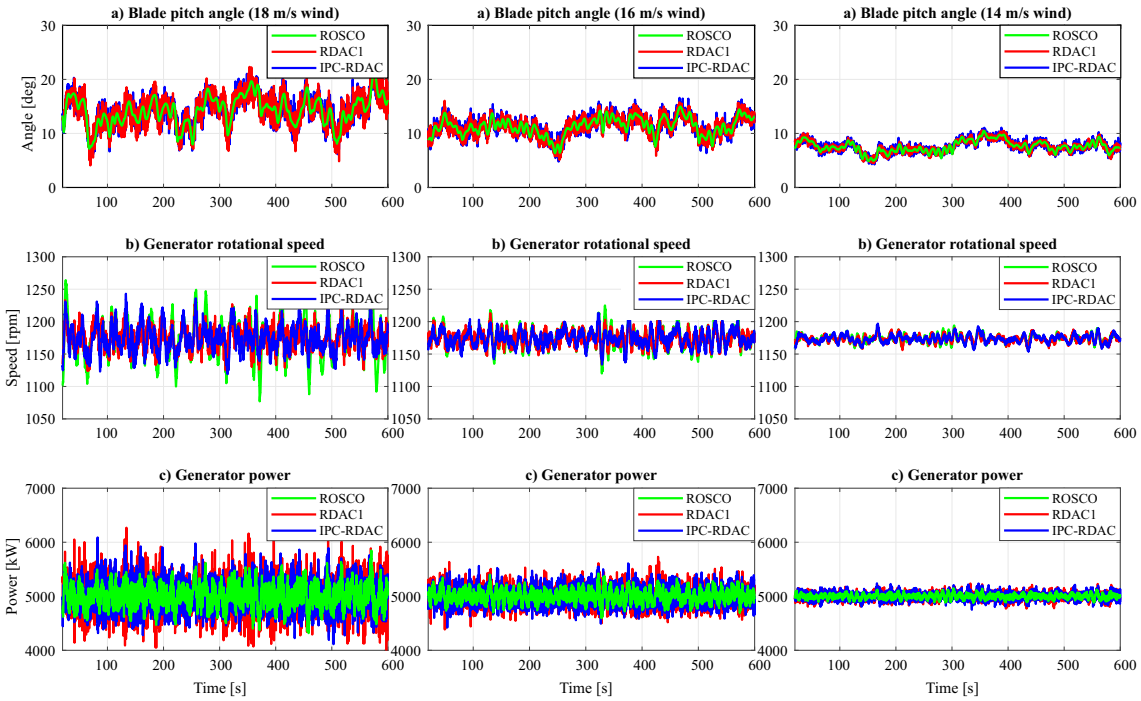

Figure 4.31: Generator speed and power regulation response [KS24]

In Figure 4.32 the average normalized RMS of blade PR and generator speed and power regulation MSE obtained from simulation results for all wind fields is shown. To ascertain that blade pitch actuation does not violate the maximum PR of 8 °/s for the 5 MW NREL RWT, the average RMS of PR is evaluated and found to be 0.37 °/s, 4.78 °/s, and 7.78 °/s for ROSCO, RDAC1, and IPC-RDAC controllers, respectively. Due to additional control objective of blade and tower load mitigation, the proposed IPC-RDAC controller shows significant pitch activity compared with ROSCO and RDAC1 as shown in Fig. 4.32. However, the graphs of generator speed and power MSE show that the proposed controller strikes a good balance between generator speed and power regulation. Therefore, the proposed controller meets all the control objectives without violating the turbine's PR constraint.

Load mitigation in other load channels

Due to coupling between the tower, blades, and drive-train dynamics in a WT, implementing a control scheme for load mitigation in one structural component can result in increased load in other WT components. For example, the using IPC control potentially excites the blade E-W and tower S-S bending modes. Therefore, additional load channels in the blades and tower are evaluated as shown in Fig. 4.33. As illustrated, the proposed controller does not excite loading in other load channels for all wind field scenarios. This is shown in Table 4.12 as the proposed controller achieves the best performance. Compared with ROSCO, the average reduction in δ for blade E-W and tower S-S moments is 2.2 % and 5.3 %, respectively. On the other hand, RDAC1 shows a slight increase in δ for both load channels. Therefore, while using RDAC1 compromises on performance in other load channels, the IPC-RDAC controller provides an optimal trade-off between load mitigation

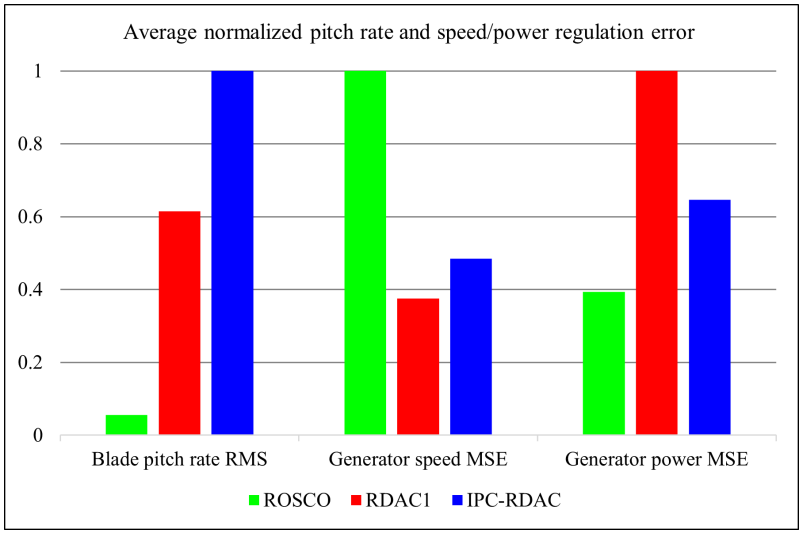

Figure 4.32: Blade pitch activity and generator speed/power regulation error [KS24]

and generator speed regulation without inducing additional loads.

Table 4.12: Blade E-W and tower S-S load mitigation performance analysis (Key: best, worst) [KS24]

Load channel [kNm]	Controller	18 m/s	16 m/s	14 m/s	Avg.	%
Blade E-W moment (δ)	ROSCO	2449.5	2489.1	2516.1	2484.9	-
	RDAC1	2453.7	2487.7	2516.7	2486	0.1
	IPC-RDAC	2393.1	2431.3	2468.0	2430.8	-2.2
Tower S-S moment (δ)	ROSCO	1779.7	1065.7	455	1100.13	-
	RDAC1	1815.7	1076.3	458.42	1116.81	1.5
	IPC-RDAC	1680.6	1023.2	421.8	1041.9	-5.3

4.4.3 Fatigue load analysis

The robustness of the proposed controller in reducing fatigue load is examined by analyzing DELs of the respective blades and tower load channels using MLife software [Hay12]. Closed-loop simulation results obtained using the wind profiles shown in Fig. 4.30(a) are used in this analysis. The wind fields cover most of the WT's above-rated operations. In Figure 4.34, the normalized DELs with respect to ROSCO for each load channel and in all wind conditions is shown. As illustrated, the blade F-W and E-W DELs are reduced by IPC-RDAC controller compared with ROSCO and RDAC1 controllers for all wind fields, with an average reduction of 11.6 % and 20.7 % for blade F-W DEL, and 1.9 % and 2.7 % for blade E-W DEL, respectively as shown in Table 4.13. Furthermore, the IPC-RDAC controller shows improvement for the tower F-A DEL compared with both ROSCO and RDAC1 with an average reduction of 6.9 %and 2.1 %, respectively. However, the proposed controller exhibits a slightly reduced performance in tower S-S DEL as it achieves an average increase of 4.9 % and 2.8 % compared with ROSCO and RDAC1 controllers, respectively. This can be attributed to use of IPC control, which typically excites the tower S-S vibration

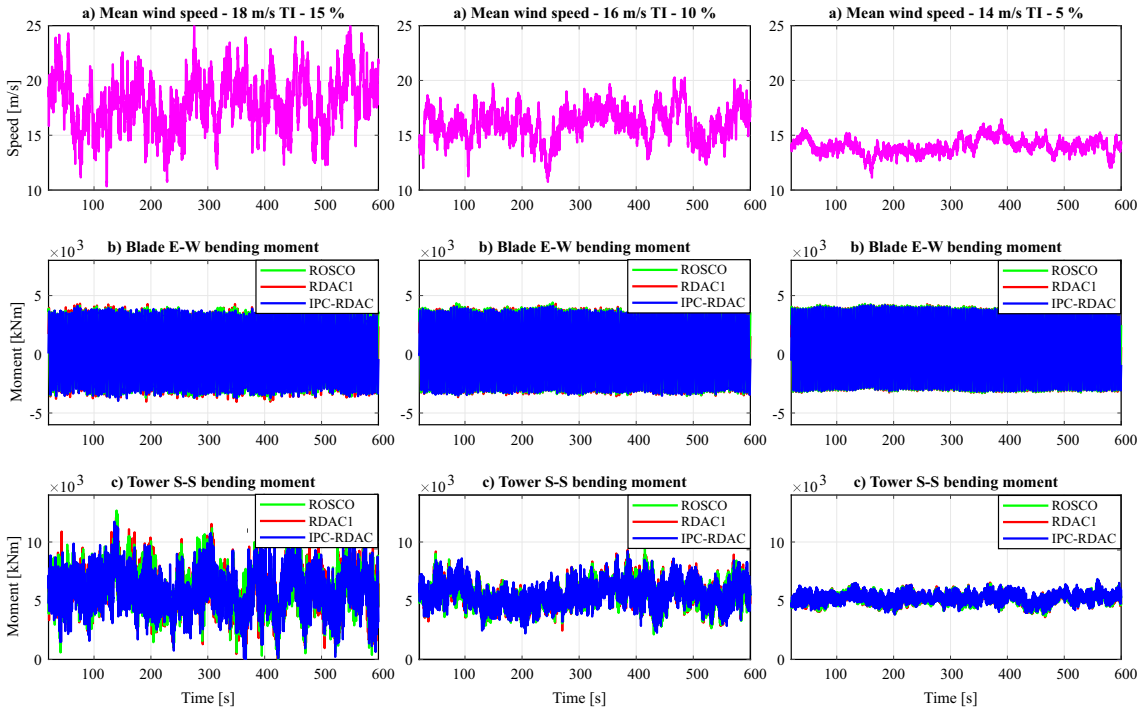

Figure 4.33: Blade E-W and tower S-S loading response [KS24]

mode. However, the performance of the proposed controller in mitigating structural loads in most load channels and aforementioned optimal performance in generator speed and power regulation far outweighs this setback. Therefore, the IPC-RDAC controller offers optimal balance in fatigue load reduction and generator speed regulation.

Table 4.13: Damage equivalent loads analysis (Key: best, worst) [KS24]

DEL channel [kNm]	Controller	18 m/s	16 m/s	14 m/s	Avg.	%
Blade F-W	ROSCO	3000	2440	1440	2293.3	-
	RDAC1	3510	2640	1520	2556.7	11.5
	IPC-RDAC	2800	2040	1240	2026.7	-11.6
Blade E-W	ROSCO	3050	3060	3060	3056.7	-
	RDAC1	3120	3070	3060	3083.3	0.9
	IPC-RDAC	3000	3000	3000	3000	-1.9
Tower F-A	ROSCO	5590	3970	1970	3843.3	-
	RDAC1	5640	3610	1710	3653.3	-4.9
	IPC-RDAC	5690	3370	1670	3576.7	-6.9
Tower S-S	ROSCO	2050	1150	506	1235.3	-
	RDAC1	2120	1150	512	1260.7	2.1
	IPC-RDAC	2110	1230	547	1295.7	4.9

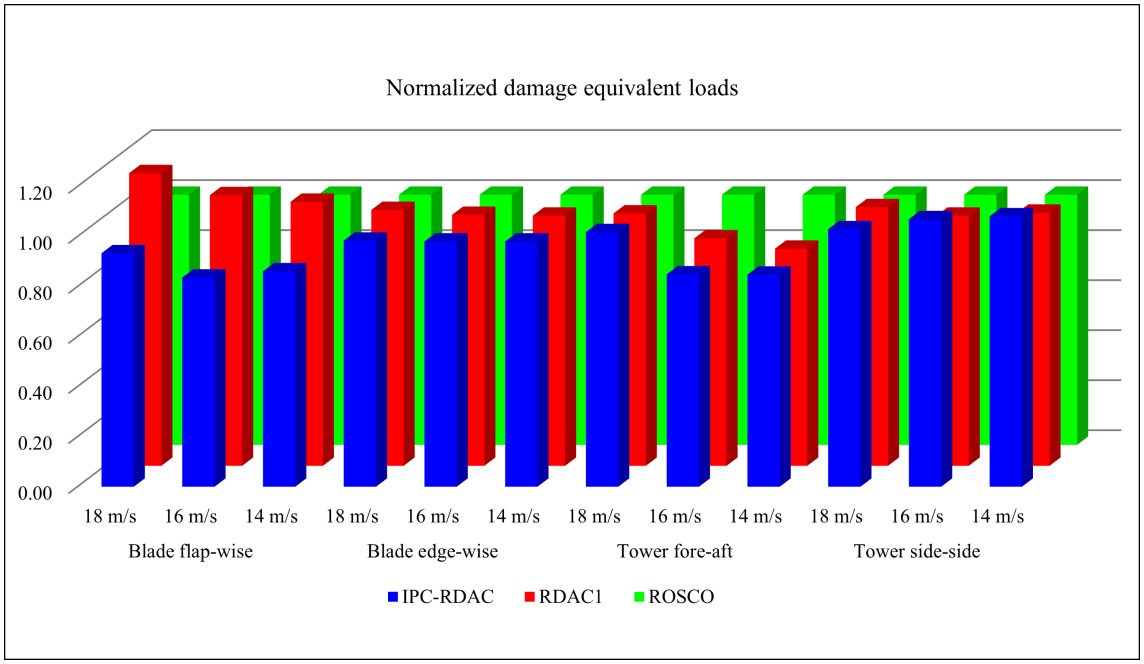

Figure 4.34: Damage equivalent loads analysis [KS24]

4.4.4 Spectral analysis

To evaluate the performance of controllers in alleviating structural loads at frequencies of interest, PSD analysis of blade F-W and tower F-A bending moments is performed. In Figure 4.35, the results of the PSD evaluation are shown. As illustrated, the IPC-RDAC controller gives the lowest response peak magnitudes of blade F-W loading at 2P and 4P frequencies compared with ROSCO and RDAC1 controllers. This means that the proposed controller alleviates the asymmetric blade F-W bending moments, ζ_{tilt} and ζ_{yaw}. This is because dynamic coupling of blade F-W bending modes, ζ_{avg}, ζ_{tilt}, and ζ_{yaw} are considered in controller design by proper selection of weighting functions. Furthermore, the IPC-RDAC controller achieves better 3P blade load reduction (related to ζ_{avg}) compared with ROSCO. Although 1P is far from the critical natural frequencies of the blades (around 4 rad/s) and the tower (2.07 rad/s) shown in Table 4.9, its higher order harmonics contribute to excitation of these frequencies. Therefore, only reduction of 2P, 3P, and 4P frequencies are considered in the design of the proposed controller. Further suppression of 1P blade excitation can be considered by designing W_{13}, and W_{14} with high magnitudes near 0P frequency. The RDAC1 controller has superior performance in suppresing blade vibration at 3P, which is accounted for in its design as it indirectly reduces 3P blade excitation experienced by the tower. This is illustrated in the tower F-A PSD analysis, where RDAC1 damps tower F-A loading at the first tower bending moment frequency TFA_1. Although the proposed controller does not show reduced damping at this frequency, it achieves lower magnitude response in tower loading at higher frequencies compared with RDAC1. In particular, it shows lower tower loading at the first drive-train torsional frequency DT_1, suggesting that using IPC-RDAC leads to lower excitation of the coupled drive-train dynamics.

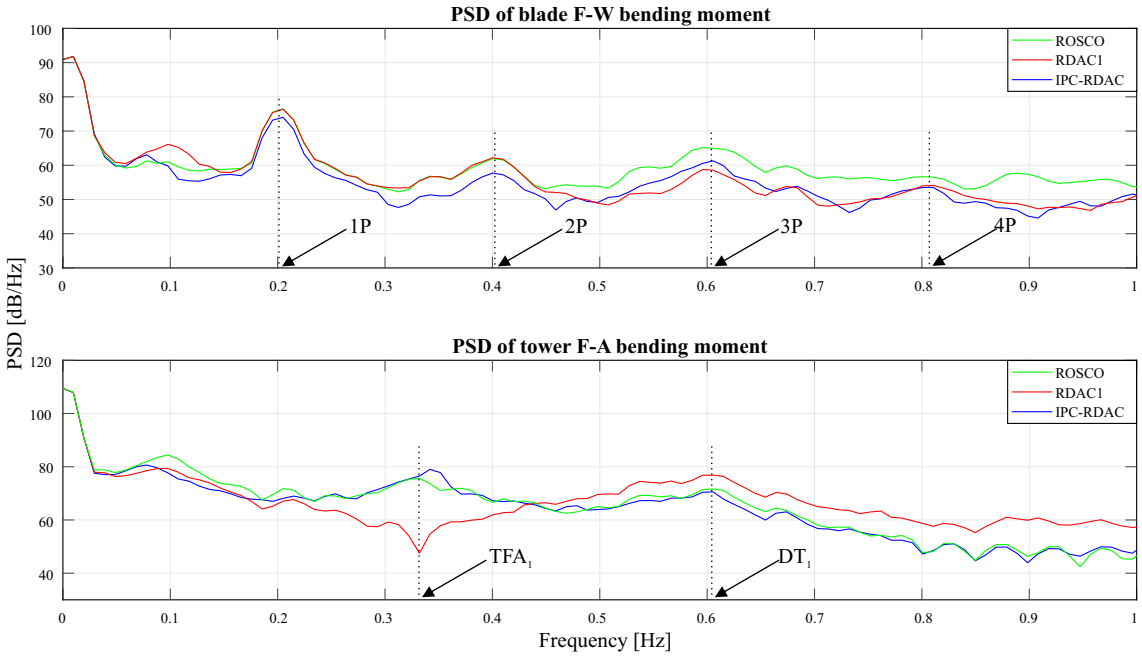

Figure 4.35: Power spectral density analysis of blade F-W and tower F-A bending moments [KS24]

4.4.5 Summary

A robust disturbance accommodating controller based on IPC control for structural load mitigation and generator speed regulation of the 5 MW NREL RWT is presented. The novel IPC-RDAC controller is designed using μ-synthesis based on the DK-iteration process by minimizing the structured singular value μ of the generalized WT system consisting of a linear model, weighting functions, and blade PA dynamics. The controller also includes an uncertainty description, which is designed from a family of linear models obtained at different operating points. Periodic 2P, 3P, and 4P frequencies as well as the first tower F-A frequency reflected in the rotor blades are reduced by designing the respective weighting functions. The proposed controller is shown by suitable simulations to be robust against model uncertainties and system nonlinearities resulting from wind speed variability. Compared with baseline ROSCO and RDAC1 controllers, dynamic simulation results show that the proposed controller reduces fatigue loading in the blades and tower without compromising on the generator speed regulation performance. It also exhibits reduced loading in other WT load channels. Fatigue load evaluation indicates a reduction of DELs in most load channels.

The limitation of the proposed control approach is that only unstructured uncertainties are considered in the uncertainty description. Furthermore, blade PA activity is particularly aggressive in wind fields having high speeds and TIs. However, these wind conditions have a low occurrence probability in a real operation of WTs, and are used to demonstrate the efficacy of the proposed controller in the event that such conditions arise. A lumped uncertainty description, which incorporates additionally plant parametric uncertainties, particularly experienced in below-rated WT operation, can be included in design to potentially improve robust performance. To further reduce 1P frequencies in the blades,

relevant weighting functions can be designed. A prognostics-based IPC-RDAC lifetime controller can also be developed to control long-term fatigue damage accumulation in multiple WT structural components.

4.5 Comparison of proposed RDAC control methods

In this section, performance of the proposed RDAC controllers are compared against each other to identify the performance improvements and limitations of each method. Based on this assessment, practical recommendations for possible applications of each controller are given. To simplify comparison, only approaches applied to the 5 MW NREL RWT are considered. Simulation results based on the stochastic wind profiles shown in Fig. 4.30 are used for the evaluation. In Table 4.14, performance in terms of blade and tower load mitigation is given. The IPC-RDAC controller provides the best performance in blade F-W load mitigation for all wind fields. In addition, this control method induces the lowest fatigue loads in other load channels not part of the control objectives, namely the blade E-W and tower S-S bending moments. On the other hand, RDAC1 achieves the best tower F-A moment mitigation. However, this is by a considerably small margin, especially compared with IPC-RDAC, which achieves best performance at near-rated wind speed (14 m/s). Given that high wind speeds (16 and 18 m/s) have a low occurence probability in real WT operation, it can be concluded that IPC-RDAC gives the best overall performance in structural load mitigation.

Table 4.14: Load mitigation performance analysis (Key: best, worst)

Load channel [kNm]	Controller	18 m/s	16 m/s	14 m/s	Avg.
Blade F-W moment(δ)	RDAC1	1972.8	1450.7	998.8	1474.1
	RDAC2	1836.2	1374.1	999.3	1403.2
	IPC-RDAC	1494.3	1118.8	792.95	1135.35
Tower F-A moment (δ)	RDAC1	5610.4	3948.9	2706.9	4088.7
	RDAC2	5658.4	4042.4	3039.2	4246.7
	IPC-RDAC	6277.9	4019.7	2697.7	4331.8
Blade E-W moment (δ)	RDAC1	2453.7	2487.7	2516.7	2486
	RDAC2	2449.4	2488.5	2516.1	2484.7
	IPC-RDAC	2393.1	2431.3	2468.0	2430.8
Tower S-S moment (δ)	RDAC1	1815.7	1076.3	458.42	1116.8
	RDAC2	1824.8	1076.9	454.27	1118.7
	IPC-RDAC	1680.6	1023.2	421.8	1041.9

In Table 4.15, blade PA usage and speed/power regulation performance is shown. The RDAC2 controller achieves the best performance in generator speed/power regulation as evidenced by the δ and MSE values. Although IPC-RDAC shows the worst performance in speed regulation, it achieves better power regulation than RDAC2 controller. All controllers have better speed regulation than ROSCO (Table 4.11) which is designed exclusively for speed regulation. However, H_∞ RDAC1 has worse power regulation than ROSCO (Table 4.11), suggesting that the μ-synthesis approach used to design RDAC2 and IPC-RDAC controllers improves robust performance in both load mitigation and speed regulation. Analysis of blade PA usage shows that all control methods place similar demands on

pitch usage to achieve their objectives. The average RMS values of PR are 4.78 $^{\circ}/s$, 2.23 $^{\circ}/s$, and 7.78 $^{\circ}/s$, for RDAC1, RDAC2, and IPC-RDAC controllers, respectively, as described in sections 4.3.2 and 4.4.2. Therefore, RDAC2 achieves the best generator/speed regulation with the lowest PA demand and is therefore recommended for speed regulation of WTs albeit with a trade-off in load mitigation. Although the RDAC1 controller has average pitch usage, it is only suitable for tower F-A moment load mitigation in high wind speeds, as IPC-RDAC provides better performance at low wind speeds. The IPC-RDAC controller is recommended for achieving multiple objectives in commercial WTs as it offers the best overall performance in blade and tower load mitigation with an optimal balance in speed/power regulation. Although it has the highest PA usage, it occurs at high wind speeds whose occurence probability is very low at most wind farm sites. In addition, pitch usage does not violate the WT's PR constraint of 8 $^{\circ}/s$.

Table 4.15: Speed/power regulation and pitch usage performance analysis (Key: best, worst)

Parameter	**Units**	**Controller**	**18 m/s**	**16 m/s**	**14 m/s**	**Avg.**
Speed (δ)	rpm	RDAC1	17.54	11.07	5.56	11.39
		RDAC2	14.61	9.62	5.88	10.04
		IPC-RDAC	20.24	12.27	6.05	12.85
Speed (MSE)	rpm	RDAC1	307.94	122.62	30.94	153.83
		RDAC2	214.5	93.33	34.71	114.2
		IPC-RDAC	409.92	150.69	36.6	199.07
Power (δ)	kW	RDAC1	304.13	165.74	61.91	177.26
		RDAC2	204.0	107.3	47.21	119.9
		IPC-RDAC	234.45	146.15	60.35	146.98
Power (MSE)	kW	RDAC1	92497	27473	3833.5	41267.8
		RDAC2	41613	11528	2230	18457
		IPC-RDAC	54966	21360	3642	26656.2
Pitch travel (mean)	$^{\circ}$	RDAC1	14.291	11.347	7.578	11.072
		RDAC2	14.289	11.339	7.570	11.066
		IPC-RDAC	14.290	11.357	7.577	11.075

5 Prognostics schemes for Lifetime Control of Commercial Wind Turbines

The figures, tables, and content in this chapter are based on the published journal paper [KDNS23] and the journal paper in preparation [KLS24].

Growing demand for wind energy has led to the development commercial wind turbines (WTs). However, these turbines are less tolerant to system performance degradation and faults [GL21]. Fatigue loads in WT components are attributed to dynamic variation of the wind field. Over the last few decades, WTs have grown in size and power rating. With larger, slender and heavier components, these utility-scale WTs are subject to increased structural loads. To ensure that commercial WTs operate within their design lifetime, advanced control strategies have been developed to reduce structural loads, particularly in the large rotor blades and tower components. These control schemes include additional objectives such as power optimization and speed control.

Wind turbines experience faults or failures due to component degradation through aging or extreme load events. This leads to system downtime and economic losses. To ensure operational safety and reliability of WT systems, structural health monitoring (SHM) and prognosis schemes for estimating and predicting degradation should be integrated to advanced multi-input multi-output (MIMO) control strategies. This ensures that the design lifetime WTs is achieved. Significant improvements in SHM has been achieved through online fault detection and condition monitoring (CM) [BNS18]. In recent years, prognosis-based lifetime control and extension of WTs has become increasingly important for ensuring power supply and operational reliability. In this context, a fatigue damage or degradation model is used to determine the consumed lifetime of a component. Subsequently, the prognostics controller gains are adapted based on the state-of-health (SOH) or remaining useful life (RUL) of the WT component to achieve the desired lifetime.

Most of the proposed reliability-oriented control methods focus on controlling the service life of a structural component of a WT, typically the rotor blade or the tower, without considering the fatigue damage level in other components. These lifetime controllers are also designed for specific operating points, hence they exhibit deteriorating performance in varying wind conditions. Stochastic wind dynamics complicates estimation of the SOH in a WT component as it causes nonstationary load profiles. Recent developments have seen the use of robust controllers combined with real-time damage evaluation models to achieve prognosis objectives. Most rely on model-based online load cycle counting algorithms to determine fatigue damage accumulation with analytical models providing the degradation estimate. However, these rely on load measurements, which may be unavailable in commercials WTs, hence limiting their practicality.

Various SHM and prognosis approaches for RUL prediction in WTs have been proposed. Physics/model-based prognosis methods use either physical or mathematical models of the

degradation patterns to predict the RUL of critical components in real-time [RKO+21]. Degradation models are obtained either through physical modeling of the degradation process or through experimental modeling, where system identification tools are used to obtain models from process measurements. Using monitoring data,these degradation models are used to predict the damage evolution and thus determine the RUL. The limitation of model-based approaches is that accurate physical modeling of the degradation process is difficult to achieve due to uncertain future operating conditions, measurement errors, and data variability. This leads to uncertainty in the predicted RUL [KAC17]. On the other hand, data-driven prognosis approaches rely on featured data of the degradation process rather than explicit input/output models, and suitable machine learning (ML) techniques to build a knowledge-base that represents an explicit dependency of system variables and a degradation model enabling prediction of future SOH and RUL [DTZX18; GL21; BZJ+22]. Data-driven approaches have been applied to prognosis of modern commercial WTs due to abundance of process monitoring data from high frequency (1 kHz) supervisory control and data acquisition (SCADA) systems [LL20]. This historical data is used to learn the WT's performance dynamics, estimate the SOH from real-time data, and predict its RUL. Data-driven prognosis approaches have a limited ability to learn complex signals with nonlinear characteristics, such as the nonstationary degradation patterns in WTs due to several failure modes [HRBA+18]. Although sufficient process data is required for accurate predictions, traditional data-driven methods have slow convergence speed and low prediction accuracy when processing large amounts of data [XWY+21]. To adress this problem, modern deep-learning methods have accelerated convergence speed and improved prediction accuracy. However, longterm dependencies hidden in sequential/timeseries data are not considered [LLJ19].

In recent years, hybrid (model-based data-riven) prognosis approaches which capitalize of the unique advantages of each approach and compensate for their limitations have been proposed. They have good prediction performance due accurate modeling of uncertainty. However, hybrid prognosis algorithms can be very sophisticated and are constrained by the requirement for physical modeling of degradation events [BMS23]. Therefore, hybrid models require a reliable physical degradation model and sufficient historical process data for successful implementation. Data-driven methods are not reliable for prognosis of WTs at the beginning of their operational life due to insufficient databases covering faulty scenarios as most of the collected data characterizes normal operation. On the other hand, useful features covering both of these operations can be generated using physical models [DBS18]. High fidelity softwares for simulating several dynamics of commercial WTs can be used for developing these physics models. Because WTs are designed to operate for decades, hybrid prognosis approaches are suitable for RUL prediction of WTs over their entire lifetime.

In this thesis, advanced robust control methods for mitigating structural loads in WTs in above-rated wind speed operation are presented in chapter 4. Although the efficacy of these controllers in load mitigation has been demonstrated, this has achieved with a short-term approach fatigue load reduction without considering the fatigue life of the WT. By integrating SHM and prognosis approaches where its SOH is estimated and its RUL is predicted [GL21], further improvements in fatigue load reduction can be achieved over the entire operational life of a WT. This ensures optimal operation of the WT, hence ensuring that reliability, cost reduction, and the desired lifetime is achieved. In this section, two prognostics-based robust lifetime control schemes are presented. First, a model-based prognosis control sheme based on the adaptive robust observer-based control strategy

described in section 4.1 is proposed. This approach is applied to the WindPACT 1.5 MW reference WT (RWT) [RD18] for lifetime control of its rotor blades. Secondly, a hybrid approach for robust lifetime control of WTs based on the μ-synthesis RDAC control scheme described in section 4.3 is outlined. The approach is applied to the larger 5 MW National Renewable Energy Laboratory (NREL) RWT [JBMS09] to control the the tower's life consumption.

5.1 Prognostics-based adaptive lifetime control

In this section, an adaptive lifetime control strategy for controlling the aging of rotor blades to achieve a desired lifetime considering the SOH of the tower is proposed. The adaptive robust observer-based control strategy described in section 4.1 is extended for lifetime prognosis of the WindPACT 1.5 MW RWT. The RDAC controller [DS22] described in section 4.1.1 is used for rotor speed regulation and load mitigation in the tower, while aIPC described in section 4.1.2, is selected as the prognostics controller for lifetime control of rotor blades. The control set-point of the aIPC controller is adapted based on both the prevailing wind speed and the SOH of rotor blades. By monitoring the accumulated damage using an online structural health evaluation model, the load mitigation level in the blades is controlled by varying the control gains in the respective IPC controllers based on a threshold assessment of the estimated lifetime. The proposed adaptive lifetime control strategy regulates fatigue loads in the rotor blades to achieve a predefined damage limit at the desired lifetime and subsequently reduce tower damage accumulation. This is realized without compromising speed/power regulation performance.

5.1.1 Fatigue damage estimation approaches

Due to wind speed variability, WT components such as blades and tower are subjected to cyclic loading. This causes damage to accumulate in these components over time causing gradual degradation until failure occurs. Therefore, SHM of WTs is important to prevent the occurrence of fatigue failure before reaching the appropriate design lifetime. Information about the damage evolution in a component can be used as a health indicator for failure detection and for developing control measures to achieve a desired lifetime. This section describes the methods used for estimating the damage accumulation in WT components.

Evaluation of damage accumulation

A WT endures varying and complex load conditions over its lifetime. Therefore, fatigue analysis is important in determining the consumed lifetime of its components. Component degradation begins at microscale as microcracks resulting from irreversible changes in the microstructure, and propagates gradually until it fails. Assumptions of underlying damage evolution laws are often used to estimate the actual damage level and predict the RUL of a component. Component-specific high-cycle fatigue experiments are used to generate S-N curves (Wöhler curve) that describe the relationship between applied stress amplitude S and the number of load cycles N that would cause failure. This forms the basis for the mathematical relation for fatigue analysis in WT components expressed as

$$s^m N = K, \tag{5.1}$$

where s denotes the stress range amplitude, m the Wöhler exponent (typically 3 for steel materials such as the tower and 10 for composites such as the rotor blade [RM07]). The material parameter of fatigue damage at failure K e.g., ultimate tensile strength depends on the number of load cycles N.

Wind turbine components are designed for a service lifetime of at least 20 years according to the International Electrotechnical Commission (IEC) standard, with these structural components subjected to roughly between 10^8 and 10^9 fatigue load cycles [ZGR+18]. A component's lifetime is typically determined using the projected number of fatigue cycles and average wind conditions it will be exposed to in its lifetime. In addition, the IEC standard specifies that a WT component should be designed to maintain its structural integrity in case it experiences 50-year extreme wind events during its lifetime.

Fatigue damage to components can be assessed using linear damage accumulation theory based on Miner's rule or nonlinear damage accumulation theories [YLH+15]. Due to its simplicity, Miner's rule [Min45] is widely used. Wind speed variability induces varying-amplitude load spectrum on WT components. To use Miner's rule, the complex spectrum of varying load is often transformed using rain-flow counting (RFC) algorithm, first proposed by [ME68], into simple uniform loading from which stress range histograms can be extracted and used to assess the accumulated damage. A schematic of this procedure is shown in Fig. 5.1.

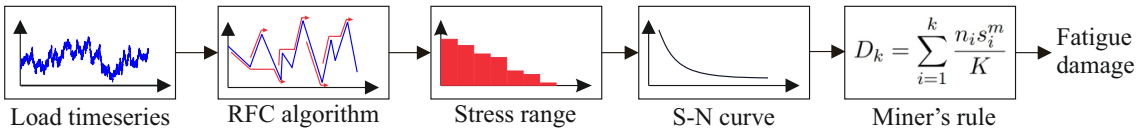

Figure 5.1: Conventional fatigue damage estimation (modified from [DS21])

By combining RFC and Miner's rule, damage accumulation D_k is calculated as

$$D_k = \sum_{i=1}^{k} d_i = \sum_{i=1}^{k} \frac{n_i}{N_i} = \sum_{i=1}^{k} \frac{n_i s_i^m}{K}, \tag{5.2}$$

where k denotes the total number of related stress range histograms, d_i the incremental damage at the i^{th} stress range histogram, n_i the number of applied load cycles in each histogram bin, N_i the number of cycles to failure at the i^{th} stress range histogram, and s_i the applied load amplitude in each histogram bin. With continuous load application, damage in a component progresses from an undamaged state $D_k = 0$ to the point it is considered to have reached its end of life when $D_k = 1$. In this case, the component is considered to have exhausted its structural reserves. Although other cycle counting algorithms exist, including level crossing counting, peak counting, and simple range counting, RFC algorithms are the most widely applied for fatigue analysis [MJ12].

Online rain-flow counting

Most standard RFC algorithms generate equivalent load cycles from complex load spectra by pairing local minima and maxima points using 3-point counting rule. Therefore, the entire load history is needed beforehand for the equivalent cycles to be generated. This process is computationally inefficient because the algorithm has to process all the stored

loading data. Therefore, standard RFC cannot be used for real-time monitoring or control of life consumption of a component [MJ12].

In [MJ12], a real-time implementation of the RFC algorithm is proposed. By employing a 3-point counting rule recursively, the extremal points of timeseries loading data are processed and stored in two flexible stacks as they occur to select the full and half cycles. For each identified cycle, the life consumption of a component is then calculated and incremented online using Miner's rule. This enables online determination of the consumed life of a component as well as implementation of lifetime control. In this thesis, the online damage evaluation algorithm [MJ12] is used to evaluate the accumulated damage in rotor blades and tower. This information is then used to adapt the lifetime controller to ensure a predefined service life of the WT components.

5.1.2 Adaptive lifetime control applied to the WindPACT 1.5 MW reference WT

The extended H_∞ RDAC control approach (RDAC+aIPC) described in section 4.1 is adapted for lifetime control. While the RDAC controller [DS22] described in section 4.1.1 is retained for regulating rotor speed and reducing of tower F-A bending moment, the aIPC controller described in section 4.1.2, is adapted to be a prognostics-based dynamic lifetime controller for reducing blade F-W bending moments in above-rated WT operation. The WindPACT 1.5 MW RWT [RD18] described in section 3.1.1, is selected for the evaluating the proposed adaptive lifetime control strategy. In this section, the aIPC controller is adapted for lifetime control using the online damage evaluation algorithm [MJ12].

To control the lifetime consumption in WT blades, the adaptive robust observer-based controller (RDAC+aIPC), implemented using two control loops is combined with an online damage evaluation model as shown in Fig. 5.2. A wind profile excites the WT dynamics in the above-rated regime. The RDAC controller [DS22], which is robust against modeling errors, generates the primary CPC signal for rotor speed regulation and tower load mitigation, while aIPC is used as a lifetime controller to dynamically control the damage accumulation of the rotor blades. The IPC angles are perturbed about the CPC signal from RDAC and forms the control input u to the WT.

The blade-root F-W bending moment measurements y are logged into memory during simulation. The online damage evaluation model based on the real-time implementation of the RFC algorithm [MJ12], calculates the accumulated damage at every time-step D_k. The estimated lifetime of the blade L_e used as a SOH indicator is calculated as

$$L_e = \frac{T_k}{D_k} D_d, \tag{5.3}$$

where T_k denotes time at the current time-step while D_d denotes the accumulated damage at the design lifetime. At every time-step T_k, the estimated RUL can be calculated as

$$RUL = L_e - T_k = T_k(\frac{D_d}{D_k} - 1). \tag{5.4}$$

Based on the threshold evaluation of L_e, the load mitigation level in the respective IPC controllers is controlled by selecting suitable gains L and K every 10 milliseconds, which is the time-step chosen for lifetime threshold evaluation. For illustrative purposes, a lifetime of 600 seconds is chosen. Three threshold levels are set such that if L_e is below the lower limit of the desired lifetime ($L_e < 580$), maximum gains of respective IPC controllers are

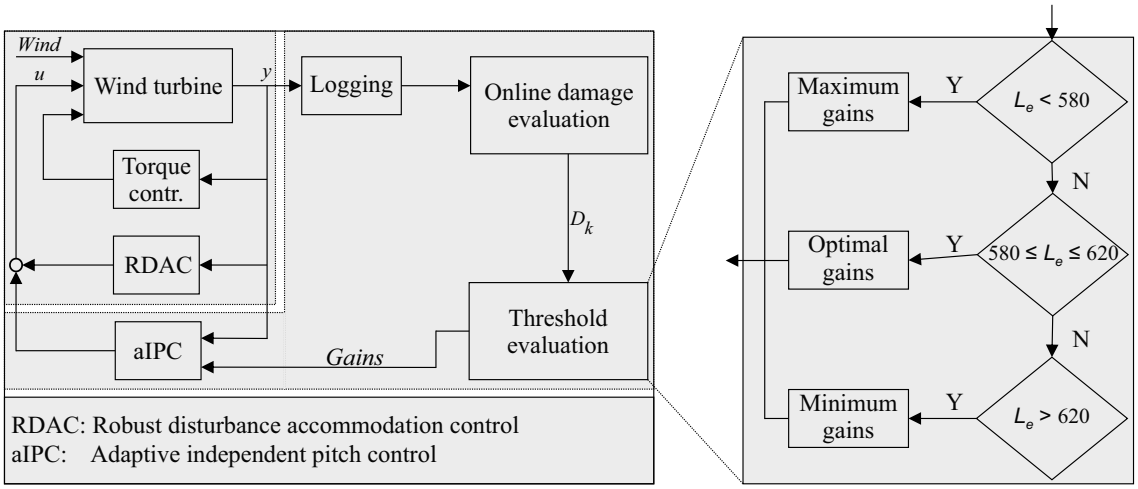

Figure 5.2: Prognostics-based adaptive lifetime control [KDNS23]

selected to increase the blade load mitigation level. If L_e falls within a range of the desired lifetime ($580 \leq L_e \leq 620$), optimal gains that strike a balance between load mitigation and speed regulation are selected. On the other hand, if the value of L_e is higher than the desired lifetime ($L_e > 620$), hence blade load mitigation level can be compromised, minimum gains are chosen.

It is important to note that two switching levels are implemented as illustrated in Fig. 5.3. The first level, used for switching between different IPC controllers, is defined based on the incoming hub-height stochastic wind speed. Highly uncertain WT anemometer measurement should suffice as strict accuracy is not required for switching. Predefined wind speed bins are used for thresholding and activate a suitable IPC controller from the designed controller bank. This ensures that a suitable IPC controller is used for the prevailing operating conditions. The second switching level relies on a lifetime estimate of the blades obtained from the online damage evaluation model to adapt both the full-state feedback gain K and observer gain L of the IPC controller activated in the first switching level to achieve the targeted lifetime. The combined switching constitutes aIPC lifetime control.

5.1.3 Simulation results and discussion

In this section, simulation results obtained from evaluating the adaptive lifetime control strategy using the 1.5 MW NREL RWT [RD18] in FAST design code [JB05] are presented and discussed. Following the IEC 61400-1 recommendation for fatigue load evaluation, a 600 seconds stochastic wind profile generated with TurbSim software [JK12] is used for closed-loop system excitation. The full-field IEC Kaimal type A wind profile shown in Fig. 5.4a has a mean hub-height wind speed of 18 m/s, a turbulence intensity (TI) of 16 % at 15 m/s, and vertical wind shear with a power-law exponent of 0.2. Although such a high wind speed has a low occurrence probability, it drives the dynamics of the WT from near rated to cut-off wind speeds. Therefore, it is useful for demonstrating the performance of the proposed control strategy over a wide range of WT operation. While blade edge-wise

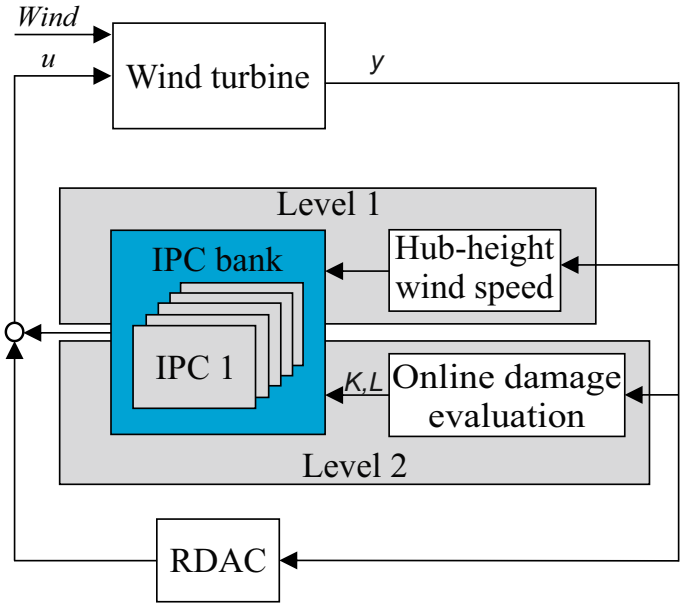

Figure 5.3: aIPC switching implementation [KDNS23]

(E-W) and tower side-side (S-S) bending moments contribute to the total fatigue damage of the respective components, in this thesis, blade F-W and tower F-A bending moments are selected because they represent the main structural loads driving fatigue damage to respective components in above-rated WT operation. This sufficiently demonstrates the application of lifetime estimation of WT components as a SOH indicator to determine a trade-off between load mitigation and speed regulation and ensure a certain damage at a desired lifetime.

The performance of the lifetime control scheme in different blade load mitigation scenarios is shown in Fig. 5.4b. As shown, the adaptive lifetime control strategy controls the damage accumulation in the blades to reach the predefined damage limit at the desired lifetime of 600 seconds. While the maximum load mitigation control strategy achieves the same desired result, the lifetime control scheme distributes the incremental damage accumulation over the entire operation window by dynamically switching between the different load mitigation levels.

The baseline controller (without lifetime control) used for comparisons is RDAC+aIPC without lifetime control, where switching in aIPC is based only on incoming wind speed as described in section 4.1.2. To evaluate the proposed controller in changing wind fields, six profiles with mean wind speeds of 18 m/s and 14 m/s and three seeds each are used. The three wind profiles with a mean wind speed of 18 m/s are shown in Fig. 5.5a. A comparison in blade F-W bending moment load mitigation performance is shown in Fig. 5.5b. On average (for the three wind fields), adaptive lifetime controller achieves standard deviation δ reduction of 9.39 % compared with the baseline controller. In addition, there is significant reduction in the accumulated damage as shown in Fig. 5.5c.

Performance of the adaptive lifetime control strategy in mitigating tower loads is also evaluated. As illustrated in Fig. 5.6a, significant reduction in tower F-A oscillation is observed, with the average δ reduced by 6.58 %. A reduction in tower damage accumulation can be seen in Fig. 5.6b. This shows that lifetime control of blades, which reduces 1P fatigue

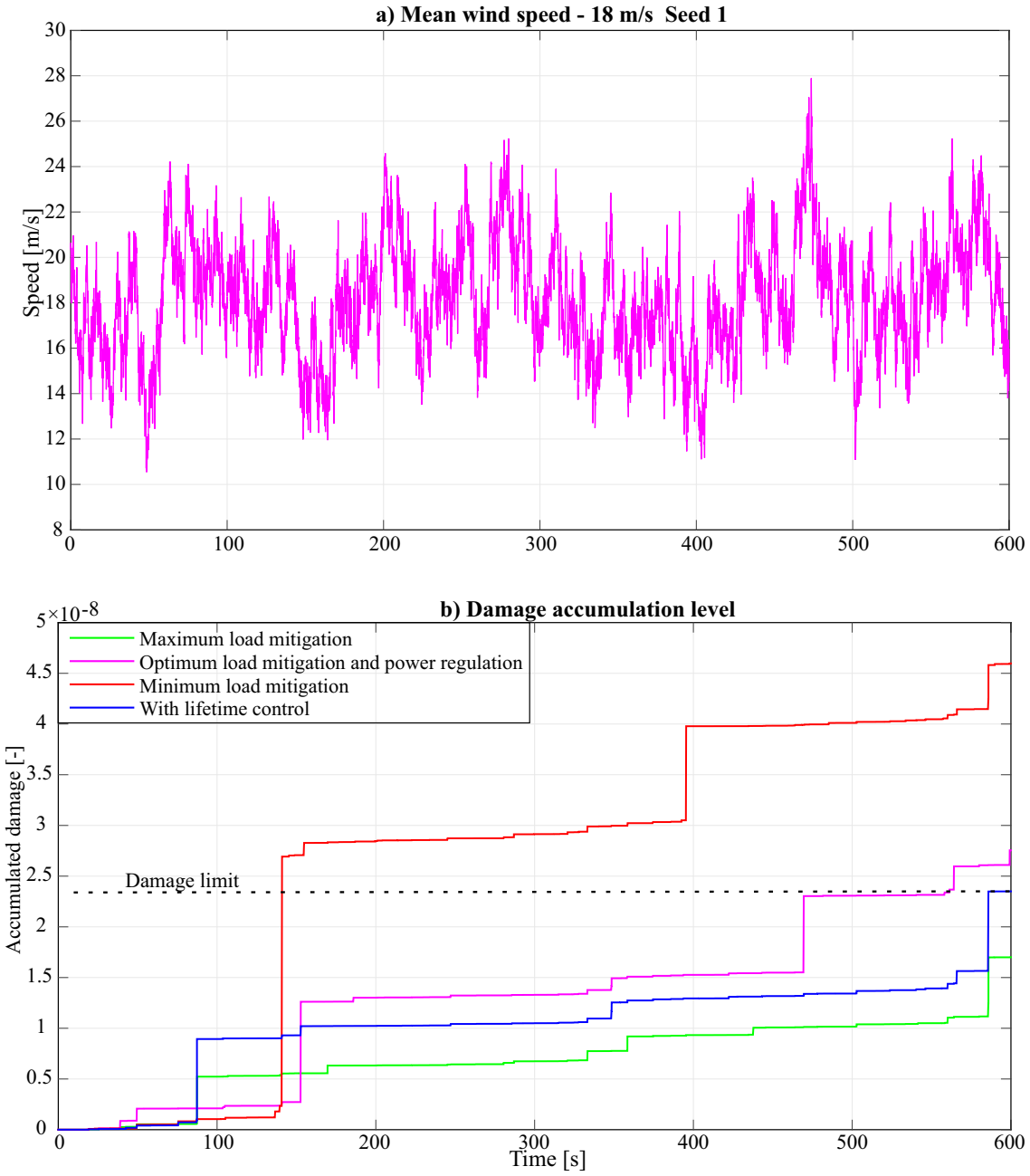

Figure 5.4: Adaptive lifetime control performance [KDNS23]

loads results in less damage accumulation in tower due to 3P fatigue loads. To evaluate the performance of the proposed lifetime control scheme in load mitigation in different tower and blades load channels, damage equivalent load (DEL) analysis is performed using MLife software [Hay12]. Based on fatigue analysis performed with results obtained using the 10-minute stochastic wind profile shown in Fig. 5.5a, the lifetime controller reduces DELs in the blade F-W and tower F-A as shown in Fig. 5.6c. No noticeable change in blade E-W DEL is achieved. However, a slight increase is observed in tower S-S DEL, which is attributed to a slight increase in pitch activity for improved load reduction.

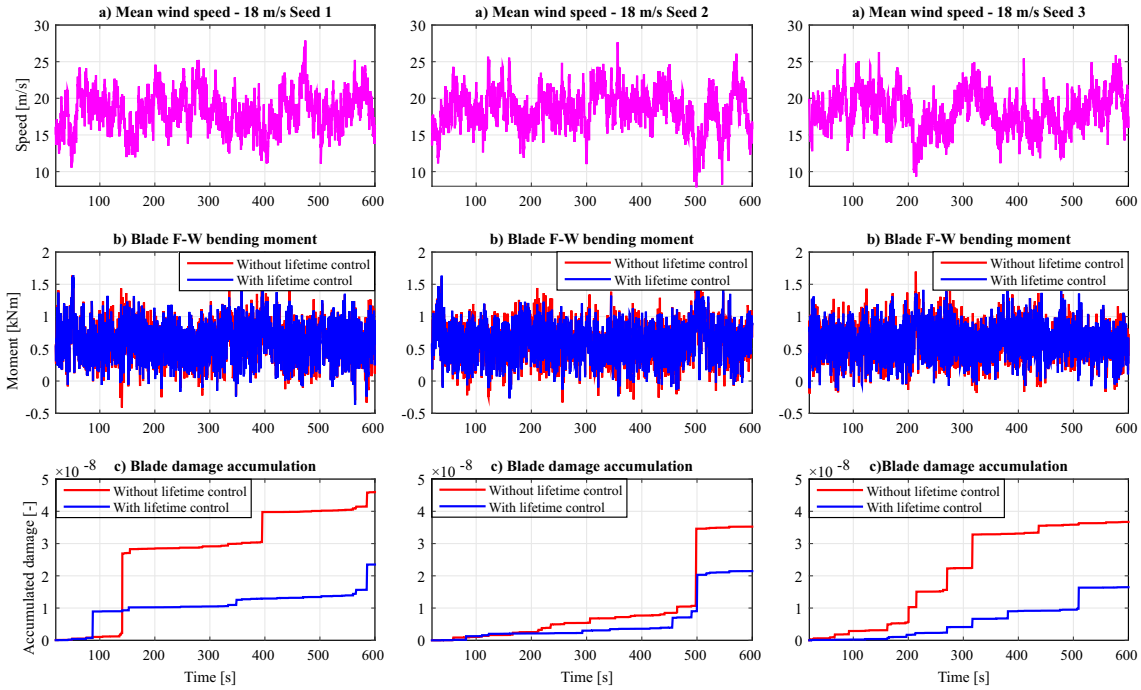

Figure 5.5: Blade fatigue load mitigation for 18 m/s wind [KDNS23]

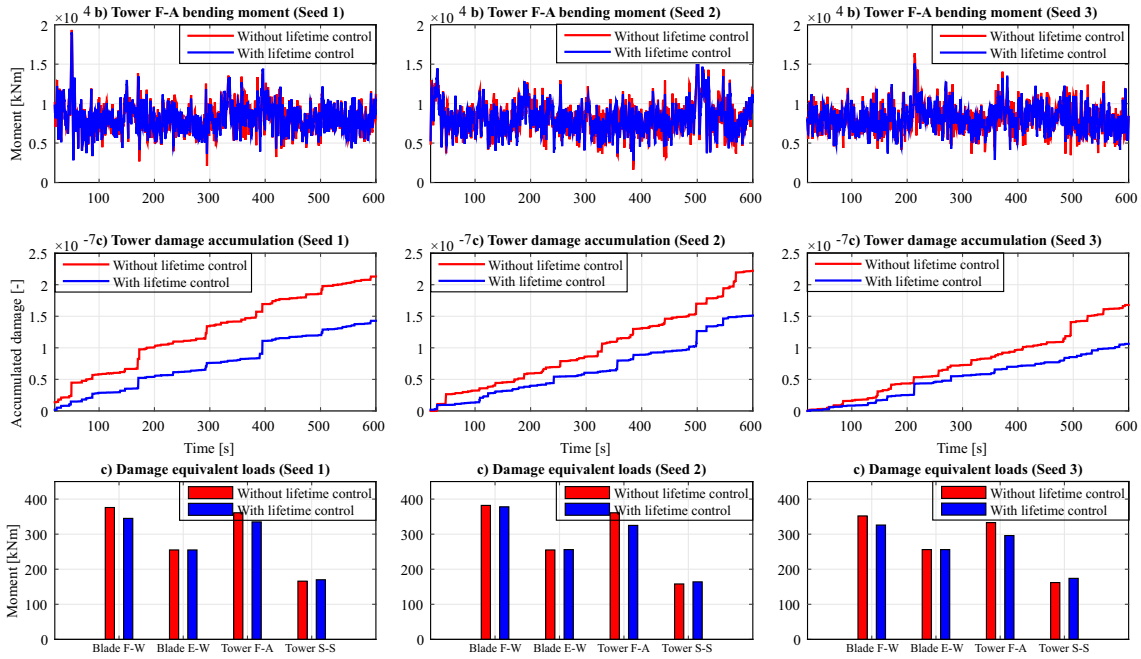

Figure 5.6: Tower fatigue load mitigation and DEL analysis for 18 m/s wind [KDNS23]

Although the adaptive lifetime controller achieves improved performance in reducing damage accumulation in both rotor blade and tower, it is important to ascertain that this does not compromise speed/power regulation performance. To illustrate this, the rotor speed and generator power are evaluated as shown in Fig. 5.7. With lifetime control, no

significant change in rotor speed regulation is realized. Although there is a slight increase of 8.7 % in power δ, the generated power fluctuates within acceptable limits. The mean power is identical at 1560.13 kW and 1559.97 kW for the baseline and lifetime controllers, respectively. Improvement in both load mitigation and rotor speed regulation is achieved with insignificant additional pitch activity as shown in Fig. 5.7c. The average total pitch travel marginally increases by 0.13 %.

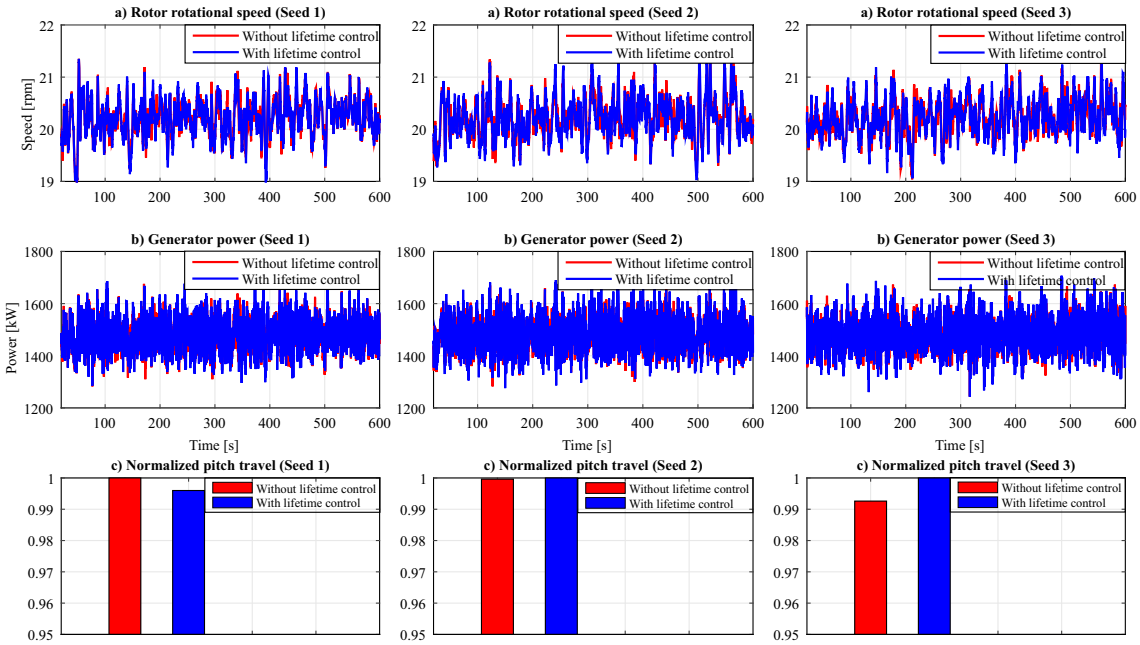

Figure 5.7: Speed/power regulation performance and pitch actuator usage for 18 m/s wind [KDNS23]

Given that a wind field realization of 18 m/s has a low occurrence probability because WTs spend most of the time operating near-rated wind conditions, the proposed adaptive lifetime control strategy is evaluated using a near-rated wind profile. For this purpose, three IEC type C stochastic wind field realizations shown in Fig. 5.8a, each with a mean speed of 14 m/s and a TI of 12 % at 15 m/s are used. Fatigue load mitigation performance of the proposed lifetime controller in the blades is evaluated against the baseline controller as shown in Fig. 5.8b. The lifetime controller achieves 10.1 % reduction in δ of the blade F-W bending moment. In addition, significant reduction in the accumulated damage is achieved.

A reduction in tower F-A loading and damage accumulation is realized as shown in Fig. 5.9a. The δ of tower load is reduced by 11.2 %. Fatigue analysis is performed using simulation results based on the wind profiles shown in Fig. 5.8a. As illustrated in Fig. 5.9c, the adaptive lifetime controller achieves reduction in DELs in all load channels except for the slight increase in tower S-S DEL.

Speed and power regulation performance of the proposed controller is also evaluated at near-rated wind conditions as shown in Fig. 5.10. With lifetime control, improvement is achieved in both speed and power regulation, with the δ of rotor speed and generated power reducing by 1.3 % and 1.2 %, respectively. The mean power is identical at 1553.5 kW and 1553.73 kW for the baseline and lifetime controllers, respectively. Improvement in

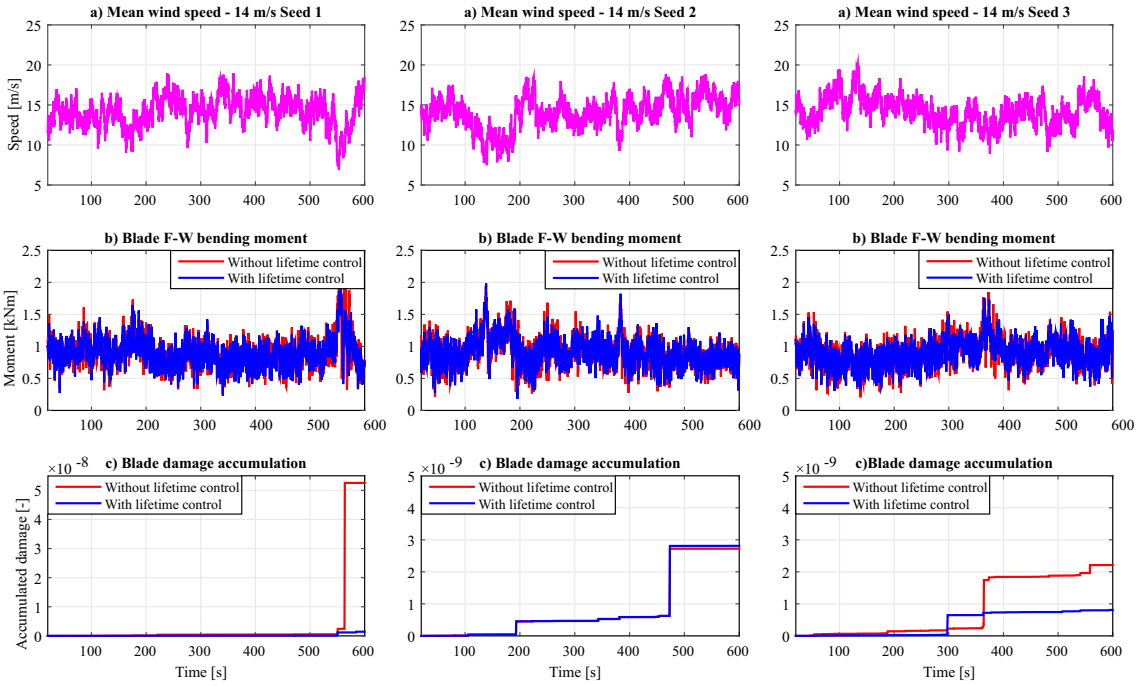

Figure 5.8: Blade fatigue load mitigation for 14 m/s wind [KDNS23]

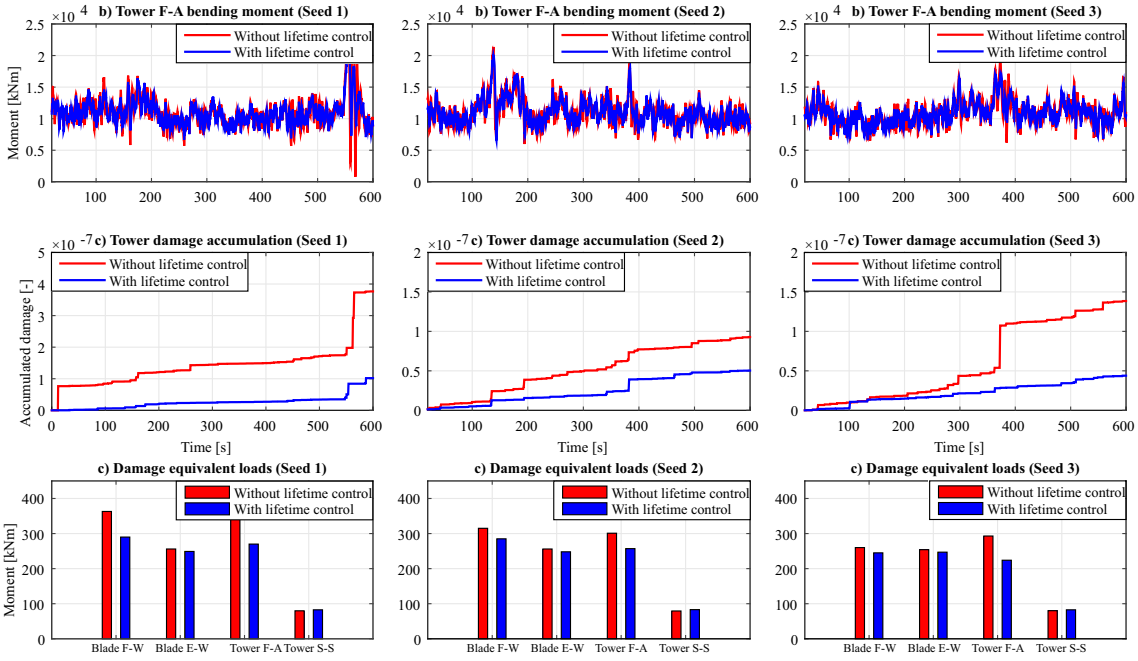

Figure 5.9: Tower fatigue load mitigation and DEL analysis for 14 m/s wind [KDNS23]

both load mitigation and speed regulation accompanied by insignificant additional pitch activity as shown in Fig. 5.10c. The average total pitch travel increases slightly by 0.5 %. Therefore, the proposed adaptive lifetime control strategy performs well in near-rated wind conditions.

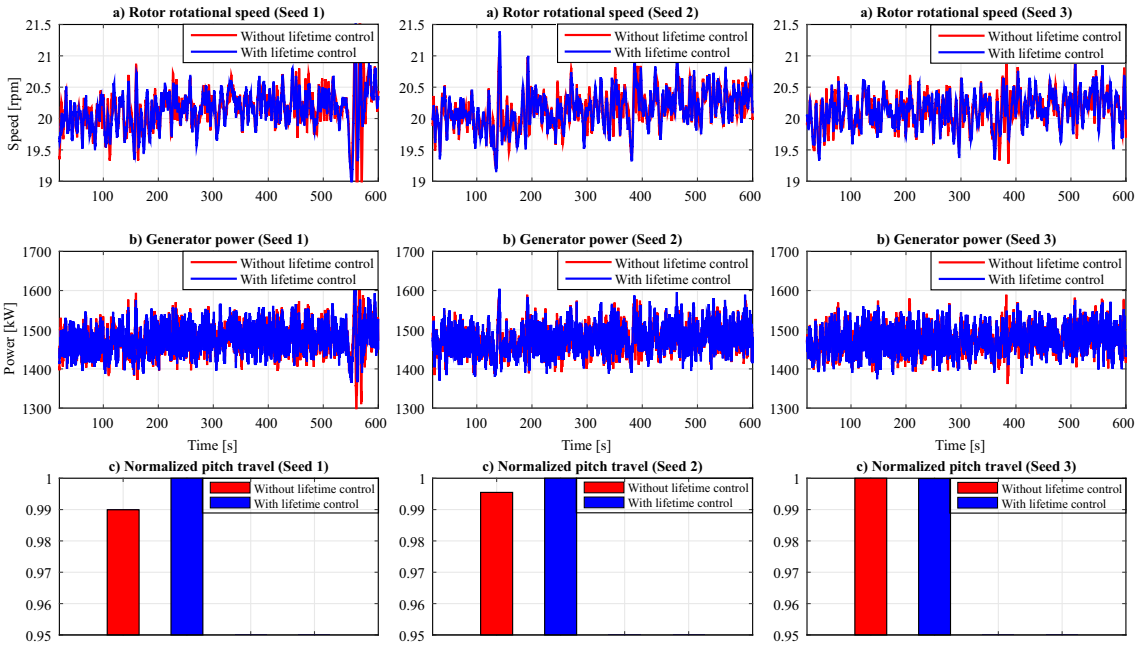

Figure 5.10: Speed/power regulation performance and pitch actuator usage for 14 m/s wind [KDNS23]

5.1.4 Summary

A prognostics-based adaptive control strategy for lifetime control of WTs is presented. A H_∞ RDAC controller is used as the primary controller for mitigating tower loads and regulating rotor speed using a CPC signal. On the other hand, aIPC controller designed using LQG control method is used as a lifetime controller. The gains of each of its five IPC controllers are adapted based on the SOH of the rotor blades, obtained using an online damage evaluation model to strike a compromise between lifetime control and rotor speed regulation. Through simulations on a 1.5 MW WT model, it is demonstrated that the adaptive lifetime control strategy controls the damage accumulation in the blades to achieve a certain damage limit at the desired lifetime. In addition, reduction in tower damage accumulation is achieved. The proposed approach can potentially be used to optimize maintenance scheduling in wind farms by synchronizing the aging of WT components, thereby reducing O&M costs and increasing operational reliability. Fatigue analysis shows reduction of DELs in most load channels. This improvement is realized without compromising speed/power regulation performance. With the lifetime control approach, these results are achieved without significantly increasing pitch actuator duty cycle.

The limitation of the proposed lifetime control approach is that although one loop is used to control fatigue damage in the blades, a separate loop is used for speed regulation and tower load mitigation. Therefore, overall system optimality is not guaranteed. In addition, the online damage evaluation model used is based on Miner's rule, which assumes of linear damage accumulation. However, WT components are subjected to complex and nonlinear degradation due to several failure modes. Therefore, nonlinear degradation models can be considered for improved lifetime control. Although, the proposed lifetime control strategy is applied to WTs in above-rated operation, this concept can be extended

for lifetime control in below-rated operation, with suitable objectives such as reducing structural loads while maximizing power extraction. A robust adaptive lifetime control approach based on hybrid SHM and prognosis method is required for improved lifetime prediction performance.

5.2 A hybrid approach for robust lifetime control

In this section, a hybrid prognosis scheme that combines data-driven load prediction and model-based damage estimation models for robust lifetime control of WTs is outlined. A support vector machine (SVM) regression model is selected for tower load prediction because it is a well-known ML method and can be directly integrated into the existing framework. The data-driven SVM regression model is trained and tested using timeseries featured data from dynamic simulations (for various wind conditions) using the μ-synthesis robust disturbance accommodating controller (RDAC2) described in section 4.3. The regression model uses available WT measurements to predict the tower load. Based on this prediction, an online RFC damage evaluation model [MJ12] described in section 5.1.1, estimates the SOH and lifetime of the tower. Using the estimated lifetime and a set of predefined thresholds, the RDAC2 controller gains are dynamically adapted to achieve a predefined damage limit and lifetime. The proposed hybrid lifetime control approach is applied to the 5 MW NREL RWT [JBMS09] described in section 3.1.2. Its performance is compared with a model-based prognosis scheme that uses ideal WT tower measurement. Simulation results demonstrate the efficacy of the proposed approach to control fatigue loading in WT components to achieve a predefined damage level and lifetime without compromising generator speed regulation.

5.2.1 Structural health monitoring and prognosis of WTs

In this section, a brief summary of the SHM and prognosis approaches applied to WTs is given. A comprehensive review is given in section 2.3.

Model-based methods are suitable for fault diagnosis and prognosis of WT in real-time. To achieve this, degradation models are obtained either through physical modeling or through system identification are used These models use the dynamic behaviour of the system, CM data, and damage evaluation models to predict the RUL of critical components [RKO$^+$21]. Model-based approaches are developed under the assumption that the failure process conforms with a physical law. Measured monitoring data is used to identify model parameters for predicting the future degradation evolution, hence obtaining the RUL. The choice of which model to use is problem-specific. The degradation model is a function of loading conditions, elapsed time/cycle, and model parameters. Loading conditions and time are often assumed to be given [KAC17]. Stochastic wind fields subject WTs to varying loads, which cause fatigue loading of structural components during operation. A number of models for lifetime prediction have been proposed, including fatigue life and progressive damage models, probabilistic damage growth models, and those based on virtual fatigue estimators. To estimate the lifetime from given fatigue stress data, RFC algorithm is used in combination with Miner's rule of linear damage accumulation and material-specific fatigue stress amplitude (S) versus number of cycles (N) curve, well known as S-N curve [CCC$^+$19]. The S-N curve defines the allowable fatigue cycles to failure. Fatigue life models calculate the RUL of a WT through extrapolation of fatigue data. Variables describing

component degradation are used in progressive damage models to estimate damage. In this thesis a real-time implementation of the RFC algorithm [MJ12] is applied for fatigue damage evaluation.

Data-driven methods rely on featured system degradation data (instead of explicit input-ouput models) in combination with suitable machine learning (ML) techniques to establish a knowledge-base representing an explicit dependency of system variables [LLJ19; JKS19; GL21]. The advantage of this approach for lifetime modeling of WTs lies in its ability to work with insufficient process data and its scalability and versality [JKS19]. However, most do not consider long-term dependencies hidden in timeseries data [LLJ19]. Modern WTs are instrumented with high frequency SCADA systems whose timeseries data such as vibration and acoustic measurements is used for fault diagnosis and prognosis. Historical WT performance data is used in ML to learn the system's dynamics, estimate the SOH, and predict its RUL. Data-driven fault diagnosis and prognosis methods have limited ability to learn complex signals with nonlinear characteristics such as degradation patterns in WTs. When used to process big data, traditional data-driven methods exhibit slow convergence speed and low prediction accuracy [XWY$^+$21]. Although modern deep-learning methods have sped up convergence speed and improved prediction accuracy, most do not consider long-term dependencies hidden in timeseries data [LLJ19]. In the proposed approach, an SVM regression model is developed and implemented for online tower load prediction.

In the recent past, hybrid approaches for fault diagnosis and prognosis in WTs have been proposed. Although model-based approaches require complex predefined physics or analytical models, they have excellent real-time capability due to their online implementation. Data-driven methods rely on historical operational data, typically acquired using SCADA and ML algorithms to establish a knowledge-base used for CM. However, they require a large amount of data with many degradation sequences for training [WLZ$^+$20; RKC$^+$20b], which is limited in practice in the context of WTs with nonstationary degradation patterns [HRBA$^+$18]. In addition, training and validation process in data-driven approaches is time consuming [GL21]. Hybrid prognosis methods that combine model-based and data-driven approaches capitalize on the advantages of aforementioned methods while counteracting their individual limitations [GL21]. Hybrid approaches have good prediction performance because they enable accurate modeling of uncertainty. However, hybrid prognosis algorithms can be extremely sophisticated and are constrained by the requirement for physical modeling of degradation events. [BMS23]. Therefore, for successful implementation of a hybrid model, the physical degradation model should be reliable and adequate historical degradation data should be available.

5.2.2 Hybrid robust lifetime control applied to the 5 MW NREL reference WT

A hybrid approach for robust lifetime control of WTs is proposed. An SVM regression model used for tower load prediction is combined with an online RFC damage accumulation model [MJ12]. The SVM regression model is trained and tested using timeseries data obtained from closed-loop simulation using the RDAC2 controller. The efficacy of the proposed approach is evaluated online on the 5 MW NREL RWT [JBMS09].

The online damage evaluation model [MJ12] is used to evaluate the tower damage accumulation at every timestep D_k. The estimated lifetime of the tower L_e=600 seconds, used as the SOH indicator, is calculated based on (5.4), where T_k denotes the time at

the current time-step while D_d denotes the accumulated damage of the tower at defined lifetime.

Due to the massive size of the towers in commercial WTs, strain gauge measurements are unreliable and are usually not used for load determination. However in OpenFAST software [NRE21], it is provided for design purposes. Therefore, to implement prognosis of tower fatigue life in an actual WT, its load should be estimated using available measurements. In this thesis, an SVM regression model is developed for predicting tower F-A bending moment. The WT measurements used as predictors include, the horizontal hub-height wind speed d, tower F-A displacement σ, rotor power p , and tower F-A acceleration γ. For training and testing, timeseries data from closed-loop simulations in various wind conditions shown in Fig. 5.11 is used. Six wind profiles having TIs of 5 % and 15 % are used for training, and three with 10 % TI are used for testing. In the training phase, the best set of hyperparametes is obtained by applying Bayesian optimization. To evaluate the performance of the model, root mean square error (RMSE) is used, with the model using a linear kernel function returning the lowest RMSE. For training and testing, the RMSE of the predicted response is 609 kNm and 597.3 kNm, respectively, corresponding to an accuracy of 98.4 % and 98.5 %, respectively. The high prediction accuracy is validated using a new set of wind profiles for simulating the proposed prognosis scheme. It is important to note that other ML regression models such as Gaussian process regression (GPR) and a neural network (NN) were used for training. Although GPR model returned the same prediction accuracy as SVM regression, the training time was quite long. On the other hand, although the NN regression model had slightly better prediction accuracy, it had slow convergence, which is not suitable for online implementation.

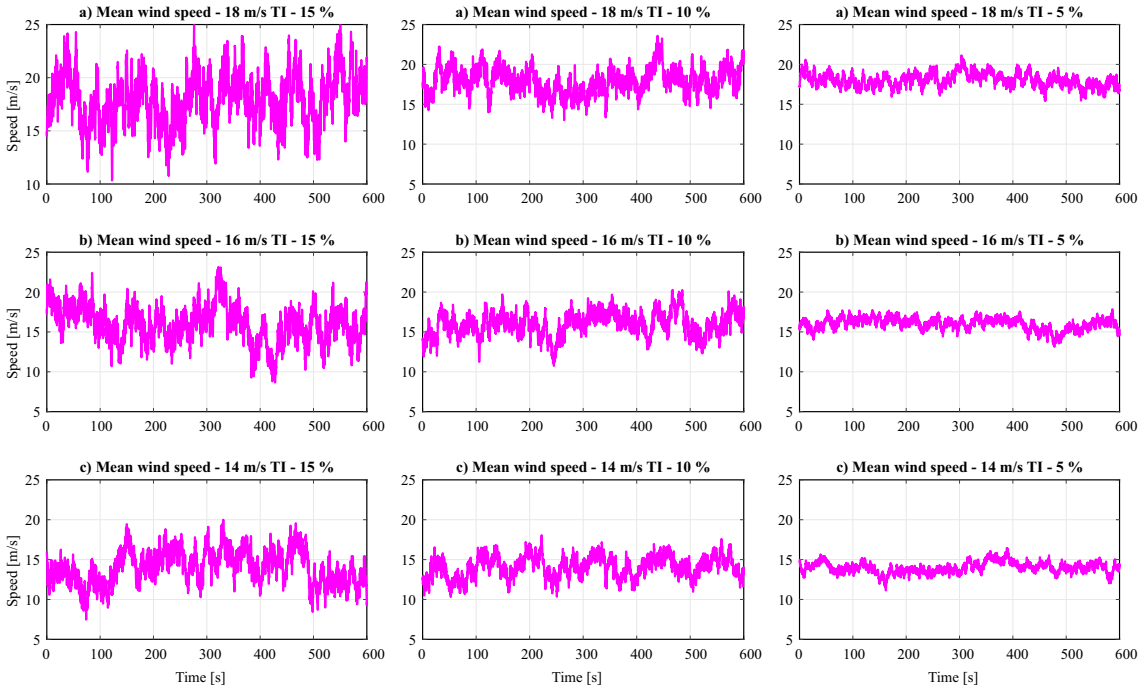

Figure 5.11: Wind profiles used for SVM regression training and testing [KLS24]

The proposed hybrid prognosis approach applied for controlling the lifetime of the 5 MW NREL RWT using RDAC2 controller is shown in Fig. 5.12. The online prognosis

scheme is realized using an SVM regression model for tower F-A load prediction ζ and a damage evaluation model for real-time calculation of D_k. The threshold evaluation model uses D_k to calculate L_e using (5.4). Based on the threshold values set for L_e, RDAC2 controller gains are adapted continuously to vary the degree of trade-off between tower load mitigation and generator speed regulation. This ensures that the predefined damage limit is not exceeded at the desired lifetime and that generator speed regulation is not compromised.

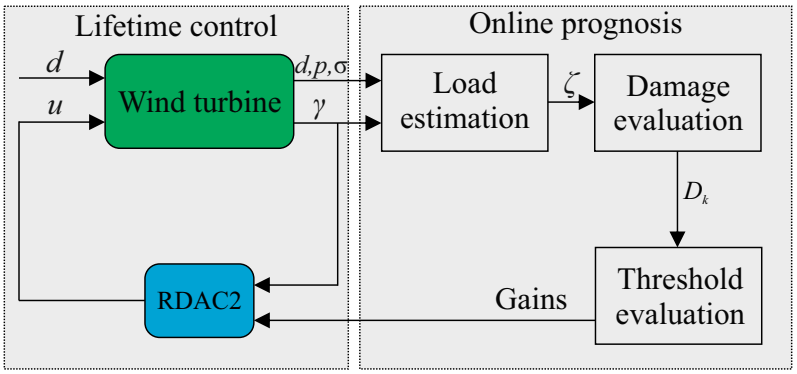

Figure 5.12: Hybrid lifetime prognosis scheme applied to the 5 MW NREL RWT [KLS24]

5.2.3 Simulation results and discussion

To validate the proposed hybrid prognosis scheme for lifetime control, closed-loop dynamic simulations are performed in OpenFAST using the 5 MW NREL RWT. The goal of the prognosis scheme is to control the fatigue life consumption of the tower while maintaining optimal generator speed regulation. The performance of the hybrid prognosis control scheme, henceforth denoted as Life2, is evaluated against a non-lifetime RDAC2 controller, henceforth denoted as Baseline, tuned for optimal trade-off between tower load mitigation and generator speed regulation. It is also compared with the model-based prognosis control scheme, henceforth denoted as Life1, which uses RDAC2 as the lifetime controller and relies on actual tower load measurements for fatigue damage evaluation using online damage accumulation model [MJ12].

Lifetime control

A new set of wind profiles shown in Fig. 5.13a are used in the simulations. In Figure 5.13b, the tower F-A load response is shown. The baseline controller exhibits the highest vibrations compared with the lifetime prognosis-based control schemes Life1 and Life2. The proposed hybrid prognosis scheme Life2 shows similar responses to Life1, hence validating the high prediction accuracy of the SVM regression model. In Table 5.1, the δ in tower F-A load is shown. Both lifetime controllers achieve 3.4 % improvement in load reduction. In Figure 5.13c, the tower damage accumulation is shown. In both 19 m/s and 17 m/s wind fields, the lifetime controllers achieve the desired damage limit at the predefined lifetime of 600 s. However, for the 15 m/s wind profile, Life1 does not achieve the damage limit due to the suboptimal trade-off in control objectives at this operating point, which can

be improved by retuning the RDAC2 controller. On the other hand, the proposed hybrid scheme meets the desired damage limit.

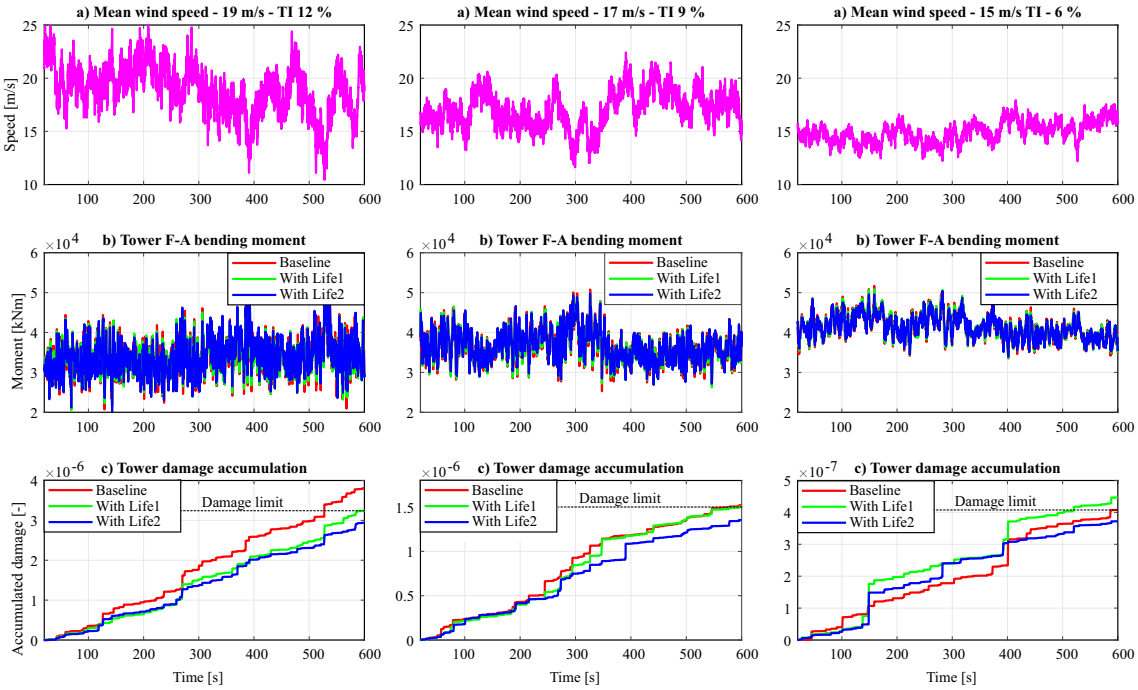

Figure 5.13: Tower F-A load response and damage accumulation [KLS24]

Table 5.1: Load mitigation, pitch activity, and generator speed/power regulation performance analysis (Key: best, worst) [KLS24]

Parameter	Units	Controller	19 m/s	17 m/s	15 m/s	Avg.	%
Tower F-A (δ)	kNm	Baseline	4438.3	3855.1	3028.4	3773.9	-
		Life1	4265.6	3709.0	2963.0	3645.9	-3.39
		Life2	4265.6	3708.7	2963.0	3645.8	-3.40
Pitch rate (RMS)	°/s	Baseline	3.946	2.152	0.976	2.358	-
		Life1	5.500	2.955	1.208	3.221	36.6
		Life2	5.500	2.959	1.208	3.223	36.7
Speed (RMSE)	rpm	Baseline	12.14	9.46	6.46	9.35	-
		Life1	12.05	9.33	6.32	9.23	-1.26
		Life2	12.14	9.45	6.46	9.35	-0.01
Power (RMSE)	kW	Baseline	166.46	106.45	55.95	136.46	-
		Life1	177.87	108.10	56.38	142.98	4.78
		Life2	166.46	106.43	55.95	136.45	-0.01

Generator speed regulation

The impact of applying the proposed hybrid prognosis scheme on generator speed and power regulation is evaluated as shown in Fig. 5.14. To reduce tower fatigue damage, the proposed scheme Life2 increases pitch activitity as illustrated in Fig. 5.14a. However, as

shown in Table 4.14, RMS of pitch rate (PR) does not exceed the maximum PR constraint of 8 ^{o}/s for the 5 MW NREL RWT. Compared with the baseline controller, Life2 ensures optimal generator speed and power regulation as shown in Fig. 5.14b and the RMSE values in Table 4.14. However, Life1 shows better speed regulation.

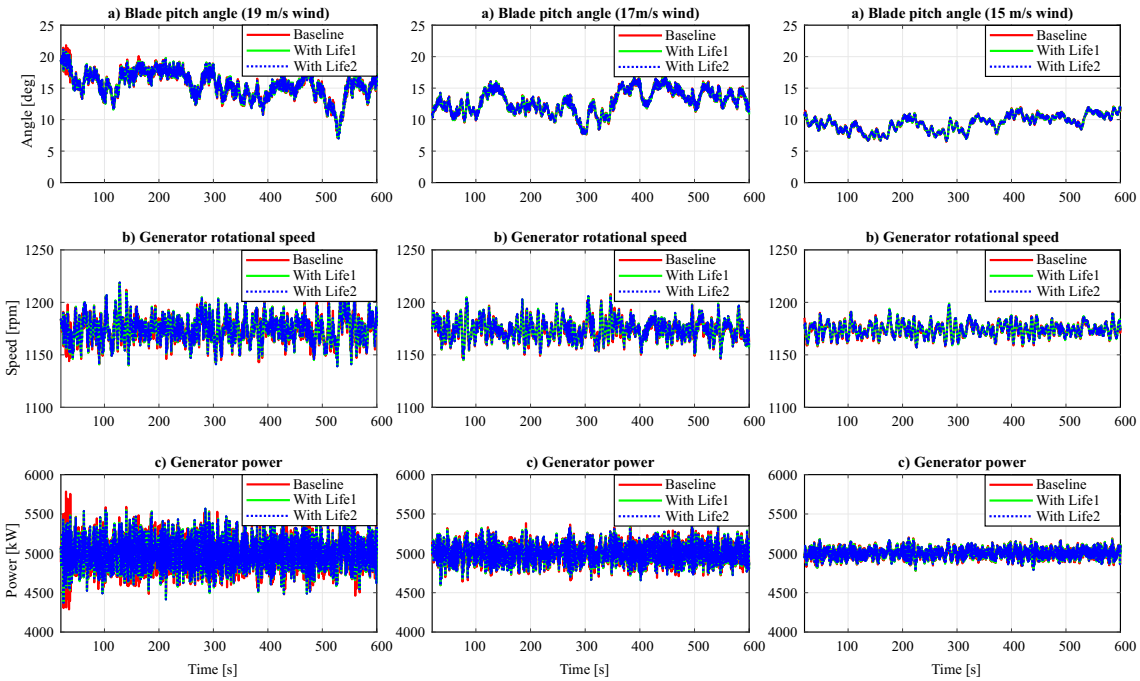

Figure 5.14: Generator speed and power regulation [KLS24]

5.2.4 Summary

A hybrid prognosis scheme for robust lifetime control of WTs is presented. To realize online prognosis, an SVM regression model is developed for tower load prediction, and a real-time RFC damage evaluation model is used for SOH estimation. The estimated lifetime of the tower is evaluated at each time-step. Based on a set of lifetime thresholds, the gains of RDAC2 controller are adapted, ensuring that the damage limit of the component is not exceeded at the desired lifetime. The 5 MW NREL RWT is used to evaluate the efficacy of the proposed approach. Its performance is compared with a model-based lifetime control scheme, which uses ideal WT load measurements. Dynamic simulation results show that the proposed approach controls the life consumption of the WT tower to achieve a predefined damage limit and lifetime without compromising generator speed regulation. The perfomance of the proposed approach is comparable to the model-based lifetime control method and is therefore suitable for practical implementation. The limitation of the proposed approach is that a linear degradation model is used for a fatigue load estimation. However, WT components experience complex nonstationary degradation patterns due to several failure modes. State-of-the-art (SOTA) model-based prognosis approaches such as Bayesian method (BM) or particle filter (PF) can be considered for improve fatigue life estimation. Furthermore, due to abundant data collected from modern high frequency SCADA systems, deep learning ML regression models can be considered for improved load

prediction accuracy. Therefore by combining physics-based models using SOTA methods such as BM or PF, and deep learning algorithms, hybrid prognostics-based robust lifetime control approaches can be developed for improved RUL prediction.

5.3 Conclusions

In this thesis, prognosis-based robust lifetime control schemes applied to commercial WTs are presented. First, the extended H_∞ RDAC controller (RDAC+aIPC) combined with an online RFC damage evaluaton model for lifetime control of the WindPACT 1.5 MW RWT is described. This model-based approach controls damage accumulation in the rotor blades to achieve a certain damage limit at the desired lifetime. In addition, reduction in tower damage accumulation is achieved without compromise in the speed/power regulation performance or blade pitch usage. However, because this approach uses two control loops to realize the desired objectives, overall system optimality can be impacted. Furthermore, the approach is applied to a small 1.5 MW RWT, which does not reflect the current trend in the size of commercial WTs. Secondly, to address the aforementioned limitations, a hybrid prognostics-based robust lifetime control approach that uses an SVM regression model for tower load prediction, and a real-time RFC damage evaluation model for SOH estimation is presented. This approach is applied for lifetime control of the larger 5 MW RWT. The μ-synthesis RDAC2 approach is used as the lifetime controller to control the life consumption of the tower. The performance of the proposed approach is comparable to a model-based lifetime prognosis method albeit with better generator speed regulation, demonstrating the practicality of the method. The common limitations of the proposed prognostics-based robust lifetime control approaches is that a linear degradation model is used for a fatigue load estimation. Degradation models based SOTA model-based prognosis approaches such BM or PF can be considered for improved performance. In addition, the proposed approaches can be extended to lifetime control in below-rated WT operation.

6 Summary, Contributions, and Outlook

6.1 Summary

In this thesis, robust approaches for structural load mitigation, speed/power regulation, and prognosis-based lifetime control of commercial wind turbines (WTs) in above-rated wind speed operation are developed. Dynamic wind speed variability causes fatigue loads, particularly in large utility-scale WTs operating in high wind speed regime. A wind disturbance model is included in the robust control approaches to suppress the influence of wind on the performance of a WT system. To compensate for uncertainities related to modeling errors and nonlinearities, the control methods are optimized using H_∞ synthesis approach. To improve robust performance, uncertainty descriptions are modeled using a family of plants and μ-synthesis approach is used to optimize the controllers. In addition to load reduction in the tower, independent pitch control (IPC) is used to reduce asymmetric blade loads caused by vertical wind shear and gravitational loads. The proposed approaches show improved performance compared with baseline gains-scheduled proportional integral (GSPI) controllers.

Wind turbines experience faults or failures due to component degradation either through aging or extreme load events. This is undesirable as it leads to system downtime and economic losses. Structural health monitoring (SHM) and prognosis schemes used for estimating state-of-health (SOH) and predicting remaining useful life (RUL), ensure operational safety and reliability of WT systems. Prognostics-based control schemes, which integrate SHM and prognosis methods are used to control the life consumption of fatigue components and extend their lifetime. These approaches rely on a fatigue damage evaluation criteria to determine the SOH and predict RUL. Control setpoints are then adapted to achieve a desired lifetime of the components. In this thesis, a comprehensive review of SHM and prognosis methods as well as prognostics-based control schemes applied to commercial WTs is presented. The developed robust control approaches are applied in reliability-oriented prognosis for lifetime control of WTs. First, a model-based robust adaptive lifetime control scheme is developed and applied to a 1.5 reference WT (RWT) to reduce the life consumption of rotor blades. Secondly, a hybrid prognostics-based robust lifetime control scheme is applied to a 5 MW RWT to reduce fatigue loads in the tower.

6.2 Contributions

Within the scope of the thesis and related published papers, the following contributions are claimed:

1. A new adaptive robust observer-based controller for reducing structural loads in multiple WT components based on CPC and IPC control is developed and evaluated.

A CPC-based H_∞ robust disturbance accommodating controller (RDAC) is used to mitigate tower loads and regulate rotor speed, while an adaptive IPC (aIPC) controller designed using linear quadratic Gaussian (LQG) control is used to reduce blade loads. The method achieves significantly better results compared with GSPI and H_∞ RDAC controllers.

2. The CPC-based H_∞ RDAC controller is designed and evaluated based on a larger high fidelity 5 MW RWT, which reflects both physical size and power rating of WTs in industry. The performance of this controller is tested on the latest reference open-source controller (ROSCO), which has modules similar to those found in industry controllers. The H_∞ RDAC controller outperforms ROSCO in tower load mitigation without a significant trade-off in generator speed regulation.

3. The RDAC controller is designed based on μ-synthesis approach following the DK-iteration process. To address the conservative robustness of the H_∞ RDAC controller, a model uncertainty description is developed using on a family of plants obtained at different operating points, and incorporated into the nominal WT model for improved robust performance. The CPC-based μ-synthesis RDAC controller is applied to the 5 MW RWT for tower load migation and generator speed regulation. The efficacy of the proposed controller is evaluated against the ROSCO and H_∞ RDAC controllers. It achieves improved robust performance compared with H_∞ RDAC in reducing tower loads and regulating generator speed without inducing significant blade loads.

4. An IPC-based RDAC (IPC-RDAC) controller is developed for structural load mitigation and generator speed regulation of the 5 MW RWT. The novel IPC-RDAC controller is designed using μ-synthesis approach for improved robust performance. The use of IPC enables load reduction in the rotor blades and tower components. Periodic twice per revolution (2P), 3P, and 4P frequencies, as well as the first-mode tower fore-aft frequency reflected in the rotor blades are reduced by the design of respective weighting functions. The performance comparison of IPC-RDAC with ROSCO, H_∞ RDAC, and μ-synthesis RDAC controllers shows that it reduces fatigue loads in the blades and tower without trading off generator speed regulation performance. It also exhibits reduced loads in other WT load channels. Damage equivalent load (DEL) evaluation shows a reduction in fatigue loads in most load channels.

5. The adaptive robust observer-based controller is applied for lifetime control of the 1.5 MW RWT. The CPC-based H_∞ RDAC is used as the primary controller for mitigating tower loads and regulating rotor speed, while aIPC controller is selected as the prognostics controller. The gains of aIPC are adapted based on the SOH of rotor blades determined using an online RFC damage evaluation model to strike a compromise between lifetime control (through load mitigation) and rotor speed regulation. The adaptive lifetime control strategy controls the damage accumulation in the blades to achieve a certain damage limit at the desired lifetime. Reduction in accumulated damage in the tower is also realized without a trade-off in generator speed regulation or significant increase in pitch activity.

6. A hybrid (model-based data-driven) prognosis scheme for robust lifetime control of commercial WTs is developed. The μ-synthesis RDAC control method is selected as the prognostics controller. To realize online prognosis, a support vector machine

(SVM) regression model is developed for tower load prediction, while a real-time RFC damage evaluation model is used for SOH estimation. Based on a set of lifetime thresholds, the gains of μ-synthesis RDAC controller are adapted, ensuring that the tower's damage limit is not exceeded at the desired lifetime. The approach is evaluated on a 5 MW RWT. Its performance is comparable to a model-based μ-synthesis RDAC prognostics controller which uses ideal tower measurements, hence demonstrating its practicality.

6.3 Outlook

In this thesis, RDAC control approaches are used in structural load reduction and speed regulation of commercial WTs in above-rated operation. These approaches can be extended to below-rated operation for to meet the objectives of structural load mitigation and power maximization. To achieve this, the control approaches should be redesigned considering the new objectives. As offshore WTs increase in size and more of these large turbines are installed in remote areas with deeper waters and stronger and steadier winds, the proposed approaches can be extended to this class of WTs for structural load reduction and lifetime control. Unique challenges that will need to be addressed include higher structural loads due to larger WT sizes and combined action of stronger wind and wave loads. Additional objectives such as stabilization of floating platforms should also be considered.

The developed control methods based on μ-synthesis approach considered only unstructured uncertainties to improve robust performance. A lumped uncertainty description, which additionally integrates plant parametric uncertainties, which arise particularly in below-rated WT operation, can be included in design to further improve robust performance. A prognostics-based lifetime control scheme based on the proposed IPC-RDAC can be developed with the goal of controlling long-term fatigue damage accumulation in multiple WT structural components. The proposed prognostics-based lifetime control approaches use a linear damage accumulation model based on Palmgren-Miner rule and rainflow counting algorithm. However, WTs are known to have complex nonlinear degradation patterns due to several failure modes. In addition, WT components exhibit different degradation rates due varied operating conditions, aging, and other factors. To accurately describe these phenomena, nonlinear multi-state degradation models based on SOTA methods such as Bayesian method (BM) or particle filter (PF) are required for improved lifetime prediction.

Although advantages of hybrid structural health monitoring (SHM) and prognosis have been shown, limited works using these approaches for lifetime control and extension strategies for WTs have been reported. In this thesis, the hybrid lifetime control scheme relies on a simple regression model for fatigue load prediction and an online linear damage evaluation model for SOH estimation. Modern commercial WTs are instrumented with high frequency (1 Hz) supervisory control and data acquisition (SCADA) systems that generate abundant performance data. Therefore, advanced hybrid prognostics-based control approaches can be developed to take advantage of the sufficient featured data by using deep-learning regression models to improve fatigue load prediction. For improved SOH and RUL prediction, physical degradation models based on SOTA approaches such BM or PF can be considered.

The developed approaches are tested on 1.5 MW and 5 MW RWTs having lower fidelity especially for rotor blades. However, modern commercial WTs have larger, slender, and highly flexible blades with bending and torsional vibrations, impacting control behavior.

Therefore, these dynamics should be considered if the developed approaches are to be commercially viable. For this purpose, higher fidelity models such as the IEA Wind 15 MW RWT can be considered. Commercial WTs are typically installed in wind farm clusters, resulting in complex wind wake interactions between turbines. Although suitable layouts can be designed to minimize wake effects, wind farm-level control is still required for wake redirection to minimize fatigue loads on the entire fleet. Therefore, by considering SOTA wake models, the proposed approaches can be extended to wind farm control.

Bibliography

[AAMO21] Adedeji, P. A. ; Akinlabi, S. A. ; Madushele, N. ; Olatunji, O. O.: Hybrid neurofuzzy wind power forecast and wind turbine location for embedded generation. In: *International Journal of Energy Research* 45 (2021), No. 1, pp. 413–428. http://dx.doi.org/10.1002/er.5620. – DOI 10.1002/er.5620. – ISSN 1099114X

[AN06] Apkarian, P. ; Noll, D.: Nonsmooth H_∞ synthesis. In: *IEEE Transactions on Automatic Control* 51 (2006), No. 1, pp. 71–86. http://dx.doi.org/10.1109/TAC.2005.860290. – DOI 10.1109/TAC.2005.860290

[AN17] Apkarian, P. ; Noll, D.: The H_∞ control problem is solved. In: *Aerospace Lab* 13 (2017), pp. 1–13. http://dx.doi.org/10.12762/2017.AL13-01. – DOI 10.12762/2017.AL13–01

[And19] Andrew, J. M.: Fundamentals of wind turbines. In: *Tribology and Lubrication Technology* 75 (2019), No. 8, pp. 32–40. – ISSN 1545858X

[ANSM19] Azizi, A. ; Nourisola, H. ; Shoja-Majidabad, S.: Fault tolerant control of wind turbines with an adaptive output feedback sliding mode controller. In: *Renewable Energy* 135 (2019), 55–65. http://dx.doi.org/10.1016/j.renene.2018.11.106. – DOI 10.1016/j.renene.2018.11.106. – ISBN 1581351666

[Apk11] Apkarian, P.: Nonsmooth μ-synthesis. In: *International Journal of Robust and Nonlinear Control* 21 (2011), 1493–1508. http://dx.doi.org/10.1002/rnc.1644. – DOI 10.1002/rnc.1644

[ARTV16] Acho, L. ; Rodellar, J. ; Tutivén, C. ; Vidal, Y.: Passive fault tolerant control strategy in controlled wind turbines. In: *2016 3rd IEEE Conference on Control and Fault-Tolerant Systems (SysTol)*. Barcelona, Spain : IEEE, 2016. – ISBN 9781509006588, pp. 636–641

[Ass12] Association, E. W. E.: *Wind energy-the facts: a guide to the technology, economics and future of wind power*. Routledge, 2012

[AYTS12] Abdullah, M. A. ; Yatim, A. H. ; Tan, C. W. ; Saidur, R.: A review of maximum power point tracking algorithms for wind energy systems. In: *Renewable and Sustainable Energy Reviews* 16 (2012), No. 5, 3220–3227. http://dx.doi.org/10.1016/j.rser.2012.02.016. – DOI 10.1016/j.rser.2012.02.016. – ISBN 1364–0321

[AZPW22] Abbas, N. J. ; Zalkind, D. S. ; Pao, L. ; Wright, A.: A reference open-source controller for fixed and floating offshore wind turbines. In: *Wind Energy Science* 7 (2022), No. 1, pp. 53–73. http://dx.doi.org/10.5194/wes-7-53-2022,2022. – DOI 10.5194/wes–7–53–2022, 2022

[Bet14] Betz, A.: *Introduction to the theory of flow machines*. Elsevier, 2014

[BGEJ14] Bitner-Gregersen, E. M. ; Ewans, K. C. ; Johnson, M. C.: Some uncertainties associated with wind and wave description and their importance for engineering applications. In: *Ocean Engineering* 86 (2014), 11–25. http://dx.doi.org/10.1016/j.oceaneng.2014.05.002. – DOI 10.1016/j.oceaneng.2014.05.002. – ISSN 00298018

[BGMO20] Bashetty, S. ; Guillamon, J. I. ; Mutnuri, S. S. ; Ozcelik, S.: Design of a robust adaptive controller for the pitch and torque control of wind turbines. In: *Energies* 13 (2020), No. 5. http://dx.doi.org/10.3390/en13051195. – DOI 10.3390/en13051195. – ISSN 19961073

[Bir10] Bir, G. S.: User's guide to MBC3: Multi-blade coordinate transformation code for 3-bladed wind turbine / National Renewable Energy Laboratory (NREL). Version: 2010. https://www.nrel.gov/docs/fy10osti/44327.pdf. – Techreport. – Online resource

[BMS23] Bousebsi, M. ; Medoued, A. ; Saidi, L.: Data-Driven and Physics-Based Approaches for Wind Turbine High-Speed Shaft Bearing Prognostics. In: *2023 International Conference on Control, Automation and Diagnosis, ICCAD 2023* (2023), pp. 1–6. http://dx.doi.org/10.1109/ICCAD57653.2023.10152369. – DOI 10.1109/ICCAD57653.2023.10152369. ISBN 9798350347074

[BNS18] Beganovic, N. ; Njiri, J. G. ; Söffker, D.: Reduction of structural loads in wind turbines based on adapted control strategy concerning online fatigue damage evaluation models. In: *Energies* 11 (2018), No. 12, pp. 3429. http://dx.doi.org/10.3390/en11123429. – DOI 10.3390/en11123429

[BS16] Beganovic, N. ; Söffker, D.: Structural health management utilization for lifetime prognosis and advanced control strategy deployment of wind turbines: An overview and outlook concerning actual methods, tools, and obtained results. In: *Renewable and Sustainable Energy Reviews* 64 (2016), 68–83. http://dx.doi.org/10.1016/j.rser.2016.05.083. – DOI 10.1016/j.rser.2016.05.083. – ISSN 18790690

[BZB+13] Bak, C. ; Zahle, F. ; Bitsche, R. ; Kim, T. ; Yde, A. ; Henriksen, L. C. ; Hansen, M. H. ; Blasques, J. P. A. A. ; Gaunaa, M. ; Natarajan, A.: The DTU 10-MW Reference Wind Turbine / DTU Wind Energy. 2013. – Techreport

[BZJ+22] Badihi, H. ; Zhang, Y. ; Jiang, B. ; Pillay, P. ; Rakheja, S.: A Comprehensive Review on Signal-Based and Model-Based Condition Monitoring of Wind Turbines: Fault Diagnosis and Lifetime Prognosis. In: *Proceedings of the IEEE* 110 (2022), No. 6, pp. 754–806. http://dx.doi.org/10.1109/JPROC.2022.3171691. – DOI 10.1109/JPROC.2022.3171691. – ISSN 15582256

[CAG+10] Choi, J. ; An, D. ; Gang, J. ; Joo, J. ; Kim, N. H.: Bayesian approach for parameter estimation in the structural analysis and prognosis. In: *Annual Conference of the Prognostics and Health Management Society, PHM 2010* (2010), pp. 1–8. ISBN 9781936263011

[CCC+19] Cetrini, A. ; Cianetti, F. ; Corradini, M. L. ; Ippoliti, G. ; Orlando, G.: On-line fatigue alleviation for wind turbines by a robust control approach. In: *International Journal of Electrical Power and Energy Systems* 109 (2019), No. October 2018, pp. 384–394. http://dx.doi.org/10.1016/j.ijepes.2019.02.011. – DOI 10.1016/j.ijepes.2019.02.011. – ISSN 01420615

[CGP17] Coronado, A. ; Gámez, M. ; Peñaloza, O.: Adaptive control of variable-speed variable-pitch wind turbines for power regulation. In: *2017 6th International Conference on Renewable Energy Research and Applications, ICRERA 2017* Vol. 2017-Janua. San Francisco, California : IEEE, 2017. – ISBN 9781538620953, pp. 479–483

[CPaN+11] Corcuera, A. D. ; Pujana-arrese, A. ; Nourdine, S. ; Camblong, H. ; Landaluze, J.: GH Bladed's linear models based H_∞ controls for off-Shore wind turbines. In: *Offshore 2011*

[CQQ18] Cheng, F. ; Qu, L. ; Qiao, W.: Fault prognosis and remaining useful life prediction of wind turbine gearboxes using current signal analysis. In: *IEEE Transactions on Sustainable Energy* 9 (2018), No. 1, pp. 157–167. http://dx.doi.org/10.1109/TSTE.2017.2719626. – DOI 10.1109/TSTE.2017.2719626. – ISSN 19493029

[CQQH19] Cheng, F. ; Qu, L. ; Qiao, W. ; Hao, L.: Enhanced Particle Filtering for Bearing Remaining Useful Life Prediction of Wind Turbine Drivetrain Gearboxes. In: *IEEE Transactions on Industrial Electronics* 66 (2019), No. 6, pp. 4738–4748. http://dx.doi.org/10.1109/TIE.2018.2866057. – DOI 10.1109/TIE.2018.2866057. – ISSN 02780046

[CS16] Chen, J. ; Song, Y.: Dynamic loads of variable-speed wind energy conversion system. In: *IEEE Transactions on Industrial Electronics* 63 (2016), No. 1, pp. 178–188. http://dx.doi.org/10.1109/TIE.2015.2464181. – DOI 10.1109/TIE.2015.2464181. – ISSN 02780046

[CSL+18] Cerrada, M. ; Sánchez, R.-v. ; Li, C. ; Pacheco, F. ; Cabrera, D. ; Oliveira, J. V. ; Vásquez, R. E.: A review on data-driven fault severity assessment in rolling bearings. In: *Mechanical Systems and Signal Processing* 99 (2018), 169–196. http://dx.doi.org/10.1016/j.ymssp.2017.06.012. – DOI 10.1016/j.ymssp.2017.06.012. – ISSN 0888–3270

[CWLW22] Chen, Y. ; Wang, L. ; Liu, S. ; Wang, G.: A Health-Oriented Power Control Strategy of Direct Drive Wind Turbine. In: *IEEE Transactions on Power Delivery* 37 (2022), No. 2, pp. 1324–1335. http://dx.doi.org/10.1109/TPWRD.2021.3084216. – DOI 10.1109/TPWRD.2021.3084216. – ISSN 19374208

[DABB21] Dali, A. ; Abdelmalek, S. ; Bakdi, A. ; Bettayeb, M.: A new robust control scheme: Application for MPP tracking of a PMSG-based variable-speed wind turbine. In: *Renewable Energy* 172 (2021), pp. 1021–1034. http://dx.doi.org/10.1016/j.renene.2021.03.083. – DOI 10.1016/j.renene.2021.03.083. – ISSN 18790682

[DBS18] Djeziri, M. A. ; Benmoussa, S. ; Sanchez, R.: Hybrid method for remaining useful life prediction in wind turbine systems. In: *Renewable Energy* 116 (2018), 173–187. http://dx.doi.org/10.1016/j.renene.2017.05.020. – DOI 10.1016/j.renene.2017.05.020. – ISSN 18790682

[DDMB19] Dhiman, H. S. ; Deb, D. ; Muresan, V. ; Balas, V. E.: Wake management in wind farms: An adaptive control approach. In: *Energies* 12 (2019), No. 7, pp. 1–18. http://dx.doi.org/10.3390/en12071247. – DOI 10.3390/en12071247. – ISSN 19961073

[DGS+20] Desai, A. ; Guo, Y. ; Sheng, S. ; Phillips, C. ; Williams, L.: Prognosis of wind turbine gearbox bearing failures using SCADA and modeled data. In: *Proceedings of the Annual Conference of the Prognostics and Health Management Society, PHM* 12 (2020), No. 1, pp. 1–10. http://dx.doi.org/10.36001/phmconf.2020.v12i1.1292. – DOI 10.36001/phmconf.2020.v12i1.1292. – ISBN 9781936263059

[DMR20] Dastres, H. ; Mohammadi, A. ; Rezaie, B.: Adaptive robust control design to maximize the harvested power in a wind turbine with input constraint. In: *Journal of Renewable Energy and Environment* 7 (2020), No. 4, pp. 30–43. http://dx.doi.org/10.30501/jree.2020.224180.1093. – DOI 10.30501/jree.2020.224180.1093

[DPAE+12] De Corcuera, A. D. ; Pujana-Arrese, A. ; Ezquerra, J. M. ; Segurola, E. ; Landaluze, J.: H_∞ based control for load mitigation in wind turbines. In: *Energies* 5 (2012), apr, No. 4, pp. 938–967. http://dx.doi.org/10.3390/en5040938. – DOI 10.3390/en5040938. – ISSN 1996–1073

[DS19] Do, M. H. ; Söffker, D.: Robust observer-based load extenuation control for wind turbines. In: *International Conference on Multibody Systems, Nonlinear Dynamics, and Control* Vol. 59261. Anaheim, CA, USA : American Society of Mechanical Engineers, aug 2019. – ISBN 978–0–7918–5926–1, pp. V006T09A039

[DS20] Do, M. H. ; Söffker, D.: Wind turbine lifetime control using structural health monitoring and prognosis. In: *IFAC-PapersOnLine* 53 (2020), No. 2, pp. 12669–12674. http://dx.doi.org/10.1016/j.ifacol.2020.12.1847. – DOI 10.1016/j.ifacol.2020.12.1847

[DS21] Do, M. H. ; Söffker, D.: State-of-the-art in integrated prognostics and health management control for utility-scale wind turbines. In: *Renewable and Sustainable Energy Reviews* 145 (2021), pp. 111102. http://dx.doi.org/10.1016/j.rser.2021.111102. – DOI 10.1016/j.rser.2021.111102

[DS22] Do, M. H. ; Söffker, D.: Wind turbine robust disturbance accommodating control using non-smooth H_∞ optimization. In: *Wind Energy* 25 (2022), No. 1, pp. 107–124. http://dx.doi.org/10.1002/we.2663. – DOI 10.1002/we.2663. – ISSN 1095–4244

[DTZX18] Ding, F. ; Tian, Z. ; Zhao, F. ; Xu, H.: An integrated approach for wind turbine gearbox fatigue life prediction considering instantaneously varying load conditions. In: *Renewable Energy* 129 (2018), 260–270. http://dx.doi.org/10.1016/j.renene.2018.05.074. – DOI 10.1016/j.renene.2018.05.074. – ISSN 18790682

[EE20] El Maati, Y. A. ; El Bahir, L.: Optimal fault tolerant control of large-scale wind turbines in the case of the pitch actuator partial faults. In: *Complexity* 2020 (2020), pp. 1–17. http://dx.doi.org/10.1155/2020/6210407. – DOI 10.1155/2020/6210407. – ISSN 10990526

[ES19] Eroglu, Y. ; Seçkiner, S. U.: Early fault prediction of a wind turbine using a novel ANN training algorithm based on ant colony optimization. In: *Journal of Energy Systems* 3 (2019), No. 4, pp. 139–147. http://dx.doi.org/10.30521/jes.613315. – DOI 10.30521/jes.613315. – ISSN 26022052

[FMC21] Fekih, A. ; Mobayen, S. ; Chen, C. C.: Adaptive robust fault-tolerant control design for wind turbines subject to pitch actuator faults. In: *Energies* 14 (2021), No. 6, pp. 1791. http://dx.doi.org/10.3390/en14061791. – DOI 10.3390/en14061791. – ISSN 19961073

[Fro09] Frost, S. A.: Adaptive control of a utility-scale wind turbine operating in region 3. In: *47th AIAA Aerospace Sciences Meeting Including The New Horizons Forum and Aerospace Exposition*. Orlando, Florida : Aerospace Research Central, 2009, pp. 480

[FVS+13] Fleming, P. A. ; Van Wingerden, J. W. ; Scholbrock, A. K. ; Van Der Veen, G. ; Wright, A. D.: Field testing a wind turbine drivetrain/tower damper using advanced design and validation techniques. In: *Proceedings of the American Control Conference* (2013), pp. 2227–2234. http://dx.doi.org/10.1109/acc.2013.6580166. – DOI 10.1109/acc.2013.6580166. – ISBN 9781479901777

[FYLW15] Fan, X. ; Yang, X. ; Li, X. ; Wang, J.: A Particle-Filtering Approach for Remaining Useful Life Estimation of Wind Turbine Gearbox. In: *Proceedings of the International Conference on Chemical, Material and Food Engineering* 22 (2015), pp. 198–200. http://dx.doi.org/10.2991/cmfe-15.2015.47. – DOI 10.2991/cmfe–15.2015.47

[GC08] Geyler, M. ; Caselitz, P.: Robust multivariable pitch control design for load reduction on large wind turbines. In: *Journal of Solar Energy Engineering* 130 (2008), aug, No. 3, pp. 031014. http://dx.doi.org/10.1115/1.2931510. – DOI 10.1115/1.2931510. – ISSN 0199–6231

[GCB+21] Gougam, F. ; Chemseddine, R. ; Benazzouz, D. ; Benaggoune, K. ; Zerhouni, N.: Fault prognostics of rolling element bearing based on feature extraction and supervised machine learning: Application to shaft wind turbine gearbox using vibration signal. In: *Proceedings of the Institution of Mechanical Engineers, Part C: Journal of Mechanical Engineering Science* 235 (2021), No. 20, pp. 5186–5197. http://dx.doi.org/10.1177/0954406220976154. – DOI 10.1177/0954406220976154. – ISSN 20412983

[GCD15] Gao, Z. ; Cecati, C. ; Ding, S. X.: A survey of fault diagnosis and fault-tolerant techniques-part I: Fault diagnosis with model-based and signal-based approaches. In: *IEEE Transactions on Industrial Electronics* 62 (2015), No. 6, pp. 3757–3767. http://dx.doi.org/10.1109/TIE.2015.2417501. – DOI 10.1109/TIE.2015.2417501. – ISSN 02780046

[GL21] Gao, Z. ; Liu, X.: An overview on fault diagnosis, prognosis and resilient control for wind turbine systems. In: *Processes* 9 (2021), No. 2, pp. 300. http://dx.doi.org/10.3390/pr9020300. – DOI 10.3390/pr9020300

[GRS+20] Gaertner, E. ; Rinker, J. ; Sethuraman, L. ; Anderson, B. ; Zahle, F. ; Barter, G.: Definition of the IEA wind 15-megawatt offshore reference wind turbine / National Renewable Energy Laboratory (NREL). Version: 2020. https://www.nrel.gov/docs/fy20osti/75698.pdf. Golden, Colorado, USA, 2020 (NREL/TP-5000-75698). – Techreport. – Online resource

[Hau13] Hau, E.: *Wind turbines: fundamentals, technologies, application, economics*. Springer Science & Business Media, 2013

[Hay12] Hayman, G.: MLife theory manual for version 1.00 / National Renewable Energy Laboratory(NREL). Version: 2012. https://www.nrel.gov/wind/nwtc/assets/pdfs/mlife-theory.pdf. Golden, Colorado, 2012. – Techreport. – Online resource

[HHS19] Habibi, H. ; Howard, I. ; Simani, S.: Reliability improvement of wind turbine power generation using model-based fault detection and fault tolerant control: A review. In: *Renewable Energy* 135 (2019), pp. 877–896. http://dx.doi.org/10.1016/j.renene.2018.12.066. – DOI 10.1016/j.renene.2018.12.066. – ISSN 18790682

[HMHN14] Hamdi, H. ; Mrad, C. ; Hamdi, A. ; Nasri, R.: Dynamic response of a horizontal axis wind turbine blade under aerodynamic, gravity and gyroscopic effects. In: *Applied Acoustics* 86 (2014), 154–164. http://dx.doi.org/10.1016/j.apacoust.2014.04.017. – DOI 10.1016/j.apacoust.2014.04.017. – ISSN 1872910X

[HRBA+18] Herp, J. ; Ramezani, M. H. ; Bach-Andersen, M. ; Pedersen, N. L. ; Nadimi, E. S.: Bayesian state prediction of wind turbine bearing failure. In: *Renewable Energy* 116 (2018), 164–172. http://dx.doi.org/10.1016/j.renene.2017.02.069. – DOI 10.1016/j.renene.2017.02.069. – ISSN 18790682

[HYS+22] He, R. ; Yang, H. ; Sun, S. ; Lu, L. ; Sun, H. ; Gao, X.: A machine learning-based fatigue loads and power prediction method for wind turbines under yaw control. In: *Applied Energy* 326 (2022), No. September, 120013. http://dx.doi.org/10.1016/j.apenergy.2022.120013. – DOI 10.1016/j.apenergy.2022.120013. – ISSN 03062619

[IEA21] IEA: Net Zero by 2050: A Roadmap for the Global Energy Sector. In: *International Energy Agency* (2021)

[IRE21] IRENA: World energy transitions outlook: 1.5°C pathway / International Renewable Energy Agency (IRENA). Version: 2021. https://irena.org/publications/2021/Jun/World-Energy-Transitions-Outlook. Abu Dhabi, 2021. – Techreport. – Online resource

[IRE23] IRENA: World energy transitions outlook 2023: 1.5°C pathway / IRENA. Version: 2023. https://irena.org/Digital-Report/World-Energy-Transitions-Outlook-2022%0Ahttps://irena.org/publications/2021/March/World-Energy-Transitions-Outlook. – Techreport. – Online resource. – ISBN 9789292603342

[JB05] Jonkman, J. M. ; Buhl, M. L.: FAST user's guide / National Renewable Energy Laboratory (NREL). Version: 2005. https://www.nrel.gov/docs/fy06osti/38230.pdf. Golden, Colorado, USA, 2005. – Techreport. – Online resource

[JBB+21] Jenkins, N. ; Burton, T. L. ; Bossanyi, E. ; Sharpe, D. ; Graham, M.: *Wind energy handbook*. John Wiley & Sons, 2021

[JBMS09] Jonkman, J. ; Butterfield, S. ; Musial, W. ; Scott, G.: Definition of a 5-MW reference wind turbine for offshore system development / National Renewable Energy Laboratory (NREL). Version: 2009. https://www.nrel.gov/docs/fy09osti/38060.pdf. Golden, Colorado, USA, 2009 (NREL/TP-500-38060). – Techreport. – Online resource

[JFPB05] Johnson, K. E. ; Fingersh, L. J. ; Pao, L. Y. ; Balas, M. J.: Adaptive Torque Control of Variable Speed Wind Turbines. In: *43rd AIAA Aerospace Sciences Meeting*. AIAA

[JGO+22] Jaramillo, F. ; Gutiérrez, J. M. ; Orchard, M. ; Guarini, M. ; Astroza, R.: A Bayesian approach for fatigue damage diagnosis and prognosis of wind turbine blades. In: *Mechanical Systems and Signal Processing* 174 (2022), 109067. http://dx.doi.org/10.1016/j.ymssp.2022.109067. – DOI 10.1016/j.ymssp.2022.109067. – ISSN 10961216

[JK12] Jonkman, B. J. ; Kilcher, L.: TurbSim user's guide: version 1.06.00 / National Renewable Energy Laboratory (NREL). Version: 2012. https://www.nrel.gov/wind/nwtc/assets/pdfs/turbsim.pdf. Golden, Colorado, USA, 2012. – Techreport. – Online resource

[JKS19] Jihin, R. ; Kögler, F. ; Söffker, D.: Data Driven State Machine Model for Industry 4 . 0 Lifetime Modeling and Identification of Irrigation Control

Parameters. In: *2019 Global IoT Summit (GIoTS)*. Aarhys, Denmark : IEEE, 2019. – ISBN 9781728121710, pp. 1–6

[JPBL06] Johnson, K. E. ; Pao, L. Y. ; Balas, M. J. ; Lee, J. F.: Control of Variable-Speed Wind Turbines: Standard and Adaptive Techniques for Maximizing Energy Capture. In: *IEEE Control Systems* 26 (2006), No. 3, pp. 70–81. http://dx.doi.org/10.1109/MCS.2006.1636311. – DOI 10.1109/MCS.2006.1636311. – ISBN 0272–1708

[JSY14] Jongmin Cheon ; Soonman Kwon ; Youngkiu Choi: Design of a pitch controller using disturbance accommodating control for wind turbines under stochastic environments. In: *2014 IEEE 23rd International Symposium on Industrial Electronics (ISIE)*. Istanbul, Turkey : IEEE, jun 2014. – ISBN 978–1–4799–2399–1, pp. 2572–2577

[JWHR19] Jonkman, J. M. ; Wright, A. D. ; Hayman, G. J. ; Robertson, A. N.: Full-System Linearization for Floating-Offshore Wind Turbines in OpenFAST. In: *ASME 2018 1st International Offshore Wind Technical Conference*. San Francisco, California, 2019, pp. 1–10

[JY20] Jain, T. ; Yamé, J.: Health-aware fault-tolerant receding horizon control of wind turbines. In: *Control Engineering Practice* 95 (2020), 104236. http://dx.doi.org/10.1016/j.conengprac.2019.104236. – DOI 10.1016/j.conengprac.2019.104236. – ISSN 0967–0661

[KAC17] Kim, N.-H. ; An, D. ; Choi, J.-H.: Prognostics and Health Management of Systems. In: *Switzerland: Springer International Publishing* (2017). http://dx.doi.org/10.1007/978-3-319-44742-1. – DOI 10.1007/978–3–319–44742–1. ISBN 9780470278024

[KBS23] Kipchirchir, E. ; Bakhshande, F. ; Söffker, D.: A μ-synthesis approach for robust control of wind turbines. In: *International Design Engineering Technical Conferences and Computers and Information in Engineering Conference 2023*. Boston, Massachusetts : ASME, 2023. – accepted

[KDNS22] Kipchirchir, E. ; Do, M. H. ; Njiri, J. G. ; Söffker, D.: Mixed-sensitivity robust disturbance accommodating control for load mitigation and speed regulation of wind turbines. In: *2022 European Control Conference (ECC)*. London, United Kingdom : IEEE, 2022. – ISBN 978–3–9071–4407–7, pp. 1012–1017

[KDNS23] Kipchirchir, E. ; Do, M. H. ; Njiri, J. G. ; Söffker, D.: Prognostics-based adaptive control strategy for lifetime control of wind turbines. In: *Wind Energy Science* 8 (2023), No. 4, pp. 575–588. http://dx.doi.org/10.5194/wes-8-575-2023. – DOI 10.5194/wes–8–575–2023. – ISSN 23667451

[KDNS24] Kipchirchir, E. ; Do, M. H. ; Njiri, J. G. ; Söffker, D.: Adaptive robust observer-based control for structural load mitigation and speed regulation in commercial wind turbines. In: *IEEE Access* 12 (2024), pp. 38335–38350. http://dx.doi.org/10.1109/ACCESS.2024.3375115.. – DOI 10.1109/ACCESS.2024.3375115.

[KLS24] Kipchirchir, E. ; Liebeton, J. ; Söffker, D.: A hybrid prognosis approach for robust lifetime control of wind turbines. (2024). – in preparation

[KRF18] Kumar, R. ; Raahemifar, K. ; Fung, A. S.: A critical review of vertical axis wind turbines for urban applications. In: *Renewable and Sustainable Energy Reviews* 89 (2018), 281–291. http://dx.doi.org/10.1016/j.rser.2018.03.033. – DOI 10.1016/j.rser.2018.03.033. – ISSN 18790690

[KS24] Kipchirchir, E. ; Söffker, D.: IPC-based robust disturbance accommodating control for load mitigation and speed regulation of wind turbines. In: *Wind Energy* 27 (2024), No. 4, pp. 382–402. http://dx.doi.org/10.1002/we.2893. – DOI 10.1002/we.2893. – ISSN 10991824

[KSE18] Kanev, S. ; Savenije, F. ; Engels, W.: Active wake control: An approach to optimize the lifetime operation of wind farms. In: *Wind Energy* 21 (2018), No. 7, pp. 488–501. http://dx.doi.org/10.1002/we.2173. – DOI 10.1002/we.2173. – ISSN 1095–4244

[LL20] Lin, Z. ; Liu, X.: Wind power forecasting of an offshore wind turbine based on high-frequency SCADA data and deep learning neural network. In: *Energy* 201 (2020), pp. 117693. http://dx.doi.org/10.1016/j.energy.2020.117693. – DOI 10.1016/j.energy.2020.117693. – ISSN 03605442

[LLJ19] Lei, J. ; Liu, C. ; Jiang, D.: Fault diagnosis of wind turbine based on Long Short-term memory networks. In: *Renewable Energy* 133 (2019), 422–432. http://dx.doi.org/10.1016/j.renene.2018.10.031. – DOI 10.1016/j.renene.2018.10.031. – ISSN 18790682

[LS18] Lei, X. ; Sandborn, P. A.: Maintenance scheduling based on remaining useful life predictions for wind farms managed using power purchase agreements. In: *Renewable Energy* 116 (2018), 188–198. http://dx.doi.org/10.1016/j.renene.2017.03.053. – DOI 10.1016/j.renene.2017.03.053. – ISSN 18790682

[LTA07] Larsen ; Torben J. Hansen ; Anders Melchior: How 2 HAWC2, the user's manual / DTU Wind Energy. Version: 2007. https://iopscience.iop.org/article/10.1088/1742-6596/1618/5/052052/pdf. Roskilde, Denmark, 2007. – Techreport. – Online resource. – ISBN 978–87–550–3583–6

[LWZQ21] Li, J. ; Wang, Y. ; Zhao, X. ; Qi, P.: Model free adaptive control of large and flexible wind turbine rotors with controllable flaps. In: *Renewable Energy* 180 (2021), pp. 68–82. http://dx.doi.org/10.1016/j.renene.2021.08.050. – DOI 10.1016/j.renene.2021.08.050. – ISSN 18790682

[LZ20] Lee, J. ; Zhao, F.: GWEC global wind report 2019 / Global Wind Energy Council (GWEC). Version: 2020. https://gwec.net/global-wind-report-2019/. Brussels, Belgium, 2020. – Techreport. – Online resource

[LZ21] Lee, J. ; Zhao, F.: GWEC global wind report 2021 / Global Wind Energy Council (GWEC). Version: 2021. https://gwec.net/

global-wind-report-2021/. Brussels, Belgium, 2021. – Techreport. – Online resource

[LZ22] Lee, J. ; Zhao, F.: GWEC global wind report 2022 / Global Wind Energy Council (GWEC). Version: 2022. https://gwec.net/wp-content/uploads/2022/03/GWEC-GLOBAL-WIND-REPORT-2022.pdf. Brussels, Belgium, 2022. – Techreport. – Online resource. – ISBN 9783981593402

[LZTT20] Li, L. L. ; Zhao, X. ; Tseng, M. L. ; Tan, R. R.: Short-term wind power forecasting based on support vector machine with improved dragonfly algorithm. In: *Journal of Cleaner Production* 242 (2020), 118447. http://dx.doi.org/10.1016/j.jclepro.2019.118447. – DOI 10.1016/j.jclepro.2019.118447. – ISSN 09596526

[Mar23] Mark Hutchinson, F. Z. C.: GWEC global wind report 2023 / Global Wind Energy Council (GWEC). Version: 2023. https://gwec.net/globalwindreport2023/. Brussels, Belgium, 2023. – Techreport. – Online resource

[MBF13] Magar, K. S. T. ; Balas, M. J. ; Frost, S. A.: Adaptive pitch control for speed regulation of floating offshore wind turbine: preliminary study. In: *51st AIAA Aerospace Sciences Meeting including the New Horizons Forum and Aerospace Exposition*. Grapevine, Texas : Aerospace Research Central, 2013, pp. 454

[ME68] Matsuishi, M. ; Endo, T.: Fatigue of metals subjected to varying stress. In: *Japan Society of Mechanical Engineers* 68 (1968), No. 2, pp. 37–40

[Min45] Miner, M. A.: Cumulative damage in fatigue. In: *Journal of Applied Mechanics* 12 (1945), No. 3, pp. A159–A164. http://dx.doi.org/10.1115/1.4009458. – DOI 10.1115/1.4009458

[MJ12] Musallam, M. ; Johnson, C. M.: An efficient implementation of the rainflow counting algorithm for life consumption estimation. In: *IEEE Transactions on Reliability* 61 (2012), No. 4, pp. 978–986. http://dx.doi.org/10.1109/TR.2012.2221040. – DOI 10.1109/TR.2012.2221040

[MN22] Moghadam, F. K. ; Nejad, A. R.: Online condition monitoring of floating wind turbines drivetrain by means of digital twin. In: *Mechanical Systems and Signal Processing* 162 (2022), No. May 2021, 108087. http://dx.doi.org/10.1016/j.ymssp.2021.108087. – DOI 10.1016/j.ymssp.2021.108087. – ISSN 10961216

[MNG22] Mehlan, F. C. ; Nejad, A. R. ; Gao, Z.: Digital Twin Based Virtual Sensor for Online Fatigue Damage Monitoring in Offshore Wind Turbine Drivetrains. In: *Journal of Offshore Mechanics and Arctic Engineering* 144 (2022), No. 6, pp. 1–8. http://dx.doi.org/10.1115/1.4055551. – DOI 10.1115/1.4055551. – ISSN 1528896X

[MNP11] Mirzaei, M. ; Niemann, H. H. ; Poulsen, N. K.: A μ-synthesis approach to robust control of a wind turbine. In: *IEEE Conference on Decision and*

Control and European Control Conference. Orlando, Florida, USA : IEEE, dec 2011. – ISBN 978–1–61284–801–3, pp. 645–650

[Mor13] Morten Hartvig Hansen ; Lars Christian Henriksen: Basic DTU Wind Energy controller / DTU Wind Energy. 2013. – Techreport. – ISBN 9788792896278

[MSMD21] Mihaly, V. ; Susca, M. ; Morar, D. ; Dobra, P.: μ-synthesis for fractional-order robust controllers. In: *MDPI-mathematics* (2021). http://dx.doi.org/10.3390/math9080911. – DOI 10.3390/math9080911

[MT22] Mazare, M. ; Taghizadeh, M.: Uncertainty estimator-based dual layer adaptive fault-tolerant control for wind turbines. In: *Renewable Energy* 188 (2022), apr, pp. 545–560. http://dx.doi.org/10.1016/j.renene.2022.02.030. – DOI 10.1016/j.renene.2022.02.030. – ISSN 09601481

[MV15] Moradi, H. ; Vossoughi, G.: Robust control of the variable speed wind turbines in the presence of uncertainties: a comparison between H_∞ and PID controllers. In: *Energy* 90 (2015), pp. 1508–1521. http://dx.doi.org/10.1016/j.energy.2015.06.100. – DOI 10.1016/j.energy.2015.06.100. – ISSN 0360–5442

[MV18] Mulders, S. P. ; Van Wingerden, J. W.: Delft Research Controller: An open-source and community-driven wind turbine baseline controller. In: *Journal of Physics: Conference Series* 1037 (2018), No. 3. http://dx.doi.org/10.1088/1742-6596/1037/3/032009. – DOI 10.1088/1742–6596/1037/3/032009. – ISSN 17426596

[NARG18] Novaes Menezes, E. J. ; Araújo, A. M. ; Rohatgi, J. S. ; González del Foyo, P. M.: Active load control of large wind turbines using state-space methods and disturbance accommodating control. In: *Energy* 150 (2018), pp. 310–319. http://dx.doi.org/10.1016/j.energy.2018.02.143. – DOI 10.1016/j.energy.2018.02.143. – ISSN 03605442

[NBDS19] Njiri, J. G. ; Beganovic, N. ; Do, M. H. ; Söffker, D.: Consideration of lifetime and fatigue load in wind turbine control. In: *Renewable Energy* 131 (2019), pp. 818–828. http://dx.doi.org/10.1016/j.renene.2018.07.109. – DOI 10.1016/j.renene.2018.07.109. – ISSN 18790682

[NCK21] Norén-Cosgriff, K. ; Kaynia, A. M.: Estimation of natural frequencies and damping using dynamic field data from an offshore wind turbine. In: *Marine Structures* 76 (2021), pp. 102915. http://dx.doi.org/10.1016/j.marstruc.2020.102915. – DOI 10.1016/j.marstruc.2020.102915. – ISSN 09518339

[Nji16] Njiri, J. G.: *Multi-Objective Control Strategies and Prognostic-Based Lifetime Extension of Utility-Scale Wind Turbines*, Universität Duisburg-Essen, Dissertation, 2016. https://duepublico2.uni-due.de/servlets/MCRFileNodeServlet/duepublico_derivate_00042219/Njiri_Diss.pdf. – Online resource

[NMV20] Nayeh, R. F. ; Moradi, H. ; Vossoughi, G.: Multivariable robust control of a horizontal wind turbine under various operating modes and uncertainties : A comparison on sliding mode and H_∞ control. In: *Electrical Power and Energy Systems* 115 (2020), pp. 105474. http://dx.doi.org/10.1016/j.ijepes.2019.105474. – DOI 10.1016/j.ijepes.2019.105474. – ISSN 0142–0615

[NRE21] NREL: OpenFAST documentation / National Renewable Energy Laboratory (NREL). Version: 2021. https://openfast.readthedocs.io/en/main/. – Techreport. – Online resource

[NRE24] NREL: *FLORIS: FLOw Redirection and Induction in Steady State*. https://www.nrel.gov/wind/floris.html. Version: 2024. – Accessed: 2024-06-16

[NS16] Njiri, J. G. ; Söffker, D.: State-of-the-art in wind turbine control: Trends and challenges. In: *Renewable and Sustainable Energy Reviews* 60 (2016), 377–393. http://dx.doi.org/10.1016/j.rser.2016.01.110. – DOI 10.1016/j.rser.2016.01.110. – ISBN 1364–0321

[ØBS07] Østergaard, K. Z. ; Brath, P. ; Stoustrup, J.: Estimation of effective wind speed. In: *Journal of Physics: Conference Series* 75 (2007), No. 1, pp. 012082. http://dx.doi.org/10.1088/1742-6596/75/1/012082. – DOI 10.1088/1742–6596/75/1/012082

[OGGP21] Ogliari, E. ; Guilizzoni, M. ; Giglio, A. ; Pretto, S.: Wind power 24-h ahead forecast by an artificial neural network and an hybrid model: Comparison of the predictive performance. In: *Renewable Energy* 178 (2021), 1466–1474. http://dx.doi.org/10.1016/j.renene.2021.06.108. – DOI 10.1016/j.renene.2021.06.108. – ISSN 18790682

[PAD23] Pandit, R. K. ; Astolfi, D. ; Durazo Cardenas, I.: A Review of Predictive Techniques Used to Support Decision Making for Maintenance Operations of Wind Turbines. In: *Energies* 16 (2023), No. 4, pp. 1–17. http://dx.doi.org/10.3390/en16041654. – DOI 10.3390/en16041654. – ISSN 19961073

[Par14] Park, S.: A novel individual pitch control algorithm based on μ-synthesis for wind turbines. In: *Journal of Mechanical Science and Technology* 28 (2014), apr, No. 4, pp. 1509–1517. http://dx.doi.org/10.1007/s12206-014-0138-y. – DOI 10.1007/s12206–014–0138–y. – ISSN 1738–494X

[PFR17] Pfaffel, S. ; Faulstich, S. ; Rohrig, K.: Performance and reliability of wind turbines: a review. In: *Energies* 10 (2017), pp. 1904. http://dx.doi.org/10.3390/en10111904. – DOI 10.3390/en10111904

[PHCW20] Pan, Y. ; Hong, R. ; Chen, J. ; Wu, W.: A hybrid DBN-SOM-PF-based prognostic approach of remaining useful life for wind turbine gearbox. In: *Renewable Energy* 152 (2020), 138–154. http://dx.doi.org/10.1016/j.renene.2020.01.042. – DOI 10.1016/j.renene.2020.01.042. – ISSN 18790682

[PJ11] Pao, L. Y. ; Johnson, K. E.: Control of Wind Turbines. In: *IEEE Control Systems* 31 (2011), No. 2, 44–62. http://dx.doi.org/10.1109/MCS.2010.939962. – DOI 10.1109/MCS.2010.939962. – ISBN 1066–033X

[PN20] Poureh, A. ; Nobakhti, A.: Robust control design for an industrial wind turbine with HIL simulations. In: *ISA Transactions* 103 (2020), pp. 252–265. http://dx.doi.org/10.1016/j.isatra.2020.05.004. – DOI 10.1016/j.isatra.2020.05.004. – ISSN 00190578

[PNJ+12] Patwardhan, S. C. ; Narasimhan, S. ; Jagadeesan, P. ; Gopaluni, B. ; L. Shah, S.: Nonlinear Bayesian state estimation: A review of recent developments. In: *Control Engineering Practice* 20 (2012), No. 10, 933–953. http://dx.doi.org/10.1016/j.conengprac.2012.04.003. – DOI 10.1016/j.conengprac.2012.04.003. – ISSN 09670661

[PSSC18] Pettas, V. ; Salari, M. ; Schlipf, D. ; Cheng, P. W.: Investigation on the potential of individual blade control for lifetime extension. In: *Journal of Physics: Conference Series* 1037 (2018), No. 3, pp. 032006. http://dx.doi.org/10.1088/1742-6596/1037/3/032006. – DOI 10.1088/1742–6596/1037/3/032006. – ISSN 17426596

[QSL+14] Qiu, W. ; Sales Junior, J. ; Lee, D. ; Lie, H. ; Magarovskii, V. ; Mikami, T. ; Rousset, J. M. ; Sphaier, S. ; Tao, L. ; Wang, X.: Uncertainties related to predictions of loads and responses for ocean and offshore structures. In: *Ocean Engineering* 86 (2014), pp. 58–67. http://dx.doi.org/10.1016/j.oceaneng.2014.02.031. – DOI 10.1016/j.oceaneng.2014.02.031. – ISSN 00298018

[RD18] Rinker, J. ; Dykes, K.: WindPACT reference wind turbines / National Renewable Energy Laboratory (NREL). Version: 2018. https://www.nrel.gov/docs/fy18osti/67667.pdf. Golden, Colorado, USA, 2018 (NREL/TP-5000- 67667). – Techreport. – Online resource

[RDT20] Rommel, D. ; Di Maio, D. ; Tinga, T.: Calculating wind turbine component loads for improved life prediction. In: *Renewable Energy* 146 (2020), 223–241. http://dx.doi.org/10.1016/j.renene.2019.06.131. – DOI 10.1016/j.renene.2019.06.131. – ISSN 18790682

[RGZ+20] Rinker, J. ; Gaertner, E. ; Zahle, F. ; Skrzypiński, W. ; Abbas, N. ; Bredmose, H. ; Barter, G. ; Dykes, K.: Comparison of loads from HAWC2 and OpenFAST for the IEA Wind 15 MW reference wind turbine. In: *Journal of Physics: Conference Series* 1618 (2020), sep, No. 5, pp. 52052. http://dx.doi.org/10.1088/1742-6596/1618/5/052052. – DOI 10.1088/1742–6596/1618/5/052052. – ISSN 1742–6588

[RJ22] Ran, Q. ; Jin, F.: Robust adaptive MPPT control of wind turbine based on prescribed performance. In: *2022 IEEE 2nd International Conference on Power, Electronics and Computer Applications, ICPECA* (2022), pp. 67–71. http://dx.doi.org/10.1109/ICPECA53709.2022.9719157. – DOI 10.1109/ICPECA53709.2022.9719157. ISBN 9781665442763

[RJP+20] Rozas, H. ; Jaramillo, F. ; Perez, A. ; Jimenez, D. ; Orchard, M. E. ; Medjaher, K.: A method for the reduction of the computational cost associated with the implementation of particle-filter-based failure prognostic algorithms. In: *Mechanical Systems and Signal Processing* 135 (2020), 106421. http://dx.doi.org/10.1016/j.ymssp.2019.106421. – DOI 10.1016/j.ymssp.2019.106421. – ISSN 10961216

[RKC+20a] Rezamand, M. ; Kordestani, M. ; Carriveau, R. ; Ting, D. S. ; Orchard, M. E. ; Saif, M.: Critical Wind Turbine Components Prognostics: A Comprehensive Review. In: *IEEE Transactions on Instrumentation and Measurement* 69 (2020), No. 12, pp. 9306–9328. http://dx.doi.org/10.1109/TIM.2020.3030165. – DOI 10.1109/TIM.2020.3030165. – ISSN 15579662

[RKC+20b] Rezamand, M. ; Kordestani, M. ; Carriveau, R. ; Ting, D. S. ; Saif, M.: An Integrated Feature-Based Failure Prognosis Method for Wind Turbine Bearings. In: *IEEE/ASME Transactions on Mechatronics* 25 (2020), No. 3, pp. 1468–1478. http://dx.doi.org/10.1109/TMECH.2020.2978136. – DOI 10.1109/TMECH.2020.2978136. – ISSN 1941014X

[RKO+21] Rezamand, M. ; Kordestani, M. ; Orchard, M. E. ; Carriveau, R. ; Ting, D. S. ; Saif, M.: Improved Remaining Useful Life Estimation of Wind Turbine Drivetrain Bearings under Varying Operating Conditions. In: *IEEE Transactions on Industrial Informatics* 17 (2021), No. 3, pp. 1742–1752. http://dx.doi.org/10.1109/TII.2020.2993074. – DOI 10.1109/TII.2020.2993074. – ISSN 19410050

[RM07] Ragan, P. ; Manuel, L.: Comparing estimates of wind turbine fatigue loads using time-domain and spectral methods. In: *Wind engineering* 31 (2007), No. 2, pp. 83–99. http://dx.doi.org/10.1260/030952407781494494. – DOI 10.1260/030952407781494494

[SBBB17] Saidi, L. ; Ben Ali, J. ; Bechhoefer, E. ; Benbouzid, M.: Wind turbine high-speed shaft bearings health prognosis through a spectral Kurtosis-derived indices and SVR. In: *Applied Acoustics* 120 (2017), 1–8. http://dx.doi.org/10.1016/j.apacoust.2017.01.005. – DOI 10.1016/j.apacoust.2017.01.005. – ISSN 1872910X

[Sko05] Skogestad, Sigurd and Postlethwaite, I.: *Multivariable feedback control: analysis and design*. John Wiley & Sons, 2005

[SKSR20] Sitharthan, R. ; Karthikeyan, M. ; Sundar, D. S. ; Rajasekaran, S.: Adaptive hybrid intelligent MPPT controller to approximate effectual wind speed and optimal rotor speed of variable speed wind turbine. In: *ISA Transactions* 96 (2020), 479–489. http://dx.doi.org/10.1016/j.isatra.2019.05.029. – DOI 10.1016/j.isatra.2019.05.029. – ISSN 00190578

[SMBN09] Stol, K. A. ; Moll, H. G. ; Bir, G. ; Namik, H.: A comparison of multi-blade coordinate transformation and direct periodic techniques for wind turbine control design. In: *47th AIAA Aerospace Sciences Meeting*

including the New Horizons Forum and Aerospace Exposition (2009), pp. 1–12. http://dx.doi.org/10.2514/6.2009-479. – DOI 10.2514/6.2009–479. ISBN 9781563479694

[SR97] Söffker, D. ; Rakowsky, U. K.: Perspectives of Monitoring and Perspectives of monitoring and control of vibrating structures by combining new methods of fault detection with new approaches of reliability engineering. In: *12th ASME conference on reliability, stress analysis and failure prevention*, ASME, 1997, pp. 671–682

[SYM95] Söffker, D. ; Yu, T. J. ; Müller, P. C.: State estimation of dynamical systems with nonlinearities by using proportional-integral observer. In: *International Journal of Systems Science* 26 (1995), sep, No. 9, pp. 1571–1582. http://dx.doi.org/10.1080/00207729508929120. – DOI 10.1080/00207729508929120. – ISSN 0020–7721

[THH+20] Teng, W. ; Han, C. ; Hu, Y. ; Cheng, X. ; Song, L. ; Liu, Y.: A robust model-based approach for bearing remaining useful life prognosis in wind turbines. In: *IEEE Access* 8 (2020), pp. 47133–47143. http://dx.doi.org/10.1109/ACCESS.2020.2978301. – DOI 10.1109/ACCESS.2020.2978301. – ISSN 21693536

[Thi05] Thiringer, Torbjörn Petersson, A.: Control of a variable-speed pitch-regulated wind turbine / CHUT, Gothenburg. Goteborg, Sweden, 2005. – Techreport

[VDDW00] Van Der Merwe, R. ; Doucet, A. ; De Freitas, N. ; Wan, E.: The unscented particle filter. In: *Advances in Neural Information Processing Systems* 13 (2000). – ISBN 0262122413

[VP19] Valeti, B. ; Pakzad, S. N.: Estimation of remaining useful life of a fatigue damaged wind turbine blade with particle filters. In: *Dynamics of Civil Structures, Volume 2: Proceedings of the 36th IMAC, A Conference and Exposition on Structural Dynamics 2018*, Springer, 2019. – ISBN 9781441998309, pp. 319–328

[VPCT23] Vidal, Y. ; Puruncajas, B. ; Castellani, F. ; Tutivén, C.: Predictive maintenance of wind turbine's main bearing using wind farm SCADA data and LSTM neural networks. In: *Journal of Physics: Conference Series* 2507 (2023), No. 1. http://dx.doi.org/10.1088/1742-6596/2507/1/012024. – DOI 10.1088/1742–6596/2507/1/012024. – ISSN 17426596

[VPPK19] Vali, M. ; Petrović, V. ; Pao, L. ; Kühn, M.: Lifetime extension of waked wind farms using active power control. In: *Journal of Physics: Conference Series* 1256 (2019), No. 1, pp. 012029. http://dx.doi.org/10.1088/1742-6596/1256/1/012029. – DOI 10.1088/1742–6596/1256/1/012029. – ISSN 17426596

[Wel67] Welch, P. D.: The use of Fast Fourier Transform for the estimation of power spectra: A method based on time averaging over short, modified

periodograms. In: *IEEE Transactions on audio and electroacoustics* AU-15 (1967), No. 2, pp. 70–73. http://dx.doi.org/10.1109/TAU.1967.1161901. – DOI 10.1109/TAU.1967.1161901

[WF08] Wright, A. D. ; Fingersh, L. J.: Advanced control design for wind turbines part I: Control design , implementation , and initial tests / National Renewable Energy Laboratory (NREL). Version: 2008. http://dx.doi.org/10.2172/927269. Golden, Colorado, USA, 2008 (NREL/TP-500-42437). – Techreport. – Online resource

[WLZ+20] Wang, J. ; Liang, Y. ; Zheng, Y. ; Gao, R. X. ; Zhang, F.: An integrated fault diagnosis and prognosis approach for predictive maintenance of wind turbine bearing with limited samples. In: *Renewable Energy* 145 (2020), 642–650. http://dx.doi.org/10.1016/j.renene.2019.06.103. – DOI 10.1016/j.renene.2019.06.103. – ISSN 18790682

[Wri04] Wright, A. D.: Modern control design for flexible wind turbines / National Renewable Energy Laboratory (NREL). Version: 2004. https://www.nrel.gov/docs/fy04osti/35816.pdf. Golden, Colorado, USA, 2004 (NREL/TP-500-35816). – Techreport. – Online resource

[WWB17] Wang, N. ; Wright, A. D. ; Balas, M. J.: Disturbance accommodating control design for wind turbines using solvability conditions. In: *Journal of Dynamic Systems, Measurement, and Control* 139 (2017), apr, No. 4, pp. 041007. http://dx.doi.org/https://doi.org/10.1115/1.4035097. – DOI https://doi.org/10.1115/1.4035097. – ISSN 0022–0434

[WWJ16] Wang, N. ; Wright, A. D. ; Johnson, K. E.: Independent blade pitch controller design for a three-bladed turbine using disturbance accommodating control. In: *American Control Conference (ACC)*. Boston, Massachusetts, 2016. – ISBN 9781467386821, pp. 2301–2306

[WWYC23] Wang, Y. ; Wei, S. ; Yang, W. ; Chai, Y.: Robust active yaw control for offshore wind farms using stochastic predictive control based on online adaptive scenario generation. In: *Ocean Engineering* 286 (2023), No. P2, pp. 115578. http://dx.doi.org/10.1016/j.oceaneng.2023.115578. – DOI 10.1016/j.oceaneng.2023.115578. – ISSN 00298018

[XA20] Xie, F. ; Aly, A. M.: Structural control and vibration issues in wind turbines: A review. In: *Engineering Structures* 210 (2020), No. September 2019, 110087. http://dx.doi.org/10.1016/j.engstruct.2019.110087. – DOI 10.1016/j.engstruct.2019.110087. – ISSN 18737323

[XLZZ19] Xiao, C. ; Liu, Z. ; Zhang, T. ; Zhang, L.: On fault prediction for wind turbine pitch system using radar chart and support vector machine approach. In: *Energies* 12 (2019), No. 14, pp. 2693. http://dx.doi.org/10.3390/en12142693. – DOI 10.3390/en12142693. – ISSN 19961073

[XWY+21] Xiang, L. ; Wang, P. ; Yang, X. ; Hu, A. ; Su, H.: Fault detection of wind turbine based on SCADA data analysis using CNN and

LSTM with attention mechanism. In: *Measurement: Journal of the International Measurement Confederation* 175 (2021), No. May 2020, pp. 109094. http://dx.doi.org/10.1016/j.measurement.2021.109094. – DOI 10.1016/j.measurement.2021.109094. – ISSN 02632241

[YCT20] Yuan, Y. ; Chen, X. ; Tang, J.: Multivariable robust blade pitch control design to reject periodic loads on wind turbines. In: *Renewable Energy* 146 (2020), feb, pp. 329–341. http://dx.doi.org/10.1016/j.renene.2019.06.136. – DOI 10.1016/j.renene.2019.06.136. – ISSN 09601481

[YLH+15] Yuan, R. ; Li, H. ; Huang, H. Z. ; Zhu, S. P. ; Gao, H.: A nonlinear fatigue damage accumulation model considering strength degradation and its applications to fatigue reliability analysis. In: *International Journal of Damage Mechanics* 24 (2015), No. 5, pp. 646–662. http://dx.doi.org/10.1177/1056789514544228. – DOI 10.1177/1056789514544228. – ISBN 1056789514

[YLL+22] Yang, Q. ; Li, Y. ; Li, T. ; Zhou, X. ; Huang, G. ; Lian, J.: Statistical extrapolation methods and empirical formulae for estimating extreme loads on operating wind turbine towers. In: *Engineering Structures* 267 (2022), No. July, 114667. http://dx.doi.org/10.1016/j.engstruct.2022.114667. – DOI 10.1016/j.engstruct.2022.114667. – ISSN 18737323

[YT16] Yuan, Y. ; Tang, J.: Adaptive pitch control of wind turbine for load mitigation under structural uncertainties. In: *Renewable Energy* 105 (2016), pp. 483–494. http://dx.doi.org/10.1016/j.renene.2016.12.068. – DOI 10.1016/j.renene.2016.12.068. – ISSN 0960–1481

[YV20] Yucesan, Y. A. ; Viana, F. A.: A hybrid model for main bearing fatigue prognosis based on physics and machine learning. In: *AIAA Scitech 2020 Forum* 1 PartF (2020), No. January. http://dx.doi.org/10.2514/6.2020-1412. – DOI 10.2514/6.2020–1412. ISBN 9781624105951

[ZGR+18] Ziegler, L. ; Gonzalez, E. ; Rubert, T. ; Smolka, U. ; Melero, J. J.: Lifetime extension of onshore wind turbines: A review covering Germany, Spain, Denmark, and the UK. In: *Renewable and Sustainable Energy Reviews* 82 (2018), 1261–1271. http://dx.doi.org/10.1016/j.rser.2017.09.100. – DOI 10.1016/j.rser.2017.09.100. – ISSN 1364–0321

[ZTG+19] Zhang, C. ; Tahoumi, E. ; Gutierrez, S. ; Plestan, F. ; Deleon-Morales, J.: Adaptive robust control of floating offshore wind turbine based on sliding mode. In: *IEEE 58th Conference on Decision and Control (CDC)*. Nice, France, 2019. – ISBN 9781728113982, pp. 6936–6941

The thesis is based on the results and development steps published/accepted/in preparation in the following journal papers and conference proceedings:

Journal papers

Kipchirchir, E. ; Do, M. H. ; Njiri, J. G. ; Söffker, D.: Prognostics-based adaptive control strategy for lifetime control of wind turbines. In: *Wind Energy Science* 8 (2023), pp. 575–588

Kipchirchir, E. ; Söffker, D.: IPC-based robust disturbance accommodating control for load mitigation and speed regulation of wind turbines. In: *Wind Energy* 27 (2024), No. 4, pp. 382–402

Kipchirchir, E. ; Do, M. H. ; Njiri, J. G. ; Söffker, D.: Adaptive robust observer-based control for structural load mitigation and speed regulation in commercial wind turbines In: *IEEE Access* 12 (2024a), pp. 382–402

Kipchirchir, E. ; Liebeton, J. Söffker, D.: A hybrid prognosis approach for robust lifetime control of wind turbines. – in preparation

Conference proceedings

Kipchirchir, E. ; Do, M. H. ; Njiri, J. G. ; Söffker, D.: Mixed-sensitivity robust disturbance accommodating control for load mitigation and speed regulation of wind turbines. In: *2022 European Control Conference (ECC)* IEEE, 2022, pp. 1012-1017

Kipchirchir, E. ; Bakhshande, F. Söffker, D.: A μ-synthesis approach for robust control of wind turbines. In: *International Design Engineering Technical Conferences and Computers and Information in Engineering Conference 2023* ASME. – accepted

In the context of research projects at the Chair of Dynamics and Control, the following student theses have been supervised by Edwin Kipchirchir M.Sc. and Univ.-Prof. Dr.-Ing. Dirk Söffker. Development results of the student theses are not included in this thesis.

[Das20] Dash, B.B.: Design and development of a small flywheel energy storage system for wind turbine application using 3D Printing. Master Thesis, 2020.

[Ham21] Hamed, A.: Review and analysis of wind turbine blade dynamics for blades modeled using different beam theories. Bachelor Thesis, 2022.

[Hus22] Hussein, R.S.H.: Advanced control of large scale floating offshore wind turbines for speed regulation, load mitigation, and platform stabilization. Master Thesis, 2022.

[Cho22] Chowdhury, B.: Disturbance accommodating control of large-scale fixed-bottom offshore wind turbines for blades and support structure load mitigation. Master Thesis, 2022.

[Babu23] Babu, J.: The characteristics, using goals and the developed models of different storage systems Master Thesis, 2023.